**UNIVERSIDAD COMPLUTENSE DE MADRID**
FACULTAD DE CIENCIAS BIOLÓGICAS


# TESIS DOCTORAL

# Physiopathological relevance of cannabinoid $CB_1$ receptor in the development of glutamatergic and gabaergic populations during cortical ontogeny

# Implicación fisiopatológica del receptor $CB_1$ cannabinoide en el desarrollo de las poblaciones glutamatérgicas y gabaérgicas durante la ontogenia cortical

MEMORIA PARA OPTAR AL GRADO DE DOCTOR

PRESENTADA POR

**Daniel García Rincón**

Directores

**Ismael Galve Roperh**
**Manuel Guzmán Pastor**

Madrid

# TESIS DOCTORAL

Departamento de Bioquímica y Biología Molecular

FACULTAD DE CIENCIAS BIOLÓGICAS

**UNIVERSIDAD COMPLUTENSE DE MADRID**


PHYSIOPATHOLOGICAL RELEVANCE OF CANNABINOID $CB_1$ RECEPTOR IN THE DEVELOPMENT OF GLUTAMATERGIC AND GABAERGIC POPULATIONS DURING CORTICAL ONTOGENY

IMPLICACIÓN FISIOPATOLÓGICA DEL RECEPTOR $CB_1$ CANNABINOIDE EN EL DESARROLLO DE LAS POBLACIONES GLUTAMATÉRGICAS Y GABAÉRGICAS DURANTE LA ONTOGENIA CORTICAL

Daniel García Rincón

Directores de la Tesis Doctoral
Dr. Ismael Galve Roperh
Dr. Manuel Guzmán Pastor

Madrid, septiembre de 2019

UNIVERSIDAD COMPLUTENSE MADRID

# DECLARACIÓN DE AUTORÍA Y ORIGINALIDAD DE LA TESIS PRESENTADA PARA OBTENER EL TÍTULO DE DOCTOR

D./Dña. Daniel García Rincón,
estudiante en el Programa de Doctorado Bioquímica, Biología Molecular y Biomedicina,
de la Facultad de Ciencias Biológicas de la Universidad Complutense de Madrid, como autor/a de la tesis presentada para la obtención del título de Doctor y titulada:

Implicación fisiopatológica del receptor CB1 cannabinoide en el desarrollo de las poblaciones glutamatérgicas y GABAérgicas durante la ontogenia cortical

Physiopathological relevance of cannabinoid CB1 receptor in the development of glutamatergic and GABAergic populations during cortical ontogeny

y dirigida por: Ismael Galve Roperh y Manuel Guzmán Pastor

**DECLARO QUE:**

La tesis es una obra original que no infringe los derechos de propiedad intelectual ni los derechos de propiedad industrial u otros, de acuerdo con el ordenamiento jurídico vigente, en particular, la Ley de Propiedad Intelectual (R.D. legislativo 1/1996, de 12 de abril, por el que se aprueba el texto refundido de la Ley de Propiedad Intelectual, modificado por la Ley 2/2019, de 1 de marzo, regularizando, aclarando y armonizando las disposiciones legales vigentes sobre la materia), en particular, las disposiciones referidas al derecho de cita.

Del mismo modo, asumo frente a la Universidad cualquier responsabilidad que pudiera derivarse de la autoría o falta de originalidad del contenido de la tesis presentada de conformidad con el ordenamiento jurídico vigente.

En Madrid, a 5 de septiembre de 2019

Fdo.:

Esta DECLARACIÓN DE AUTORÍA Y ORIGINALIDAD debe ser insertada en la primera página de la tesis presentada para la obtención del título de Doctor.

*A las miles de vidas animales que esta Tesis ha extinguido...*

# AGRADECIMIENTOS

Cuando uno se embarca en el proceso de escribir una Tesis (y esto se hace algunos años antes de ponerse delante de la página en blanco por primera vez, quizá antes incluso de decidirse realmente a empezar un doctorado), acepta entregar una parte de su vida. Una parte que no se entrega como un todo indivisible, sino que se va repartiendo en partes alícuotas entre cada persona que, de alguna manera, forma parte del proyecto. Le das un poco a tus supervisores, otro poco a las personas que te llevan de la mano en la poyata cuando empiezas, un trocito va para cada persona que conoces en el laboratorio. La propia Ciencia demanda su correspondiente paquete de acciones en tu vida. Y también merece su parte cada persona (muchas veces ajena al laboratorio) en la que depositas tus ratos de ilusión, frustración, amenazas de abandono, conatos fallidos de descubrimiento y (también ☺), con la que compartes cada vez que el programa estadístico de turno te dice que sí, que las diferencias son estadísticamente significativas, que quizá todo tiene algún sentido después de todo. Son tantas personas, tantos sitios, tantos momentos en los que entregas una parte de ti, que de no ser por todo lo que recibes a cambio, llegarías al "final" del proceso, al momento de la página en blanco, siendo menos de lo que eras al empezar. Pero creo que nadie tiene esa sensación, sea como sea su *Viathesis*, si se me permite la licencia. Para mí, al menos, ha sido justo al contrario. Y no por todas las destrezas, científicas o no, que se adquieren a lo largo de estos años. Sino porque siento que por cada fragmento de mi vida que he entregado, he recibido a cambio otro para tomar el lugar del que yo daba.

Sea lo que sea lo que venga después de esta fase, estará sustentado, directa o indirectamente, en las ideas, ánimos, esfuerzos, convenientes dosis de realidad, y ratos de refugio que me han regalado decenas de personas a lo largo de estos años. Espero que estéis casi tan contentos con el resultado como lo estoy yo. Gracias a todos. Y un gracias adicional a todos los habitantes del L1 ♥.

Gracias también a la Fundación Tatiana Pérez de Guzmán el Bueno, ya que de no ser por su compromiso y su generosidad para con la Ciencia, esta Tesis no habría podido llegar a término. Mi más sincero agradecimiento por financiar la estancia que realicé en Ámsterdam, que supuso un antes y un después (para bien ☺) en mi vida personal y profesional.

I finally want to thank the people I met in Amsterdam, as they not only contributed to the data I show in this Thesis, but also became my family abroad. Thanks, Pascal, Taco, Femke, Tabitha, Eline, Sabine, Laila, Giulia, Rebecca and Thomas for your experimental effort. This Thesis is also yours.

# Table of Contents

# Resumen

El cerebro es el órgano más complejo del organismo, y dada la cantidad de información que tiene que computar e integrar, no resulta sorprendente la enorme diversidad de células y circuitos que lo conforman. Esta diversidad tiene su origen en un cantidad relativamente pequeña de células madre indiferenciadas que experimentan un complicado proceso de desarrollo que culmina con un cerebro maduro. Cientos de moléculas y sistemas de señalización celular orquestan sucesivas oleadas de proliferación de progenitores neurales, así como su diferenciación en los linajes específicos que pueblan el parénquima cerebral, y la posterior migración de su progenie desde los nichos germinativos en los que nace, hacia las áreas definitivas que ocupará en un cerebro adulto. A lo largo de estos procesos, neuronas, astrocitos y oligodendrocitos deben madurar y adquirir las características que las distinguirán como células funcionales, asegurando su inclusión en circuitos cerebrales específicos. Hoy día sabemos que una ligera desviación del programa ontogénico predeterminado puede tener consecuencias muy perjudiciales, ya que puede a su vez condicionar la aparición de diferentes malformaciones y patologías, que van desde enfermedades psiquiátricas a retraso mental de diversos grados, sin olvidar las enfermedades del espectro epiléptico. Por tanto, resulta crucial entender qué sistemas de señalización específicos regulan qué procesos concretos, y cómo se solapan unos con otros durante todo el proceso de desarrollo, para así poder predecir las consecuencias de su alteración y diseñar contramedidas efectivas.

Uno de los sistemas de señalización que participa en esta colección de procesos es el de los endocannabinoides. El sistema endocannabinoide regula multitud de funciones ya conocidas en el organismo adulto, funciones que van desde la actividad sináptica al balance energético. Pero su papel durante el desarrollo es un aspecto que, pese a estar ya plenamente aceptado, aún necesita ser investigado en profundidad.

Con esto en mente, decidimos investigar la implicación del receptor $CB_1$ en el desarrollo tanto de neuronas de proyección como de interneuronas GABAérgicas durante la ontogenia cortical. A tal fin, postulamos los siguientes objetivos para la presente Tesis Doctoral:

**Objetivo 1:** Analizar la conexión entre una función endocannabinoide alterada y la displasia cortical focal, una patología humana asociada con epilepsia infantil, así como evaluar si las neuronas de proyección que ven su expresión de $CB_1$ alterada durante el desarrollo experimentan cambios permanentes en su plasticidad y excitabilidad.

**Objetivo 2:** dilucidar la implicación del receptor $CB_1$ en el establecimiento de las interneuronas GABAérgicas, analizando el impacto a largo plazo de la exposición prenatal a THC en la población hipocampal de células en cesta CCK-positivas, junto con cualquier correlato comportamental o funcional.

Con respecto al **Objetivo 1**, hemos evaluado la expresión del receptor $CB_1$ en muestras de tejido provenientes de resecciones de pacientes con displasia cortical focal, así como su posible relación causal con la sobreactivación de la vía mTOR típica de esta patología. Además, hemos analizado la existencia de polimorfismos de un solo nucleótido específicos en genes del sistema endocannabinoide, para abordar la cuestión de si existe alguna alteración genética en el sistema endocannabinoide que pueda contribuir a la aparición de la enfermedad. Finalmente, mediante técnicas de electroporación *in utero* de ARNip en ratones, hemos atenuado transitoriamente la expresión del receptor $CB_1$ en neuronas corticales de proyección, para después estudiar su estado de maduración en diferentes estadios postnatales.

En resumen, hemos encontrado no solo que el receptor $CB_1$ se encuentra enriquecido en muestras de displasia cortical focal, sino también que su bloqueo farmacológico disminuye la fosforilación de la proteína ribosomal S6, que constituye un marcador *bona fide* de la actividad de mTOR. Además, hemos demostrado la asociación de un polimorfismo en el gen *DAGLA*, que codifica la enzima responsable de la síntesis del endocannabinoide 2-araquidonilglicerol, con la aparición de la enfermedad. Por último, hemos observado un retraso en la migración radial de las células electroporadas con ARNip, que además muestran una maduración alterada, demostrada por sus propiedades electrofisiológicas anómalas.

Nuestros hallazgos contribuyen a demostrar la implicación del sistema endocannabinoide en el desarrollo y maduración de neuronas corticales de proyección, y establecen una relación causal entre un defecto en dicho sistema y la aparición de malformaciones del desarrollo cortical, como la displasia cortical focal.

En relación al **Objetivo 2**, decidimos administrar una dosis baja de THC a ratonas gestantes durante una ventana temporal restringida del desarrollo embrionario, para después analizar a su descendencia en la edad adulta. Así, hemos comprobado el estado de la población de células en cesta CCK-positivas en la región hipocampal, así como la actividad oscilatoria propia de dicha estructura cerebral mediante el implante de electrodos de registro intracerebrales. También hemos evaluado si la descendencia de las

ratonas tratadas muestra algún efecto perjudicial del tratamiento sobre la ejecución de dos tests de memoria diferentes, así como si su equilibrio excitación-inhibición muestra alguna susceptibilidad diferencial frente a la inyección del fármaco proconvulsivo pentilenotetrazol. Finalmente, utilizamos el mismo paradigma de administración prenatal en ratones que carecen selectivamente de expresión del receptor $CB_1$ bien en neuronas glutamatérgicas telencefálicas, bien en interneuronas GABAérgicas, y verificamos el efecto de la deleción genética condicional sobre los efectos provocados por el THC.

Los datos obtenidos en estos experimentos mostraron que la alteración prenatal de la señalización del receptor $CB_1$ provocada por la administración de THC condiciona una disminución a largo plazo en la densidad de células en cesta CCK-positivas en la región CA1, disminución que afectó únicamente a la progenie masculina. Esta interneuronopatía específica de los machos ocurre concomitantemente con una alteración de las oscilaciones hipocampales y con una mayor frecuencia de rizaduras específicamente en los machos tratados. También encontramos alteraciones en la memoria espacial dependiente de hipocampo, mientras que la memoria de reconocimiento de objetos no sufrió alteraciones. El uso de ratones modificados genéticamente nos permitió adscribir los efectos observados exclusivamente a la acción del THC sobre receptores $CB_1$ presentes en neuronas GABAérgicas recién formadas, y no sobre el mismo receptor en neuronas glutamatérgicas nacientes.

En conjunto, estos datos señalan la importancia de una función endocannabinoide correcta durante fases tempranas del desarrollo cerebral para el establecimiento de una subpoblación GABAérgica específica, así como para la adquisición de una memoria espacial apropiada y un equilibrio excitatorio-inhibitorio estable. Además, nuestros hallazgos sientan las bases para un mejor entendimiento de las consecuencias a largo plazo producidas por la exposición prenatal a cannabinoides.

# Summary

The brain is the most complex organ in the body. Given the amount of information that it has to compute and integrate in behavioural and somatic responses, it comes as no surprise the enormous amount of different cells and circuit assemblies that build it up. All this diversity originates from a relatively small amount of undifferentiated stem cells that undergo an intricate development proccess culminating with a mature brain. Hundreds of molecules and signalling systems orchestrate consecutive waves of progenitor cell proliferation, their differentiation in the specific cell lineages that populate the cerebral parenchyma, as well as the migration of their progeny from the germinative niches in which they are born to the definitive areas they will occupy in the adult brain. Meanwhile, neurons, astrocytes and olygodendrocytes need to maturate and acquire the traits that characterize functional cells, including their assembly in specific brain circuits. Today we know that a slight deviation from the default program may lead to deleterious consequences and to the onset of different malformations and pathologies, which range from psychiatric diseases to diverse grades of mental retardation, without forgetting conditions belonging to the epileptic spectrum. Thus, it is crucial to understand which specific steps are regulated by which specific signalling systems, and how they imbricate themselves during the whole developmental process in order to predict the consequences of their malfunction and design effective countermeasures.

One of the signalling systems participating in this fine-tuned collection of processes is the endocannabinoid system. The endocannabinoid system regulates a well-characterized plethora of functions in the adult body, ranging from synaptic activity to energy balance, but its role during brain development is an issue that, despite being extensively accepted, needs to be further investigated.

Bearing this in mind, we sought to investigate the involvement of the $CB_1$ receptor in the development of both projection neurons and GABAergic interneurons during cortical ontogeny. To that end, we put forward the following aims for the present Thesis:

**Aim 1:** To analyse the link between altered endocannabinoid system function and focal cortical dysplasia, a human pathology associated with childhood epilepsy, as well as to assess if projection neurons that have got their $CB_1$ receptor signalling genetically disrupted during development suffer from permanent changes in plasticity and

excitability.

**Aim 2:** To assess the involvement of the $CB_1$ receptor in the establishment of GABAergic interneurons, by analysing the long-term impact of prenatal THC exposure in the hippocampal CCK-containing basket cell population, along with any cognitive or behavioural outcome.

With regard to **Aim 1**, we evaluated $CB_1$ receptor expression in tissue samples obtained from focal cortical dysplasia patient resections, as well as its causal link with the overactivation of the mTORC1 pathway, which constitutes a hallmark in this pathology. Next, we analysed the existence of specific single nucleotide polymorphisms within endocannabinoid system element genes in the same samples in order to address if there exists a genetically-encoded endocannabinoid malfunction that can contribute to the onset of the disease. Finally, by means of siRNA *in utero* electroporation, we transiently knocked-down $CB_1$ receptor expression in murine cortical projection neurons, and then studied their maturation state at different postnatal stages.

We found not only that $CB_1$ receptor is highly enriched in focal cortical dysplasia, but also that blocking its signalling attenuates the phosphorylation of a *bona fide* readout of mTORC1 activity, the ribosomal S6 protein. In addition, we demonstrated the association of a single nucleotide polymorphism affecting the *DAGLA* gene, which encodes the enzyme responsible for synthesizing the endocannabinoid 2-arachidonoylglicerol, with the occurence of the disease. Last, we observed a delay in the radial migration of $CB_1$-knocked-down neurons, which also show an impaired maturation as reflected by altered electrophysiological properties.

Altogether, these findings strongly support the involvement of the endocannabinoid system in the development and maturation of cortical projection neurons, and establish a yet-to-be-studied causal link between its malfunction and the appearance of malformations of cortical development, as focal cortical dysplasia.

In respect of **Aim 2**, we decided to administer a mild dose of THC to pregnant mice during a restricted developmental window, and then analyse their offspring at adult stages. In this way, we evaluated the state of the CCK-containing basket cell population in the hippocampal region, as well as the oscillatory activity arising from that brain structure, by implatation of intracranial recording electrodes. We also assessed if the offspring of the treated dams exhibited any detrimental trait in the execution of two different memory tasks, and challenged their excitatory-inhibitory balance by inject-

ing a proepileptic drug, pentylenetetrazol. Finally, we used the same administration paradigm in mice that lack $CB_1$ receptor expression selectively in either telencephalic glutamatergic neurons or GABAergic interneurons, and verified the effect of the genetic deletion over our previously observed THC-elicited effects.

The data obtained from these experiments showed that prenatal disruption of $CB_1$ receptor signalling by THC administration fosters a long-term and male-specific decrease in CCK-containing basket cell density in CA1. This sex-dimorphic interneuronopathy ensues along with altered hippocampal oscillations and a higher sharp-wave ripple rate specifically in the treated males. Hippocampal-dependent spatial memory was also impaired in that group, while object recognition memory remained unaffected. The use of genetically modified mice let us adscribe these effects exclusively to the action of THC on $CB_1$ receptors present on developing GABAergic neurons, and not those expressed by nascent projection neurons.

As a whole, these data unveil the importance of a proper endocannabinoid function during early brain development for the establishment of a specific GABAergic subpopulation, as well as for the refining of an appropriate spatial memory and a stable excitation-inhibition balance. In addition, our findings pave the way to a better understanding of the long-term consequences evoked by prenatal cananbinoid exposure.

# Abbreviations

**2-AG:** 2-arachidonoylglycerol

**AC:** adenylyl ciclase

**ACSF:** artificial cerebrospinal fluid

**AEA:** anandamide

**AHP:** afterhyperpolarization

**AP:** action potential

**BC:** balloon cell

**BLBP:** brain lipid-binding protein

**CAT:** chloramphenicol acetyltransferase

**$CB_1R$:** cannabinoid receptor type 1

**$CB_2R$:** cannabinoid receptor type 2

**CBD:** cannabidiol

**CBR:** cannabinoid receptor

**CCK:** cholecystokinin

**CGE:** caudal ganglionic eminence

**CNS:** central nervous system

**CP:** cortical plate

**CPN:** callosal projection neuron

**CR:** calretinin

**CRC:** Cajal-Retzius cell

**CSMN:** corticospinal motor neuron

**CthPN:** corticothalamic projection neuron

**DAG:** diacylglycerol

**DAGL:** diacylglycerol lipase

**DN:** dysmorphic neuron

**DTT:** dithiothretiol

**E:** embryonic day, as in E10 or E17

**eCB:** endocannabinoid

**ECS:** endocannabinoid system

**EEG:** electroencephalography

**EGTA:** ethylene glycol tetraacetic acid

**EPSC:** excitatory postsynaptic current

**ERK:** extracellular-signal regulated kinase

**FAAH:** fatty acid amide hydrolase

**FCD:** focal cortical dysplasia

**FDG:** fluorodeoxyglucose

**GABA:** γ-aminobutyric acid

**GE:** ganglionic eminence

**GFAP:** glial fibrillary acidic protein

**GFP:** green fluorescent protein

**GLAST:** glutamate aspartate transporter

**GPCR:** G protein-coupled receptor

**HCN:** hyperpolarization-activated cyclic nucleotide-gated (channel)

**HEPES:** 4-(2-hydroxyethyl)-1-piperazine-ethanesulfonic acid

**HFO:** high frequency oscillation

**IHC:** immunohistochemistry

**IKM:** interkinetic nuclear migration

**IN:** interneuron

**IPC:** intermediate progenitor cell

**IPSC:** inhibitory postsynaptic current

**ISH:** *in situ* hybridization

**ISI:** interspike interval

**IUE:** *in utero* electroporation

**IZ:** intermediate zone

**LFP:** local field potential

**LGE:** lateral ganglionic eminence

**LTD:** long term depression

**MCD:** malformation of cortical development

**MGE:** medial ganglionic eminence

**MGL:** monoacylglycerol lipase

**mPFC:** medial prefrontal cortex

**MRI:** magnetic resonance imaging

**mTOR:** mammalian target of rapamycin
**MZ:** marginal zone
**NAPE:** N-acylphosphatidylethanolamine
**NAPE-PLD:** NAPE-specific phospholipase D
**NEC:** neuroepithelial cell
**NOR:** novel object recognition
**NSC:** neural stem cell
**Oct4:** octamer-binding transcription factor 4
**OL:** object-location
**oRGC:** outer radial glia cell
**oSVZ:** outer subventricular zone
**Oxt1:** orthodenticle homeobox 1
**P:** postnatal day, as in P1 or P14
**Pax6:** paired box protein 6
**PBS:** phosphate buffered saline
**PET:** positron emission tomography
**PFC:** prefrontal cortex
**PI3K:** phosphatidylinositol 3-kinase
**PKA:** protein kinase A
**PN:** projection neuron
**POA:** preoptic area
**PP:** preplate
**pS6:** phosphorylated ribosomal protein S6
**PTZ:** pentylenetetrazol
**PV:** parvalbumin
**qPCR:** quantitative PCR
**RGC:** radial glia cell
**Rheb:** Ras homolog enriched in brain
**RMP:** resting membrane potential
**S6:** ribosomal protein S6
**SD:** standard deviation
**Shh:** sonic-hedgehog
**ShNP:** short neural precursor
**SNP:** single nucleotide polymorphism
**Sox2:** SRY-box transcription factor 2
**SP:** subplate
***sp*:** *stratum pyramidale*
**SST:** somatostatin
**STD:** short term depression
**Svet1:** subventricular expressed transcript 1
**SVZ:** subventricular zone
**SWR:** sharp-wave ripples
**Tbr1:** T-box brain protein 1
**Tbr2:** T-box brain protein 2
**TF:** transcription factor
**THC:** $\Delta^9$-tetrahydrocannabinol
**TSC:** tuberous sclerosis complex
**VIP:** vasointestinal peptide
**VZ:** ventricular zone

# Introduction

The brain. The organ that orchestrates every single complex behaviour that defines us as humans. The flagship of our complexity as mammals. The master operator of the body's functions. An organ composed by several hundred billions of cells, which assemble in turn billions of circuits. Countless populations and subtypes of neurons, astrocytes, oligodendrocytes and microglial cells receiving inputs from the surrounding world and the body itself, computing herculean amounts of information in order to integrate it in biological responses pursuing one major goal: our adaption and survival.

The ontogeny of the nervous system is a delicate process in which subtle alterations may lead to highly noxious consequences. A slight deviation from the default genetic programs that encode the blueprint for a functional brain may produce outcomes that endanger the survivability of the individual. Hence and not surprisingly, brain development has become an area of knowledge that attracts growing attention and effort, in search not only of understanding about the molecular mechanisms underlying this complex process, but also of insight regarding the consequences of its deregulation and the possible treatments or countermeasures.

## 1. Ontogeny of the nervous system: the basics

Understanding how a cluster of embryonic undifferentiated neural stem cells (NSCs) gives rise to a fully mature and functional brain is a question that scientists have been trying to answer for decades. Pioneer neuroscientists, as Camilo Golgi, Korbinian Brodmann and Santiago Ramón y Cajal, among others, fuelled with their seminal works the race for brain comprehension. Ramón y Cajal first described the neuron as the functional and cellular unit of the brain (Ramón y Cajal, 1899) and, from that point, thousands of neuroscientists have dedicated their lives to understand how a mature brain arises from NSCs. Thanks to their efforts, nowadays we have a precise, although far from concluded, idea of how brain development works.

The more we know about this field, the more evident becomes that every single developmental step must be meticulously and tightly regulated by multiple genetic programs. These programs, established and maintained primarily by molecules termed morphogens, give rise to spatiotemporal patterns, which in turn define the types and quantities of neural cells that are generated in a given moment in a specific brain region. Morphogens are molecules released by organizers or patterning nodes during development in a way that creates a concentration gradient, being higher in the surroundings of the node, and decreasing progressively as the distance to the node

increases. A given cell will be exposed to different concentrations of diverse morphogens depending on its position relative to distinct nodes. As different morphogens trigger specific signalling pathways, the integration of all the morphogen levels that a cell receives will determine its molecular identity, since pathways activated or inhibited by morphogens are related to patterns of transcription factor (TF) expression that subsequently regulate gene expression and ultimately control cell fate.

### 1.1. Primordial morphogenesis of the brain

To begin with, and taking a mammalian embryo (like that of human and mouse species) as example, at an early stage of ontogeny, a regionalization of the dorsal ectoderm leads to the formation of the neural plate, a planar sheet of neuroepithelium (Rubenstein *et al*., 1998). In a later stage [embryonic day 8 (E8) in mice], the neural plate will form the neural tube after neurulation (Copp *et al*., 2003). Although antero-posterior identity is still present in the neural plate, driven by the antagonistic signalling between the embryonic organizer and the anterior visceral endoderm, neural tube and subsequent phases of development are characterized by a deeper, more complex and irreversible specification and patterning (Hébert and Fishell, 2008). The neural tube suffers a set of constrictions that establish the boundaries of the primary brain vesicles: prosencephalon, mesencephalon and rhombencephalon, which will grow into forebrain, midbrain and hindbrain, respectively, as development progresses. The prosencephalon will subsequently suffer a new division in order to form the secondary vesicles: telencephalon (the most rostral) and diencephalon (the most caudal) (Figure 1).

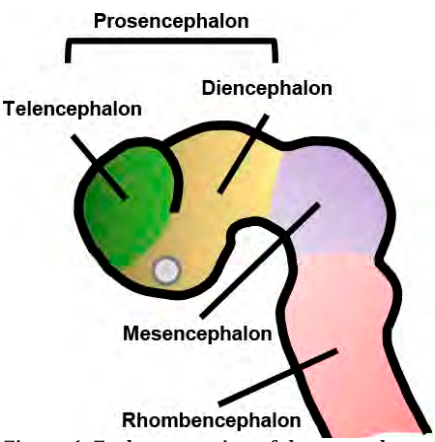


**Figure 1. Early patterning of the central nervous system.** Primary and secondary brain vesicles in the developing mammalian brain.

Afterwards, by E10, the telencephalon will further specialize in two areas. The dorsal telencephalon, or pallium, will be the origin of the three cortical ultrastructures that characterize a mature brain: neocortex, paleocortex (olfactory piriform cortex) and archicortex (subiculum, hippocampus, entorhinal and retrosplenial cortices) (Figure 2). The vast majority of cortical projection neurons (PNs) are born in this region (O'Leary *et al*., 2007). On the other hand, the ventral telencephalon, or subpallium, will give rise to another three different regions:

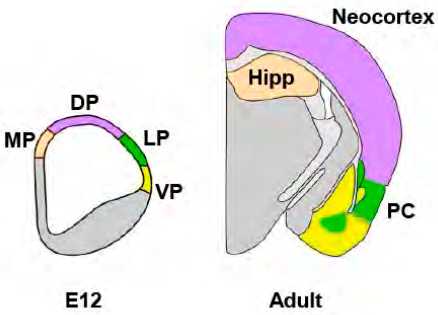


**Figure 2. The dorsal telencephalon gives rise to three different cortical structures.** Cortical structures in the adult (right) mice brain [(the neocortex, the hippocampal formation (Hipp) or archicortex, and the olfactory piriform cortex (PC) or paleocortex] originate from specific pallial domains present in the embryonic (left) brain [medial pallium (MP), dorsal pallium (DP), lateral pallium (LP), ventral pallium (VP)]. Adapted from Luzzati, 2015.

lateral (LGE), medial (MGE) and caudal (CGE) ganglionic eminences (GEs), that will serve as the prospective territories for the basal ganglia and as origin for the majority of inhibitory neurons that populate the forebrain (Figure 3) (Hansen *et al*., 2013; Huang, 2014; Marín and Müller, 2014).

This primordial shaping constitutes only the beginning of a puzzling process, as the developing cerebral tissue needs to further subdivide in order to reach the characteristic complexity of a mature brain.

## 1.2. Radial and tangential patterning within the cortex

The neocortex is the most complex area of the brain, being also the most recent in phylogeny. To understand its complexity, one should notice the heterogeneity generated in its two axes: radial and tangential, the former being perpendicular to the ependymal layer of the lateral ventricles and the latter parallel to it. The tangential axis is divided into several areas which are functionally different from each other. These differences come along with a characteristic patterning in gene expression, hodology and cytoarchitecture (O'Leary and Sahara, 2008). Four cortical main areas

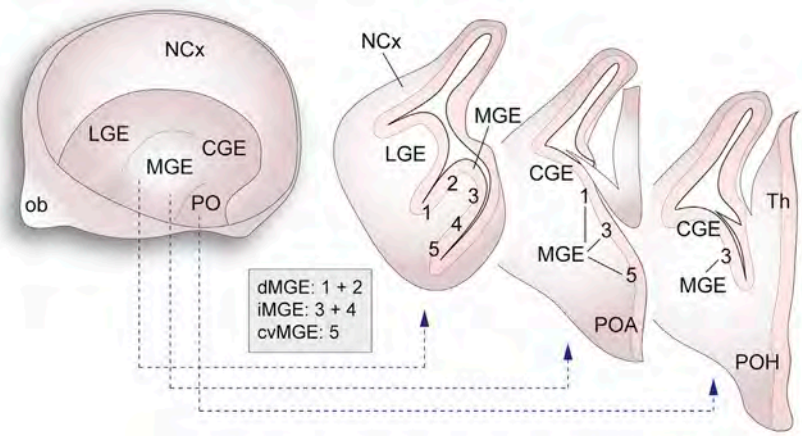


**Figure 3. Regional organization of the embryonic subpallium.** Developing telencephalic hemisphere (left) as viewed from the midline. On its right, three coronal sections depicting the ganglionic eminences. CGE, caudal ganglionic eminence; LGE, lateral ganglionic eminence; MGE, medial ganglionic eminence (d, dorsal; i, intermediate; cv, caudoventral); NCx, neocortex; ob, olfactory bulb; PO, preoptic region; POA, preoptic area; POH, preoptic-hypothalamic border; Th, thalamus. From Lim *et al*., 2018.

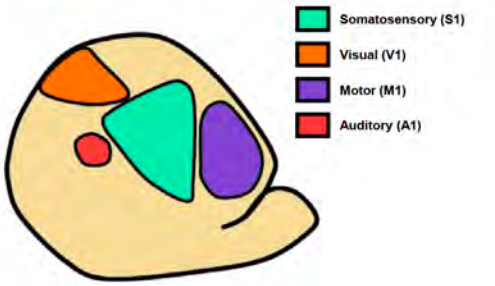


**Figure 4. Area patterning within the neocortex.** Embryonic arealization defines four areas that are divergent in gene expression, connectivity pattern and cognitive function. Adapted from Bertacchi *et al*., 2018.

(Figure 4) can be distinguished attending to their functionality: one pledged to motor function (M1), and three engaged in sensory function [auditory (A1), somatosensory (S1) and visual (V1)] (O'Leary *et al*., 2007). To generate these different areas, a process known as arealization must take place. Arealization is a direct consequence of the existence of morphogen gradients [like those of bone morphogenetic proteins, fibroblast growth factors and sonic-hedgehog (Shh)], which determine the expression of TFs such as Pax6, Sp8, Emx2, Coup-TFI and others. These TFs enforce different genetic programs that condition cellular identity of the progenitor cells in the developing cortex and, consequently, the identity of the neural cells derived from them. Although this process is strongly conserved in different mammalian species, which suggests common programs securing the correct patterning of the neocortex, the plasticity shown by neocortex regionalization after trauma points also to some degree of freedom in the acquisition of cortical identity (Alfano and Studer, 2013).

Regarding the radial axis, within the neocortex, and specifically in mammals, six different layers numbered from I (outermost) to VI (innermost) can be distinguished (Box 1), each one populated with its own assortment of neurons that differ in gene expression, morphology and connectivity (Molyneaux *et al*., 2007). Amniotes other than mammals possess cortices comprising only three layers (Puelles *et al*., 2000; Cheung *et al*., 2007).

The first comprehensive theory that brought together the discoveries about radial and tangential axes was the radial unit theory (Figure 5), which stands that "*the ependymal layer of the embryonic cerebral ventricle consists of proliferative units that provide a proto-map of prospective cytoarchitectonic areas. The output of the proliferative units is translated via glial guides to the expanding cortex in the form of ontogenetic columns, whose final number for each area can be modified through interaction with afferent input*" (Rakic, 1988; Mountcastle, 1997). Although partially modified and amended by recent findings, the cortical column model remains valid today. It is important to note that currently we know that the neurons which are born in a particular column are not completely restricted to that column, as, in contrast, they have some plasticity and can finally be part of surrounding columns (Torii *et al*., 2009; Dimidschstein *et al*., 2013).

**BOX 1. The six-layered neocortex**

The neocortex, also known as isocortex, is one of the most complex regions within the brain, its structure and composition differing across the different areas it encompasses. Nevertheless, and with some exceptions, it keeps a six-layered composition in almost its whole extension. Each one of its layers possess its own microstructure and cell composition, and so its own connectivity pattern.

»**Layer I:** the molecular layer, populated by scattered GABAergic INs. It also contains glial cells and the dendritic arborisation and horizontally oriented axons from neurons populating the other layers.

»**Layer II:** the external granular layer, vastly occupied by small pyramidal neurons that receive afferences from the contralateral hemisphere also projecting onto it, as well as by numerous stellate neurons.

»**Layer III:** the external pyramidal layer, populated by small and medium-sized pyramidal neurons that form the main corticocortical efferences.

»**Layer IV:** the internal granular layer, in which pyramidal and stellate neurons receive thalamocortical and intrahemispheric corticocortical afferents.

»**Layer V:** the internal pyramidal layer, which contains large pyramidal neurons that project to subcortical (other than thalamic) and subcerebral structures.

»**Layer VI:** the multiform or polymorphic layer, occupied by a few large pyramidal neurons and many small spindle-like pyramidal and multiform neurons. From this layer the efferences to the thalamic region depart.

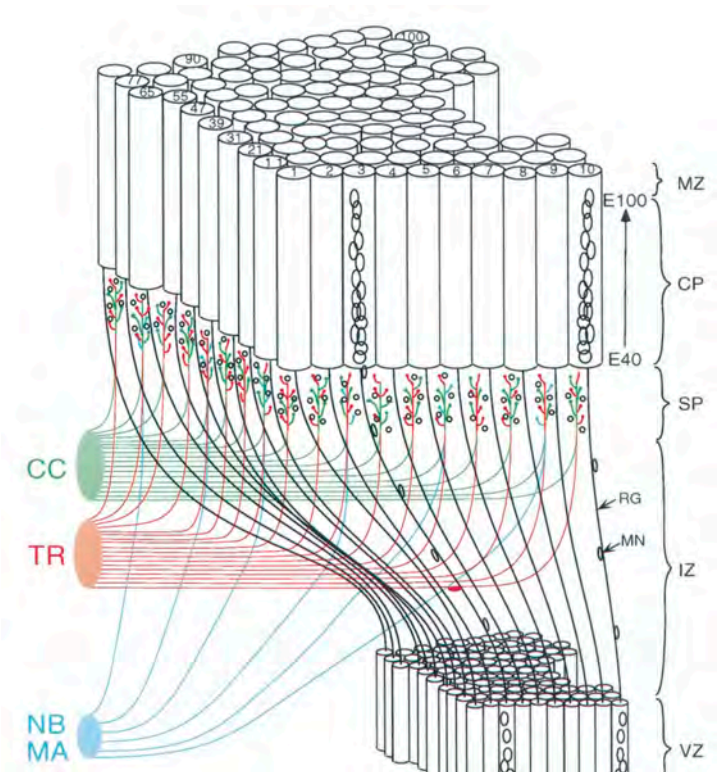


**Figure 5. Radial unit model: 3D representation of the column model in the monkey cortex.** Migrating neurons (MN), using radial glia (RG) as a scaffold, traverse the intermediate zone (IZ) and the subplate (SP), where they interact with afferents from monoamine nuclei of the brainstem (MA), from the nucleus basalis (NB), from the thalamic radiation (TR) and from corticocortical bundles (CC). MG settle in an inside-out manner, occupying always the interface between cortical plate (CP) and the marginal zone (MZ). In this way, neurons arising from a specific "column" in the ventricular zone (VZ) maintain the topology in the CP, althoug there exist lateral displacement at some extent. In the schematic, columns in the VZ are identified by numbers, maintained by the cortical columns that they give rise to. From Mountcastle, 1997.

## 2. Establishing cortical diversity: one step beyond

After introducing neocortical heterogeneity, it is time to try to understand where it stems from. Briefly, the whole brain primordium, which is composed at first by a homogenous neuroepithelium, will undergo different expansion and specification processes to give rise to the cortex and other structures. In this point, it becomes convenient to introduce some topological terms that will be extensively used, terms that correspond to the different strata in the early telencephalic wall. Spanning from the dorsalmost part of the neural tube, underlying what will become the pial surface, and until the ventralmost part of pallium, just over the embryonic ventricle, the different zones that compose the developing brain receive the names of marginal zone (MZ), intermediate zone (IZ), subventricular zone (SVZ) and ventricular zone (VZ). These zones contain, in different time points, the diverse progenitor populations that shape the origin of cortical cell diversity.

### 2.1. Diversity of progenitor cells

As stated, the homogenous neuroepithelial population will undergo consecutive rounds of symmetric divisions, each one further refining their genetic program, which will guide the cells through a complex process that culminates with neurogenesis. During that process, several types of progenitors can be distinguished attending to their genetic profile and mitotic behaviour.

#### 2.1.1. Neuroepithelial cells

Cells forming the brain primordium are known as neuroepithelial cells (NECs). These cells have their bipolar soma so elongated that they contact both surfaces of the developing cortex, pial and ventricular surfaces, with their basal and apical process, respectively (Sidman and Rakic, 1973). Even if NECs are committed to neural lineage, they retain some attributes typical from epithelia: they are highly polarized and strongly attached, as they form tight junctions to each other in the apical part, and are affixed to basal part through integrins (Aaku-Saraste *et al*., 1996; Graus-Porta *et al*., 2001). NECs experience a process called interkinetic nuclear migration (INM), during which their nuclei move along the apicobasal axis depending on the specific phase of the cell cycle that they are in. Hence, during G1, the bulk of their soma, containing the nucleus, moves to the basal pole, near the pial surface. Once there, the cell undergoes S phase, and then, while proceeding to G2, the soma moves to the opposite

pole, the apical wall, where the M phase will take place. This way, cell divisions happen only in the VZ (Sauer, 1934; Takahashi *et al*., 2018). NECs divide almost exclusively in a symmetric fashion, thus increasing the size of the NSCs pool. In a later phase, NECs start losing their epithelial identity and gradually transform in radial glia cells (RGCs), with molecular markers more typical of astrocytes. That point marks the outbreak of neurogenesis (Kriegstein and Alvarez-Buylla, 2009).

### 2.1.2. Radial glia cells

RGCs take their name from the fact that they form radial processes to the apical and basal edges of the cortical primordium (Figure 6). In this stage, the characteristic tight junctions from NECs are replaced by adherens junctions (Martynoga *et al*., 2012). RGCs also undergo INM and retain some of the protein expression from NECs, as Pax6, nestin or vimentin can be found in both cell types (Götz *et al*., 2002; Osumi *et al*., 2008). On the other hand, RGCs express astrocyte markers such as GFAP, GLAST or BLBP (Hartfuss *et al*., 2001). The main difference between NECs and RGCs is that the latter are capable not only of symmetrical division, which yields two identical RGCs, but also of two modes of asymmetrical self-renewing divisions: non-neurogenic, in which one of the offspring cells is a RGC and the other is an intermediate progenitor

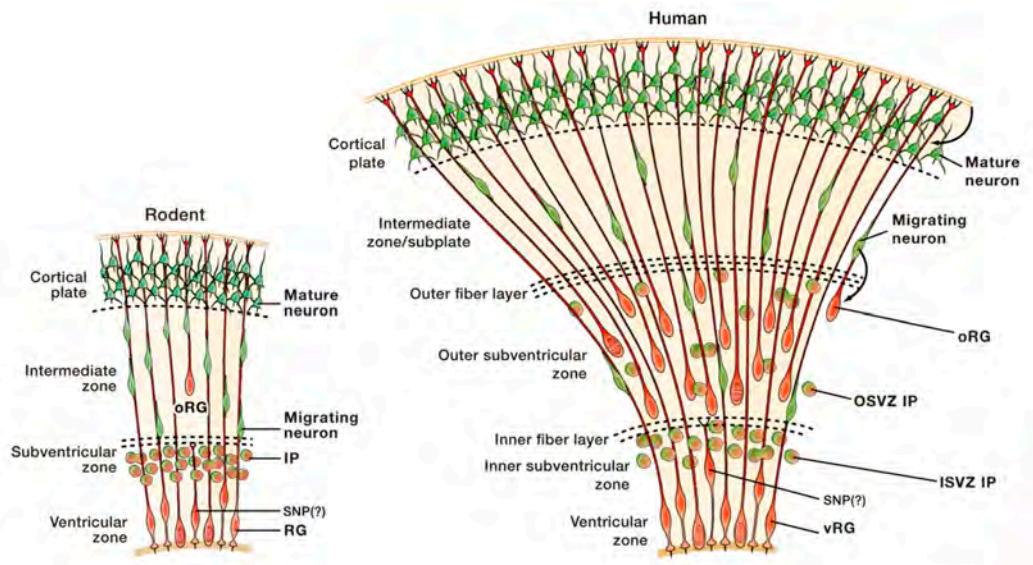


**Figure 6. Overview of neocortical development in rodents and humans.** Schematic depicting different types of necortical progenitor cells and the compartments in which they reside. In rodents (left), radial glia (RG) cells divide in the VZ, while intermediate progenitor (IP) cells undergo their division processes in the SVZ. Only a small fraction of RG detach from the VZ, creating an incidental outer SVZ (OSVZ). In contrast, humans (right) develop a thick OSVZ, which is populated by its own cohort of outer IP cells (OSVZ IP). Given the huge expansion achieved by a thick OSVZ, tissue expands not only radially from the column units in the VZ, but also tangentially, giving rise to the folded neocortex that defines gyrencephalic animals. Adapted from Lui *et al*., 2011.

cell (IPC); and neurogenic, which yields a RGC and a newborn neuron (Noctor *et al*., 2004). At the time RGCs appear and start their asymmetrical divisions, the once single-layered neuroepithelium grows in thickness and complexity, and the neurons arising in the apical compartments start their migration to the cortical plate using RGCs as a radial scaffold (Malatesta *et al*., 2000; Miyata *et al*., 2001; Noctor *et al*., 2001).

### 2.1.3. Intermediate progenitor cells

Also known as basal progenitors because they translocate their soma to the SVZ, thus making them "basal" with respect to RGCs, which are typically located in the VZ (Takahashi *et al*., 1995), these cells work as a secondary population of progenitor cells. Once they are born, they lose their processes and adopt a multipolar morphology. IPs will not undergo INM anymore (Noctor *et al*., 2008; Borrell *et al*., 2012; Wilsch-Brauninger *et al*., 2012). They switch their expression profile from that of RGCs to a new one without epithelial markers like Pax6, as instead, IPCs start expressing the TFs Svet1 and Tbr2/Eomes (Tarabykin *et al*., 2001; Englund *et al*., 2005). IPCs experience in most cases symmetrical division in their first stages, shifting to self-consuming neurogenic divisions later. Thus, the SVZ, which by mouse E13 is barely emerging, becomes the main contributor to neurogenesis by E16, when the IPC pool has reached its maximum size after several amplifying symmetric divisions. Currently, the fact that the majority of cortical neurons, regardless of their specific lineage, originate from IPCs is something generally accepted in the field (Noctor *et al*., 2004; Kowalczyk *et al*., 2009; Mihalas *et al*., 2016).

### 2.1.4. Other progenitor populations in the dorsal telencephalon

Although NECs, RGCs and IPCs constitute the main populations of progenitor cells in the developing brain, at least two additional populations are worth to be mentioned: short neural precursors (ShNPs) and outer radial glia cells (oRGCs).

ShNPs are a special population of RGCs that have lost their basal process, while retaining the apical one (Gal *et al*., 2006). In spite of expressing Pax6 and not Tbr2, and being located in the VZ, ShNPs behave like IPCs in that they are likely to directly generate neurons in the VZ (Stancik *et al*., 2010). They also respond to niche-derived cues, like Notch, which are typical from IPCs (Mizutani *et al*., 2007). Thus, some consider them as a population of RGCs undergoing the transformation into IPCs.

oRGCs are another population of RGCs located in a zone known as outer subven-

tricular zone (oSVZ). The oSVZ was once believed to be present only in gyrencephalic mammals, although its existence has been confirmed to a lesser extent in the mouse cortex (Shitamukai *et al*., 2011). oRGCs resemble RGCs without their apical process, thus losing their connection with the ventricular wall. They retain the basal process, Pax6 expression and self-renewal capacity. They are considered to be the population that gives rise to the massive tangential expansion in the cortex of primates, otherwise hardly explained (Reillo *et al*., 2011).

### 2.2. Neurogenic waves and projection neuron diversity

Different progenitor cells populate the primordium of the cortex at different time points, but each one of them participates in a series of spatiotemporal events that drive the onset of neurogenesis. Neurons generated from pallial progenitors belong to subpopulations which will colonise specific layers of the neocortex, depending on the exact day when they are born. This event occurs in an inside-out fashion, so that the neurons which are born in early embryonic days populate the layers near VZ and SVZ (deep layers), while the ones born later will migrate through the previously established deep layers and will populate the upper ones.

Approximately from E10 to E12, cortical progenitors start undergoing asymmetrical divisions which will generate neurons. These neurons will radially migrate using RGCs as scaffold, forming the preplate (PP). PP neurons will, in a later developmental stage, establish transient glutamatergic synapses with newly generated neurons to regulate their multipolar-to-bipolar morphology transition, a step that will be crucial for their migration towards neocortical layers (Ohtaka-Maruyama *et al*., 2018). At the same time, the Cajal-Retzius cells (CRCs) originating from different foci at the borders of pallium colonise the pial surface of the developing cortex and transiently establish in the MZ (Marín-Padilla, 1998; Soriano and Del Río, 2005). Once there, they start releasing reelin, that acts as a directional cue for migrating neurons.

A second surge of newborn neurons arises at E12. After migrating through the PP [which is splitting into the MZ and a deep subplate (SP) by that time], they form the cortical plate (CP), the real primordium of the six-layered neocortex. Concomitantly, the SVZ makes its debut, and starts growing in size and progenitor cell number that will subsequently boost the growth of the CP.

In the next five days, overlapping neurogenic waves will generate diverse PN populations (Figure 7), as previously stated, in an inside-out fashion, giving origin to rough-

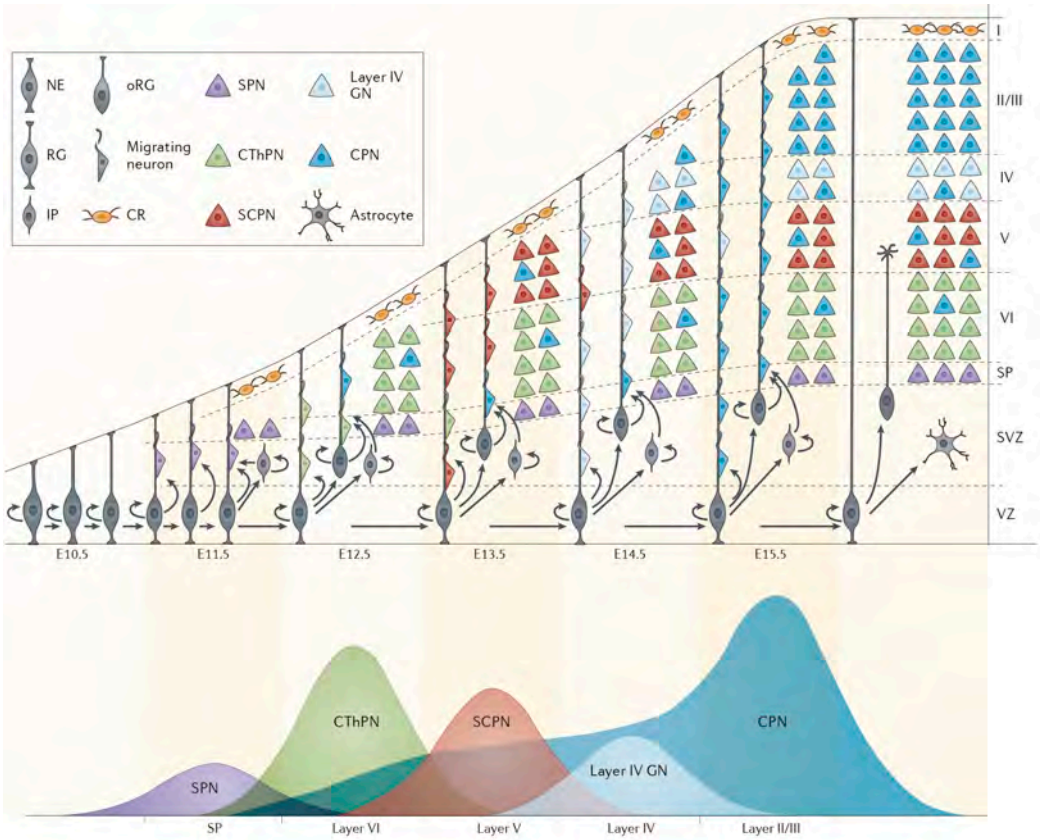


**Figure 7. Sequential neurogenic waves give rise to projection neurons populating the neocortex.** Cortical PNs generate sequentially from different progenitor types in the VZ/SVZ. RGCs begin to produce neurons around E11.5, while also producing Ips and oRGCs. CRCs populate layer I from non-cortical areas. According to their birthdate, PNs acquire a specific subtype and migrate to their corresponding cortical layer, populating and thickening the CP in an inside-out manner. Briefly, subplate neurons (SPN) are born around E11.5, just before the peak of CThPNs and SCPNs (E12.5 and E13.5, respectively) Layer IV granular neurons (GN) are born around E14.5, while most CPNs are generated between E14.5 and E16.5. Peak sizes in the lower diagram ara proportional with the estimate number of neurons born each day. Adapted from Greig *et al*., 2013.

ly 80 % of the neurons that populate the cortex. Peaking at E12, the birth of neurons destined to migrate to layer VI gives rise to corticothalamic PNs (CThPNs) and callosal PNs (CPNs). Then, with peak at E13, layer V neurons, including corticospinal motor neurons (CSMNs) and more CPNs, are born. Layer IV neurons, which include locally projecting stellate cells, appear at E14. Between E15 and E17, diverse subpopulations of CPNs and intracortical PNs bound for layers II/III arise. Layer I, which originates from MZ, lacks PN somata, and will be populated only by GABAergic interneurons (INs) and glial cells in the mature brain, as CRCs disappear gradually in early postnatal life (Martynoga *et al*., 2012; Greig *et al*., 2013; Huang, 2014).

This clockwork mechanism defining the fate of newborn neurons also affects the generation of the rest of cell types that conform the cortex (with the exception of mi-

croglia, whose origin is myeloid): NSCs generate neurons, astrocytes and oligodendrocytes in a sequential manner (Abney *et al*., 1981; Qian *et al*., 2000). Although astrogliogenesis starts during embryonic development (around E16 in mice) and oligodendrogenesis begins just after birth, both cell types have the main part of their populations generated in the first postnatal month (Cameron and Rakic, 1991; Misson *et al*., 1991; Rowitch and Kriegstein, 2010).

### 2.3. Interneurons in the cortex: origin and diversity

Inhibitory neurons constitute the remaining 20% of cortical neurons. The majority of them hold γ-aminobutyric acid (GABA) as their main neurotransmitter. They typically dampen neurotransmitter release in closely located neurons, and so they are termed INs. Different criteria have been proposed in the past years in order to classify them, but single and simple criteria appear to be insufficient to apprehend their full diversity (Figure 8) (Ascoli *et al*., 2008; Bartolini *et al*., 2013; DeFelipe *et al*., 2013).

The vast majority of INs populating the neocortex arises from the subpallial regions known as GEs (Figure 3), which act as the proliferative niche in the subpallium. GEs possess, as their pallial counterpart, VZ and SVZ compartments that contain progenitor cells very similar to those found in the pallium not only in morphology and time-restricted presence, but also in their proliferative and neurogenic behaviour (Flames and Marín, 2005). However, neurons derived from these progenitors are eminently INs. Although these traits are valid for GEs as a whole, GEs is a term that encompasses three spatially segregated regions characterized by the expression of different TFs: LGE, MGE and CGE. The latter two give rise to the INs that will afterwards migrate to the cortex. The MGE is believed to give rise to roughly 60% of cortical INs, including parvalbumin- (PV) and somatostatin- (SST) containing INs. As for the CGE, it produces cholecystokinin- (CCK), calretinin- (CR) and vasointestinal peptide (VIP)- containing INs. Additionally, a small percentage (less than 10%) of cortical INs are born in a different subpallial area, the preoptic area (POA), which is the origin of a small though diverse group of SST-, PV- and neuropeptide Y (NPY)- containing INs, with different morphological idiosyncrasy from those born in MGE in the SST and PV groups (Figure 8) (Lim *et al*., 2018).

The mechanisms underlying the generation of IN diversity seem to be similar to those responsible for PN diversity in the cortex. Both pallial and subpallial progenitor cells' potentiality are determined by the area from which they derive, that provides them in turn with a specific molecular identity (spatial patterning). The final lineage

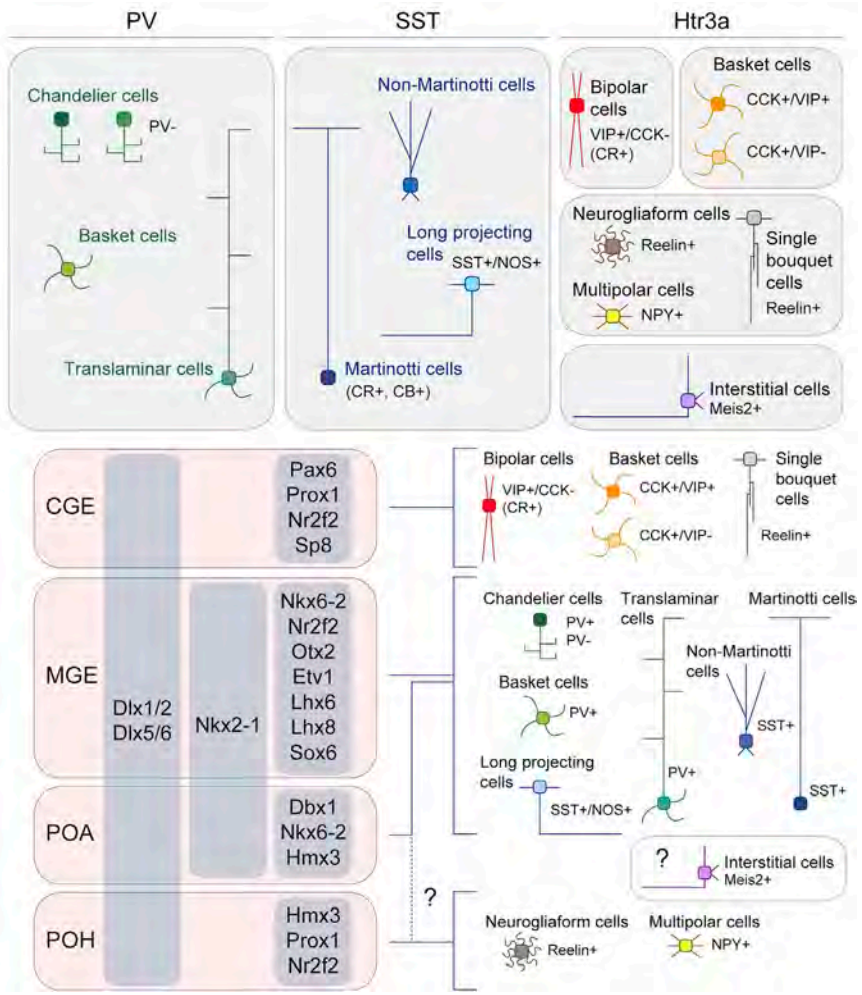


**Figure 8. Diversity of GABAergic neurons in the neocortex. Upper panel depicts major IN clases according to their expression profile.** Three extensive groups [PV-, SST- and serotonin receptor 3A (Htr3a)-containing INs] may be distinguished and subsequently subdivided attending to morphology, laminar identity, electrophysiological properties and the expression of markers other than the abovementioned. Lower panel links specific IN types with their prospective area, as well as with the TF signature that characterizes their progenitor cells. CB, calbindin; NOS, nitric oxide synthase; POH, preoptic region. Adapted from Lim *et al*., 2018.

a given neuron arising from a progenitor belongs to (and so, the cortical layer it will migrate to) is then also determined by the specific moment at which its progenitor cell undergoes the neurogenic division that originates that neuron (temporal patterning), as different moments of the developmental time line also determine slightly different programs and potentialities in a given progenitor cell. Spatial and temporal patterning operating together greatly amplify the number of different populations that arise from a progenitor pool, which otherwise may seem insufficient to explain cortical diversity (Greig *et al*., 2013; Marín and Müller, 2014; Lim *et al*., 2018).

## 3. Neuronal migration: a pilgrimage for diversity

PNs and INs populating the cortex arise from distant progenitor pools; therefore, they undergo distinct migration processes (Figure 9) to reach their destiny: the specific cortical layer to which they are bound for according to their birthdate. Neuronal migration is a very complex process, during which cells need to integrate a plethora of auto- and paracrine signals that work as permissive/repulsive or directional cues. Those signals trigger downstream cascades that foster dynamic cytoskeletal reorganizations in a way that facilitates nucleokinesis and translocation of the soma using the extracellular matrix, the somata of other neurons, and the processes emitted by RGCs, as a scaffold (Rakic, 1972; Nguyen and Hippenmeyer, 2014).

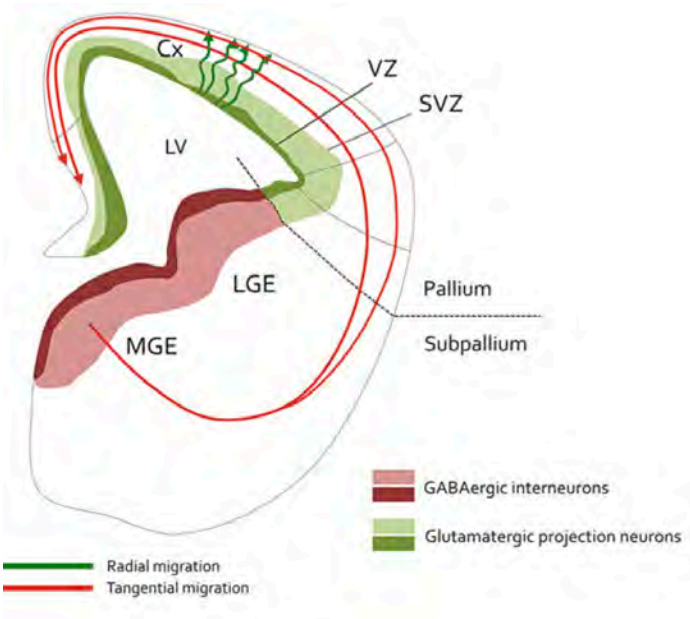


**Figure 9. Neurons arising from distant proliferative areas undergo different types of migration to reach the neocortex.** In order to arrive to their final destination, PNs arising from pallial germinal niches (VZ and SVZ, green regions) migrate radially (green arrows) towards their specific cortical layer, whereas INs born in the subpallial progenitor pools (as the MGE, red regions) undergo a longer tangential migration (red arrows) following migratory streams to reach the cortex, followed by a subsequent radial migration step to correctly allocate themselves within neocortical layers when they arrive to the specific area they are bound to. Adapted from Nguyen and Hippenmeyer, 2014.

Although intermediate filaments are also important to maintain cell morphology and to determine migration mode, microtubules, and especially actin filaments, are the leading players in neuronal migration. While microtubules are key regulators of the elongation of the leading process and nucleokinesis, actin filaments work as the crucial driving force for cell migration, given their strong capacity to physically translocate the soma while they rearrange (Heng *et al*., 2010; Govek, Hatten and Van Aelst, 2011).

### 3.1. Pyramidal neurons and radial migration

As PNs are born in the pallial VZ or SVZ, their migration is shorter than that of INs and relies almost exclusively in radial migration steps. Thus, a PN travels from its birthplace, near the ventricle, to the neocortical layer in which it may establish in accordance with its birthdate. Thus, early-born neurons will form the deep layers of the cortex, whereas late-born neurons will populate the upper ones.

As the regions a PN has to travel through display a strong heterogeneity, both defined by the position in the dorsoventral axis and the specific moment of development, the migration mode used within each compartment also varies (Figure 10). Thus, in early stages of development (between E10 and E14 in the murine brain), when the cortical wall is still relatively thin, neurons and sometimes RGCs may undergo direct somal translocation (Miyata *et al*., 2001; Nadarajah *et al*., 2001). During somal translocation, the cell exhibits a long radial process that reaches the pial surface and a shorter trailing process that detaches from the ventricular wall. The basal process constantly shrinks, thus provoking a fast nucleokinesis in the same direction (Noctor *et al*., 2004; Taverna *et al*., 2014).

In contrast, when cortical thickness expands (from E14 onwards), newborn cells rely on the scaffold composed by their mother RGC and its process to properly migrate. During this event, known as RGC-aided locomotion, migrating neurons possess leading process and a short trailing process, none of them attached to the pial or ventricular surfaces. Both processes seem to embrace the radial fibre of the RGC during migration (Nguyen and Hippenmeyer, 2014).

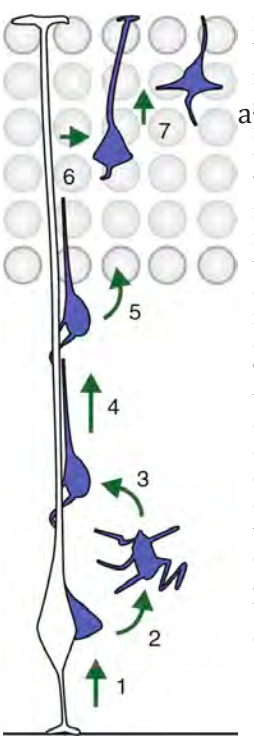


**Figure 10. Sequence followed by cortical projection neurons during their radial migration.** Newborn PNs detach, if yet attached, from the ventricular surface and travel through VZ/SVZ (1). After undergoing multi-to-bipolar shift (2), neurons, engage RGC-aided migration (3) using the basal process of their mother cell as a scaffold, until they reach the SP and enter their target CP area (4). Then, neurons further migrate towards their corresponding cortical layer (5), where they detach from the RGC (6), and execute terminal somal translocation (7). During this sequential steps, PNs follow different cues present both in the millieu and in the surface of neighbouring cells (not represented). Adapted from Nguyen and Hippenmeyer, 2014.

Lastly, a different mode of migration is transiently observed in neurons in the SVZ and IZ, while they detach from radial fibres and pause their migration. At this moment, they acquire multipolar morphology, more appropriate to sense cues from several directions. After a

short time, they undergo a short tangential migration, reaching the radial process of a RGC other than their mother cell (Tabata and Nakajima, 2003).

Putting everything together, newborn PNs must first detach from the apical surface and migrate towards the SVZ/IZ, where they acquire a transient multipolar morphology, which helps them to sense the extracellular milieu in search for promigratory cues. Later, they re-engage RGC-aided locomotion and invade the CP (Tabata and Nakajima, 2003; Noctor *et al*., 2004; Nguyen and Hippenmeyer, 2014). It is important to note that, in this last step, as they recover the bipolar morphology needed to migrate towards CP, they also establish neuronal (*i.e*., axon-dendrite) polarity, as it derives from the leading-trailing process polarization (Barnes and Polleux, 2009).

### 3.2. Interneurons and tangential migration

As opposed to PN, cortical INs are born in the subpallium. They need to reach the cortex, migrating through the developing telencephalon, and then acquire their laminar identity, establishing in the proper neocortical layer. IN migration is also a heterogeneous process that can be subdivided in three major phases: tangential migration to the pallium, intracortical dispersion and laminar allocation, covering consecutive steps of the whole journey (Marín, 2013; Lim *et al*., 2018).

INs migrating to the pallium need to find their route from their birthplaces (namely CGE, MGE and POA) to the pallium-subpallium boundary. Although their TF signature is different, and so is the subset of guidance factors they respond to, INs arising from these distinct regions exhibit an undistinguishable morphology while migrating (Marín *et al*., 2006), being the major feature the formation of a leading process that is permanently branching while migration cycle goes on (Yanagida *et al*., 2012). This process senses the extracellular milieu in search for chemorepulsive or chemoattractant cues that help the cell to find its route to the cortex. INs from different origins seem to follow differential paths to reach the cortex, supporting the idea that each progenitor pool generates INs that use their own unique subset of extracellular signals. As an example, Slit1 and Sema3A work as repulsive signals for MGE-derived INs, while Nrg1 constitutes an attractant for them. Little is known about the specific cues that CGE- and POA-derived INs need to complete a proper migration, although some neurotransmitters have been proposed (Riccio *et al*., 2012; Zimmer-Bensch, 2018). Interestingly, cannabinoid receptor type 1 ($CB_1R$) has been proposed to regulate CCK-IN migration (Berghuis *et al*., 2005).

Once they reach the pallial-subpallial boundary, cortical INs enter a new phase of their migration: the so-called intracortical dispersion (Figure 11), in which the subpallium becomes repulsive to them, and they organize into migratory streams. The two main migratory streams course through the MZ and SVZ, respectively, although a small fraction of INs migrate through the SP. A common trait of intracortical dispersion seems to be that INs actively avoid entering the CP (Marín and Rubenstein, 2001; Wichterle *et al.*, 2001). Whether a given IN selects a migratory stream over another responds to the specific complement of guidance receptors it possess, and, as their origin (MGE *versus* CGE *versus* POA) does not seem to influence this decision, it has been proposed, though not demonstrated, that specific IN subtypes use specific migratory streams to travel (Miyoshi and Fishell, 2011).

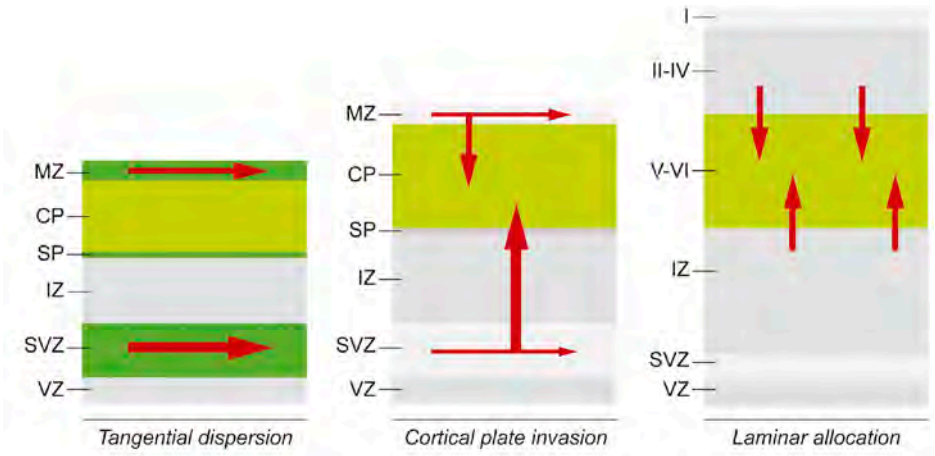


**Figure 11. Interneurons colonising the cortex follow three consecutive phases of migration.** When migrating INs reach the pallium, they join one of the stereotyped migratory streams in order to travel towards their target region (tangential dispersion, left). Subsequently, they switch their migration type and engage radial migration in order to invade the CP (center). Finally, INs translocate to their final destination (right) following chemoattractive cues expressed by PNs. Adapted from Marín, 2013.

The last step of cortical IN migration is their laminar allocation. This last process requires that INs switch from a tangential migration mode to a radial one, a shift which is believed to be triggered by the loss of responsiveness to the attractant Cxcl12 (Li *et al.*, 2008). This radial migration step allows INs to enter the CP, where they will finally migrate into the cortical layer that constitutes their final destination. Even though some classes of IN appear equally distributed across many layers, the majority of them have a more restricted pattern within cortical layers, a trend that is strongly echoed in the hippocampus (Klausberger and Somogyi, 2008; Ciceri *et al.*, 2013).

### 3.3. Neuronal migration defects and malformations of cortical development

Neuronal migration is a tightly regulated succession of processes that ends with PNs and INs residing in their definitive neocortical layer. Belonging to a specific layer determines not only the physical proximity to a specific subset of neurons, but also establishes the microenvironment surrounding a neuron, its ability to create specific interactions (its efferences), and the origin of the connections it receives (its afferences), thus conditioning the microcircuits that it can, and will, assemble. But, what happens if something fails?

Disruption of neuronal migration causes cortical malformations, whose severity and features depend on the specific process that becomes disrupted and on the specific brain region in which it occurs. There is a wide spectrum of potential functional consequences: from mental retardation and intellectual disabilities, to autism or epilepsy (Guerrini and Parrini, 2010; Barkovich *et al*., 2012). Clinically, this broad selection of alterations and pathologies is gathered under the extensive term "malformations of cortical development" (MCDs; Box 2). The general classification scheme of MCDs includes three major types of malformations, attending to the developmental step at which a healthy development becomes first disrupted: malformations of cell proliferation, of neuronal migration, and of postmigrational cortical organisation and connectivity (Guerrini and Dobyns, 2014). These entities comprise a bulk of pathologies that are also highly heterogeneous and in constant change, as knowledge about their causes and features advances. Remarkable examples of these conditions are lissencephaly, polymicrogyria, periventricular heterotopia, hemimegalencephaly and focal cortical dysplasia (FCD). Only the latter will be extensively introduced here.

FCD is also a heterogeneous group of disorders that are characterized by relatively localized histological alterations in any cortical region, and can appear with a hugely varying size range. The common trait that identifies an FCD is that it courses with epilepsy. FCDs that differ in size, location or shape cause diverse degrees of epilepsy. Debut age and seizure semiology vary among patients, although it is very common that first seizures appear in early childhood. Children affected by FCD may also show behavioural disturbances, and their seizures tend to be antiepileptic drug-resistant. A set of electroencephalographic recordings is frequently used in order to diagnose FCD, which is characterized by focal and rhythmic epileptiform discharges that correlate spatially with the lesion (Gambardella *et al*., 1996).

**BOX 2. Malformations of cortical development**

A wide range of conditions affecting the cortex fall under this denomination. What they have in common, though, is that they originate from the disruption of different steps in the ontogeny of the neocortex. Their severity and functional outcome vary, depending on the area they occupy, their size, and their intrinsic nature, but the most common consequences are some extent of neurological disability and epilepsy with an early onset. Although multiple criteria have been proposed to classify MCDs, their heterogeneity and the fact that in some occasions a single lesion displays features typical of different clinical categories make them hard to apprehend. A short description of the most common and well-established MCDs other than focal cortical dysplasia, reviewed in the main text, is included here.

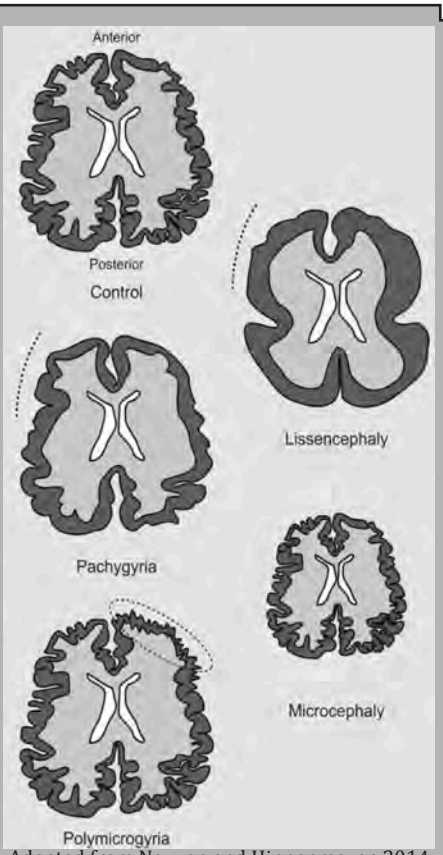

Adapted from Nguyen and Hippenmeyer, 2014.

»**Megalencephaly:** this term refers to an abnormally large brain, exceeding the mean for age and gender by 3 standard deviations (SD). The origin of this abnormal size is believed to be an excessive neural progenitor proliferation and/or a reduced rate of apoptosis. It is relatively common that megalencephaly appears combined with MCDs such as polymicrogyria, as explained below.

»**Microcephaly:** opposite to megalencephaly, this condition includes brains smaller than the mean by 3 SDs. Its causes are also believed to be related with defects in progenitor proliferation and/or cell survival. It also courses commonly with polymicrogyria.

»**Polymicrogyria:** in this case, the major feature is that cortical surface appears irregular or pebbled. It size varies ranging from a small cortical area to both hemispheres, and it usually shows microscopically overfolded cortices (thus, excessive gyration at the microscopic scale, although macroscopically, the altered structure may be confounded with pachygyria). It is also common that the affected area possess an altered or absent lamination.

»**Lissencephaly:** at some extent, it can be considered the opposite to polymicrogyria, as it comprises cases in which the cortical folding and sulcation are reduced (pachygyria) or absent (agyria). Sometimes, both phenotypes are present in distinct areas of the same patient. In a subset of lissencephalies, known as cobblestone, neurons overflow from the meninges, creating a "bumpy" appearance.

»**Subcortical band heterotopia:** although the gyral pattern is often altered in subcortical band heterotopias, its main feature is a smooth band of grey matter in the superficial and middle portions of the subcortical white matter, composed of dense nodes of heterotopic neurons. In most cases, the neocortical portion just atop the heterotopia appears normal in lamination.

»**Periventricular nodular heterotopia:** in this case, patients show nodular masses of grey matter that line the ventricular walls and protrude into its lumen. The number of nodules varies amply among patients. Individual nodules may possess a rudimentary lamination.

Attending to the nature of each specific alteration, three subtypes of FCD may be distinguished (Blümcke *et al*., 2011; Najm *et al*., 2018). FCD Type I consists on malformations that affect cortical layering, whether in a radial (FCD Type Ia) or a tangential (FCD Type Ib) fashion. In some cases, both kinds of malformations appear at the same time (FCD Type Ic). FCD Type I usually shows a less sharply demarcated white matter border, due to the presence of ectopic neurons. Although

the underlying causes are still unclear, disruption of neuronal migration appears as one of the most plausible. FCD Type II, on the other hand, comprises alterations that display not only cortical layering defects, but also specific cytological abnormalities that define its both subtypes: FCD Types IIa and IIb. The hallmark of FCD Type IIa is the presence of dysmorphic neurons (DNs), with an enlarged cell body and nucleus, malorientation and accumulation of neurofilament proteins 2F11 and SMI-32 in their cytoplasm. On the other hand, FCD Type IIb shows the presence not only of DN identical to those found in FCD Type IIa, but also of balloon cells (BCs). BCs are cells with a large rounded cell body that possess a glassy eosinophilic cytoplasm. They tend to accumulate vimentin and nestin filaments and may show a concomitant expression of neuronal and glial markers, as neurofilaments and GFAP. Although contribution of DNs and BCs to epileptiform activity is not well established, it has been demonstrated that DNs may possess hyperexcitable intrinsic membrane properties (Cepeda *et al*., 2006; André *et al*., 2007). A third type of FCD, FCD Type III, is characterized by cortical lamination abnormalities which are associated with a primary lesion that defines its subtype. Thus, FCD Type IIIa is associated with hippocampal sclerosis, FCD Type IIIb with tumours, FCD Type IIIc with vascular malformations, and FCD Type IIId with any other lesion acquired during early life.

Even though a genetic origin has been proposed for FCD, and a growing body of evidence points to mutations on genes involved in the mammalian target of rapamycin (mTOR) pathway as one of the major candidates to FCD etiopathology (Crino, 2015; Lim *et al*., 2015; Majolo *et al*., 2018), there is no general consensus yet, and it is very likely that a heterogeneous spectrum of abnormalities, as those found in FCD cases, is caused by different mutations in each case. mTOR-related mutations have been mainly associated with FCD Type II, which possess some resemblances to tuberous sclerosis complex (TSC), a genetic disorder caused by mutations affecting TSC1 and TSC2 proteins that lead to an overactivation of mTOR signalling. Important to note, mTOR-related mutations have been also identified in hemimegalencephaly cases. This finding has taken some authors to theorize that hemimegalencephaly and FCD are, in fact, a continuum of the same pathology, in which the extent of the dysplastic lesion is determined by the specific moment and area in which mutations appear (D'Gama *et al*., 2017), with an earlier onset resulting in a larger and more severe dysplastic areas, as those observed in hemimegalencephaly cases.

## 4. The endocannabinoid system and brain development

Being a highly intricate process, it comes as no surprise that hundreds of signalling pathways are implicated (and imbricated) in brain development. From early morphogens as Shh or Wnt to late pathfinding signals as netrins and semaphorins, a profusion of different molecules participates in the control of the central nervous system (CNS) ontogeny. One of the signalling systems that orchestrates its appropriate completion is the endocannabinoid system (ECS), composed by endocannabinoid (eCBs) ligands, cannabinoid receptors (CBRs) and eCB-metabolising enzymes that are, as a whole, amply expressed throughout the body, although with varying relevance depending on the specific tissue. In particular, $CB_1R$, a protein that humans have been engaging with plant-derived compounds due to its psychoactive potential since ancient times (Box 3),

**BOX 3. *Cannabis sativa***

The vascular plant *Cannabis sativa* L., also known as cannabis, marijuana, or hemp, among others, has been cultivated since times as ancient as the Neolithic. By 5000 years ago, in the ancient China, it was recognized as an herbal medicine for multiple afflictions. Later, by 2000 BC, it was used by Assyrians with similar applications, and its acknowledgment gradually shifted its influence area towards the Middle East and India, until circa 1800 AC, when French soldiers returning from Egypt introduced it definitely in Europe. By that time, its uses where not only medicinal, but also textile (as hemp fibres were the main component of ropes and sails) and recreational, its most-widely application nowadays. *C. sativa* and its subspecies are to date the only ones among the whole plant kingdom that produce cannabinoids (phytocannabinoids attending to their origin). Although a single plant may produce more than a hundred different phytocannabinoid compounds, the most relevant ones, both in abundance and in pharmacological action, are Δ9-tetrahydrocannabinol (THC) and cannabidiol (CBD). Although THC was structurally characterized by Raphael Mechoulam and his group in the 1960s, it was not until 30 years later that its molecular targets (the cannabinoid receptors) in the mammalian brain were discovered. Thus, the receptor stimulated by THC, responsible for its psychoactive effects, was named after the plant that produces THC: type-1 cannabinoid receptor, and when the full signalling system was discovered, it maintained the name, thus becoming the endogenous cannabinoid system, or endocannabinoid system.

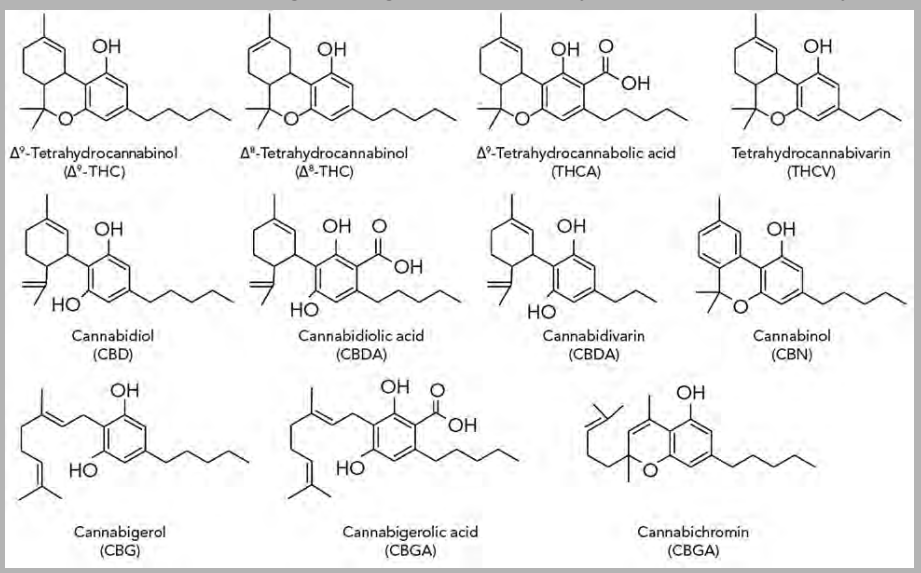

captures most of the attention when it comes to CNS, as the other known CBR ($CB_2R$) is less represented in brain tissue. See Box 4 for a description of the ECS and its components other than $CB_1R$.

**BOX 4. The endocannabinoid system**

The ECS is a biological system which participates in the control of diverse functions throughout the body. It acts as an attenuator of neurotransmitter release in virtually every single synapse in the brain, thus regulating a wide range of brain processes, but it is also involved in immune modulation and the control of energy balance, among others. Its name comes from the fact that its receptors were first identified as the endogenous targets of the phytocannabinoid THC in the brain, not being until a few years later that the endogenous ligands were isolated. As a cell signalling system, the ECS is composed by an assortment of receptors (CBRs), ligands (eCBs), and the enzymes responsible of their synthesis, degradation and bioconversion.

»**Cannabinoid receptors:** the two main cannabinoid receptors are known as type-1 and type-2 cannabinoid receptors, or $CB_1$ and $CB_2$ receptors ($CB_1R$ and $CB_2R$, respectively). Both are classical GPCRs with seven transmembrane helixes, and signal through their coupling to different G proteins, although non-canonical signalling through their interaction with other intracellular proteins and membrane receptors has been described. Although $CB_1R$ and $CB_2R$ have typically been considered brain- and immune system-bound, respectively, it is now accepted that they are expressed in multiple tissues. They share not only 42 % of their amino acid sequence, but also the collection of ligands by which they are engaged. Nevertheless, even if they share their ability to bind both phytocannabinoids and eCBs, binding affinity and specificity is different for each receptor. This, together with their distinct tendency to select intracellular interacting partners, give each CBR a unique signalling signature. In addition to $CB_1R$ and $CB_2R$, other receptors as TRPV1, GPR18, GPR55 and GPR119 are known to bind eCBs, but are no formally considered as cannabinoid receptors because they do not fulfil all the "official" IUPHAR requirements.

»**Endocannabinoids:** they are a diverse group of lipid molecules derived from arachidonic acid that share the ability to engage CBRs. The two main eCBs, by abundance and relevance, are N-arachidonoylethanolamine (anandamide, AEA) and 2-arachidonoylglicerol (2-AG). Even though both are capable of binding to $CB_1R$ and $CB_2R$, their affinity for the receptors differs, as it does its potency (AEA is, in fact, a partial agonist, while 2-AG is a full one); furthermore, their bioavailability depends on the specific tissue in which they exert their functions. There might be additional, less classical, and still controversial (since they have not been univocally proven to bind CBRs and exert CBR-evoked biological actions) examples of eCBs, such as oleoylethanolamide, virodhamine and N-arachidonoyldopamine.

»**Synthesis enzymes:** as already mentioned, the main eCBs are arachidonic acid derivatives. Their dynamics are different to those of the classical neurotransmitter synthesing enzymes, as eCBs are synthesized "on demand", not stored in vesicles until an action potential determines their release to the synaptic cleft. The enzymes responsible for eCB synthesis are mainly the N-acylphosphatidylethanolamine (NAPE)-specific phospholipase D (NAPE-PLD), which gives rise to AEA after hydrolysing NAPÊs, and diacylglycerol lipase (DAGL; from which two isoforms, α and β, are known), which produces 2-AG from diacylglycerol (DAG). Both enzymes are sensitive to neuronal activity, as they are activated upon intracellular $Ca^{2+}$ increases.

»**Degradation enzymes:** after binding to their receptors and triggering their signalling, eCBs are inactivated by specific intracellular serine hydrolases: fatty acid amide hydrolase (FAAH) degrades AEA, while monoacylglycerol lipase (MGL) breaks down 2-AG. eCBs and their deactivation products are themselves precursors of other lipid mediators, such as prostaglandins, prostamides and other eicosanoids, which increases the complexity of eCB bioconversion and ECS signalling.

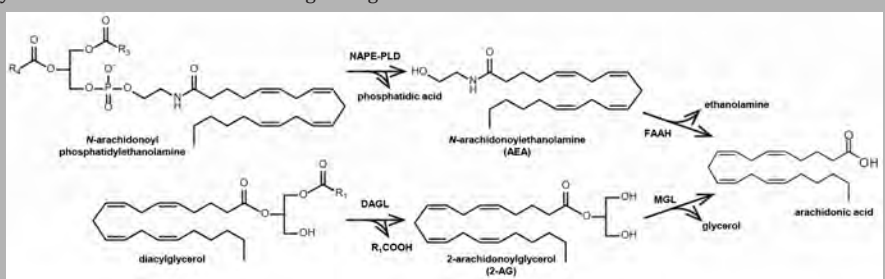


Adapted from Blankmann and Cravatt, 2013.

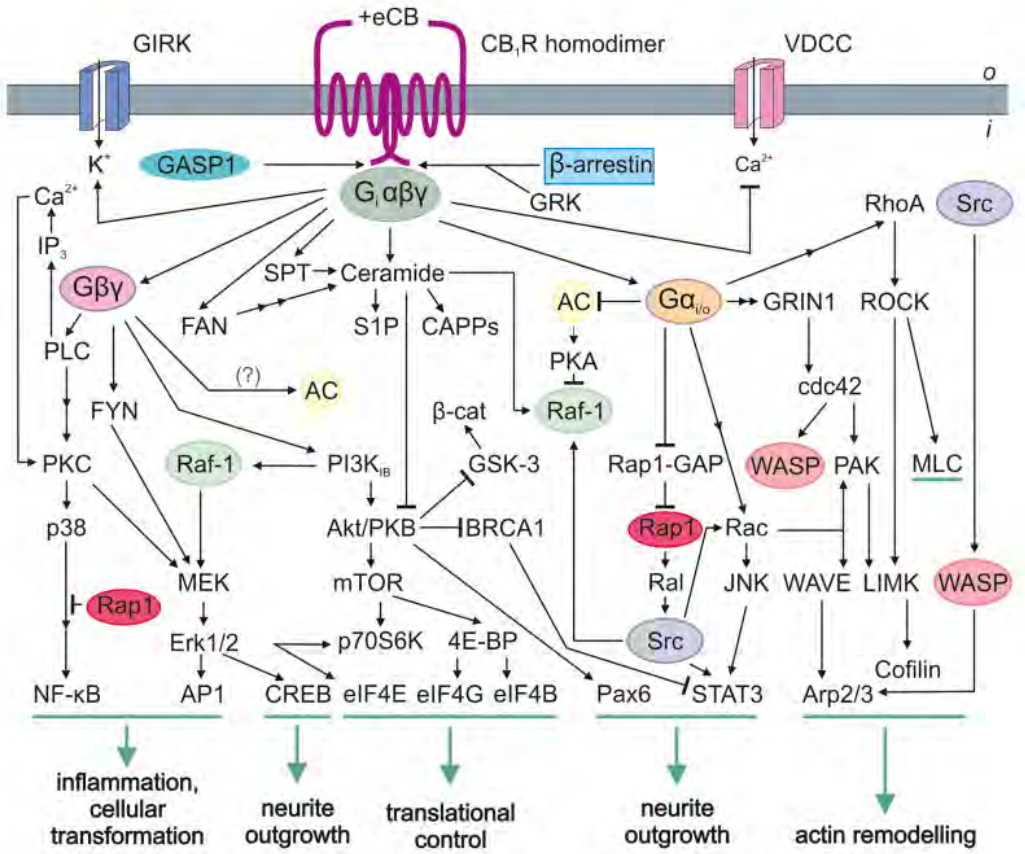


**Figure 12. Intracellular signalling through $CB_1$ receptor.** $CB_1R$ exerts pleiotropic effects upon activation, as it is involved in a wide range of sinalling cascades. The most classical downstream effects of $CB_1R$ activation are the inhibition of PKA through $G\alpha_{i/o}$-dependent inactivation of AC and the activation of MAPKs (MEK, Erk1/2) by means of βγ subunits, althoug its contribution to mTORC1 activation *via* PI3K-Akt recruitment is also well established. Less canonical pathways are also depicted, as its interaction with cofilin through RhoA activation, the inactivation of voltage-dependent calcium channels (VDCCs) or the activation of G protein-copuled inward rectifying potassium channels (GIRKs). From Keimpema *et al*. 2011.

$CB_1R$ is one of the, if not the, most abundant metabotropic G protein-coupled receptors (GPCRs) in the adult mammalian brain (Herkenham *et al*., 1990). As $CB_2R$, it belongs to the Class A GPCR superfamily, which defines it as an integral membrane protein with its N-terminal region oriented to the extracellular space. It also possess seven transmembrane domains, connected by six loops, of which one half is intracellular and the other half is extracellular. Finally, the C-terminal domain is located towards the cytoplasm. Both CBRs share 42 % of their amino acid sequence, a percentage that increases to 70 % when taking into account only the transmembrane regions, which are key for ligand binding, affinity and specificity (Munro *et al*., 1993; Hua *et al*., 2016, 2017; Shao *et al*., 2016). $CB_1R$ usually couples to $G_{i/o}$ heterotrimeric proteins, and thus its activation typically dampens adenylyl ciclase (AC) activity, thus

lowering cAMP levels (Howlett, 1985). Nevertheless, $CB_1R$ signalling also activates extracellular signal-regulated kinase (ERK) by protein kinase A (PKA) inhibition (Davis *et al*., 2003; Howlett *et al*., 2004) or by βγ-dependent activation of phosphatidylinositol 3-kinase (PI3K) (Galve-Roperh *et al*., 2002), as well as interacting with β-arrestins, which are not only involved in GPCR internalization but also trigger G protein-independent signalling (Figure 12) (Jin *et al*., 1999; Laporte and Scott, 2019). Its plausible signalling cascades, though, are even more complex, as CBRs are able to couple to other heterotrimeric G proteins (Lauckner *et al*., 2005; Roland *et al*., 2014), and they have been shown to homo- (with additional CBR molecules) or heteromerize (with other GPCRs or even with tyrosine kinase receptors), increasing the intricacy of their signalling (Moreno *et al*., 2018; Blasco-Benito *et al*., 2019).

### 4.1. $CB_1$ receptor in the adult brain

$CB_1R$ is profusely expressed throughout the mature mammalian CNS (Figure 13). Specifically, it is particularly enriched in the striatum, hippocampus, cerebellum and olfactory bulb, but it can also be easily detected in the cortex, as in other subcortical regions like the amygdala, septum, hypothalamus and some nuclei in the brainstem and dorsal spinal cord (Kano *et al*., 2009). Nonetheless, although $CB_1R$ expression covers virtually every single region in the brain, its pattern highly differs from one cell type to other. GABAergic INs possess the highest $CB_1R$-expression levels among brain cell types, while PNs tend to show a much lower, though remarkably functional, $CB_1R$ load (Marsicano and Lutz, 1999). Thus, although PNs exhibit lower $CB_1R$ levels than INs, it appears that the coupling of the receptor is much more efficient in the former

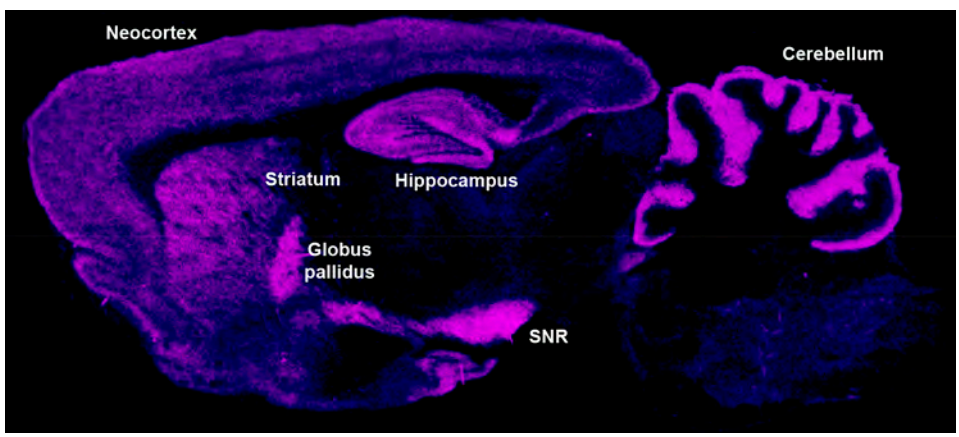


**Figure 13. $CB_1$ receptor ubiquitous expression in the rat brain.** Image showing autoradiography of 10 nM $^3$H-CP55,940, a radioactively marked $CB_1R$ agonist, in a sagital section of an adult rat brain. Purple indicates saturation whereas dark blue indicates low signal. SNR, *substantia nigra pars reticulata*. Adapted from Herkenham *et al*., 1991.

than in the latter (Steindel *et al*., 2013). At even lower levels, $CB_1R$ has been found in astrocytes, where it might play a key role in astrocyte-dependent neuronal plasticity (Martín *et al*., 2015); oligodendrocytes (Molina-Holgado *et al*., 2002); microglia (Stella, 2010) and neural progenitors present in the adult brain (Aguado *et al*., 2005, Khatri *et al*., 2018, Zimmerman *et al*., 2018, Aguareles *et al*., 2019). Noteworthy, $CB_1R$ levels in a given cell are not the only feature that predicts its ability to respond to agonists, as the efficiency in its coupling to G proteins is also important, as well as the presence of additional $CB_1R$-interacting proteins, as CRIP1a (Guggenhuber *et al*., 2016; Blume *et al*., 2017).

Regarding the processes in which $CB_1R$ is involved, they can be analysed at both the circuit and the behavioural level. On the one hand, $CB_1R$ is broadly known because of its role in cannabinoid retrograde signalling, the well-established mechanism by which eCBs produced by a postsynaptic neuron bind to presynaptic $CB_1R$, initiating an intracellular cascade that results in a decrease in intracellular free $Ca^{2+}$ concentration, turning down neurotransmitter release by the presynaptic neuron. In this way, $CB_1R$ controls synaptic plasticity, thereby participating in short- and long-term depression (STD and LTD, respectively) processes (Katona and Freund, 2008; Ohno-Shosaku *et al*., 2012). During STD, as abovementioned, the increment in postsynaptic $Ca^{2+}$ triggers the production of DAG by phospholipase C-β. DAG is then used by DAGLα to synthetize 2-AG, which signals backwards and targets presynaptic $CB_1R$, inhibiting

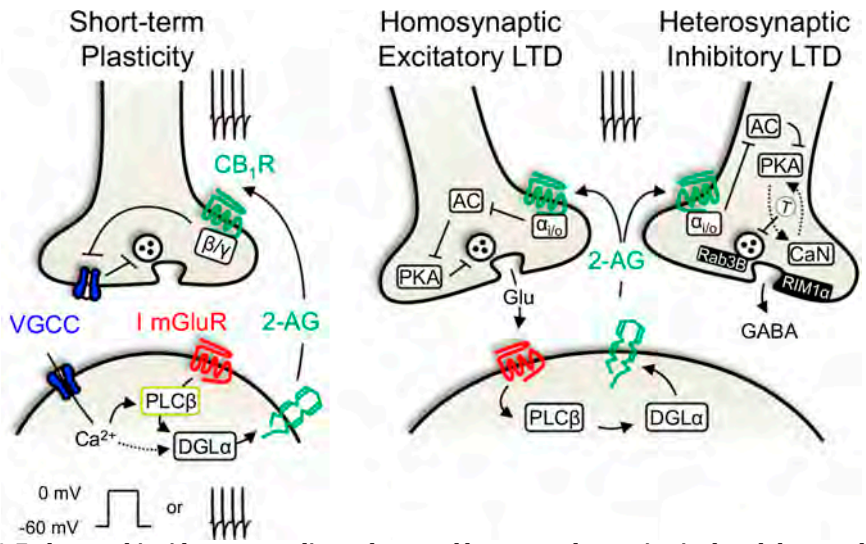


**Figure 14. Endocannabinoid system mediates short- and long-term depression in the adult central nervous system.** $CB_1R$ signalling induces retrograde synaptic plasticity upon activation by 2-AG. STD relies on inactivation of voltage-gated calcium channels (VGGC), while LTD depends on inhibition of AC. Adapted from Castillo *et al*., 2012.

$Ca^{2+}$ entry in a Gi β/γ subunit-dependent manner, thus dampening neurotransmitter release (Castillo *et al*., 2012). In contrast, LTD requires the action of the $G_i$ α subunit, which inhibits AC, rendering PKA inactive, which in turn also prevents neurotransmitter release (Figure 14) (Castillo, 2012).

In a higher organizational level, $CB_1R$ physiological engagement regulates a vast number of complex functions (Figure 15), like memory consolidation (Puighermanal *et al*., 2012) or extinction (Marsicano *et al*., 2002), control of nociception together with $CB_2R$ (Cravatt and Lichtman, 2004), control of stress (Morena *et al*., 2016), energy balance (Quarta *et al*., 2010), feeding behaviour (Bellocchio *et al*., 2010; Soria-Gómez *et al*., 2014), motor learning (Kishimoto and Masanobu, 2006), protection against excitotoxicity (Gutiérrez *et al*., 2003; Monory *et al*., 2006; Chiarlone *et al*., 2014; Bravo-Ferrer *et al*., 2017), to list only a fraction of the whole picture (Mechoulam and Parker, 2013; Piazza *et al*., 2017).

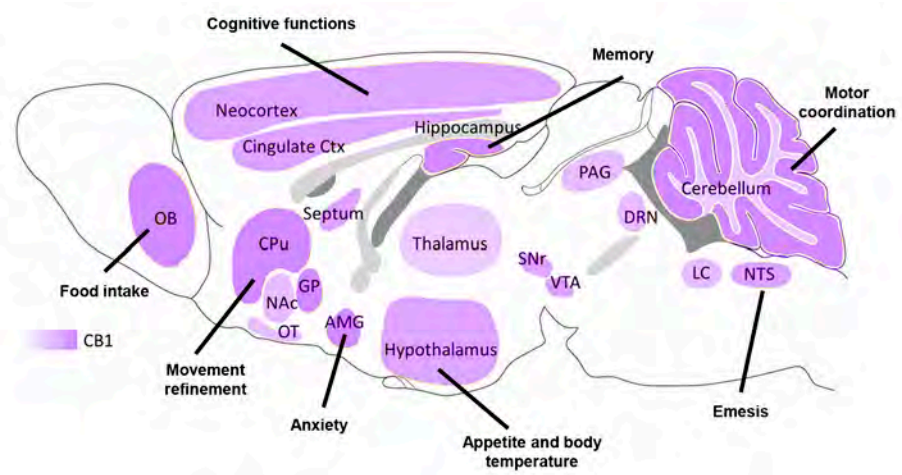


**Figure 15. Main physiological functions regulated by endocannabinoid system.** $CB_1R$ is involved in the regulation of a multitude of behavioural functions, from which the best-established are shown in the schematic. Purple intensity correlates with $CB_1R$ protein expression levels. Adapted from Flores *et al*., 2013.

## 4.2. $CB_1$ receptor during brain development

The presence of ECS elements during brain development, including regional CBRs distribution and eCBs levels, has been well characterized for some time now. Summarizing, ECS function is patent at stages as early as neural plate formation (Psychoyos *et al*., 2008). eCB levels in the developing CNS, especially in the case of 2-AG, are comparable to those in an adult brain (Fernández-Ruiz *et al*., 2000; Keimpema *et al*., 2010), whereas the embryonic $CB_1R$ distribution, although evident in numerous brain areas

(Berrendero *et al*., 1998, 1999; Fernández-Ruiz *et al*., 2000), is clearly different from its expression pattern in the mature CNS. At early stages, $CB_1R$ is atypically detected in the white matter (Romero *et al*., 1997; Fernández-Ruiz *et al*., 2000), which is strikingly devoid of its mRNA. This suggests that the observed $CB_1R$ protein belongs to immature projections of neuronal-lineage committed cells (Harkany *et al*., 2007). Altogether, these findings paved the way to theorize, as it has been extensively demonstrated, that the ECS exerts a complex role during brain development. In fact, evidence has been growing during the last twenty years showing that the early presence of the ECS in the developing brain is not a mere seed of its characteristic expression in the mature CNS, but it is in fact crucial for the appropriate consecution of several developmental processes (Galve-Roperh *et al*., 2006; Harkany *et al*., 2007). Nowadays it is widely recognised that eCBs, by acting through $CB_1R$, have a relevant role in diverse processes ranging from NSC proliferation to neuronal differentiation and migration.

### 4.2.1. $CB_1$ receptor regulation of neural progenitor proliferation

Despite being hard to assess at the time that ECS first came to the neural development scene, CBRs expression have been now extensively documented in NSCs (Figure 16) (Molina-Holgado *et al*., 2007; Palazuelos *et al*., 2012; Compagnucci *et al*., 2013; Maccarrone *et al*., 2014). From early stages, $CB_1R$ activation has been linked with incremented NSC proliferation and neurogenesis, a positive association being found in both embryonic and adult brains (Jin *et al*., 2004; Galve-Roperh *et al*., 2013; Díaz-Alonso *et al*., 2015), upon both pharmacological manipulation and increasing eCB tone

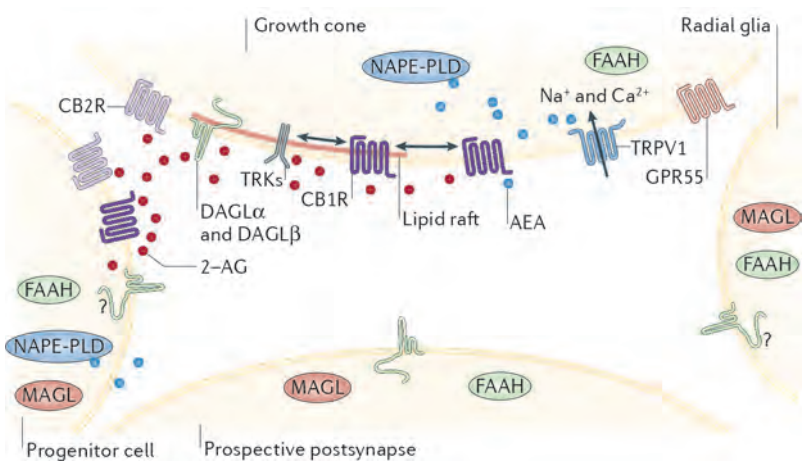


**Figure 16. Endocannabinoid system is present in neural stem cells, as well as in immature synapses.** ECS has been confirmed to play multiple roles during brain development. Thus, it is to be expected that at least some of its components are expressed by neural progenitor cells and developing neurons. The image summarizes the evidence found so far regarding to ECS expression in the immature brain. Adapted from Maccarrone *et al*., 2014.

by FAAH genetic ablation. Consequently, $CB_1R$ knockout mice show impaired neural progenitor proliferation in the embryonic VZ/SVZ (Mulder *et al*., 2008; Díaz-Alonso *et al*., 2015). $CB_1R$ seems to fulfil this role through diverse intracellular cascades (as activation of ERK or PI3K), which gives it the potential to regulate, for instance, the transition from apical progenitor ($Pax6^+$) to basal progenitor ($Tbr2^+$) in the developing cortex by engaging mTORC1 signalling (Díaz-Alonso *et al*., 2015).

### 4.2.2. $CB_1$ receptor regulation of neural differentiation

One step ahead from NSC proliferation, $CB_1R$ is also involved in cell-fate acquisition, not only in the transition from one type of progenitor to another, but also in neuronal (Mulder *et al*., 2008; Díaz-Alonso *et al*., 2012), astroglial (Aguado *et al*., 2006; Soltys *et al*., 2010) and oligodendroglial (Gómez *et al*., 2010) differentiation and maturation. Focusing on its role in neuronal specification, $CB_1R$ promotes long-range PN fate (Mulder *et al*., 2008; Stanslowsky *et al*., 2017), specifically by regulating the balance between the antagonic TFs Ctip2 and Satb2, thus favouring the activation of the former in detriment of the latter, which drives the expansion of CSMN pool. Accordingly, $CB_1R$-deficient mice exhibit an increased number of $Satb2^+$ cells, decreased CSMN numbers, and impaired skilled motor function (Díaz-Alonso *et al*., 2012).

### 4.2.3. $CB_1$ receptor regulation of neuronal migration

After neuroblasts have been specified, they have to reach their final destination by means of neuronal migration, a process that is also regulated by $CB_1R$. Even though the engagement of the receptor has been positively linked with CCK-containing IN migration (Berghuis *et al*., 2005), other studies have shown antithetical effects, confirming a relation between cannabinoid function and neuronal migration (Oudin *et al*., 2011; Tortoriello *et al*., 2014; Vargish *et al*., 2016). In addition, although pharmacological stimulation of $CB_1R$ signalling also impairs tangential migration (Sáez *et al*., 2014), it has not been until recently that a molecular mechanism has been proposed to explain the association between $CB_1R$ activation and migration of pyramidal neurons (Díaz-Alonso *et al*., 2017). This study not only proposes degradation of the monomeric G protein RhoA as a downstream $CB_1R$ effector that mediates its promigratory action, but also demonstrates that transient $CB_1R$ loss of function exerts a deleterious effect in neural development independently of the classical neuromodulatory role of the receptor.

### 4.2.4. $CB_1$ receptor regulation of neuronal maturation

$CB_1R$ signalling also participates in the various steps that a neuron must follow in order to reach a mature and functional stage. For instance, $CB_1R$ activation regulates neurite outgrowth, although different studies have reported opposite effects (Jordan *et al*., 2005; Vitalis *et al*., 2008), thus pointing to a complex and context-dependent effect. In addition, there is an increasing body of studies supporting a $CB_1R$-dependent regulation of axon-related events like growth cone collapse (Argaw *et al*., 2011), specialization of the initial segment (Tapia *et al*., 2017) and axonal pathfinding (Berghuis *et al*., 2007). Disruption of $CB_1R$ function in this context leads to significant fasciculation deficits (Mulder *et al*., 2008; Wu *et al*., 2010; Tortoriello *et al*., 2014), although little is known about neuronal functionality and electrophysiological properties under these circumstances.

## 4.3. Consequences of prenatal exposure to cannabinoids

As the ECS regulates several steps of cortical neuron development, it is easy to hypothesize that prenatal disruption of cannabinoid signalling may lead to deleterious consequences for the developing brain. The fact that marijuana is the most commonly used illegal drug by pregnant women (Figure 17) (Young-Wolff *et al*., 2017), together with the increase of THC content in the smoked cannabis observed in the last two decades (Pijlman *et al*., 2005; Mehmedic *et al*., 2010), make this topic even more relevant. A raising cohort of longitudinal studies in humans (Fried, 1980; Day and Richardson, 1991; Hofman *et al*., 2004) and their subsequent reviews (Goldschmidt *et al*., 2000; Jutras-Aswad *et al*., 2009; Goldschmidt *et al*., 2012) have pointed that prenatal cannabinoid exposure is associated with a full range of paediatric and adolescent alterations, as lower short-term memory, increased aggressive behaviours, higher impulsivity, hyperactivity, problems in visual and abstract reasoning, and increased risk to develop addictions. In addition, research conducted with human samples has found opioid and dopaminergic neurotransmission systems altered (Wang *et al*., 2006; Morris *et al*., 2011), which may have a conceivable causative link with the abovementioned long-term outcomes, and which may emerge from epigenetic disturbances as changes in histone metilation and shifts in the microRNA load (Morris *et al*., 2011).

Furthermore, multiple studies encompassing prenatal administration of different cannabinoid molecules to animal models show numerous long-lasting consequences in neurotransmitter systems and animal behaviour (Pinky *et al*., 2019).

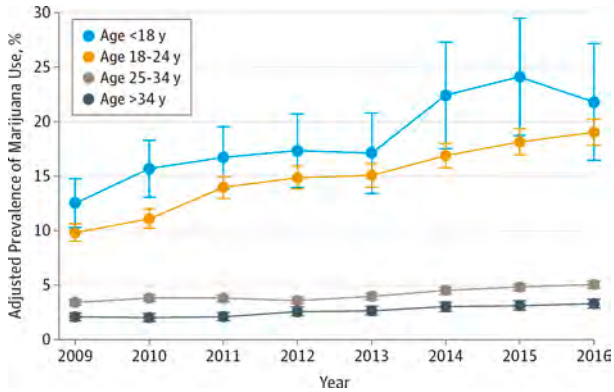


**Figure 17. Increasing trends in marijuana use among pregnant females.** Graphs show Poisson regresion models regarding self-reported and positive toxicology screening of marijuana use by ≈280 thousand pregnant women between 2009 and 2016. From Young-Wolff *et al.*, 2017.

Summarizing, prenatal cannabinoid exposure has been linked with decreased CSMN generation and impaired skilled motor function, as well as increased seizure susceptibility that persist in the adulthood (de Salas-Quiroga *et al.*, 2015); disrupted fasciculation and miswiring of cortical circuits (Tortoriello *et al.*, 2014); altered memory retention and glutamatergic transmission in the hippocampus and prefrontal cortex (PFC) (Mereu *et al.*, 2003; Antonelli *et al.*, 2004); reduced GABA outflow in the hippocampus (Beggiato *et al.*, 2017); persistent disruption of social behaviour and reduced numbers of CCK-containing INs in the hippocampus (Vargish *et al.*, 2016); increased brain tyrosine hydroxylase activity (Bonnin *et al.*, 1995); sex-dimorphic alterations in opioid transmission (Pérez-Rosado *et al.*, 2000, 2002); and a male-specific impairment of social behaviour and synaptic plasticity in the PFC (Bara *et al.*, 2018), to name just some processes. Remarkably, the described alterations show a tendency to gather on cortical and hippocampal regions, and some of them have a marked sexually dimorphic trend (Pinky *et al.*, 2019).

Altogether, this body of evidence supports the importance of fully addressing the short- and long-term consequences of prenatal exposure to cannabinoids, as they may have great impact in the modern society, which is nowadays struggling under intense debate to find a proper regulation for cannabis consumption.

### 4.4. Cannabinoids as therapeutic agents

On the other side of the coin, the implication of the ECS on a profuse collection of physiological processes and its striking pleiotropic capacity give CBRs the potential to be therapeutic targets in a wide range of diseases (Kaur *et al.*, 2016). In humans, the ECS participates not only in central and peripheral nervous system functions, but is

also involved in immune modulation, as well as control of blood pressure, bronchodilation, energy balance, and emesis, among others. But, although the ECS could be out forward as a therapeutic target aiming to alleviate symptoms of diseases affecting the cited body functions, clinical and preclinical evidence points to the ECS as a promising target in many other conditions, such as cancer (Velasco *et al*., 2016; Blasco-Benito *et al*., 2018; López-Valero *et al*., 2018); chronic pain (Romero-Sandoval *et al*., 2017; Sun *et al*., 2017); brain trauma derived from stroke or neurodegenerative diseases (Blázquez *et al*., 2015; Fernández-Ruiz *et al*., 2015); anxiety (Bergamaschi *et al*., 2011; Piper *et al*., 2017); fragile X syndrome (Busquets-García *et al*., 2013; Tartaglia *et al*., 2019); to mention but a few.

Although from a theoretical perspective, both synthetic cannabinoids and phytocannabinoids could be developed and distributed as treatments, the use of the former is usually not favourable in terms of efficacy/safety balance (Ozturk *et al*., 2019; Yeruva *et al*., 2019). Thus, phytocannabinoid extracts, which are easily isolated and accurately standardized from C. sativa cultivars, are becoming the actual investment in the medical cannabis framework. In fact, among the cannabinoid drugs approved in different countries, the vast majority are exclusively composed of phytocannabinoids. THC, under the trademark of dronabinol (and also its synthetic analogue, nabilone) is approved for palliative therapy in cancer patients, for the treatment of nausea driven by chemotherapies, and for the anorexic syndrome secondary to AIDS or cancer (Velasco *et al*., 2012). Nabiximols, a standardized cannabinoid extract containing CBD and THC in a 1:1 ratio, has been approved, under the trademark of Sativex, to alleviate spasticity and overactive bladder derived from multiple sclerosis. Sativex is also utilised for the treatment of neuropathic and cancer-associated pain (Giacoppo *et al*., 2017). More recently, a CBD preparation (Epidiolex) has been approved by the FDA for the treatment of seizures in two paediatric epileptic syndromes (Dravet and Lennox-Gastaut), while its use for other conditions associated to refractory epilepsy, as TSC or febrile-infection related epilepsy syndrome, also looks promising (O'Connell *et al*., 2017).

In a context in which cannabinoid therapeutic potential is starting to prevail over its social stigma, both sides of cannabis should be taken into account to elaborate a rational and well-informed verdict about whether, when and how targeting CBRs to maximize positive effects on each given condition while reducing side effects as much as possible.

## Aims of this Thesis

In the past decades, multiple groups have shown that $CB_1R$ regulates different steps of both cortical PNs and INs development. In particular, our group has demonstrated that both genetic and pharmacological disruption of $CB_1R$ signalling during brain ontogeny impairs the establishment and migration of cortical PNs, concomitantly increasing seizure susceptibility. Nevertheless, a link between ECS malfunction and the onset of epileptic pathologies has been not yet established, as neither has been a mechanistic explanation for the observed seizure-prone phenotype. In addition, the susceptibility of GABAergic INs to the appearance of persistent effects upon early ECS disturbance has not been extensively studied.

In this regard, we defined the following objectives for this Doctoral Thesis:

**Aim 1:** To analyse the link between altered ECS function and FCD, a human pathology associated with childhood epilepsy, as well as to assess if PNs that have got their $CB_1R$ signalling genetically disrupted during development suffer from permanent changes in plasticity and excitability.

**Aim 2:** To assess the involvement of $CB_1R$ in the establishment of GABAergic interneurons, by analysing the long-term impact of prenatal THC exposure in the hippocampal CCK-containing basket cell population, along with any cognitive or behavioural outcome.

# Materials & Methods

### Constructs

For *in utero* electroporation (IUE) experiments, pCAG-Green fluorescent protein (GFP) expression vector was kindly provided by Dr. François Guillemot (The Francis Crick Institute, London, UK). Regarding transfection experiments in P19 cells, pCAG-RHEB and pCAG-RHEB Q64L (a constitutively active Rheb mutant) expression vectors were kindly provided by Dr. Tomohiko Maehama (Kobe University, Kobe, Japan). pCAG-Tbr2 was kindly provided by Prof. Robert F. Hevner (University of California, San Diego, CA, USA).

### Animals

Experimental designs and procedures were approved by the Complutense University Animal Research Committee in accordance with the European Commission regulations. All efforts were made to minimize the number of animals and their suffering throughout the experiments. Nex-$CB_1^{-/-}$ and Dlx5/6-$CB_1^{-/-}$ colony-founding mice were provided by Prof. Beat Lutz (Johannes Gutenberg University, Mainz, Germany). Mice were maintained in standard conditions, keeping littermates grouped in breeding cages, at a constant temperature (20±2 °C) on a 12 hours light/dark cycle with food and water ad libitum. The generation and genotyping of Nex-$CB_1^{-/-}$, Dlx5/6-$CB_1^{-/-}$ and wild-type littermates has been reported elsewhere, and was performed accordingly (Monory *et al*., 2007). Mouse embryonic tissues were obtained upon timed mating as assessed by vaginal plug observation (E0).

### Human samples

The FCD cases included in this thesis were obtained from the archives of the Departments of Neuropathology of the Academic Medical Center (University of Amsterdam, The Netherlands), the University Medical Center in Utrecht (The Netherlands), Hospital Infantil Niño Jesús (Madrid, Spain) and Hospital Sant Joan de Déu (Barcelona, Spain). A total of 30 surgical specimens (10 FCD Type I and 20 FCD Type II), resected from patients undergoing surgery for intractable epilepsy, were examined (Table 1). Tissue was obtained and used in accordance with the Declaration of Helsinki and informed consent was obtained for the use of brain tissue and for access to medical records for research purposes. All cases were reviewed by the corresponding neuropathologist and the diagnosis was confirmed according to ILAE classification system (Blümcke *et al*., 2011; Najm *et al*., 2018). Control brains from patients that were not diagnosed with neurologic disorders were also employed [n = 6; age (years) = 53; 40; 34; 21; 51; 25].

Formalin-fixed, paraffin-embedded tissue (one representative paraffin block per case containing the complete lesion or the largest part of the lesion resected at surgery) was sectioned at 6 µm and mounted on pre-coated glass slides (Star Frost, Waldemar Knittel GmbH, Braunschweig, Germany). Sections of all specimens were processed for haematoxylin-eosin, luxol-fast blue and Nissl stainings and neuronal and glial markers for classification and selection.

**Table 1. Clinical features of patients analysed in this Thesis.**

| Patient | Age at surgery (years) | Duration of epilepsy (years) | Diagnosis | Location | Engel's class |
|---|---|---|---|---|---|
| 01 | 14.0 | 8.0 | FCD Ia | Parietal | II |
| 02 | 19.0 | 10.0 | FCD Ia | Frontal | I |
| 03 | 23.0 | 16.0 | FCD Ia | Temporal | I |
| 04 | 16.0 | 11.0 | FCD Ia | Frontal | I |
| 05 | 24.0 | 17.0 | FCD Ia | Temporal | I |
| 06 | 16.0 | 12.0 | FCD Ia | Frontal | II |
| 07 | 4.5 | 4.0 | FCD Ia | Temporal | I |
| 08 | 3.0 | 3.0 | FCD Ia | Frontal | I |
| 09 | 2.0 | 1.5 | FCD Ia | Multilobar | IV |
| 10 | 3.0 | 2.0 | FCD Ia | Frontal | I |
| 11 | 29.0 | 21.0 | FCD IIb | Temporal | I |
| 12 | 23.0 | 18.0 | FCD IIb | Temporal | I |
| 13 | 21.0 | 19.0 | FCD IIb | Frontal | I |
| 14 | 17.0 | 9.0 | FCD IIb | Temporal | I |
| 15 | 13.0 | 10.0 | FCD IIb | Frontal | I |
| 16 | 5.0 | 5.0 | FCD IIb | Multilobar | II |
| 17 | 8.0 | 5.0 | FCD IIb | Multilobar | III |
| 18 | 8.0 | 7.5 | FCD IIb | Frontal | II |
| 19 | 0.5 | 0.5 | FCD IIb | Multilobar | III |
| 20 | 19.0 | 17.0 | FCD IIb | Multilobar | II |
| 21 | 1.0 | 0.5 | FCD IIb | Multilobar | II |
| 22 | 21.0 | 21.0 | FCD IIb | Multilobar | III |
| 23 | 3.5 | 2.5 | FCD IIb | Temporal | I |
| 24 | 15.0 | 15.0 | FCD IIb | Parietal | II |
| 25 | 12.0 | 6.0 | FCD IIb | Occipital | I |
| 26 | 6.0 | 5.0 | FCD IIb | Frontal | I |
| 27 | 0.5 | 0.5 | FCD IIa | Occipital | II |
| 28 | 6.0 | 5.0 | FCD IIa | Temporal | I |
| 29 | 7.0 | 5.0 | FCD IIa | Multilobar | I |
| 30 | 3.0 | 3.0 | FCD IIb | Frontal | I |

**Focal cortical dysplasia organotypic cultures**

Resected brain tissue was transported from the operating theatre to the laboratory in a solution containing 310 mM sucrose, 25 mM $NaHCO_3$, 3 mM KCl, 1 mM $CaCl_2$, 10 mM $MgCl_2$ and 10 mM D-glucose, equilibrated with carbogen, maintained at 2-10 °C. Capillaries and damaged tissue were dissected away from the tissue block in the cold sucrose-based solution in sterile conditions while equilibrating with carbogen. Slices were cut at thickness 300 μm in a vibratome (VT1200S; Leica, Wetzlar, Germany). Slices were then placed on an semiporous insert in sterile conditions (insert diameter = 30 mm, pore diameter = 0.4 μm; Merck Millipore, Burlington, MA, USA) at the interface between air and a medium containing 20 mM HEPES and the antibiotics penicillin and streptomycin (50 U/mL). They were maintained in an incubator, at 37 °C in 95 % $O_2$/5 % $CO_2$. After 1 hour, slices on inserts were transferred to a six-well plate, pre-equilibrated in the incubator and containing the same solution except that HEPES was omitted. The medium was changed on a daily basis during 7 days. Slices were then subjected to pharmacological regulation and, after incubation, they were fixed and sectioned for immunofluorescence characterization. Alternatively, proteins were extracted after cell lysis in a buffer containing 50 mM Tris, 0.1 % Triton X-100, 1 mM ethylenediaminetetraacetic acid, 1 mM ethylene glycol tetraacetic acid (EGTA), 50 mM NaF, 10 mM sodium β-glicerophosphate, 5 mM sodium pyrophosphate and 1 mM sodium orthovanadate (pH 7.5) supplemented with a protease inhibitor cocktail (Roche, Basel, Switzerland), 0.1 mM phenylmethane-sulphonylfluoride, 0.1 % β-mercaptoethanol and 1 μM microcystin for Western blot analyses.

**Immunofluorescence and confocal microscopy**

P19 murine carcinoma cells, coronal embryonic and postnatal murine brain slices (14 and 30 μm-thick, respectively), organotypic human brain slices (20 μm-thick) and FCD samples were fixed in paraformaldehyde solution [4 % in phosphate buffered saline (PBS)] at 4 °C and immunofluorescence performed.

After a 2 hours blockade with 5 % goat serum, overnight incubation at 4 °C with the indicated primary antibodies was performed (Table 2). Samples were subsequently incubated for 2 hours at room temperature with the appropriate highly cross-adsorbed anti-mouse, rat, guinea pig, and rabbit AlexaFluor 488, AlexaFluor 546, Alexa Fluor 594, and AlexaFluor 647 secondary antibodies (1:500 in every case; Invitrogen, Carlsbad, CA, USA). Confocal fluorescence images were acquired by using either Leica

TCS-SP2 or LAS-X software with a SP2 or a SP8 microscope respectively, with 3 passes by Kalman filter and a 1024x1024 or a 2048x2048 collection box respectively. Immunofluorescence data were obtained in a blinded manner and sample code remained unsealed during the whole data processing and analysis.

**Table 2. Primary antibodies used in this Thesis.**

| Target | Host species | Application | Concentration | Company |
|---|---|---|---|---|
| β-actin | Rabbit | WB | 1:5000 | Cell Signaling Technology (Barcelona, Spain) |
| $CB_1R$ | Rabbit | IF, WB | 1:500 | Frontier Institute (Hokkaido, Japan) |
| $CB_1R$ | Guinea Pig | IF | 1:500 | Frontier Institute |
| c-Myc | Mouse | IF | 1:500 | Sigma-Aldrich España (Madrid, Spain) |
| GABA | Mouse | IHC | 1:100 | Sigma-Aldrich España |
| NeuN | Mouse | IHC | 1:500 | Merck Millipore |
| pS6 S235/S236 | Rabbit | IF, WB | 1:100, 1:1000 | Cell Signaling Technology |
| pS6 S240/S244 | Rabbit | IF, WB | 1:800, 1:1000 | Cell Signaling Technology |

Immunoreactivity was measured using Fiji open source software establishing a threshold to measure only specific signal. The resulting binary mask was then used along the built-in measure function to acquire the total integrated grey density among all the pixels inside the binary mask overlaid on top of the original image. The obtained value was then referred to the number of $DAPI^+$ cell nuclei present in the optic field.

In $CB_1R$ knockdown experiments by IUE, cell migration was measured by determining the position of $GFP^+$ cells along the cortical wall, assigning each cell to their corresponding cortical compartment attending to histological criteria defined by DAPI staining.

### Western blot assays

Protein extracts were prepared as abovementioned. Equal amount of protein samples were electrophoretically separated and transferred to polyvinylidene difluoride membranes. After blocking with 5 % BSA, membranes were incubated overnight at 4 °C with the indicated primary antibodies (Table 2). PVDF membranes were then incubated with the corresponding secondary antibodies coupled to horseradish peroxidase for 1.5 hours at room temperature. Optical density of the specific immunoreactive band was quantified with Fiji software and normalized to those β-actin for the corresponding samples in the same membranes.

### $CB_1$ receptor promoter transcriptional assays

Embryonic carcinoma P19 cells were transfected with Lipofectamine 2000 (Thermo Fisher Scientific, Waltham, MA, USA) following manufacturer's instructions. Cells were co-transfected with one of the following constructions: pCAG-RHEB, pCAG-RHEB Q64L, pCAG-Tbr2, mouse TSC2 short hairpin RNA (shRNA, 5'-TGAGCCTTGCTGGAAGTTGAT-GCGTAACC-3') or control (scrambled) shRNA (Origene, Rockville, MD, USA) and a construct encoding the -3016 to +142 sequence (referring to the first nucleotide of exon 1) of the human *CNR1* gene promoter fused to the chloramphenicol acetyltransferase (CAT) reporter gene (ph$CB_1$-3016-CAT) (Blázquez *et al*., 2011). The reporter gene construct was based on the pBLCAT2/pBLCAT3 system, in which the thymidine kinase minimal promoter was replaced for the human *CNR1* promoter upstream of CAT. CAT levels were subsequently analysed with CAT ELISA kit (Roche, distributed by Sigma-Aldrich España) following manufacturer's instructions.

### DNA single nucleotide polymorphisms analyses and sequencing

Genomic DNA was obtained by standard methods and Sequenom single nucleotide polymorphism (SNP) analyses were performed by Centro Nacional de Genotipado (CEGEN-PRB2 USC node, Santiago de Compostela, Spain) using the iPlex Gold chemistry and MassARRAY platform, according to manufacturer's instructions (Sequenom, San Diego, CA, USA). 48 SNPs within different ECS element genes were analysed (Table 3). Genotyping assays were designed using the Sequenom MassARRAY Assay Designer 4.1 software. SNPs were genotyped in 3 assays, PCR reactions were set up in a 5 μL volume and contained 20 ng of template DNA, 1x PCR buffer, 2 mM $MgCl_2$, 500 μM dNTPs and 1 U/reaction of PCR enzyme. A pool of PCR primers (Metabion, Steinkirchen, Germany) was made at a final concentration of each primer of 100 nM. The thermal cycling conditions for the reaction consisted on an initial denaturation step at 94 °C for 2 minutes, followed by 45 cycles of 94 °C for 30 seconds, 56 °C for 30 seconds and 72 °C for 1 minute, and a final extension step of 72 °C for 1 minute. PCR products were treated with 0.5 U shrimp alkaline phosphatase, followed by enzyme inactivation to neutralize unincorporated dNTPs.

**Table 3. SNPs analysed in this Thesis.** Table includes the gene within each specific SNP is located and their functional consecuence, if known.

| Gene | SNP | Functional consequence |
|---|---|---|
| *CNR1* | rs806365 | unknown |
| *CNR1* | rs7766029 | unknown |
| *CNR1* | rs806366 | unknown |
| *CNR1* | rs806368 | utr variant 3 prime |
| *CNR1* | rs12720071 | utr variant 3 prime |
| *CNR1* | rs4707436 | utr variant 3 prime |
| *CNR1* | rs1049353 | synonymous codon |
| *CNR1* | rs806369 | intron variant, upstream variant 2KB |
| *CNR1* | rs2023239 | intron variant |
| *CNR1* | rs1535255 | intron variant |
| *CNR1* | rs806379 | intron variant |
| *CNR1* | rs9444584 | intron variant |
| *CNR1* | rs9450898 | intron variant |
| *CNR1* | rs806380 | intron variant |
| *CNR1* | rs6454674 | intron variant, utr variant 5 prime |
| *CNR1* | rs2180619 | upstream variant 2KB |
| *DAGLA* | rs4963304 | upstream variant 2KB |
| *DAGLA* | rs7931563 | upstream variant 2KB |
| *DAGLA* | rs7942387 | upstream variant 2KB |
| *DAGLA* | rs198430 | synonymous codon |
| *DAGLA* | rs198444 | synonymous codon |
| *DAGLA* | rs34365114 | synonymous codon |
| *DAGLA* | rs144674730 | missense |
| *DAGLB* | rs143650244 | downstream variant 500B |
| *DAGLB* | rs187296513 | downstream variant 500B |
| *DAGLB* | rs3813518 | downstream variant 500B |
| *DAGLB* | rs3813517 | downstream variant 500B |
| *DAGLB* | rs836559 | utr variant 3 prime |
| *DAGLB* | rs2303361 | missense |
| *MGL* | rs76802560 | downstream variant 500B |
| *MGL* | rs6801421 | downstream variant 500B |
| *MGL* | rs72969613 | utr variant 3 prime |
| *MGL* | rs4881 | synonymous codon |
| *MGL* | rs115970931 | utr variant 3 prime |
| *FAAH* | rs932816 | upstream variant 2KB |
| *FAAH* | rs4141964 | intron variant |
| *FAAH* | rs324420 | missense |
| *FAAH* | rs324419 | synonymous codon |
| *FAAH* | rs2295632 | downstream variant 500B |
| *FAAH* | rs12029329 | downstream variant 500B |

| Gene | SNP | Functional consequence |
|---|---|---|
| *CNR2* | rs12744386 | unknown |
| *CNR2* | rs1130321 | utr variant 3 prime |
| *CNR2* | rs1106 | utr variant 3 prime |
| *CNR2* | rs2229579 | missense |
| *CNR2* | rs2501431 | synonymous codon |
| *CNR2* | rs41311993 | missense |
| *CNR2* | rs35761398 | missense |
| *CNR2* | rs2501432 | missense |

The iPLEX GOLD reactions were set up in a final 9 μL volume and contained 0.222x iPLEX buffer Plus, 1x iPLEX termination mix and 1x iPLEX enzyme. An extension primer mix (Metabion) was made to give a final concentration of each primer between 0.52 μM and 1.57 μM. The thermal cycling conditions for the reaction included an initial denaturation step at 94 °C for 30 seconds, followed by 40 cycles of 94 °C for 5 seconds, with an internal 5 cycles loop at 52 °C for 5 seconds and 80 °C for 5 seconds, followed by a final extension step of 72 °C for 3 minutes. The iPLEX Gold reaction products were desalted, dispensed onto a 384 Spectrochip II using an RS1000 Nanodispenser and spectra were acquired using the MA4 mass spectrometer, followed by manual inspection of spectra by trained personnel using MassARRAY Typer software, version 4.0. All assays were performed in 384-well plates, including negative controls and a trio of Coriell samples (Na10830, Na10831 and Na12147) for quality control. Seven samples were tested in duplicate and they were 100 % concordant. Genomic DNA sequencing of the *CNR1* gene coding exon was performed by the Sanger method under standard conditions by Secugen (Madrid, Spain).

**Quantitative PCR**

RNA was isolated using RNeasy Plus kit (Qiagen, Hilden, Germany) following manufacturer's instructions. cDNA was obtained with Transcriptor (Roche). Real-time quantitative PCR (qPCR) assays were performed using the FastStart Master Mix with Rox (Roche) and probes were obtained from the Universal Probe Library Set (Roche). Amplifications were run in a 7900 HT-Fast Real-Time PCR System (Applied Biosystems, Foster City, CA, USA). Each value was adjusted by using 18S RNA and β-actin levels as reference.

### *In utero* electroporation

Timed-pregnant C57Bl/6J mice were injected subcutaneously with buprenorphine (0.1 mg/kg) and meloxicam (1 mg/kg) 30 minutes before surgery at E14. The surgery was performed on a heating blanket and breathing and temperature were monitored throughout. Under isoflurane anaesthesia (induction: 4 %, maintenance: 2.5 %), the eyes of the dam were covered with eye ointment to prevent damage just before the uterine horns were exposed and moistened with warm sterile PBS (37 °C). Solution containing pCAG-GFP (0.5 μg/μL) and ON-TARGETplus mouse *Cnr1* siRNA smart pool (target sequences 5'-GGUAGUCCCUUCCAAGAAA-3', 5'-CCACAGAAAUUCCCUCUAA-3', 5'-GGGAAGAUGAACAAGCUUA-3', 5'-GUGUUUGCCUUCUGUAGUA-3'; further referred as $siCB_1$) or control siRNA (further referred as siCo; Dharmacon, Lafayette, CO, USA), as well as 0.1 % Fast Green was injected into the lateral ventricle of individual embryos using pulled borosilicate glass capillaries with a sharp and long tip. Plasmid DNA was purified with NucleoBond EF (Macherey-Nagel, Düren, Germany) in order to assure the absence of endotoxin. Injected embryos were then placed between the electroporation tweezer-type paddles (5 mm diameter; Sonidel Limited, Dublin, Ireland) that were oriented at a rough 20° leftward angle from the midline and a rough 10° angle downward from anterior to posterior. By these means, neural precursor cells from the SVZ, which radially migrate into the medial prefrontal cortex (mPFC), were transfected. Electrode pulses (30 V, 50 ms) were applied five times at intervals of 950 ms controlled by an electroporator (NEPA21; Sonidel Limited). Uterine horns were placed back into the abdominal cavity after electroporation. The abdominal cavity was filled with warm sterile PBS (37 °C) and abdominal muscles and skin were sutured individually with absorbable and non-absorbable suture thread, respectively. After recovery, pregnant mice were returned to their home cages. After birth, GFP expression was assessed in the pups with a portable fluorescent flashlight (Nightsea, Lexington, MA, USA) or under a fluorescence binocular through the intact skull and skin at P1-P3. Pups without expression in the mPFC were excluded from the analysis. Mice of both sexes were used.

### Patch clamp and electrophysiological recordings

Mice electroporated with either $siCB_1$ or siCo at E14 were sacrificed at different ages (P7, P14, P21 and P60) and their brains were quickly removed and immediately placed in oxygenated (95 % $O_2$/5 % $CO_2$), ice-cold (4 °C) slicing artificial cerebrospinal fluid

(sACSF) containing 120 mM choline chloride, 10 mM D-glucose, 25 mM $NaHCO_3$, 6 mM $MgSO_4$, 3.5 mM KCl, 1.25 mM $NaH_2PO_4$ and 0.5 mM $CaCl_2$. Brain was then sliced using a vibratome (VT1200S; Leica). Coronal slices (300 µm) of the mPFC were selected and transferred to a holding chamber placed in a water bath at 32 °C. Slices were kept in oxygenated recording ACSF (rACSF) for 15-30 min. rACSF contained 120 mM NaCl, 3.5 mM KCl, 1.3 mM $MgSO_4$, 1.25 mM $NaH_2PO_4$, 2.5 mM $CaCl_2$, 10 mM D-glucose and 25 mM $NaHCO_3$. Subsequently, slices recovered at room temperature for at least 30 minutes before recording.

Recordings were made using either an EPC-10 amplifier controlled by PatchMaster Software (HEKA, Lambrecht, Germany) or an Axopatch 200b (Molecular Devices, San José, CA, USA) and an in-house software running under Matlab 9.3 (MathWorks, Natick, MA, USA). Signals were low-pass filtered at 2.9 kHz and sampled at 10 kHz. All experiments were performed at 30-32 °C. Whole-cell current clamp recordings were made from the soma of $GFP^+$ upper layer II/III neurons that visually appeared pyramidal in shape. Patch pipettes were pulled from borosilicate glass capillaries to an open pipette resistance of 2-4 MΩ when filled with pipette solution. Pipette solution contained 110 mM potassium gluconate, 30 mM KCl, 0.5 mM EGTA, 10 mM HEPES, 4 mM Mg-ATP and 0.5 mM Na-GTP and biocytin at a concentration of 2 mg/mL. Series resistance ranged from two to three times the pipette resistance (4-12 MΩ) and was compensated to 70 %. Signals were corrected for liquid junction potential (+15 mV). Neurons were excluded from the analysis when their series resistance changed by more than 50 % during an experiment. Actual recordings started after 5 minutes of stabilization. The protocols mentioned below were used to determine firing properties (average firing frequency and time constant of adaptation for firing), passive (RMP, input resistance and membrane time constant) and active cell properties (spike properties, voltage sag and rheobase), as well as spontaneuos synaptic activity. In order to achieve appropriate filling of the recorded neurons with biocytin the whole-cell configuration was maintained for at least 15-20 minutes. Subsequently, the pipette was retracted carefully to avoid damaging or removing the cell.

For the passive cell properties, current-voltage relationship was used for the calculation of the input resistance. Input resistance was determined as the slope of the linear fit between -60 and -70 mV. The membrane time constant was determined with a mono-exponential fit of the voltage response after a current step of -10 pA. RMP was read in current clamp immediately after rupturing the cell membrane.

Regarding active cell properties, rheobase, which is the minimal current that evoked an action potential (AP), was estimated using small current steps of 10 pA. The voltage sag was measured at a hyperpolarizing current injection of -100 pA. The AP threshold was determined using the membrane potential at the peak of the second derivative in a phase plot. The AP amplitude was calculated as the voltage difference between the AP peak and the threshold. The AP half-width was measured as the width in ms at the half-maximal spike amplitude. The amplitude of the afterhyperpolarization (AHP) was calculated as the voltage difference between the AP threshold and the most negative voltage reached during the AHP. As for AP threshold, AP amplitude and AP half-width, the average of all spikes that occurred during the first five current steps where spikes were detected was taken. When the first five sweeps comprised less than 10 spikes more sweeps were included to average at least 10 spikes. For the average of the AHP amplitude all spikes from repetitive AP firing traces were included.

Respecting spike firing properties, the frequency of the firing rate was determined by counting the spikes during current injection step. The interspike interval (ISI) was calculated as the time between subsequent spikes. ISIs were used to determine the instantaneous spike frequency, which was in turn plotted against the time points of the spikes for every current step. The time constant of adaptation was estimated by fitting a standard exponential function to the instantaneous frequency for all current injections that resulted in repetitive firing of at least five spikes. In the end, one time constant of adaptation was obtained for each current step.

Finally, when assessing spontanueos synaptic activity, miniature postsynaptic currents were isolated. The amplitude and instantaneous frequency were determined for every miniature synaptic event, detected using a combined threshold and template matching procedure. Distribution of binned inhibitory and excitatory postsynaptic currents (IPSCs and EPSCs, respectively), instantaneous frequencies and amplitudes (40–50 bins) were constructed for every cell and then averaged. For IPSCs, at least 100 events were analysed per cell; while at least 250 events were analysed per cell for EPSCs. Average amplitudes and frequencies were calculated per 5 minutes.

**THC administration**

THC (≥99 % HPLC; THC Pharm, Frankfurt am Main, Germany) was diluted in 0.9 % NaCl (saline) solution containing 3 % (v/v) DMSO and 2 % (v/v) Tween-80 and administered intraperitoneally (i.p.) at a final dose of 3 mg/kg to pregnant

dams (at 10 µL/g) for 8 consecutive days, from E10 to E17. Control mice were injected with vehicle solution.

### *In situ* hybridization

Coronal sections (30 µm) of P60 mouse brains were mounted on SuperFrost Ultra Plus glass slides (Thermo Fisher Scientific). When completely dry, they were subjected to *in situ* hybridization (ISH) using CCK digoxygenin-labelled riboprobes obtained by PCR amplification and retrotranscription (forward primer 5'-AGAGAGCGGCGTATGTCTGT-3', reverse primer 5'-CTGCATTGCACACTCTGGAC-3'). Briefly, samples were acetylated and then incubated in a hybridization buffer containing 0.5-1.0 µg/mL DIG-labelled riboprobes at 65 °C overnight. Sections were sequentially washed twice in a medium containing 2x standard saline citrate and 50% formamide for 1 hour at 60 °C and then 20 minutes at 37 °C in 2x SSC. The hybridized probe was detected after incubation with alkaline phosphatase-conjugated anti-digoxygenin antibody (Roche) and subsequent incubation with NBT/BCIP (Roche) in alkaline buffer (pH 9.5). The resulting blue precipitate was post-fixed by incubation in PFA 4% during 10 minutes. There were no apparent signal in control sections with the sense probes.

### Immunohistochemistry

Samples from ISH assays were subsequently used for immunohistochemistry (IHC). Briefly, after washing, slides were subjected to a heat-induced antigen retrieval step with sodium citrate buffer (10 mM, pH 6) at 96 °C, as well as a 1 hour blockade, prior to exposure to a mouse anti-GABA primary antibody (A0310; Sigma-Aldrich España). Immunodetection was achieved using the Envision+ Dual Link System-HRP (DAB+) kit (Dako-Agilent Technologies, Santa Clara, CA, USA), following manufacturer's instructions. Samples were then mounted using Entellan resin.

### Stereological analysis of cell density

Samples stained by CCK ISH and GABA IHC were analysed using a Olympus BX61 microscope (Olympus, Tokyo, Japan) operated by VIS software with newCAST incorporated (Visiopharm, Hoersholm, Denmark). Hippocampal *strata* were manually delineated within CA1 region before performing a stereological counting of the total number of $CCK^+GABA^+$ cells. The frame area was set to 625 $\mu m^2$ with a sampling interval of 120 µm at the z level. Results are expressed as the number of double positive cells per $mm^2$. Gundersen's coefficient of error was always below 0.1. Data were

obtained in a blinded manner and sample code remained unsealed during the whole data processing and analysis.

**THC determination**

Analysis of THC in embryonic brain tissue was performed as follows: samples were homogenized on ice with 700 µL of a mixture of 50 mM Tris-HCl buffer (pH 7.4):methanol (1:1) and the homogenates were transferred to 12 mL glass tubes. The homogenizer was washed twice with 0.9 mL of the same mixture and the contents were combined into the tube giving an approximate volume of 2.5 mL of homogenate. The homogenization process took less than 5 minutes per sample and homogenates were kept on ice until organic extraction. After the homogenization step, 5 mL of hexane:ethyl acetate was added into each 12 mL glass tube and were placed in a rocking mixer over 20 minutes. Tubes were centrifuged at 1700 g over 5 minutes at room temperature and organic phase was then transferred to clean tubes, and evaporated under nitrogen stream. Extracts were subjected to a derivatization step using dansyl chloride. This reaction is selective for phenol functions present in THC and improves the separation and ionization efficiency. Extracts were reconstituted in 100 µL of a mixture of water:acetonitrile (1:9, v/v) with 0.1% formic acid (v/v) and transferred to HPLC vials. 20 µL were injected into an Agilent 6410 Triple Quadrupole Liquid-Chromatograph equipped with a 1200 series binary pump, a column oven and a cooled autosampler at 4 °C (Agilent Technologies). Chromatographic separation was carried out with a Waters C18-CSH column (3.1 x 100 mm, 1.8 µm particle size; Waters, Milford, MA, USA) maintained at 40 °C with a mobile phase flow rate of 0.4 mL/min. The composition of the mobile phase was: A: 0.1 % (v/v) formic acid in water; B: 0.1 % (v/v) formic acid in acetonitrile. THC was separated by gradient chromatography.

**WIN-55,212-2 stimulated [35S]GTPγS binding assays**

Tissue samples were homogenized using a Teflon-glass grinder in 30 volumes of homogenization buffer (1 mM EGTA, 3 mM $MgCl_2$, 1 mM dithiothreitol (DTT), and 50 mM Tris-HCl, pH 7.4) supplemented with 250 mM sucrose. The crude homogenate was centrifuged for 5 minutes at 1000 g (4 °C). The resulting supernatant was centrifuged at the same conditions. Pellet was washed twice in 20 volumes of homogenization buffer and centrifuged in similar conditions. Binding assays were carried out in a final volume of 250 µL in 96 well plates, containing 1 mM EGTA, 3 mM $MgCl_2$, 100 mM NaCl, 0.2 mM DTT, 50 µM guanosine 5′-GDP, 50 mM Tris-HCl at pH 7.4 and

0.5 nM [$^{35}$S]GTPγS (Perkin Elmer Life Sciences, Waltham, MA, USA). Stimulation curves were carried out by incubating increasing concentrations of the $CB_1R$ agonist WIN-55,212-2 ($10^{-12}$-$10^{-4}$ M). The incubation started by addition of the membrane suspension (30 μg of membrane proteins per well) and was performed at 30 °C for 2 hours with shaking (600 rpm). Incubations were terminated by rapid filtration under vacuum (Perkin Elmer Life Sciences) through GF/C glass fibre filters (Perkin Elmer Life Sciences) pre-soaked in ice-cold incubation buffer. The filters were then rinsed, air dried, and counted for radioactivity (5 minutes) by liquid scintillation spectrometry using a MicroBeta TriLux counter (Perkin Elmer Life Sciences). Non-specific binding was defined as the remaining [$^{35}$S]GTPγS binding in the presence of 10 μM unlabelled GTPγS, and the basal binding as the signal in the absence of WIN-55,212-2.

**Intrahippocampal electric field recording**

Mice were implanted with fixation bars under isoflurane anaesthesia (1.5-2 %). The recording chamber was aligned to target the right dorsal hippocampus at -1.8 mm posterior from Bregma and -1.25 mm lateral from midline. At least two jeweller's screws were inserted into the skull for providing additional anchoring and reference/ground connections (over the cerebellum). If required, an additional screw was located over the frontal skull. The implant was secured with dental cement.

One week after surgery, mice were habituated to the head-fixed setup consisting on a cylinder (20 cm radius) coupled to a stereotactic frame. Habituation sessions included handling, running freely around the setup and mounting/dismounting the head during brief periods of time. After 2-3 days, animals were water deprived, and they started daily sessions of 10 minutes running for reward (water), till they were fully habituated to the procedure. Once they consistently run for water in the 10 minutes session, time in the setup was increased over steps of 5 minutes, until animals got habituated to behave freely. They typically alternated periods of running and immobility during a maximum of 60 minutes each day. Water port was removed after the first 10 minutes session to keep deprivation level. Once mice were habituated to 30-60 minutes sessions, they were briefly anesthetized under isoflurane to open the craniotomy. Afterwards, craniotomy was covered with low toxicity silicone elastomer (Kwik-Sil; World Precision Instruments, Sarasota, FL, USA) and recordings started the following day. Every animal was recorded in two independent sessions of 1 hour.

For recordings, 16-channels silicon probes (100 μm resolution, 413 $\mu m^2$ electrode area) were used (Neuronexus, Anne Arbor, MI, USA). Extracellular signals were pre-amplified (4x) and recorded with a 16-channel AC amplifier (Multichannel Systems, Reutlingen, Germany), further amplified by 100, filtered by analogous means at 1 Hz to 5 kHz, and sampled at 20 kHz/channel with 12 bits precision. The animal speed was stored to evaluate periods of running and immobility.

Analysis of electrophysiological signals was implemented in Matlab 9.3. Local field potential (LFP) signals from sites at *stratum lacunosum moleculare* were used for identifying theta periods during running (band-pass 4-12 Hz). Forward-backward-zero-phase finite impulse response filters of order 512 were used to preserve temporal relationships between channels and signals. The mean power spectra during theta was fitted to the 1/f decay for frequencies > 60 Hz and a reference level was established at 0 dB. Spectral values fitted to 1/f were similar between groups and were discarded for the analysis. Consequently, only the theta (4-12 Hz) and low gamma bands (30-60 Hz) were included in the analysis.

For detection of sharp-wave ripples (SWR), LFP signals from *stratum radiatum* were low-pass filtered (100 Hz) while signals from *stratum pyramidale* (*sp*) were bandpass filtered (100-600 Hz). Filtered signals were smoothed by a Gaussian kernel and candidate events were detected by thresholding (> 4 SDs). The power spectra was evaluated in a window of ±0.2 ms around each detected event. Time-frequency analysis was performed by applying the multitaper spectral estimation in sliding windows with 97.7 % overlap and frequency resolution of 10 Hz in the 90-600 Hz frequency range. The normalized power in the 90-600 Hz band was treated as a statistical distribution, from which we extracted the mode to estimate the oscillatory frequency peak, the entropy and fast ripple index, as previously described (Foffani *et al*., 2007). Slow (90-120 Hz) and fast ripples (>120 Hz) were separated using individual spectra for visualization purposes.

**Pentylenetetrazol-induced seizures assay**

Pentylenetetrazol (PTZ) (Sigma-Aldrich España) was dissolved in 0.9 % saline and administered i.p. to mice at P60 at a concentration of 22.5 mg/kg (at 10 μL/g). Mice were then placed in Plexiglas cages and re-injected with the PTZ-containing solution every 10 minutes until generalized seizures occurred. This was considered the end of the experiment. All the procedure was video-recorded and analysed later by an experimenter blinded to the experimental groups, who determined the precise moment of generalized seizure onset.

### Novel object recognition task

P60 mice were habituated to an arena consisting on a grey methacrylate open field of 70 x 70 x 40 cm under uniform lightning conditions of 25 lux. Mice were allowed to freely explore the arena for 10 minutes the day before the novel object recognition (NOR) test to let them familiarize with the arena and minimize cage-exploring-derived distractions during the subsequent test. Test consisted of two parts: training and test sessions. During the former mice were allowed to individually explore two objects for 10 minutes. Then mice were returned to the home cage and the open field and objects were cleaned to avoid olfactory cues. After an inter-trial interval of 50 minutes, mice were placed back into the same open field for the test session, in which one of the familiar objects had been replaced by a novel object. Mice were allowed to explore the objects for 10 minutes. Mice did not show preference for any object before trials. Mice were excluded from the analysis only if the total time of exploration for each mouse was lower than 5 seconds in the test session. Object exploration was defined as the mouse being within 2 cm of an object, directing its nose at the object, and being involved in active exploration such as sniffing. A discrimination index was calculated to measure recognition memory as follows:

$$I_d = (t_{\text{new object}} - t_{\text{familiar object}})/(t_{\text{new object}} + t_{\text{familiar object}})$$

All tests were video-recorded and systematically analysed by mean of the SMART 3.0 video tracking software (Panlab, Barcelona, Spain).

### Object location task

The day after NOR test, mice were subjected to an object-place recognition, or object location (OL), task in the same open field arena. This test was also structured in two sessions: similar to NOR, mice were first exposed to two identical objects that they were left to explore during 10 minutes. After that, mice were placed back in their home cage and the arena and object were cleaned to remove any odour cue. After 50 minutes, in the test session, one of the objects was placed in a different position maintaining its distance relative to the walls, and mice were allowed to explore the objects for an additional 10 minutes. Mice were excluded from the analysis only if the total time of exploration for each mouse was lower than 5 seconds in the test session. A discrimination index was calculated to measure recognition memory as follows:

$$I_d = (t_{\text{displaced object}} - t_{\text{undisplaced object}})/(t_{\text{displaced object}} + t_{\text{undisplaced object}})$$

All tests were video-recorded and systematically analysed by mean of the SMART 3.0 video tracking software (Panlab).

**Cannabinoid-induced tetrad**

A classical cannabinoid tetrad test (Metna-Laurent et al., 2017) was performed on P60 mice, which were injected i.p. with THC (10 mg/kg) or its vehicle following the same preparation protocol as abovementioned. Basal temperature was measured with a rectal probe just before injection. 45 minutes after injection mice were placed in an open field arena and recorded for 10 minutes to evaluate hypolocomotion. Just after removing the mice from the open field arena, rectal temperature was taken again to assess hypothermia. 60 minutes after injection, mice were subjected to a catalepsy test. Briefly, mice were set up in a standing position with both forepaws resting on a horizontal bar separated 3 cm from the floor of a standard cage. Time until mice descended from the bar (i.e. both forepaws are touching the floor) was measured with a cut-off time of 2 minutes. Lastly, 90 minutes after injection, mice were placed in a hot plate set at 52 ºC and time until first sign of pain was quantified. In absence of signs of pain, mice were removed from the hot plate at a cut-off time of 30 seconds in order to avoid wounds to the animals. A naive cohort from each genotype was injected with vehicle and used to establish the baseline for both parameters.

**Data and statistical analyses**

Results shown represent the means ± S.E.M., and the number of experiments is indicated in every case. Statistical analysis was performed with GraphPad Prism 6.07 (GraphPad Software, La Jolla, CA, USA). All variables were first tested for nomality (Kolmogorov-Smirnov test) and homocedasticity (Levene's test). When variables satisfied these conditions, one-way or two-way ANOVA and Student-Newman-Keuls or LSD Fisher *post hoc* tests were used to assess differences between groups. Disease-Genotype association test was performed by the SNPator online tool (Morcillo-Suárez *et al*., 2008) to examine genotype and allele frequencies between patients and controls. p values of $< 0.05$ were regarded as statistically significant.

# Results

## Aim 1: Summary

MCDs are associated with refractory epilepsy in children and young adults (Iffland and Crino, 2017). These alterations are originated by the disruption of key processes during brain development, such as neural progenitor cell proliferation or neuronal migration. Within MCD, some types of FCD are associated with overactivation of the mTORC1 signalling pathway (Aronica and Crino, 2014; Najm *et al*., 2018). Whereas the origin of the different FCD subtypes is still unclear, recent research has demonstrated the involvement of alterations of the PI3K/Akt/mTORC1 pathway particularly in FCD Type II (Jansen *et al*., 2015; Lim *et al*., 2015; D'Gama *et al*., 2017). Nevertheless, further investigation on the mechanisms responsible for the epileptogenic network is required for the development of novel therapeutic strategies aimed to manage FCDs.

The ECS, and especially $CB_1R$, exerts an essential neuromodulatory role in the adult brain *via* the retrograde lipid messengers 2-AG and AEA (Soltesz *et al*., 2015). In addition, $CB_1Rs$ are expressed during human cortical development (Mato *et al*., 2003; Wang *et al*., 2003). During early stages in brain development, $CB_1Rs$ are required for proper radial migration during cortical development, and their genetic inactivation induces brain hyperexcitability (Díaz-Alonso *et al*., 2017). Interestingly, $CB_1R$ is expressed in FCD (Zurolo *et al*., 2010), a pathology that may be related to PN migration defects, although its contribution to FCD severity remains unclear. Thus, here we sought to investigate the potential contribution of aberrant cannabinoid signalling to FCD developmental pathogenesis. Additionally, we aimed to characterize the long-term electrophysiological alterations of PNs that suffer embryonic $CB_1R$ signalling disruption in order to find the mechanism underlying the hyperexcitability found in previous studies.

## Aim 1. Impact of altered endocannabinoid signalling in focal cortical dysplasia and in projection neuron maturation

### R1.1. $CB_1$ receptor expression in focal cortical dysplasia is associated with overactive mTORC1 pathway

To assess the pathophysiological relevance of $CB_1R$ signalling in MCDs we analysed $CB_1R$ immunoreactivity in control and dysplastic brain areas (Figure R1.1). FCD cases (n=30) were included with a mean patient age of 11.4 years and a male/female distribution of n=18 and 12, respectively (Table 1). Double immunofluorescence analysis with anti-pS6 (recognizing the phosphoS240/S244 sites) and anti-$CB_1R$ antibodies confirmed the selective overactivation of the mTORC1 pathway in FCD Type II but not FCD Type I samples (Figure R1.1A, B). Quantification of $CB_1R$ immunoreactivity revealed that receptor expression is notably enriched in the dysplastic areas of FCD Type II when compared with control brain tissue, but not in FCD type I (Figure R1.1A, C). A more detailed analysis of double immunofluorescence images showed that $CB_1R^+$ cells largely colocalized with pS6 immunoreactivity in FCD Type II, and $CB_1R^+pS6^+$ cells were highly enriched in the dysplastic areas when compared to control cortical tissue (Figure R1.1D). Moreover, the intensity of pS6 immunoreactivity was selectively increased when comparing FCD Type II and I (1.61 ± 0.14 *versus* 1.00 ± 0.07 respectively; $p < 0.018$, $n = 4$).

Next we analysed $CB_1R$ expression in BCs and DNs based in morphological characterization and mTORC1 overactivation (Figure R1.2A). This indicated that 2.43 ± 0.92 and 0.57 ± 0.29 % of total $CB_1R$ tissue immunoreactivity corresponded to these cell subpopulations, respectively. FCD Type II is characterized by the expression of undifferentiated markers in BC including Sox2, Oct4, Pax6, Tbr1, Otx1 and others (Hadjivassiliou *et al*., 2010; Orlova *et al*., 2010; Arai *et al*., 2012; Yao *et al*., 2016). Thus, we analysed the expression of $CB_1Rs$ in FCD Type II neurons together with undifferentiated-cell markers. Whereas in FCD Type II sparse c-$Myc^+$ cells could be detected, this was never the case in FCD Type I samples. Importantly, c-$Myc^+$ cells expressed $CB_1R$ and showed active mTORC1 signalling ($pS6^+$) (Figure R1.2B). Hence, in FCD Type II we determined that 72.74 ± 11.04 % c-$Myc^+$ cells were also $pS6^+$.

### R1.2. $CB_1$ receptor expression is not induced by mTORC1 signalling

To determine if $CB_1R$ enrichment in FCD lesions was a cause or a consequence of mTORC1 overactivation we analysed if this signalling pathway can regulate $CB_1R$

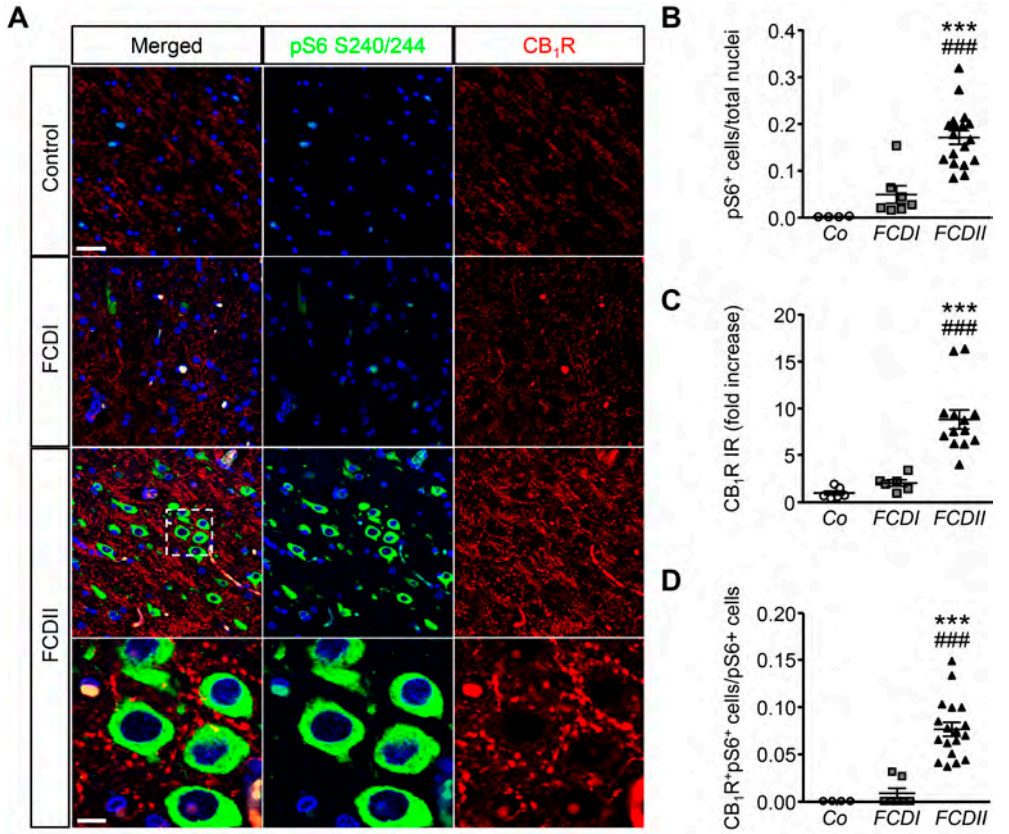


**Figure R1.1. $CB_1$ receptor is enriched in focal cortical dysplasia Type II in cells with overactive mTORC1 signalling.** (**A**) Representative immunofluorescence images showing the presence of $CB_1R$ in samples from Type I and II FCD and control brains, revealed with an anti-$CB_1R$ antibody (red). Cells with over-active mTORC1 signalling are stained with anti-pS6 S240/244 antibody (green). High magnification images of $CB_1R$ expression associated with mTORC1 overactivation in FCD Type II are shown. (**B-C**) $pS6^+$ cells and $CB_1R$ immunoreactivity (IR) were quantified in the dysplastic area and referred to total cell number (DAPI counterstaining). Control, FCD Type I and FCD Type II cases (**B**, n = 4, 7 and 18, respectively; **C**, n = 6, 8, 13). (**D**) $CB_1R^+pS6^+$ double-labelled cells were quantified and referred to total $pS6^+$ cells. Control, FCD Type I and FCD Type II cases (n = 4, 7 and 18, respectively). Statistical comparison *versus* control samples: ***, $p < 0.001$. Statistical comparison *versus* FCD Type I samples: ###, $p < 0.001$. Scale bars: 45 μm; inset: 10 μm.

expression. P19 cells were transfected with a plasmid encoding a constitutively active mutant of the mTORC1 upstream activator Rheb (RhebQ64L) or a Tsc2 specific short-hairpin RNA coding plasmid (shTSC2). In these conditions, as compared to control cells, mTORC1 pathway activity increased as evidenced by the strong increase of $pS6^+$ immunoreactive cells (Figure R1.3A). However, under the same conditions of overactive mTORC1 signalling, $CB_1R$ protein levels were not induced (Figure R1.3B).

We also performed $CB_1R$ promoter transcriptional assays by co-transfection with a CAT gene reporter in frame with a minimal *CNR1* promoter (Blázquez *et al.*, 2011). Again, in cells with overactive mTORC1 pathway *CNR1* promoter activity was not induced (Figure R1.3C). As a control of the sensitivity of this assay, P19 cells

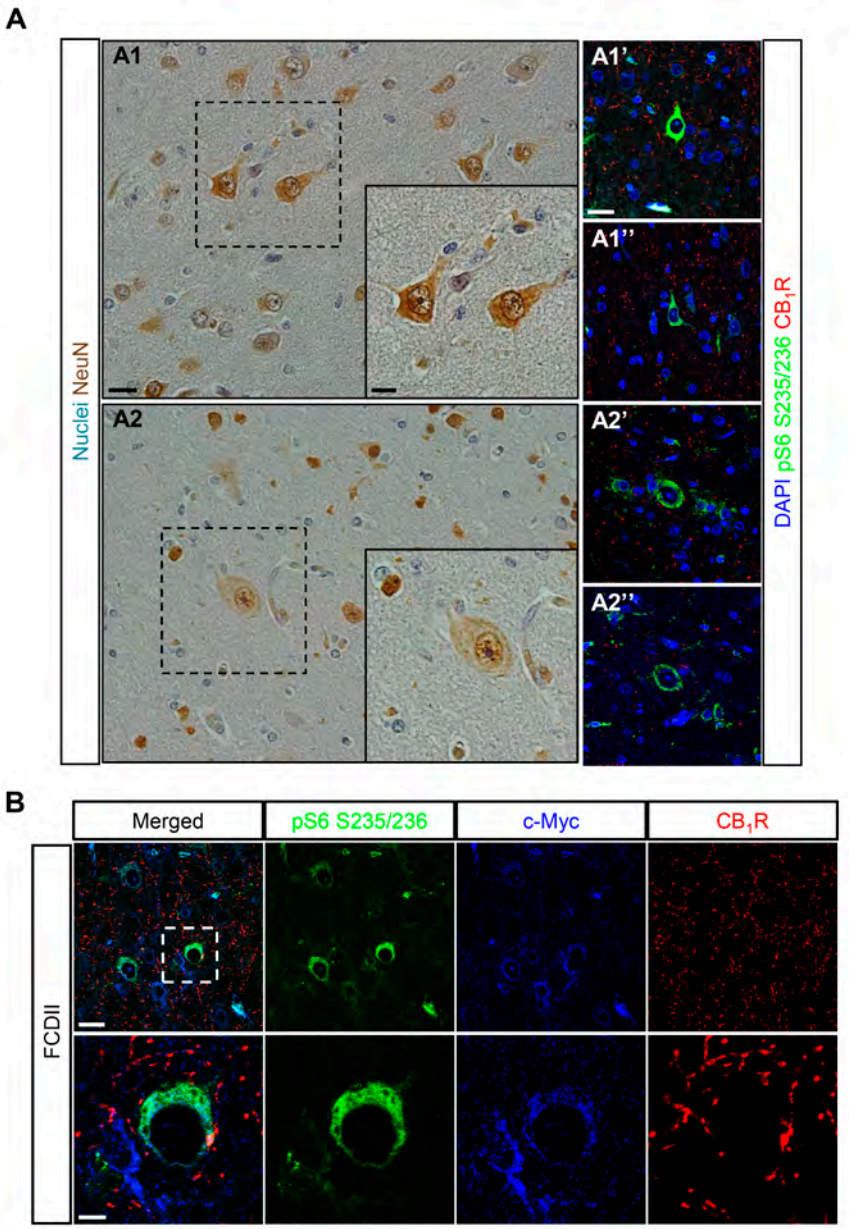


**Figure R1.2. $CB_1$ receptor is present in undifferentiated cells.** (**A**) DNs (**A1, A1'** and **A1''**) and BCs (**A2, A2'** and **A2''**) were identified based in morphological criteria in hematoxylin/eosin sections stained with anti-NeuN antibody (**A1, A2**). $CB_1R$ expression and mTORC1 activity status was analysed by immunofluorescence with anti-$CB_1R$ and anti-pS6 antibodies, respectively (**A1', A1'', A2'** and **A2''**). (**B**) Representative immunofluorescence images showing co-expression of $CB_1R$ (red) and the undifferentiated cell marker c-Myc (blue), as well as pS6 as a readout of mTORC1 activity (green). High magnification insets are shown (lower panels). Scale bar: 25 μm, insets, 6.5 μm.

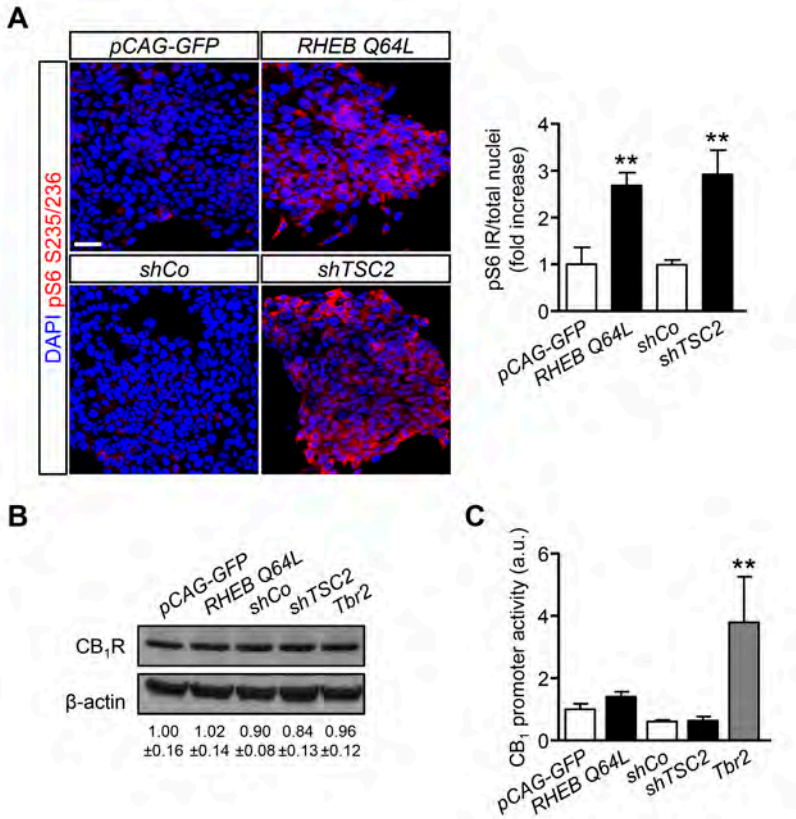


**Figure R1.3. The mTORC1 pathway does not regulate $CB_1$ receptor expression.** (**A**) Representative images and quantification of mTORC1 activation in P19 cells after transfection with the Rheb constitutively active mutant Q64L, shTSC2, a scrambled shRNA-encoding vector (shCo), or a GFP-encoding plasmid. mTORC1 activation was analysed by means of $pS6^+$ cells quantification. (**B**) Western blot analysis of $CB_1R$ levels in the same conditions as above. Representative immunoblot luminograms and quantification for $CB_1R$ and β-actin as loading control are shown (mean ± SEM is provided, n = 3). (**C**) *CNR1* promoter activity was analysed using a CAT construct 24 hours after transfection (n = 6). Statistical comparison *versus* the corresponding control samples: **, $p < 0.01$. Scale bar: 50 μm.

were transfected with the intermediate progenitor transcription factor Tbr2. The *CNR1* promoter has several putative Tbr2-binding sites (Table 4), and its expression was indeed sufficient to increase the promoter reporter activity (Figure R1.3C), but failed to increase protein levels (Figure R1.3B). In summary, these results indicate that the increased $CB_1R$ levels in FCD are not a direct consequence of an overactive mTORC1 pathway.

## R1.3. Genetic characterization of the endocannabinoid system in focal cortical dysplasia

The observation that $CB_1R$ levels are increased in the dysplastic cells of FCD Type II cases prompted us to expand the analyses to other elements of the ECS that may contribute to cannabinoid signalling deregulation. Genomic DNA and messenger RNA

**Table 4. Putative Tbr2 binding sites within *CNR1* locus.** Detected using Matinspector (Genomatix, München, Germany)).

| Species | Gene location | Binding site position | | Strand | Matrix similarity |
|---|---|---|---|---|---|
| | | Start | End | | |
| Human | 6q15 | 88164872 | 88164900 | + | 0.941 |
| | | 88166737 | 88166765 | + | 0.963 |
| | | 88166645 | 88166673 | + | 0.989 |
| | | 88166554 | 88166568 | + | 0.902 |
| | | 88168289 | 88168317 | + | 0.990 |
| Mouse | 4A5 | 33936594 | 33936608 | - | 0.896 |
| | | 33925880 | 33925908 | + | 0.901 |
| | | 33944561 | 33944589 | - | 0.999 |

**Table 5. Endocannabinoid system elements analysed by qPCR in FCD Type II and control samples.** (n = 4 and 22, control and FCD Type II, respectively, for *CNR1* transcript; 4 and 8, control and FCD Type II, for the rest). Statistical comparison *versus* control samples: *, $p < 0.05$; ns, non significant.

| Transcript | Condition | Mean | SEM | Statistical significance |
|---|---|---|---|---|
| *CNR1* | Control | 1.00 | 0.2397 | * |
| | FCD Type II | 33.70 | 5.3080 | |
| *DAGLA* | Control | 1.00 | 0.0004 | ns |
| | FCD Type II | 0.45 | 0.1286 | |
| *DAGLB* | Control | 1.00 | 0.0106 | ns |
| | FCD Type II | 0.84 | 0.2274 | |
| *MGL* | Control | 1.00 | 0.0005 | ns |
| | FCD Type II | 0.88 | 0.3061 | |
| *NAPE-PLD* | Control | 1.00 | 0.0264 | ns |
| | FCD Type II | 0.72 | 0.1176 | |
| *FAAH* | Control | 1.00 | 0.0182 | ns |
| | FCD Type II | 0.36 | 0.1910 | |

from the FCD collection were obtained. Real time PCR expression analysis confirmed increased levels of $CB_1R$ transcripts in FCD Type II *versus* control brain extracts (Table 5), further supporting the results obtained at the protein level by immunofluorescence characterization (Figure R1.1). Transcript levels of other elements of the ECS (DAGLα, DAGLβ, MGL, FAAH and NAPE-PLD) were also quantified and no differences were observed (Table 5). To further characterize if cannabinoid signalling alterations may contribute to overactive mTORC1 in FCD Type II, we performed SNP analysis of various genes of ECS elements including $CB_1R$, DAGLα and β, MGL, FAAH and $CB_2R$. A total 48 SNPs of the ECS were selected (Table 3), based on previous evidences that point to their potential involvement in different nervous system disorders. Genotype disease association analysis revealed the existence of 3 polymorphisms in the *DAGLA* gene differentially expressed in FCD Type II *versus* control specimens (Table 6).

**Table 6. SNPs. analysed in focal cortical dysplasia Type II and control brain genomic DNA extracts.** SNPs appear listed in the same order as in Table 3. (n= 4 and 22, control and FCD Type II, respectively). Disease-Genotype association test carried out by SNPator online tool. *, $p < 0.05$.

| SNP | Major/minor alleles | % major homozygosity | | % heterozygosity | | % minor homozygosity | | Disease association |
|---|---|---|---|---|---|---|---|---|
| | | Control | FCD | Control | FCD | Control | FCD | |
| rs806365 | C/T | 20.0 | 36.4 | 70.0 | 45.4 | 10.0 | 18.2 | |
| rs7766029 | T/C | 20.0 | 31.8 | 50.0 | 54.5 | 30.0 | 13.6 | |
| rs806366 | T/C | 40.0 | 31.8 | 40.0 | 31.8 | 20.0 | 36.4 | |
| rs806368 | T/C | 60.0 | 54.5 | 20.0 | 36.4 | 20.0 | 9.0 | |
| rs12720071 | A/G | 60.0 | 86.4 | 40.0 | 13.6 | 0.0 | 0.0 | |
| rs4707436 | G/A | 60.0 | 59.1 | 30.0 | 40.9 | 10.0 | 0.0 | |
| rs1049353 | G/A | 80.0 | 68.2 | 10.0 | 31.8 | 10.0 | 0.0 | |
| rs806369 | C/T | 60.0 | 45.5 | 30.0 | 40.9 | 10.0 | 13.6 | |
| rs2023239 | T/C | 60.0 | 63.6 | 40.0 | 36.4 | 0.0 | 0.0 | |
| rs1535255 | T/G | 70.0 | 63.6 | 30.0 | 36.4 | 0.0 | 0.0 | |
| rs806379 | A/T | 30.0 | 18.2 | 60.0 | 77.3 | 10.0 | 4.5 | |
| rs9444584 | C/T | 60.0 | 54.5 | 30.0 | 45.5 | 10.0 | 0.0 | |
| rs9450898 | C/T | 70.0 | 63.6 | 30.0 | 36.4 | 0.0 | 0.0 | |
| rs806380 | A/G | 60.0 | 54.5 | 30.0 | 40.9 | 10.0 | 4.5 | |
| rs6454674 | T/G | 40.0 | 63.6 | 40.0 | 31.8 | 20.0 | 4.5 | |
| rs2180619 | A/G | 30.0 | 31.8 | 50.0 | 45.5 | 20.0 | 22.7 | |
| rs4963304 | G/A | 10.0 | 68.2 | 50.0 | 31.8 | 40.0 | 0.0 | * |
| rs7931563 | T/G | 50.0 | 40.9 | 50.0 | 40.9 | 0.0 | 18.2 | |
| rs7942387 | C/A | 90.0 | 100.0 | 10.0 | 0.0 | 0.0 | 0.0 | |
| rs198430 | C/T | 30.0 | 77.3 | 40.0 | 22.7 | 30.0 | 0.0 | * |
| rs198444 | T/C | 40.0 | 4.5 | 60.0 | 45.5 | 0.0 | 50.0 | * |
| rs34365114 | G/A | 100.0 | 95.5 | 0.0 | 4.5 | 0.0 | 0.0 | |
| rs144674730 | C/T | 100.0 | 100.0 | 0.0 | 0.0 | 0.0 | 0.0 | |
| rs143650244 | AAA/- | 90.0 | 100.0 | 10.0 | 0.0 | 0.0 | 0.0 | |
| rs187296513 | C/T | 100.0 | 100.0 | 0.0 | 0.0 | 0.0 | 0.0 | |
| rs3813518 | G/A | 50.0 | 77.3 | 50.0 | 18.2 | 0.0 | 4.5 | |
| rs3813517 | A/G | 100.0 | 95.5 | 0.0 | 4.5 | 0.0 | 0.0 | |
| rs836559 | C/G | 10.0 | 36.4 | 40.0 | 45.4 | 50.0 | 18.2 | |
| rs2303361 | T/C | 40.0 | 72.8 | 30.0 | 22.7 | 30.0 | 4.5 | |
| rs76802560 | G/T | 100.0 | 100.0 | 0.0 | 0.0 | 0.0 | 0.0 | |
| rs6801421 | G/A | 90.0 | 63.6 | 10.0 | 36.4 | 0.0 | 0.0 | |
| rs72969613 | C/T | 100.0 | 100.0 | 0.0 | 0.0 | 0.0 | 0.0 | |
| rs4881 | A/G | 70.0 | 81.8 | 20.0 | 18.2 | 10.0 | 0.0 | |
| rs115970931 | A/G | 100.0 | 100.0 | 0.0 | 0.0 | 0.0 | 0.0 | |
| rs932816 | G/A | 80.0 | 50.0 | 20.0 | 45.5 | 0.0 | 4.5 | |
| rs4141964 | G/A | 30.0 | 40.9 | 30.0 | 40.9 | 40.0 | 18.2 | |
| rs324420 | C/A | 30.0 | 59.1 | 50.0 | 22.7 | 20.0 | 18.2 | |
| rs324419 | G/A | 80.0 | 81.8 | 20.0 | 18.2 | 0.0 | 0.0 | |
| rs2295632 | C/A | 30.0 | 54.5 | 40.0 | 27.3 | 30.0 | 18.2 | |
| rs12029329 | G/C | 30.0 | 54.5 | 40.0 | 27.3 | 30.0 | 18.2 | |

| SNP | Major/minor alleles | % major homozygosity | | % heterozygosity | | % minor homozygosity | | Disease association |
|---|---|---|---|---|---|---|---|---|
| | | Control | FCD | Control | FCD | Control | FCD | |
| rs12744386 | C/T | 10.0 | 31.8 | 70.0 | 50.0 | 20.0 | 18.2 | |
| rs1130321 | A/G | 20.0 | 27.3 | 80.0 | 54.5 | 20.0 | 18.2 | |
| rs1106 | G/C | 20.0 | 27.3 | 80.0 | 54.5 | 20.0 | 18.2 | |
| rs2229579 | C/T | 70.0 | 63.6 | 30.0 | 27.3 | 0.0 | 9.1 | |
| rs2501431 | A/G | 20.0 | 27.3 | 80.0 | 54.5 | 20.0 | 18.2 | |
| rs41311993 | G/T | 100.0 | 100.0 | 0.0 | 0.0 | 0.0 | 0.0 | |
| rs35761398 | CC/TT | 20.0 | 23.8 | 80.0 | 57.2 | 20.0 | 19.0 | |
| rs2501432 | C/T | 20.0 | 27.3 | 80.0 | 54.5 | 20.0 | 18.2 | |

The rest of SNPs analysed for *CNR1*, *DAGLB*, *MGL*, *FAAH* and *CNR2* did not show any difference between pathologic samples and controls. To further investigate the potential involvement of $CB_1R$ in FCD we sequenced the *CNR1* gene exon in FCD and control genomic DNA samples. *CNR1* exon 1 sequencing revealed normal wild-type sequence in most samples and only rs1049353 SNP (c.1359G>A; p.Thr453) was identified with similar distribution among dysplastic and control DNA.

In summary, these results suggest that the DAGLα-evoked generation of the endocannabinoid 2-AG might be altered in FCD Type II and can contribute to its etiopathology. However, the exact contribution of endocannabinoid tone alterations in MCDs would require more complex genetic studies to identify its potential association with the origin of the disease.

### R1.4. $CB_1$ receptor crosstalk with the mTORC1 pathway in focal cortical dysplasia resections

Additional specimens derived from surgical resection for intractable epilepsy were analysed *ex vivo* for mechanistic studies. 3T magnetic resonance imaging (MRI), positron emission tomography with fluorodeoxyglucose (FDG-PET) scan, scalp electroencephalography (EEG) recording and invasive neurophysiological studies were employed to identify the origin of epileptic seizures (Figure R1.4A). Representative images of one case prior and after surgery are shown. In this particular patient, a small FCD Type II involving the left rolandic region and superior frontal gyrus (arrowheads, Figure R1.4A) was associated with daily focal motor seizures and Epilepsia Partialis Continua involving the left arm and the face. Scalp EEG analyses revealed continuous focal epileptiform discharges (arrowhead, Figure R1.4B) in accordance with a hypermetabolic FDG-PET focus. Intracraneal EEG exploration of the dysplastic lesion, using a combination of subdural electrodes and depth electrodes, better defined a characteristic EEG pattern, indicative of FCD.

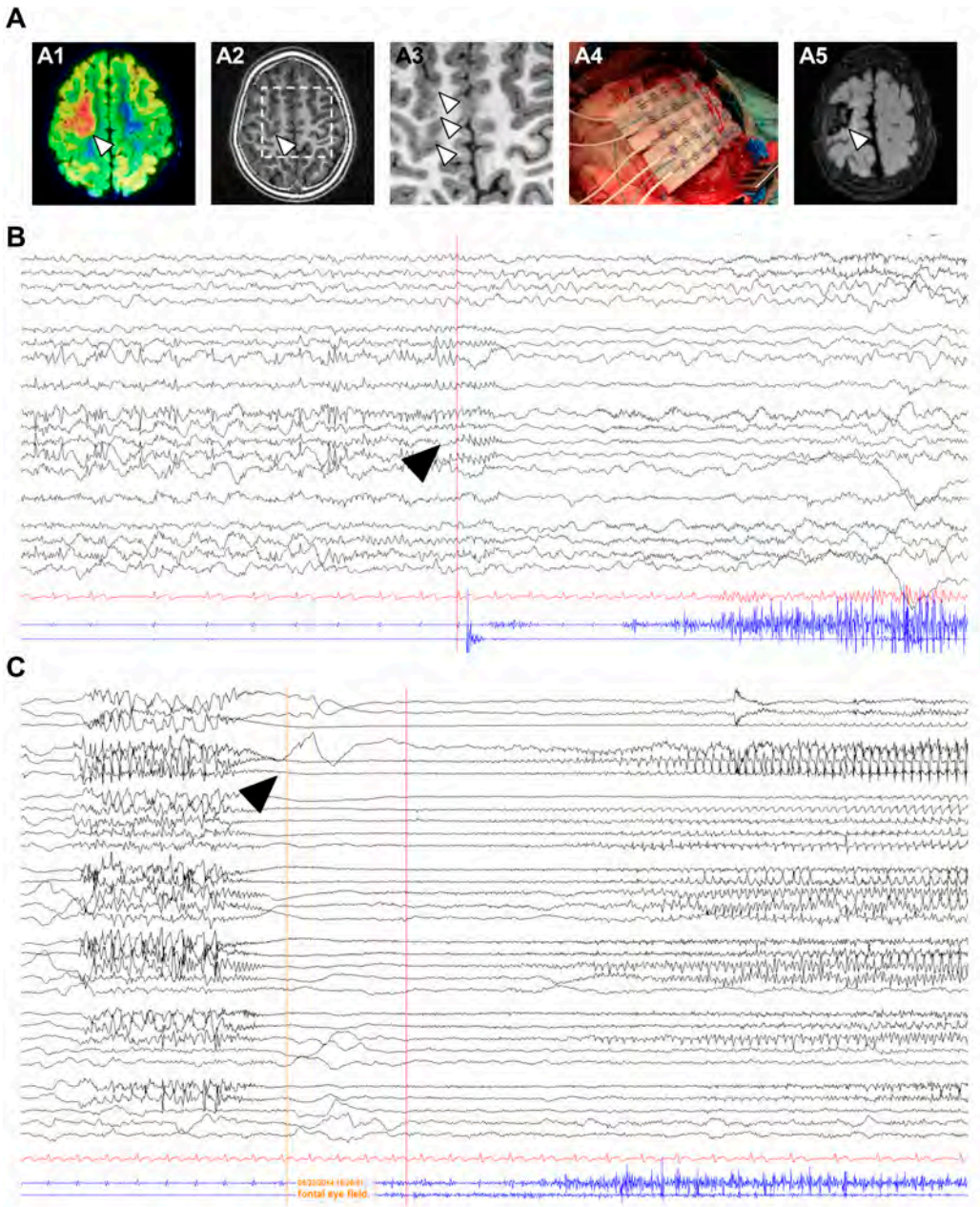


**Figure R1.4. EEG characterization of a representative FCD case subject to surgery.** (**A**) FDG-PET scan (**A1**) co-registered with 3T MRI imaging (**A2**, an inset is included in **A3**) of a 5 years old affected by a "malignant rolandic epilepsy" with daily motor seizures and Epilepsia Partialis Continua. (**A4**) Representative example of the electrode grid used during surgeries. (**A5**) MRI one year after epilepsy surgery. White arrowheads indicate hypermetabolic FDG-PET focus (red zone, **A1**), small FCD involving the left rolandic region and superior frontal gyrus (**A2**), grey-white matter blurring (**A3**), and resected tissue (**A5**). (**B-C**) Scalp and intracraneal EEG recording, respectively, of the previous patient, using a combination of subdural electrodes and depth electrodes, prior resection of the epileptogenic zone. Black arrowheads indicate epileptiform activity.

This characteristic EEG pattern shows continuous repetitive burst of epileptiform activity turning into focal EEG ictal patterns (arrowhead, Figure R1.4C), in association with the onset of clinical seizure signs. After tailored resection of the epileptogenic zone, one year follow-up after surgery revealed a seizure-free clinical status, MRI and EEG showed absence of the lesion and normalization of hyperexcitability.

Considering the regulatory role of $CB_1R$ in cortical progenitor cell identity *via* mTORC1 signalling (Díaz-Alonso *et al.*, 2015), we next sought to investigate the impact of the receptor in FCD-derived neurons. We obtained FCD Type II organotypic cultures derived from fresh resections that were maintained for 7 days *in vitro* and subjected to pharmacological manipulation. Quantification of pS6 immunoreactivity revealed that $CB_1R$ activation with the cannabinoid agonist HU-210 was without effect on mTORC1 activation, whereas the mTORC1 inhibitor rapamycin was effective in reducing mTORC1 overactivation (Figure R1.5A). Western blot analysis confirmed that $CB_1R$ agonism did not influence mTORC1 activation, whereas the $CB_1R$ inverse

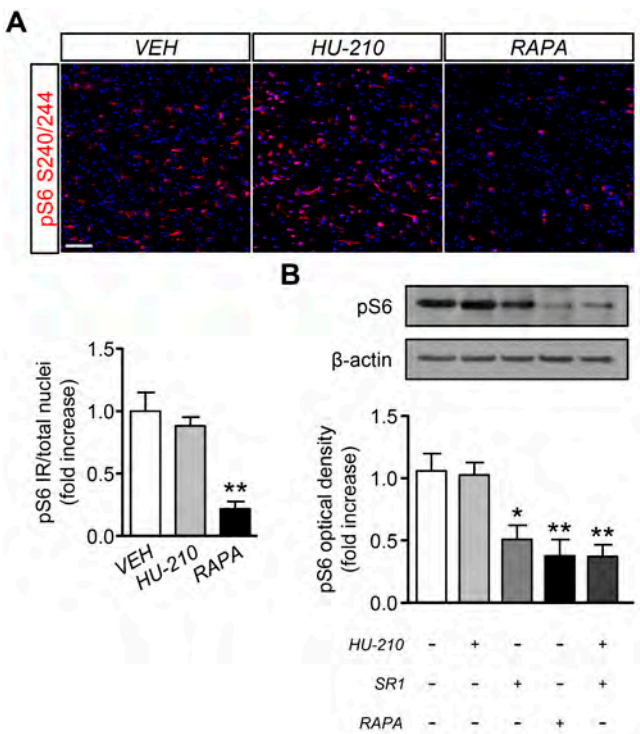


**Figure R1.5. $CB_1$ receptor blockade attenuates mTORC1 overactivation in FCD organotypic cultures.** Organotypic cultures of FCD resections were cultured 7 days *in vitro* and exposed to the $CB_1R$ agonist HU-210 (1 μM), and rapamycin (1 μM) for 90 min. (**A**) Representative images of immunofluorescence characterization with anti-pS6 S240/244 antibody were quantified and pS6 immunoreactivity was referred to the total number of cells revealed by DAPI counterstaining (n = 4 experiments). (**B**) Western blot analysis of pS6 S240/244 levels was performed in slice extracts after 90 min incubation with HU-210 alone or together with SR141716 (25 μM), SR141716 alone or rapamycin (n = 4 experiments). Statistical comparison *versus* vehicle samples: *p < 0.05; **, p < 0.01. Scale bar: 80 μm.

agonist SR141716 (rimonabant), as well as rapamycin, reduced mTORC1 activation as assessed by pS6 S240/244 levels (Figure R1.5B). Overall, these results indicate that inhibition, but not activation of the $CB_1R$, may tune the overactive mTORC1 pathway found in FCD Type II dysplastic brain.

### R1.5. Transient $CB_1$ receptor knockdown alters maturation and impaired circuit integration in upper-layer neurons

The added value of experiments with human tissue obtained from resections of MCDs cases is hampered by the extreme difficulty inherent to use this kind of material as well as the limitations that it offers in terms of approaching mechanistic questions. Hence, the use of human derived tissue generally does not allow to fully address if the observed alterations are a primary direct consequence of the disease or just a secondary maladaptation. With this in mind, we moved to a developmental approach by performing IUE experiments in animal models. Previous findings have demonstrated that embryonic $CB_1R$ acute knockdown fosters a delay in the radial migration of cortical PNs, which in turn increases seizure susceptibility (Díaz-Alonso *et al*., 2017). However, the impact of this migration delay in the acquisition of a mature neuronal phenotype, in regard of excitability, remains unknown. Thus, we decided to perform whole-cell patch-clamp experiments on acute brain slices obtained at different time points (P7, P14, P21, P60) from wild type mice subjected to IUE in the mPFC with either $siCB_1$ or siCo at E14, in order to determine if there is a causal link between an early ECS malfunctioning and the seizure-prone phenotype observed in animal models.

After confirming that a radial migration delay was apparent at E17 (Figure R1.6A), we verified that in adult stages (P60) the majority of the $GFP^+$ neurons had properly reached the upper layers, the laminar fate determined by their birthdate, as neurons born at E14 are bound to migrate towards layers II/III (Greig *et al*., 2013). We first characterized these properly-migrated neurons.

By means of current-clamp experiments, we analysed passive properties of $GFP^+$ neuron membranes (Figure R1.6B, C). In general terms, RMP became hyperpolarized with age in both experimental conditions, due to maturation of neurons and cortical circuits, although we recorded a slight depolarization in adults from the control group with respect of the immediate preceding age (P21). When comparing conditions, we found a depolarized RMP in $CB_1R$-knocked down cells at P7 and in the adult mice (P60) (Figure R1.6B). Input resistance also decreased with age, although showing different

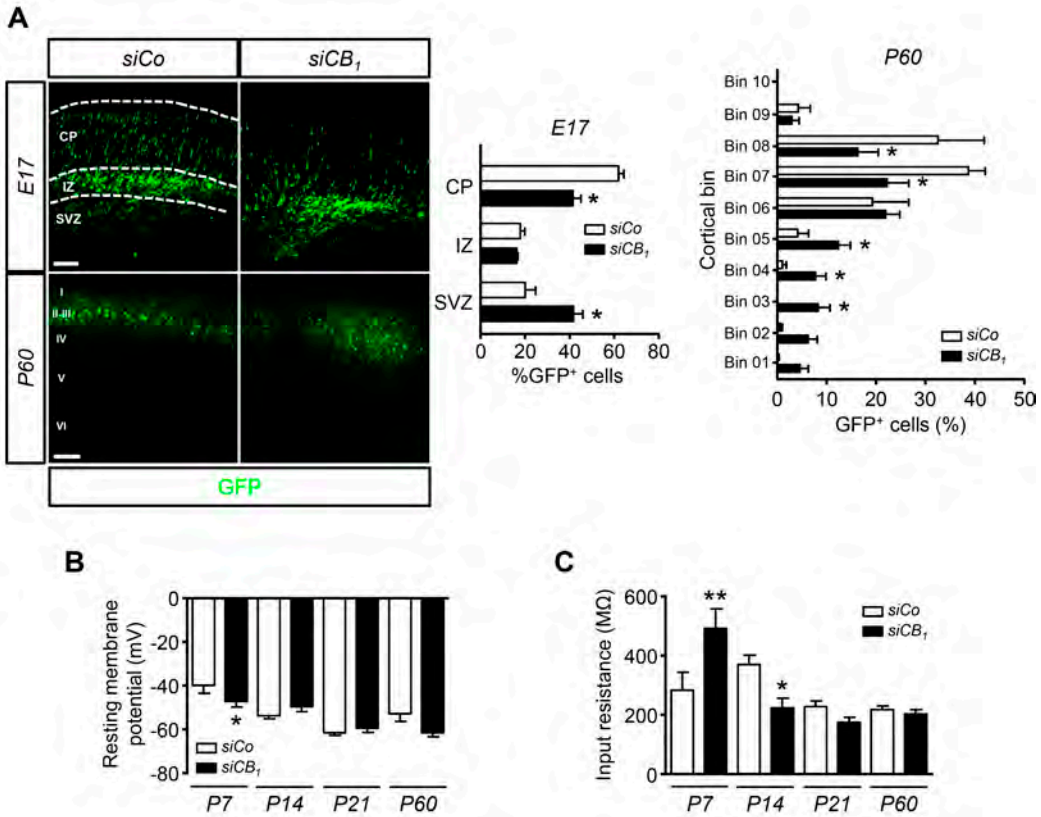


**Figure R1.6. Transient $CB_1$ receptor knockdown impairs radial migration and alters passive electrophysiological properties.** Murine embryos were electroporated at E14 with either $siCB_1$ or siCo. Brains were dissected at different ages and analysed by immunofluorescence or whole-cell patch clamp. (**A**) Representative immunofluorescence images and quantification showing altered neuronal migration at E17, expressed as percentage of $GFP^+$ cells located within each compartment of the developing cortical wall (VZ/SVZ, IZ and CP). At P60, although most of the cells have reached the upper cortical layers, $GFP^+$ cells arrested in the deep layers can be observed only in $siCB_1$-electroporated animals. (n = 5 animals per group). (**B**) RMP measured in whole-cell current clamp experiments at four different ages (P7, P14, P21, P60). [n = (siCo: 17, 29, 19 and 13 cells; P7, P14, P21 and P60, respectively); ($siCB_1$: 22, 20, 13 and 16 cells; P7, P14, P21 and P60, respectively)]. (**C**) Input resistance measured in the same conditions. Same dataset as RMP. Statistical comparison *versus* the corresponding siCo group: *, $p < 0.05$; **, $p < 0.01$. Scale bars: E17: 100 µm, P60: 150 µm.

trends in the two groups. While control neurons reached a plateau at P21, $siCB_1$-targeted cells stabilized earlier, at P14. After showing a 2-fold increase at P7 with respect to the control group, input resistance of the $siCB_1$-targeted neurons quickly decreased and by P14 it had reached its stabilization value (Figure R1.6C). Changes in passive membrane properties may indicate a shift in the neuronal ionic channel expression profile, a trait that evolves with neuronal maturation. Thus, these findings, especially when their age pattern is taken into account, support that the migration delay elicited by acute $CB_1$R-knockdown provokes in turn a disruption in the maturation pace of developing neurons.

Still in current-clamp configuration, we evaluated the active electrophysiological properties of the targeted cells (Figure R1.7). We determined the firing frequency in the three

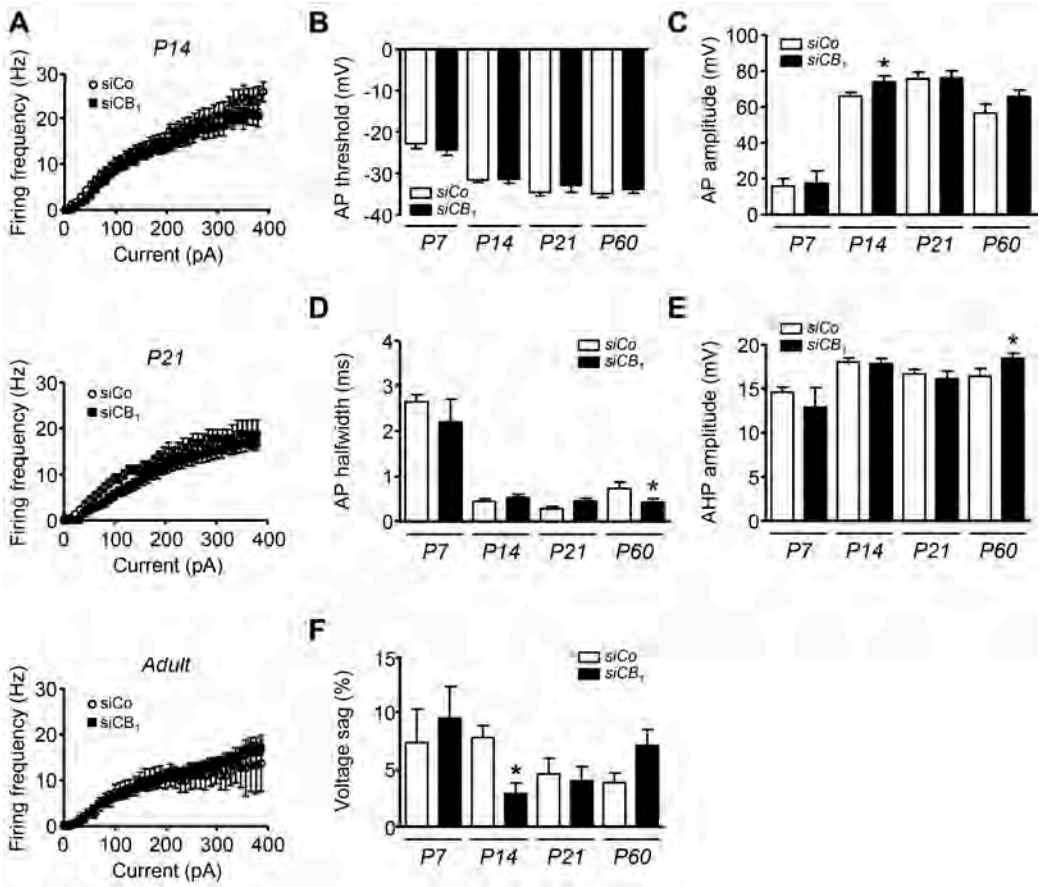


**Figure R1.7. Transient $CB_1$ receptor knockdown alters the maturation pace of properly migrated neurons.** Active electrophysiological properties were evaluated in the same cells, also in whole-cell current clamp configuration. (**A**) AP firing rate was measured at P14, P21 and P60, as it was inconsistent at P7. (**B-F**) Other active properties were recorded in the four time points, including P7. Specifically, we evaluated: (**B**) AP threshold, (**C**) AP amplitude, (**D**) AP halfwidth, (**E**) AHP amplitude and (**F**) voltage sag. The trends observed among the different time stages point to a differential expression of ionic channels, which suggest a divergent maturation rate upon transitory $CB_1$R-expression reduction by $siCB_1$ electroporation. [n = (siCo: 17, 29, 19 and 13 cells; P7, P14, P21 and P60, respectively); ($siCB_1$: 10, 20, 13 and 16 cells; P7, P14, P21 and P60, respectively)]. Statistical comparison *versus* the corresponding siCo group: *, $p < 0.05$.

older time points (P14, P21, P60), as patched cells in P7, even though they were able to develop APs, did it in a much slower and irregular pace. Nevertheless, firing frequency was similar in the two conditions across all the different ages (Figure R1.7A). We found similar age-dependent tendencies in both groups for AP threshold, AP half-width and AP amplitude. While the two former showed higher values at P7 that decreased and stabilized at P14 (Figure R1.7B, D), the latter exhibited the opposite trend, stabilizing at P14 after increasing from P7 (Figure R1.7C). Among all the time points studied in the three parameters, we found differences in the AP amplitude at P14 (higher in knocked down cells) and the AP half-width at adulthood (lower in $siCB_1$-targeted cells). We also measured the amplitude of the AHP that follows an AP and its voltage sag (Figure R1.7E, F).

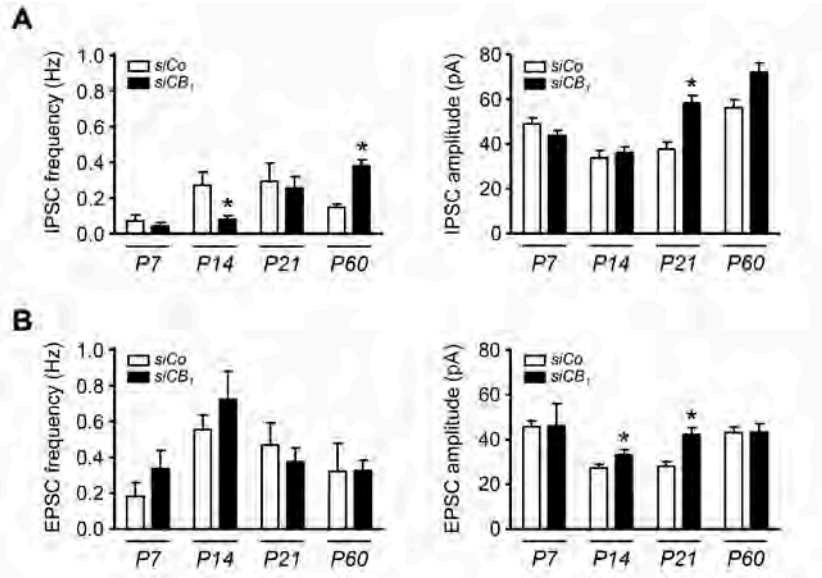


**Figure R1.8. Neurons that reach their proper laminar destination show a defective integration in cortical circuits.** Cells analysed in current clamp configuration were also studied under voltage clamp conditions in order to assess the frequency and amplitude of postsynaptic events affecting them. Both parameters were analysed for (**A**) IPSC events, and (**B**) EPSC events. The differences found when comparing both experimental conditions at multiple stages suggest that siCB$_1$-electroporated neurons, even if they reach their destination, do not integrate in circuit assemblies in the same way as their siCo-electroporated counterparts. [n = (siCo: 10, 31, 12 and 4 cells; P7, P14, P21 and P60, respectively); (siCB$_1$: 3, 16, 9 and 12 cells; P7, P14, P21 and P60, respectively)]. Statistical comparison *versus* the corresponding siCo group: *, $p < 0.05$.

Although AHP in both groups presented again similar age-related trends (a slight increase and stabilization from P7 to P14), it was increased in adult neurons from the siCB$_1$-targeted group. Voltage sag, which decreased with age, was lower in siCB$_1$-electroporated cells at P14 with respect to siCo neurons. These data reinforces the rationale that the transient depletion of CB$_1$R during embryonic development influences neuronal maturation and likely modifies the the ion channel expression signature.

Moving to a voltage-clamp configuration, we determined the spontaneous synaptic activity (i.e. IPSCs and EPSCs) that patched cells developed in response to synaptic inputs coming from the circuits in which they assemble, to assess if there was any difference in circuit integration among both conditions (Figure R1.8). While IPSCs frequency was decreased at P14 and increased in adult CB$_1$R-knocked down neurons (Figure R1.8A), no changes were appreciable in EPSCs (Figure R1.8B). Conversely, IPSCs amplitude was increased in P21 in siCB$_1$-electroporated cells (Figure R1.8A), but also EPSCs amplitude was higher in those cells both at P14 and P21 (Figure R1.8B). These observations point that transient CB$_1$R knockdown alters not only the maturation pace of cortical PNs, but also the way in which they integrate in their corresponding cortical circuits.

## Aim 2: Summary

Exposure of the immature brain to cannabinoids exerts deleterious functional consequences in adulthood by interfering with neural cell development, as well as with neuronal differentiation and connectivity (Grant *et al*., 2018). Thus, perinatal THC exposure induces changes in glutamatergic and noradrenergic signalling that are, at least in part, responsible of the cognitive deficits observed in adults (Mereu *et al*., 2003; Campolongo *et al*., 2007). Embryonic THC exposure impairs NMDAR-dependent LTD (Tortoriello *et al*., 2014). Similarly, maternal cannabis consumption results in a selective dopaminergic D2R (but not D1R) impairment in the mesolimbic system (Dinieri *et al*., 2011; Morris *et al*., 2011).

THC interferes with the neurodevelopmental role of the ECS (Galve-Roperh *et al*., 2013; Maccarrone *et al*., 2014). $CB_1R$, upon engagement by 2-AG and AEA, regulates crucial steps of cortical development as IN migration and morphogenesis. Thus, the number of hippocampal CCK-containing basket cells can be influenced by embryonic THC (Berghuis *et al*., 2005), or WIN-55,212-2 (Vargish *et al*., 2016) exposure. However, embryonic THC administration can also interfere with pyramidal neuron development (de Salas-Quiroga *et al*., 2015), which leads to an unbalanced excitation/inhibition state and higher susceptibility to seizures. Studies using both conditional $CB_1R$ knock-out and $CB_1R$-rescue in a null background demonstrated that THC-induced proconvulsive status relies at least in part in alterations in both PNs and GABAergic INs. In this chapter, we investigated the neurodevelopmental consequences of prenatal THC exposure by focusing on hippocampal plasticity and sex-dependent dimorphic sensitivity, given the role of temporal lobe circuits in memory function and epilepsy.

## Aim 2. Implication of $CB_1$ receptor in the establishment of CCK-containing interneurons in the hippocampus

### R2.1. Embryonic THC exposure evokes long-term interneuronal alterations in a sex-dimorphic manner

To assess the impact of prenatal THC administration throughout IN embryonic development, we defined the temporal window of drug delivery at 3 mg/kg (i.p.) from E10 to E17. At P20, analysis of $CB_1R$ immunoreactivity in the dorsal hippocampus of wild type mice prenatally exposed to THC showed a male-specific decrease of $CB_1R$ levels with respect to vehicle-treated mice (Figures R2.1A and R2.2A, B). Interestingly, no significant differences were found for sex or treatment in other areas as the PFC or somatosensory cortex (SSC) (Figure R2.2C, D). Of note, the vast majority of immunoreactivity that is detected under these experimental conditions corresponds to $CB_1R^+$ terminals of GABAergic INs (Monory *et al*., 2006; de Salas-Quiroga *et al*., 2015). Hence, we decided to focus on CA1 CCK-containing basket cells, the population of hippocampal INs that expresses the highest levels of $CB_1R$ in the mouse forebrain (Marsicano and Lutz, 1999). Perisomatic $CB_1R$ immunoreactivity at CA1 *sp* was reduced in the THC-exposed male progeny compared to its vehicle-treated counterpart (Figure R2.1B). No differences were found for females treated with either THC or its vehicle.

Next, we evaluated whether these alterations are due to a previously described morphogenetic role of $CB_1R$ in developing INs (Berghuis *et al*., 2007) or to a decrease in the total numbers of $CCK^+$ INs. To address this question, we performed ISH with a riboprobe against CCK, combined with anti-GABA IHC, to unequivocally identify CCK-containing hippocampal INs, given the broad expression of CCK by CA1 pyramidal neurons (Figures R2.1C and R2.2E). Stereological analysis showed a selective reduction of CA1 $CCK^+$ IN density in THC-treated males as compared either to vehicle-treated males, or to females, irrespective of the treatment. Taken together, these findings support that adult mice exposed to THC during embryonic development exhibit an overt interneuronopathy with a remarkable sexual dimorphism. To rule out the possibility that sexual differences emerge from pharmacokinetic factors, such as THC bioavailability, we measured THC levels in E17-brain tissue (i.e., 12 hours after the last THC injection) and found similar values in both sexes (Figure R2.2F). In addition, as protracted embryonic THC exposure leads to a transient downregulation of $CB_1R$ (de Salas-Quiroga *et al*., 2015), we asked whether a sex-dimorphic $CB_1R$ down-

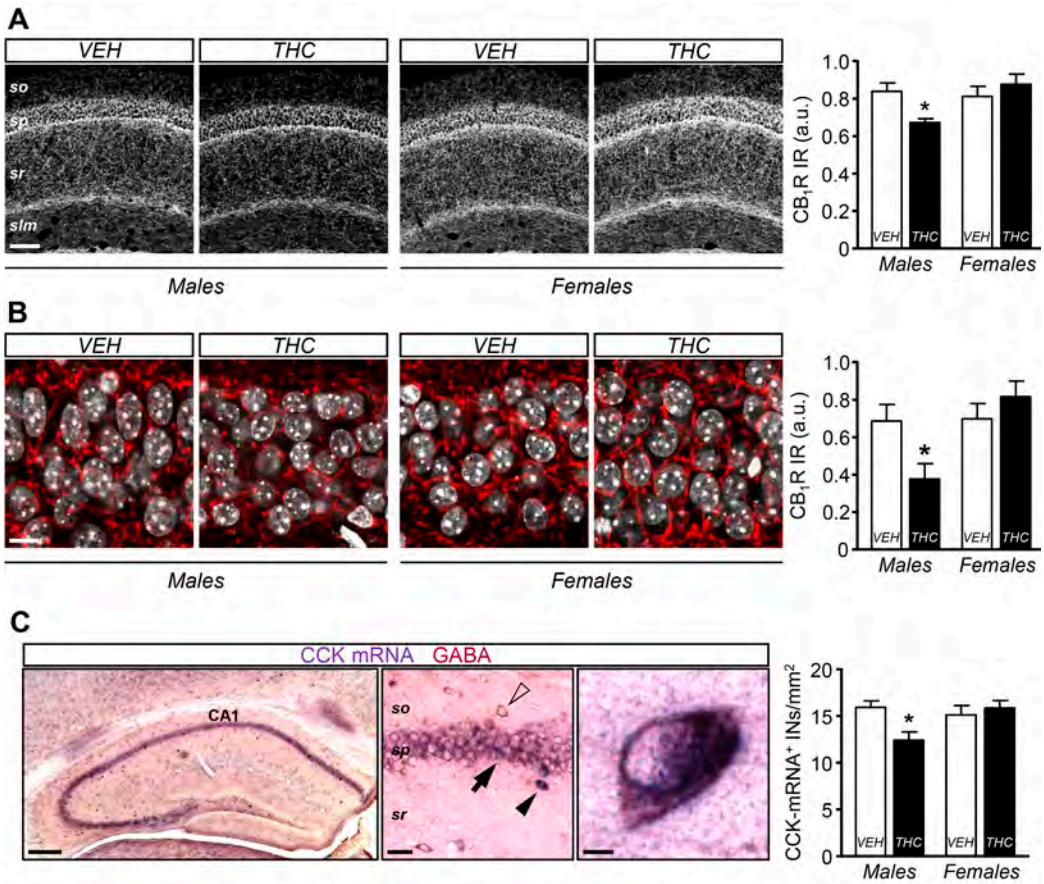


**Figure R2.1. Prenatal THC exposure induces a sex dimorphic long-lasting hippocampal $CB_1$ receptor adaptation and $CCK^+$ basket cell interneuronopathy.** (**A**) Representative images and quantification of $CB_1R$ immunoreactivity (IR) measured in the CA1 hippocampal region of P20 mice prenatally exposed to THC (3 mg/kg) or its vehicle. (**B**) $CB_1R$ immunoreactivity quantified in the *sp* of CA1 in the same mice. (**C**) Representative images of CCK ISH and GABA IHC in the hippocampus, and quantification of basket cells identified as $CCK^+/GABA^+$ double-positive cells (black arrowhead). $CCK^+/GABA^-$ (arrow) and $GABA^+/CCK^-$ (hollow arrowhead) cells were excluded from the quantification. (n = 7 animals per group). Statistical comparison *versus* the corresponding vehicle group: *, $p < 0.05$. Scale bars: **A**: 50 µm; **B**: 10 µm; **C**: left: 150 µm, center: 25 µm, right: 5 µm.

regulation might be responsible for the observed effects. [$^{35}$S]GTPγS binding analysis in E17-brain tissue revealed an evident downregulation of $CB_1R$ after embryonic THC exposure, but comparable curves were obtained for both sexes (Figure R2.2G).

## R2.2. Prenatal THC exposure alters main hippocampal oscillations in adult males

CCK-containing basket cells are essential for proper hippocampal physiology and function (del Pino *et al*., 2017). Hence, we decided to further characterize the aforementioned THC-induced deficits *via* intrahippocampal recordings. Specifically, we performed *in vivo* electrophysiological recordings of the LFP throughout CA1 in the hippocampus of head-fixed freely moving P60 mice (Figure R2.3A).

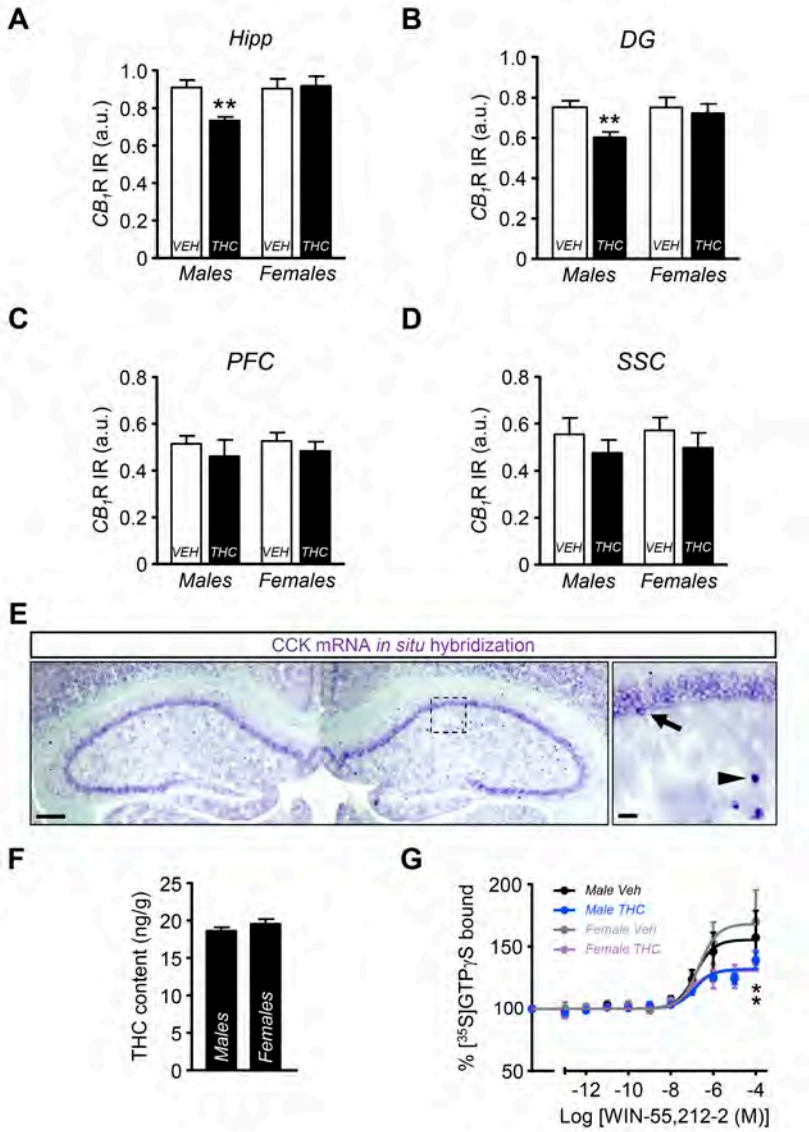


**Figure R2.2. Sex divergent and long-lasting $CB_1$ receptor expression plasticity affects selectively hippocampal region.** (**A-D**) $CB_1R$ immunoreactivity (IR) quantification in the progeny of vehicle- or THC- treated pregnant dams. $CB_1R$ levels were analysed in the whole hippocampus (**A**), dentate gyrus (**B**), prefrontal (**C**) and somatosensory (**D**) cortices (n= 5 animals per group). (**E**) Hippocampal formation stained by CCK ISH without GABA IHC. Inset: positive cells outside *sp* (arrowhead) can be considered as $CCK^+$ basket cells safely, whereas positive cells inside *sp* (arrow) may be basket or pyramidal cells, needing an additional interneuronal marker as GABA to be fully identified. (**F**) THC levels were determined in brain extracts from E17 embryos after prenatal exposure to THC or its vehicle (n = 6 animals per group). (**G**) $[^{35}S]GTP\gamma S$ binding was determined in brain membrane extracts obtained from the same embryo cohorts (n = 6 pooled samples per group, each pool consisting of 3 E17.5 brains). Statistical comparison *versus* corresponding vehicle group: *, $p < 0.05$; **, $p < 0.01$. Scale bars: 150 µm; inset: 25 µm.

During running, theta (4-12 Hz) and gamma oscillations (30-60 Hz) typical of exploratory behaviour were recorded across layers (Figure R2.3B). Spectral analyses of the LFP signal revealed changes in the theta band that were confined to the *sp* of CA1 (Figures R2.3C, D and R2.4A, B). THC treatment was associated with a non-significant reduction of the gamma power at *sp* in both males and females, thus suggesting that some alterations may not have a dimorphic component (Figure R2.3E). These data are consistent with the idea of a complementary role of CCK-containing basket cells in hippocampal theta and gamma oscillations (Klausberger *et al*., 2005).

Next, we analysed SWR (Figure R2.3F), a major hippocampal high-frequency oscillation (HFO) recorded during immobility and sleep that is crucial for learning and memory consolidation (Buzsáki, 2015). SWR emerge from the oscillatory firing of pyramidal cell ensembles, controlled by the interplay between excitation and basket cell-mediated inhibition (Stark *et al*., 2014). In diseases affecting the hippocampal formation, such as temporal lobe epilepsy and Alzheimer's disease, SWR are pathological and associated to severe cognitive deficits and epileptiform activities (Gillespie *et al*., 2016; Valero *et al*., 2017). Spectral analysis of SWR in mice treated with THC confirmed some differences with a clear sex dimorphism (Figure R2.3G). First, the SWR rate was significantly higher in males exposed to THC as compared to females or vehicle-treated males, independently of the detection threshold (Figure R2.3H, I). Second, the typical bimodality of the spectral SWR peaks (Sullivan *et al*., 2011) was remarked in THC-treated male mice (Figure R2.3G), with many more slower (<120 Hz) than fast events (>120 Hz) (Figure2.3J). This reflects a larger proportion of high-gamma SWR in THC-exposed males as compared to the other groups (Figure R2.3K). No significant changes were found in other measures of spectral distribution such as entropy and fast ripple index (Figure R2.4C-F). Taken together, these observations provide functional evidence for aberrant hippocampal microcircuit function caused by a persistent reduction of CCK-containing INs and oscillatory defects that predict cognitive alterations in males prenatally exposed to THC. To test this idea further, we conducted NOR and OL memory tests. The former evaluates non-spatial, conceptual learning of object identity, which depends on multiple brain regions, while the latter provides a measure of spatial learning, which strongly relies on hippocampal function (Langston and Wood, 2010). We did not observe any interference of prenatal THC in the NOR paradigm, but THC-treated males performed poorly in the OL test as compared to females or their vehicle-treated counterparts (Figure R2.3L, M), consistent with the

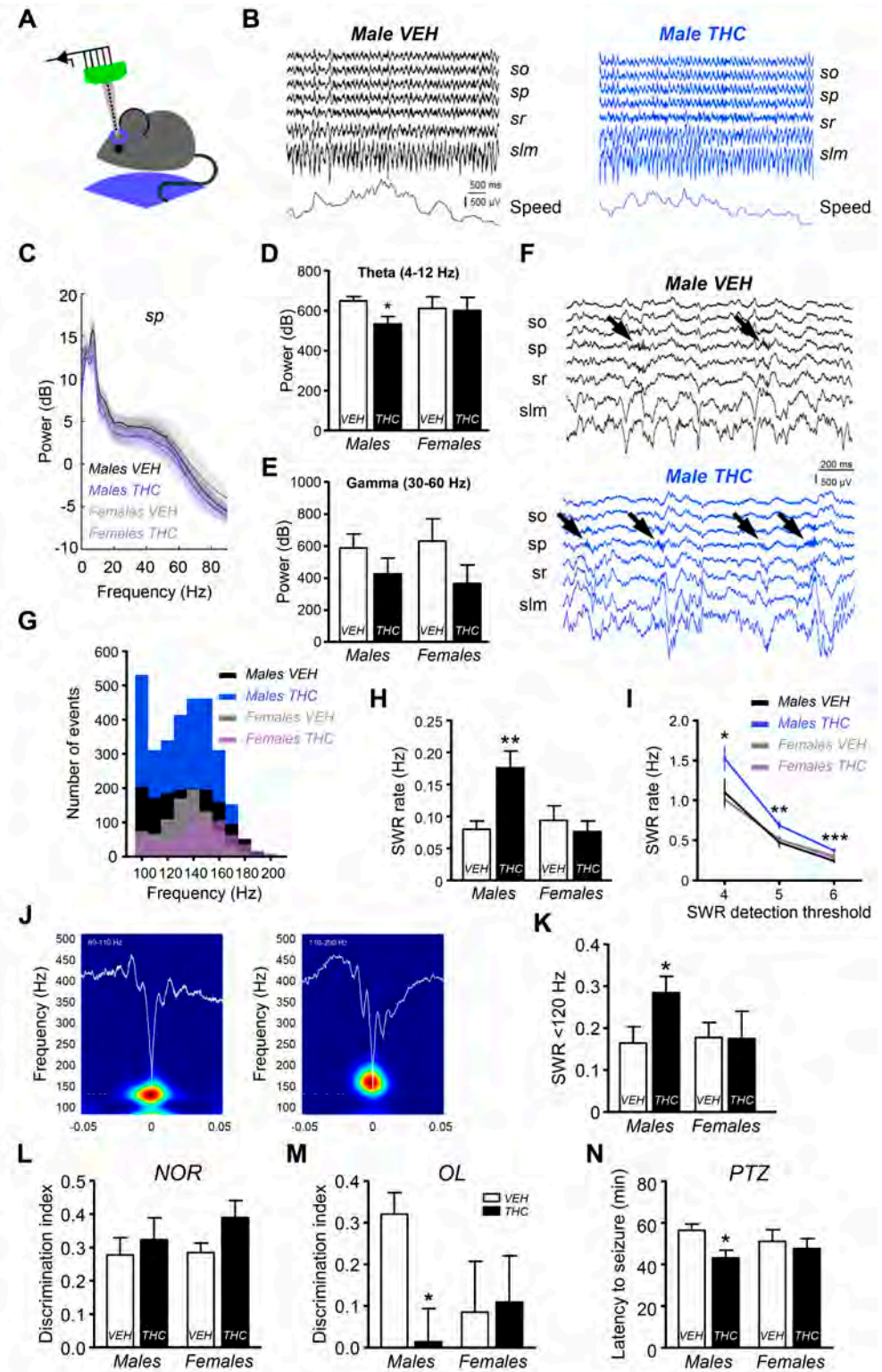


**Figure R2.3. Prenatal THC exposure induces sex-dimorphic alterations of hippocampal oscillations and spatial cognitive deficits.** See next page for detailed description.

**Figure R2.3. Prenatal THC exposure induces sex-dimorphic alterations of hippocampal oscillations and spatial cognitive deficits.** (**A**) Scheme of experimental set up. Mice were recorded head-fixed while running freely in a wheel. (**B**) Laminar recordings of LFP signals from a representative male mouse from each group (vehicle and THC). The running speed is shown at bottom. *so*, *stratum oriens*; *sp*, *stratum pyramidale*; *sr*, *stratum radiatum*; *slm*, *stratum lacunosum moleculare*. (**C**) Mean power spectra of running episodes show representative peaks at theta and gamma recorded at the pyramidal cell layer (*sp*). [n = (males: 15 and 15, vehicle- and THC-treated, respectively); (females: 8 and 4, vehicle- and THC treated, respectively)]. (**D**) Group differences of theta power were specific for male THC mice. Same dataset as above. (**E**) No differences were found in gamma power. (**F**) SWR events were recorded during immobility. Note higher event rate in THC treated males. (**G**) Distribution of spectral peaks per SWR events in the different groups. Note more number of events in THC-treated males and a larger contribution of slow ripple events. (**H**) SWR mean rate was higher in THC-treated males. (**I**) Consistent larger SWR rate across detection thresholds (in number of SD). (**J**) Examples of mean traces of slow (80-110 Hz) and fast (110-200 Hz) SRW events. (**K**) The proportion of slow SWR was significantly higher in the THC-treated male group. Same dataset as above. (**L**) Discrimination index in the NOR task was unchanged accross groups. [n = (males: 6 and 7, vehicle- and THC-treated, respectively); (females: 3 and 5, vehicle- and THC treated, respectively)]. (**M**) Discrimination index in the OL task was reduced specifically in THC-treated male mice. Same dataset as NOR task. (**N**) Latency to PTZ-induced seizures was significantly lower in the male THC group. [n = (males: 6 and 6, vehicle- and THC-treated, respectively); (females: 6 and 8, vehicle- and THC treated, respectively)]. Statistical comparison *versus* the corresponding vehicle group: *, $p < 0.05$; **, $p < 0.01$.

aforementioned electrophysiological data. In addition, we analysed susceptibility to PTZ-induced seizures and found selective effects in the male offspring (Figure R2.3N). Altogether, these data support deleterious sex-dimorphic effects of prenatal THC exposure caused by a CCK interneuronopathy.

## R2.3. $CB_1$ receptor located on GABAergic neurons is responsible for the sex-dimorphic interneuronopathy induced by embryonic THC exposure

To understand better the developmental mechanisms leading to CCK interneuronopathy in adulthood, we sought for a direct link between THC action and specific cellular targets. $CB_1R$ are expressed in various neuronal lineages throughout development (Galve-Roperh *et al*., 2013). To unequivocally assess the involvement of a specific subset of $CB_1R$ in the abovementioned defects, we made use of conditional knockout mice (Monory *et al*., 2006) lacking $CB_1R$ exclusively in dorsal telencephalic glutamatergic pyramidal cells ($CB_1R^{floxed/floxed}$::Nex-$Cre^{+/-}$ mice; herein referred to as Glu-$CB_1R$-KO) or in forebrain GABAergic neurons ($CB_1R^{floxed/floxed}$::Dlx5/6-$Cre^{+/-}$ mice; herein referred to as GABA-$CB_1R$-KO). Immunofluorescence analysis of perisomatic $CB_1R^+$ basket cell synapses at CA1 *sp* revealed a selective long-term decrease in $CB_1R^{f/f}$ males exposed to THC that was preserved in Glu-$CB_1R$-KO animals, pointing to an involvement of $CB_1R$ located on developing GABAergic INs in mediating THC actions (Figure R2.5A). In contrast, the remnant hippocampal $CB_1R$ immunoreactivity of GABA-$CB_1R$-KO mice exhibited no differences by sex or treatment. Additionally, we carried out anti-CCK ISH combined with anti-GABA IHC to label $CCK^+$ hippocampal INs in every genotype, sex, and treatment. Stereological analysis confirmed a persistent reduction of $CCK^+$ INs in $CB_1R^{f/f}$

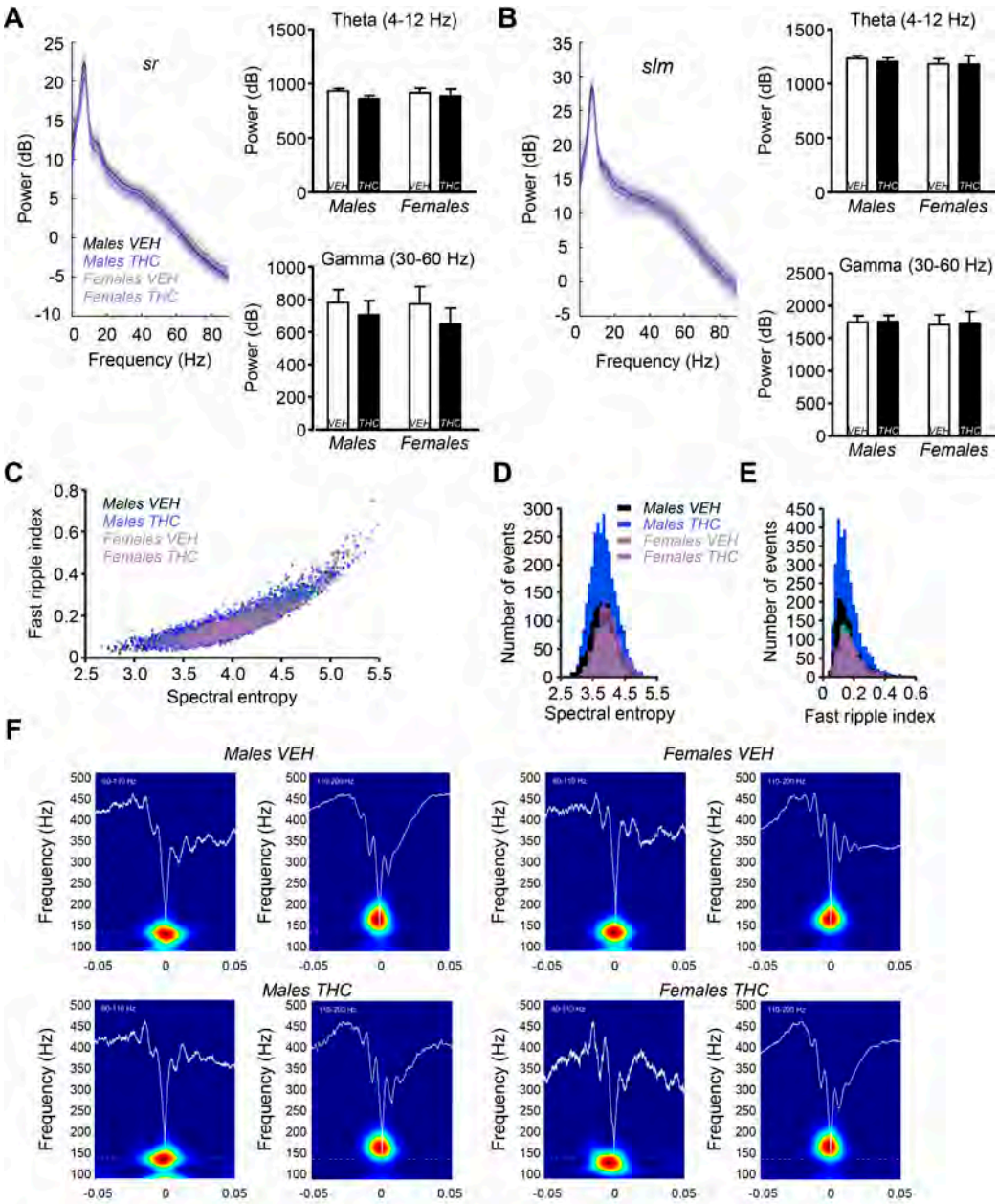


**Figure R2.4. Analysis of hippocampal oscillations.** (**A**) Mean power spectra of running episodes recorded at *stratum radiatum* (left) with mean group values for the theta and gamma band (right). (**B**) Mean power spectra of running episodes recorded at *stratum lacunosum moleculare* (left) with mean group values for the theta and gamma band (right). (**C**) Distribution of the spectral entropy and fast ripple index of all SWR events recorded from different groups. (**D**) Mean group histograms of spectral entropy of SWR show no overt differences. (**E**) Same for fast ripple index. (**F**) Mean traces of slow and fast SWR recorded from representative mice from each group.

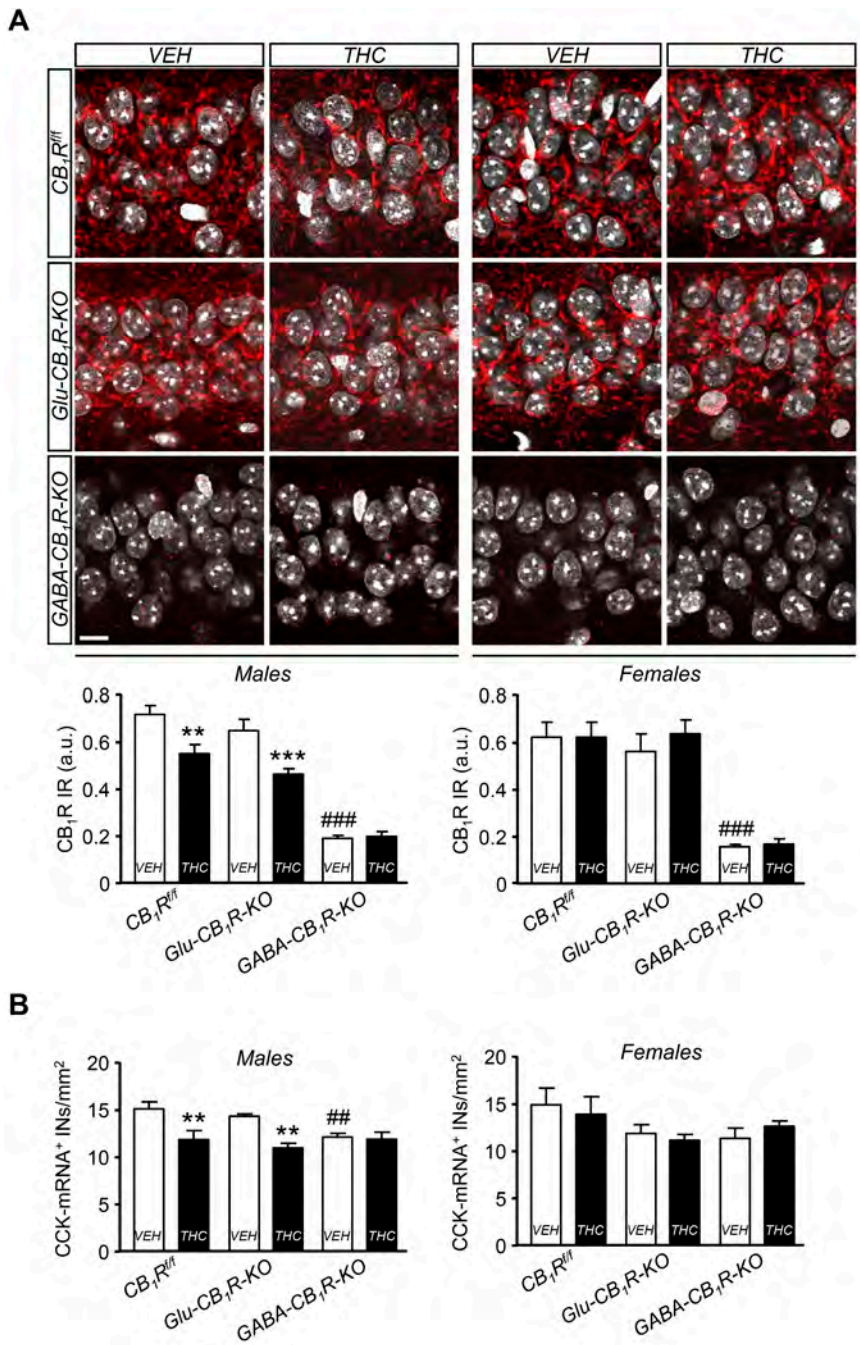


**Figure R2.5. Sex specific interneuronopathy elicited by prenatal THC exposure requires $CB_1$ receptor located on GABAergic neurons.** (**A**) Representative images and quantification of $CB_1R$ immunofluorescence in the *sp* of the CA1 region of Glu-$CB_1R$-KO, GABA-$CB_1R$-KO and $CB_1R^{f/f}$ P60 mice prenatally exposed to THC or its vehicle. (n = 5 animals per group). (**B**) Quantification of $CCK^+$ INs in the same animal groups. (n = 5 animals per group). Statistical comparison *versus* the corresponding vehicle group: **, $p < 0.05$; ***, $p < 0.001$. Statistical comparison *versus* the corresponding $CB_1R^{f/f}$ vehicle group: ##, $p < 0.01$; ###, $p < 0.001$. Scale bar: 10 μm.

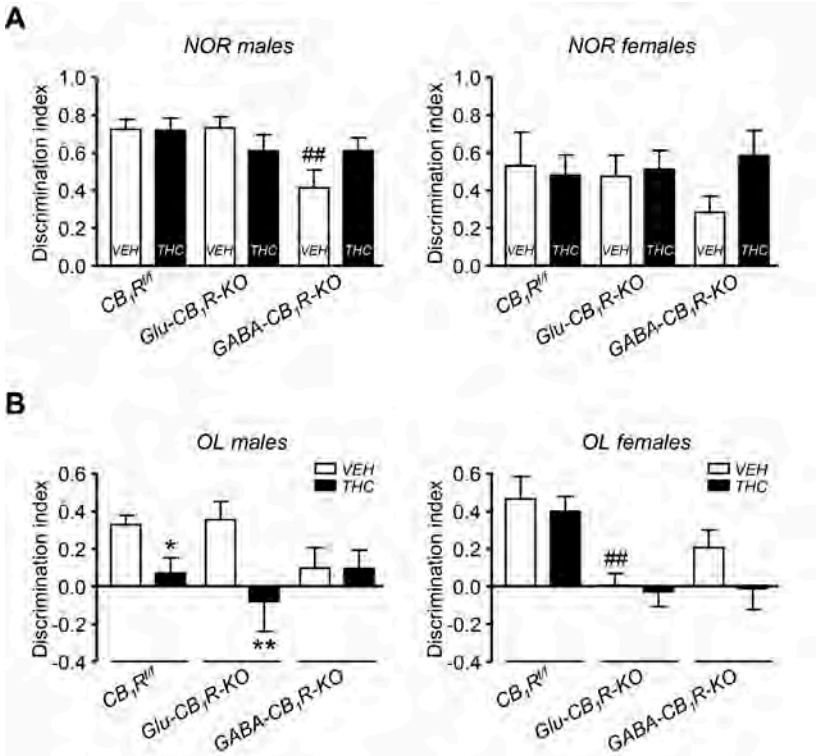


**Figure R2.6. Hippocampal-dependent spatial memory, but no object recognition memory, is altered by prenatal THC exposure specifically in males that preserve $CB_1$ receptor in GABAergic neurons.** (**A**) Novel object recognition test was performed in Glu-$CB_1$R-KO, GABA-$CB_1$R-KO and $CB_1R^{f/f}$ P60 mice, and a discrimination index was calculated for both males and females. (n = 5 animals per group). (**B**) Object location test was performed in the mentioned groups, a similar index was then calculated for males and females. (n = 5 animals per group). Statistical comparison *versus* the corresponding vehicle group: *, $p < 0.05$; **, $p < 0.01$. Statistical comparison *versus* the corresponding $CB_1R^{f/f}$ vehicle group: #, $p < 0.05$; ##, $p < 0.01$.

males prenatally exposed to THC compared to vehicle-treated ones (Figure R2.5B), while $CB_1R^{f/f}$ females exhibited comparable densities irrespective of treatment. Likewise, similar data were obtained in Glu-$CB_1$R-KO mice, whereas GABA-$CB_1$R-KO mice appeared refractory to THC impact in both males and females. Remarkably, conditional deletion of $CB_1$R in the GABAergic lineage *per se* led to a decrease in the density of $CCK^+$ hippocampal INs, only reaching statistical significance in the male population. These findings demonstrate the involvement of $CB_1$R located on hippocampal GABAergic INs as a main cellular substrate for the sex-dimorphic impact of embryonic THC exposure.

## R2.4. Cell-type specific sex dimorphism of $CB_1$R signalling is critical for adult hippocampal function

To unequivocally identify the neuronal population responsible for the prenatal THC-induced cognitive impairment, we performed the NOR and OL tests in condi-

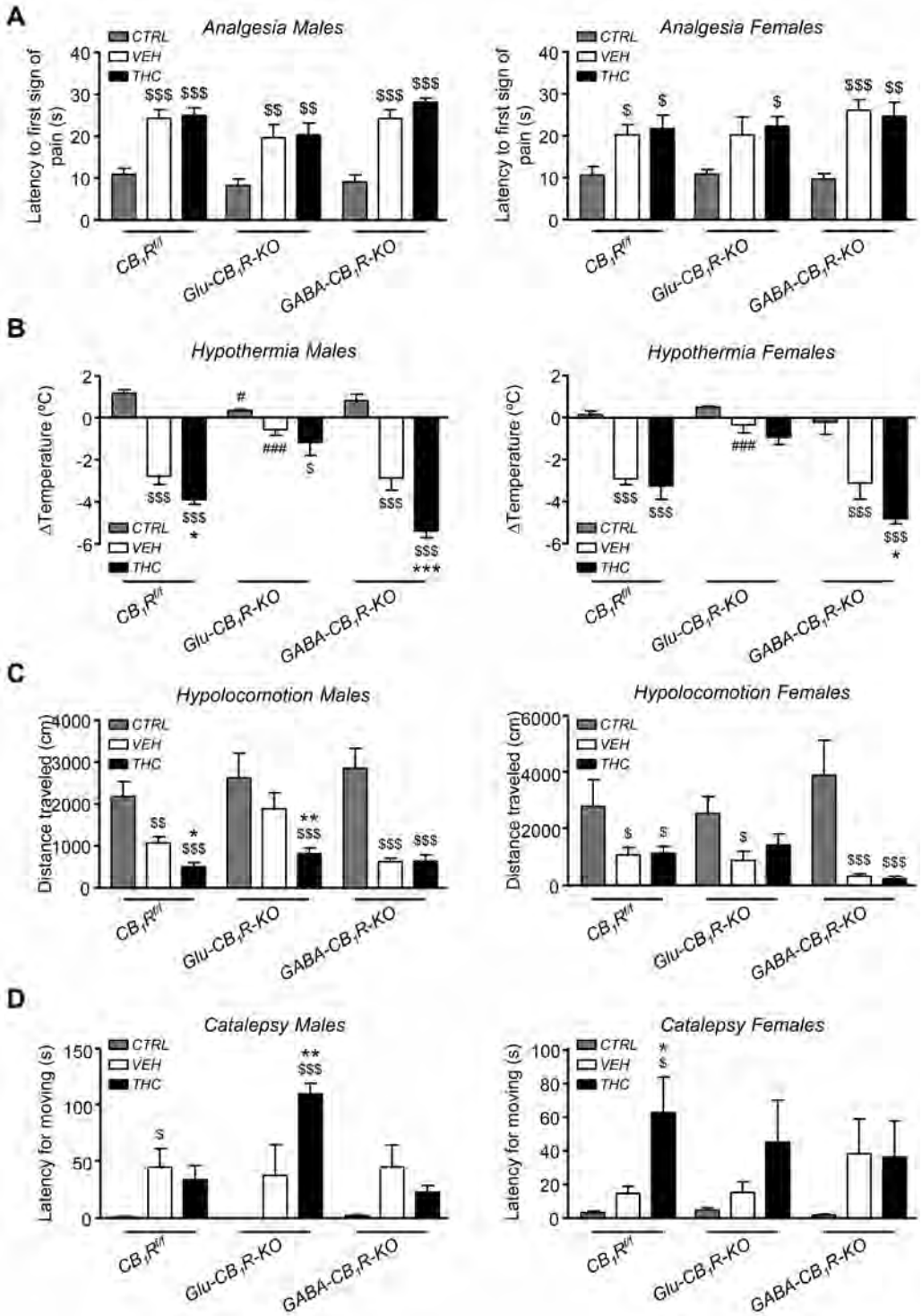


**Figure R2.7. THC-induced actions that depend on neurons other than GABAergic are not sex-dimorphic.** A classical THC-induced cannabinoid tetrad experiment consisting on (**A**) analgesia, (**B**) hypothermia, (**C**) hypolocomotion, and (**D**) catalepsy, was analysed in vehicle and THC-treated Glu-$CB_1$R-KO, GABA-$CB_1$R-KO and $CB_1R^{f/f}$ P60 male and female mice. (n= 5 animals per group). Statistical comparison *versus* the corresponding vehicle group: *, $p < 0.05$; **, $p < 0.01$; ***, $p < 0.001$. Statistical comparison *versus* the corresponding vehicle $CB_1^{f/f}$ group: #, $p < 0.05$; ###, $p < 0.001$. Statistical comparison *versus* the corresponding naive control group: $, $p < 0.05$; $$, $p < 0.01$; $$$, $p < 0.001$.

tional $CB_1R$-deficient mice. Prenatal THC administration did not induce significant differences in the NOR task by sex or treatment in $CB_1R^{f/f}$ and Glu-$CB_1R$-KO mice (Figure R2.6A). In contrast, we found robust spatial memory impairment in THC-treated $CB_1R^{f/f}$ and Glu-$CB_1R$-KO male mice in the OL task (Figure R2.6B). THC exerted no effect in GABA-$CB_1R$-KO males, which exhibited worse spatial memory as compared to vehicle-treated $CB_1R^{f/f}$ and Glu-$CB_1R$-KO males. Surprisingly, a different mechanism seems to operate in females, which exhibited an interaction between genotype and treatment. Interestingly, both vehicle-treated GABA-$CB_1R$-KO male and female mice presented impairment of conceptual memory (statistically significant only in males), which was not evident upon embryonic THC administration. Together, these data support a requirement of $CB_1R$ signalling in developing GABAergic neurons for the adequate maturation of CCK-dependent hippocampal function in male mice, and so point to remarkable sex-dimorphic actions of $CB_1R$ signalling along development.

To further assess the specific involvement of $CB_1R$ located on GABAergic INs in the sex-dimorphic developmental consequences of THC exposure, we analysed the impact of THC on the so-called "cannabinoid tetrad" that corresponds to well-established $CB_1R$-mediated actions: hypothermia, hypolocomotion, analgesia, and catalepsy. These behavioural traits have been ascribed to $CB_1R$ located on particular neuronal populations (Monory et al., 2007), and so they are informative of the status of $CB_1R$ in those neurons.

Regardless of sex or treatment, no differences were observed in THC-induced analgesia, a trait that relies on PNs located outside the neocortex (Figure R2.7A). Moreover, cannabinoid-induced hypothermia, which is mediated mainly by $CB_1R$ on dorsal telencephalic glutamatergic neurons, did not reveal sex- or treatment-dependent effect in Glu-$CB_1R$-KO mice, but was differentially affected by treatment, in a non sex-dimorphic way, in GABA-$CB_1R$-KO animals (Figure R2.7B). Regarding cannabinoid-induced hypolocomotion, Glu-$CB_1R$-KO males prenatally exposed to THC exhibited an enhanced response to acute THC (Figure R2.7C), while no differences were found in females. Finally, the cataleptic effect of acute THC is believed to result from a complex and concerted action of THC on $CB_1R$ located on neurons of the basal ganglia, as well as on principal serotonergic and noradrenergic cells (Monory et al. 2007). We found a sex dimorphic effect of acute THC on catalepsy as well as differential contribution of glutamatergic and GABA INs (Figure R2.7D). Noteworthy, GABA-$CB_1R$-KO females were resistant to embryonic THC action.

# Discussion

Overall, our results reveal, on the one hand, a striking increase of $CB_1R$ expression levels in FCD Type II, an enrichment that occurs selectively in neurons with overactive mTORC1 signalling. In addition, characterization of genomic DNA in dysplastic human brain resections unveiled the differential expression of three SNPs affecting the *DAGLA* gene in FCD Type II patients. Furthermore, pharmacological manipulation of organotypic slices from human resections demonstrated that $CB_1R$ signalling contributes to overactive mTORC1 signalling, one of the major hallmarks of the disease. Finally, altered maturation and integration of transiently $CB_1R$ knocked-down PNs points to an abnormal wiring of cortical circuits that may contribute to an imbalance in excitation/inhibition.

On the other hand, our data confirm a pivotal and sex-dimorphic role of embryonic $CB_1R$ in the development of hippocampal CCK-containing basket cell populations, as prenatal THC exposure led to a persistent interneuronopathy that affected only the male progeny. We also found a concomitant sex-dimorphic decrease in perisomatic $CB_1R$ innervating pyramidal cells within the *sp* and a deficit in spatial memory, both persisting in the adulthood.

**$CB_1$ receptor overexpression in focal cortical dysplasia. Cause or consequence?**

Here we report highly increased $CB_1R$ levels in BCs and DNs in FCD samples. As ECS activity is coupled to the mTORC1 signalling pathway both at early stages of neocortex formation (Díaz-Alonso *et al*., 2015) and in the adult brain (Puighermanal *et al*., 2009), it is important to address whether the overexpression of $CB_1R$ is a direct consequence of an altered cellular state elicited by overactive mTORC1 or if, conversely, it can be one of the causes of mTORC1 overactivation. Gene expression assays indicated that $CB_1R$ enrichment is not a direct consequence of an overactive mTORC1 pathway, pointing to other signalling events as up-regulators of $CB_1R$ levels in this context.

We therefore analysed $CB_1R$ downstream signalling in FCD-derived organotypic slices. The $CB_1R$ agonist HU-210 was unable to further increase mTORC1 activation, suggesting that the pathway is already saturated. Nevertheless, the $CB_1R$ inverse agonist rimonabant was as efficient as rapamycin in reducing S6 protein phosphorylation, suggesting that a basal cannabinoid signalling tone sustains exacerbated mTORC1 activity in FCD Type II. It would be worth assessing whether this $CB_1R$-dependent mTORC1 overactivation contributes to epileptic activity or not, as dampening overactive $CB_1R$ activity with rimonabant in other settings, as the Fmr1 knockout mice,

efficiently decreases not only exacerbated mTORC1 activity but also disease symptoms (Busquets-García *et al*., 2013; Navarro-Romero *et al*., 2019). In the adult brain, presynaptic $CB_1R$ engaged by retrograde eCBs constitutes an efficient regulatory mechanism of excessive neurotransmitter release. Hence, ECS signalling is a crucial pathway controlling neuronal activity, and its activation or blockade modulates seizures and epilepsy development (Soltesz *et al*., 2015). It has been shown that patients with temporal lobe epilepsy have decreased $CB_1R$ expression (Ludányi *et al*., 2008; Goffin *et al*., 2011), and, likewise, selective loss of function of presynaptic $CB_1Rs$ in PN populations in the mouse brain results in an imbalance of the excitatory/inhibitory tone and a higher susceptibility to seizures (Monory *et al*., 2006). Thus, the enrichment in $CB_1R$ expression observed in FCD samples could also represent a compensatory mechanism aimed to attenuate the imbalance of excitatory/inhibitory neuronal activity. As stated, ECS signalling is linked to mTORC1 stimulation, and, therefore, a deregulation in this compensatory ECS activity could become a drawback by further overactivating mTORC1 pathway.

**The endocannabinoid system and the genetic origin of focal cortical dysplasia**

Somatic mutations of mTOR signalling pathway, including upstream regulators as PI3K/Akt, TSC1, TSC2 and DEPDC5, have been recently found in FCD Type II (Jansen *et al*., 2015; Lim *et al*., 2015; Ricos *et al*., 2016). This led us to assess if a similar association with ECS-related mutations may be established. SNPs analyses and genomic DNA sequencing of the *CNR1* exon did not reveal any mutation associated with FCD Type II. However, we confirmed the existence of a selective enrichment in three SNPs of the *DAGLA* gene, suggesting the potential involvement of 2-AG metabolism in FCD Type II. The impact of these *DAGLA* SNPs in 2-AG production is still unknown, as they correspond to non-coding regions of the gene. Nevertheless, *DAGLA* transcript levels were slightly reduced in FCD when compared to control tissue. This is important to note, as decreased 2-AG, either caused by diminished DAGLα levels or activity, may foster a $CB_1R$ upregulation similar to that found in FCD samples. In addition, these results are in agreement with a recent study that described *DAGLA* polymorphisms associated with neurodevelopmental disorders and seizures in humans, while *CNR1* polymorphisms were associated with pain sensitivity, sleep, memory deficit or anxiety, but not seizures (Smith *et al*., 2017). Bearing this in mind, although a clear link is far from being established, the possibility that some FCD cases could be associated to mutations in ECS genes may not be completely dismissed.

**The impact of transient loss of $CB_1$ receptor function in projection neuron maturation and excitability**

FCD Type II is believed to originate from the dorsal telencephalic progenitor pool and their excitatory neuronal progeny, the PNs (D'Gama *et al*., 2017). Noteworthy, in experimental models of MCDs mimicking mTORopathies, unbalanced deep and upper layer neuronal development occurs as a consequence of aberrant expression of neural fate determinants. Hence, a contribution of $CB_1R$ signalling to neural precursor alterations responsible for FCD Type II cannot be excluded, as during embryonic development, $CB_1R$ controls the RGC-to-IP transition *via* mTORC1 signalling (Díaz-Alonso *et al*., 2015), deep cortical neuron differentiation (Mulder *et al*., 2008; Díaz-Alonso *et al*., 2012) and neuronal migration (Díaz-Alonso *et al*., 2017). A transient prenatal ablation of $CB_1R$ as that used in this Thesis, results in ectopic neuron accumulations and increased seizure susceptibility. Here, we targeted mPFC and observed a long-term effect in cortical circuit integration that was accompanied by an impaired neuronal maturation in the siRNA-targeted cells, subsequent to a delay in neuronal migration. As the developing brain is a tissue in constant change, we hypothesize that, as they travel, neurons delayed in migration are exposed to a different extracellular context than properly-migrating neurons. The same applies for the context that delayed neurons would find when they finally arrive to their laminar destination, for they can reach a layer in which afferents and efferents have been already formed. These different contexts may condition specific and divergent protein-expression profiles, which, in turn, may account for the alterations in electrophysiological properties we observed. Additionally, as $CB_1R$ have been shown to modulate transcriptional activity in different developmental contexts (Díaz-Alonso *et al*., 2012; Alpár *et al*., 2014; Tortoriello *et al*., 2014) and $CB_1R$ knockout mice show altered expression of synaptic activity-related markers, as enkephalin or glutamic acid decarboxylase (Steiner *et al*., 1999), it is worth to further investigate if $CB_1R$ activity regulates the expression of proteins (i.e. ionic channels, neurotransmitter receptors, and others) that determine the electrophysiological behaviour and/or the synaptic activity of specific neuronal subpopulations.

Taken together, the consequences of our genetic manipulation resemble some traits found in FCD cases. Therefore, either hyper- or hypoactive $CB_1R$ signalling during cortical development may have the potential to elicit cortical alterations, thus driving long-term neuronal plasticity and abnormalities that underlie FCD hyperexcitability.

The precise contribution of $CB_1R$ activity to the hyperexcitable neuronal circuits of the dysplastic brain remain unknown. Among other mechanisms involved in FCD, decreased hyperpolarization-activated cation currents contribute to pyramidal layer V hyperexcitability (Albertson *et al*., 2011) near dysplastic lesions. Interestingly, a particular pool of somatodendritic $CB_1Rs$ can regulate Ih currents and this explains in turn some of the cognitive consequences of $CB_1R$ signalling (Maroso *et al*., 2016). Ih current, which is determined by the presence of hyperpolarization-activated cyclic nucleotide-gated (HCN) channels, also determines the amplitude of voltage sag (Albertson *et al*., 2017), a trait we have found altered at different time points upon $siCB_1$ IUE, further supporting a conceptual link between an ECS malfunction and miswired dysplastic circuits. Important to note, our analyses were restricted to the well-positioned neurons, those that finally reach their laminar destination. It would be of great interest to characterize misplaced neurons and elucidate whether they electrophysiologically behave as upper-layer neurons (their identity according to their birthdate) or deep-layer neurons (the compartment in which they stop their migration); and if they contribute to altered cortical excitability.

**Ribosomal S6 protein phosphorylation: in search for a better treatment**

Ribosomal S6 protein is regulated by phosphorylation at multiple sites (Meyuhas, 2015). S6 phosphorylation at Ser240/244 is selectively mediated by S6-kinases 1 and 2, providing a *bona fide* readout of mTORC1 upstream activation, whereas Ser235/236 phosphorylation is regulated by different signalling pathways (cAMP/PKA, casein kinase 1, MAPK-activated protein kinase-1 and mTORC1 *via* S6 kinases 1 and 2). Initial studies have revealed increased levels of S6 protein phosphorylated at Ser235/236 in FCD and TSC (Baybis *et al*., 2004; Aronica *et al*., 2007), which suggests that pathways other than mTORC1 may contribute to the increased levels found of pS6 in FCD, and that different mechanisms phosphorylating S6 protein may have different functional consequences in FCD (Ljungberg *et al*., 2006; Biever *et al*., 2015).

Considering the finding that $CB_1R$ antagonism attenuates the phosphorylation of S6 protein at different amino acid residues (Ser235/236 and Ser240/244) in the same magnitude observed upon mTOR inhibition with rapamycin (Discussion Figure 1), this could indicate that the mTOR overactivation observed in FCD Type II samples requires the existence of active $CB_1R$ signalling, although the precise crosstalk between $CB_1R$ downstream effectors and the PI3K/Akt/mTOR altered context remains unknown.

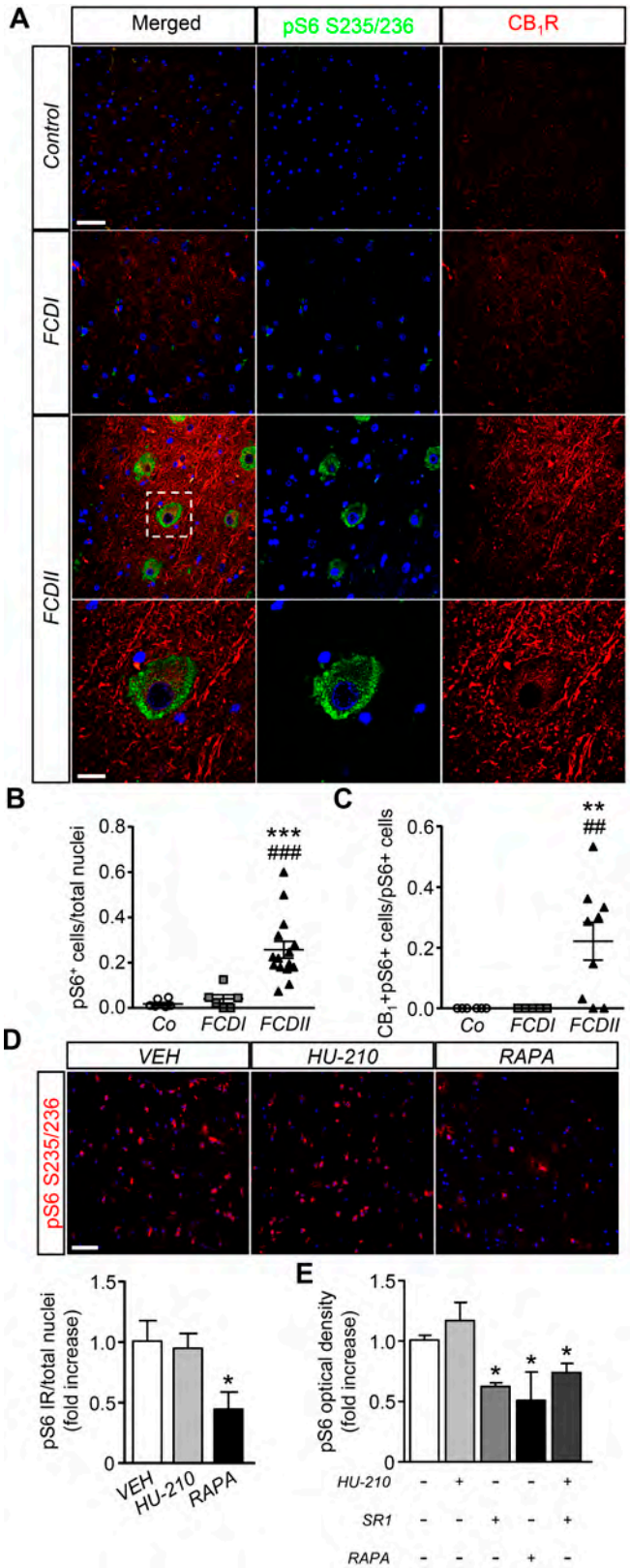


**Discussion Figure 1. Findings previously observed are replicated when using anti-pS6 Ser235/Ser236, a non-selective for mTOR activity antibody.** (**A**) Representative immunofluorescence images showing the presence of $CB_1R$ in samples from FCD Type I, II and control brains, stained with an anti-$CB_1R$ antibody (red) and an anti pS6 Ser235/Ser236 antibody (green). High magnification images of $CB_1R$ expression associated with S6 phosphorylation in FCD Type II are shown. (**B**) $pS6^+$ cells were quantified in the dysplastic area and referred to total cell number (DAPI counterstaining). Control, FCD Type I and FCD Type II cases. (**C**) $CB_1R^+pS6^+$ double-labelled cells were quantified and referred to total $pS6^+$ cells. Control, FCD Type I and FCD Type II cases (n= 6, 8 and 9, respectively). Statistical comparison *versus* control samples: **, $p < 0.01$; ***, $p < 0.001$. Statistical comparison *versus* FCD Type I samples: ##, $p < 0.01$; ###, $p < 0.001$. (**D, E**) Organotypic cultures of FCD resections were cultured 7 days *in vitro* and exposed to HU-210 (1 µM), and rapamycin (1 µM) for 90 minutes. (**D**) Representative images of immunofluorescence characterization with anti-pS6 Ser235/236 antibody. $pS6^+$ cells were quantified and referred to the total number of cells revealed by DAPI counterstaining. (**E**) Western blot analysis of pS6 Ser235/236 was performed in slice extracts after 90 minutes of incubation with HU-210 alone or together with SR141716 (25 µM), SR141716 alone or rapamycin (n= 4 experiments). Statistical comparison *versus* vehicle samples: *, $p < 0.05$. Scale bars: **A**: low magnification: 25 µm; inset: 10 µm. **D**: 50 µm.

Hence, regulation of cannabinoid signalling could constitute an attractive target for various mTORopathies. In the past years, CBD, a non-psychotomimetic cannabinoid with multiple targets, marketed as Epidiolex, has demonstrated its efficacy as antiepileptic drug in refractory epilepsies including TSC, Dravet and Lennox-Gastaut syndromes, and is under clinical trial for FCDs (Devinsky *et al*., 2016; Hess *et al*., 2016; Thiele *et al*., 2018).

Together with our previous findings (Mulder *et al*., 2008; Díaz-Alonso *et al*., 2012, 2017), this Thesis reinforces the role of developmental $CB_1R$ function in the correct establishment of cortical PN populations and highlight the pathological implication of altered developmental cannabinoid signalling in refractory epilepsy.

**Impact of prenatal exposure to cannabinoids on GABAergic transmission: from laboratory animals to humans**

The demonstration of a functional endocannabinoid signalling in modulating crucial neurodevelopmental processes (Galve-Roperh *et al*., 2013; Maccarrone *et al*., 2014) has contributed to the understanding of the consequences of prenatal cannabinoid exposure in developing neuronal circuits. In the present Thesis, we demonstrate that prenatal THC exposure exerts a sex-dimorphic interference with CCK-containing basket cell development, leading to a long-term interneuronopathy, altered hippocampal function, and impaired spatial cognition. Our results are in partial agreement with previous findings showing that prenatal WIN-55,212-2 administration interferes with the development of CCK-containing basket cells, which in turn impacts feedforward and feedback inhibition, an effect that was associated with reduced social interaction (Vargish *et al*., 2016). Likewise, WIN-55,212-2 administration during early and mid, but not late, adolescence interferes with maturation of GABAergic function, leading to layer V prefrontal cortex disinhibition (Cass *et al*., 2014). Hence, both perinatal and adolescent exposure to cannabinoids result in GABAergic hypofunction in animal models. Strikingly, a recent study demonstrated that lactational exposure to THC or WIN-55,212-2 delays the excitatory-to-inhibitory switch that GABAergic transmission undergoes during perinatal development, a process that is determined by a shift in the expression ratio of two ionic transporters: KCC2, which increases as development progresses, and NKCC1, which decreases (Scheyer *et al*., 2018).

In humans, among the neuropsychiatric traits induced by early cannabinoid exposure, the increased risk of psychosis and schizophrenia has been mainly associated to GABAergic hypofunction (Volk and Lewis, 2016). Alternatively, cannabinoid-induced

remodelling and plasticity of GABAergic circuits can contribute to explain cognitive impairment, as $CB_1R$ signalling is critical in modulating cognition and memory and hence cannabis use interferes with working and episodic memory (Curran *et al*., 2016). Nevertheless, while in adult animals acute and chronic THC administration impairs novel object recognition, our results indicate that embryonic THC exposure does not affect conceptual learning, but instead blunts spatial memory, and this occurs in a striking sex-dimorphic manner.

We did not find psychotic-like features in the THC-exposed offspring (startle response and prepulse inhibition were unaffected; data not shown). One possible explanation is that cannabinoid agonists used in the laboratory, as WIN-55,212-2, are likely to induce a stronger impact than THC and other phytocannabinoid molecules. Phytocannabinoids possess important differences in solubility, potency, and hence pharmacokinetic and pharmacodynamic behaviour from other synthetic cannabinoid drugs (e.g., WIN-55,212-2, HU-210). Moreover, different cannabinoid ligands contribute differentially to biased $CB_1R$ signalling and can target additional receptors and binding proteins (Al-Zoubi *et al*., 2019). Noteworthy, a severe cannabinoid-induced impairment of cortical oscillations was observed upon administration of the WIN-55,212-2 compound (Cass *et al*., 2014; Raver and Keller, 2014). Hence, it would be desirable that, when attempting to extrapolate to humans the consequences of cannabinoid exposure from experimental models based on small laboratory animals, exquisite care is taken in the pharmacological regulation strategy and the experimental design that were used. Evidence for the impact of sex-dimorphic cannabinoid prenatal exposure on human brain development is scarce, and its interpretation is extremely complex due to a wide array of confounding factors. Nonetheless, it has been suggested that early cannabinoid exposure may promote the development of aggressiveness differently in girls and boys (Marroun *et al*., 2011).

**$CB_1$ receptor, hippocampal function and spatial memory processing**

At the circuit level, and consistent with the role of CCK-containing basket cells in hippocampal oscillations (Klausberger *et al*., 2005; del Pino *et al*., 2017), we found changes in the theta and the low ripple band exclusively in THC-treated male mice. As theta-nested gamma oscillations were not affected, we confirmed that these effects were frequency- and circuit-specific. Within the hippocampus, $CB_1R$ differentially contributes to perisomatic inhibition of superficial *versus* deep CA1 pyramidal cells

(Valero *et al*., 2015). Possibly, the frequency-specific effect found in ripple distribution of THC-treated males can be associated with the emerging concept of different microcircuit organization along the deep-superficial hippocampal sublayers (Soltesz and Losonczy, 2018; Valero and de la Prida, 2018).

At the cellular level, CCK-containing basket cells in the CA1 region are known to control the activity of place cells. These hippocampal pyramidal neurons encode the cognitive map of the surrounding space, and specific groups (or spatial units) of place cells fire when the individual is located in the specific spatial context they encode within the map (Moser *et al*., 2015). CCK-containing basket cells, which maintain a perisomatic tonic inhibition over place cells, determine when (and where) to suppress inhibition in order to permit the firing from specific place cells (del Pino *et al*., 2017). Thus, a reduced number of CCK-containing basket cells, as that observed in this Thesis, may condition a lesser ability to regulate clusters of place cells, subsequently reducing the number of spatial units. This, in turn, impairs spatial memory encoding and discrimination. Additionally, other groups have proposed that $CB_1R$ controls spatial memory by regulating HCN channels and Ih current, an effect that is specific of CA1 superficial PNs (Maroso *et al*., 2016). Interestingly, the immediate/early gene transcription factor NPAS4, whose expression is triggered in a sensory experience-driven manner, mediates recruitment of CCK-evoked cannabinoid inhibition (Hartzell *et al*., 2018). Thus, enriched environment may constitute a valuable strategy to counteract the detrimental consequences of prenatal cannabinoid exposure, as an alternative to ongoing studies aimed to prevent deleterious cannabinoid maladaptive plasticity by pharmacological manipulation (Vallée *et al*., 2014). Overall, our findings underline the influence that ECS signalling possess over spatial processing, and establish a connection between the observed THC-induced interneuronopathy and the decline in spatial memory.

**Sex-dimorphic trends in endocannabinoid system function**

The findings presented here highlight the importance of addressing sex differences when investigating the neurodevelopmental changes induced by cannabis exposure and the functional consequences in the offspring (Sanchis-Segura and Becker, 2016). Males and females exhibit different expression levels for diverse ECS elements, and respond differently to THC (Rubino and Parolaro, 2011; Cuttler *et al*., 2016). In animal models, prenatal cannabinoid exposure induces sex-dimorphic changes in pyramidal neuron

intrinsic properties and synaptic plasticity in the PFC that are associated to social interaction deficits (Bara *et al*., 2018). Our data show that sex-dimorphic and THC-induced CCK-containing basket cell interneuronopathy contributes to the observed spatial cognitive impairment.

Interestingly, there is a collection of different studies describing prenatal exposure to diverse chemicals or stressors that elicit deleterious consequences only in males, or with male-biased intensity (Sickmann *et al*., 2014; Chalkiadaki *et al*., 2019; Winterbottom *et al*., 2019). This general trend could be explained by a generalist mechanism dependent on sex hormones and their concentration/functionality in the developing brain, although a specific mechanism underlying each prenatal insult may not be excluded. Brain-wide-mapping studies have recently revealed cell-type specific contributions to cortical and subcortical sexual dimorphism (Kim *et al*., 2017), suggesting that many effects should be identified at the system level.

### $CB_1$ receptor-dependent cell-autonomous regulation of interneuron development

This Thesis demonstrates that conditional $CB_1R$ ablation in the telencephalic IN lineage mimics the consequences of THC treatment, thus pointing to $CB_1R$ downregulation as the main mechanism of THC action in the studied context. Repeated cannabinoid exposure in the immature brain results in functional antagonism of $CB_1R$

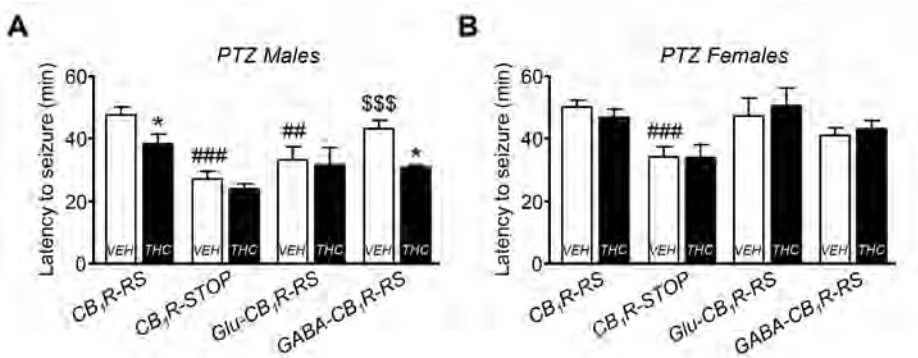


**Discussion Figure 2. Sex-dimorphic seizure susceptibility in $CB_1R$ rescue mice.** (**A, B**) Seizure susceptibility to subconvulsive doses of PTZ was determined in the offspring of mice that had been prenatally exposed to vehicle or THC [data taken from their original source (de Salas-Quiroga *et al*., 2015) and herein just segregated in males and females]. Latency to seizures was determined in $CB_1R$-RS, Glu-$CB_1R$-RS, GABA-$CB_1R$-RS and $CB_1R$-STOP, which express $CB_1R$ globally, in the glutamatergic neuronal lineage, in the GABAergic neuronal lineage, or lack $CB_1R$ expression, respectively. [n = (males: 9 and 9, vehicle- and THC-treated $CB_1R$-RS, respectively; 12 and 7, vehicle- and THC-treated $CB_1R$-STOP, respectively; 4 and 4, vehicle- and THC-treated Glu-$CB_1R$-RS, respectively; 4 and 6, vehicle- and THC-treated GABA-$CB_1R$-RS, respectively); (females: 9 and 10, vehicle- and THC-treated $CB_1R$-RS, respectively; 7 and 7 , vehicle- and THC-treated $CB_1R$-STOP, respectively; 5 and 2, vehicle- and THC-treated Glu-$CB_1R$-RS, respectively; 5 and 6, vehicle- and THC-treated GABA-$CB_1R$-RS, respectively)]. Statistical comparison *versus* the corresponding vehicle group: *, $p < 0.05$. Statistical comparison *versus* the corresponding $CB_1R$-RS vehicle group: ##, $p < 0.01$; ###, $p < 0.01$. Statistical comparison *versus* the corresponding $CB_1R$-STOP vehicle group: $$$, $p < 0.001$.

signalling in principal neurons (de Salas-Quiroga *et al*., 2015) and CCK-containing basket cells (present results). As a consequence of THC-elicited activation, $CB_1R$ desensitizes, and cannabinoid signalling becomes impaired, which favours the development of seizures and spatial cognitive deficits in a sex-dimorphic manner. In fact, post hoc sex-segregated analysis of a dataset in which both sexes were previously pooled (de Salas-Quiroga *et al*., 2015), further supports the involvement of GABAergic INs, but not PNs, in prenatal THC-induced hyperexcitability, as measured by PTZ-evoked seizure susceptibility and by using a lineage-specific $CB_1R$-rescue mice model generated in a null background and subjected to a prenatal THC treatment similar to that used in the present Thesis (Discussion Figure 2). In summary, the study of functional consequences (hyperexcitability, cognition, and other behavioural traits), *in vivo* electrophysiological recordings, and neuron-lineage tracking in conditional $CB_1R$-deficient mice, as shown herein, provides a strong support to the idea that neurodevelopmental exposure to THC exerts selective actions in different neuronal populations with a remarkable sex dimorphism.

Taken together, the results presented in this Thesis reinforce the pivotal role that ECS signalling possess in the development of both PNs and INs. We have demonstrated that $CB_1R$ disruption during embryonic periods may trigger long-term deleterious consequences, whose extent and severity depend on the specific neuronal population and the precise step of development that becomes targeted, as well as on the sex of the animal. Thus, our findings contribute to pave the way for the understanding of the neurodevelopmental role of the ECS, and provide fundamental knowledge for evidence-based decision regarding the benefits and risks that the use of medical cannabis may imply, which is crucial when deciding if therapeutic cannabis may be chosen over other therapies when treating a specific condition.

# Conclusions

The following conclusions summarize the main findings presented and discussed within this Doctoral Thesis:

**I.** Endocannabinoid signalling is altered in focal cortical dysplasia type II. Increased expression of the $CB_1$ receptor is associated with an overactivation of the mTORC1 pathway, which, in turn, is dampened upon $CB_1$ receptor antagonism. Thus, the endocannabinoid system might be explored as a therapeutic target in this pathology.

**II.** The existence of genetic polymorphisms affecting the *DAGLA* gene in focal cortical dysplasia type II suggests that a causal link between early disrupted endocannabinoid function and the onset of the disease might not be excluded.

**III.** The $CB_1$ receptor participates in the maturation of neocortical projection neurons, as a transient developmental loss of its function fosters a delay in cell migration. This delay occurs concomitantly with a long-term impairment of neuronal excitability.

**IV.** The endocannabinoid system regulates the establishment of CCK-containing interneurons in the hippocampus, since prenatal exposure to THC evokes a long-lasting interneuronopathy affecting this GABAergic subpopulation.

**V.** THC-elicited interneuronopathy, which relies exclusively on $CB_1$ receptors located on GABAergic neurons, shows a striking sex dimorphism, affecting solely the male progeny. This finding points to an endocannabinoid system-dependent regulation of interneuron development, which operates divergently among sexes.

**VI.** A correct endocannabinoid signalling during early development seems to be crucial for the proper acquisition of adult brain functions such as hippocampal oscillatory activity, spatial memory processing, and fine-tuned brain excitability, as transient interference with prenatal endocannabinoid signalling exerts marked detrimental effects on them that persist in adulthood.

# References

Aaku-Saraste E, Hellwig A, Huttner WB. "Loss of occludin and functional tight junctions, but not ZO-1, during neural tube closure-remodeling of the neuroepithelium prior to neurogenesis". *Dev Biol* **180**:664–679 (1996).

Abney ER, Bartlett PP, Raff MC. "Astrocytes, ependymal cells, and oligodendrocytes develop on schedule in dissociated cell cultures of embryonic rat brain". *Dev Biol* **83**:301–310 (1981).

Aguado T, Monory K, Palazuelos J, Stella N, Cravatt B, Lutz B, Marsicano G, Kokaia Z, Guzmán M, Galve-Roperh I. "The endocannabinoid system drives neural progenitor proliferation". *FASEB J* **19**:1704–1706 (2005).

Aguado T, Palazuelos J, Monory K, Stella N, Cravatt B, Lutz B, Marsicano G, Kokaia Z, Guzmán M, Galve-Roperh I. "The endocannabinoid system promotes astroglial differentiation by acting on neural progenitor cells. *J Neurosci* **26**:1551–1561 (2006).

Aguareles J, Paraíso-Luna J, Palomares B, Bajo-Grañeras R, Navarrete C, Ruiz-Calvo A, García-Rincón D, García-Taboada E, Guzmán M, Muñoz E, Galve-Roperh I. "Oral administration of the cannabigerol derivative VCE-003.2 promotes subventricular zone neurogenesis and protects against mutant huntingtin-induced neurodegeneration". *Transl Neurodegener* **8**:9 (2019).

Al-Zoubi R, Morales P, Reggio PH. "Structural insights into CB1 receptor biased signaling". *Int J Mol Sci* **20**:1837 (2019).

Albertson AJ, Bohannon AS, Hablitz JJ. "HCN channel modulation of synaptic integration in GABAergic interneurons in malformed rat neocortex". *Front Cell Neurosci* **11**:109 (2017).

Albertson AJ, Yang J, Hablitz JJ. "Decreased hyperpolarization-activated currents in layer 5 pyramidal neurons enhances excitability in focal cortical dysplasia". *J Neurophysiol* **106**:2189–2200 (2011).

Alfano C, Studer M. "Neocortical arealization: evolution, mechanisms and open questions". *Dev Neurobiol* **73**:411–447 (2013).

Alpár A, Tortoriello G, Calvigioni D, Niphakis MJ, Milenkovic I, Bakker J, Cameron GA, Hanics J, Morris CV, Fuzik J, Kovacs GG, Cravatt B, Parnavelas JG, Andrews WD, Hurd YL, Keimpema E, Harkany T. "Endocannabinoids modulate cortical development by configuring Slit2/Robo1 signalling". *Nat Commun* **5**:4421 (2014).

André VM, Wu N, Yamazaki I, Nguyen ST, Fisher RS, Vinters HV, Mathern GW, Levine MS, Cepeda C. Cytomegalic interneurons: a new abnormal cell type in severe pediatric cortical dysplasia. *J Neuropathol Exp Neurol* **66**:491–504 (2007).

Antonelli T, Tanganelli S, Tomasini MC, Finetti S, Trabace L, Steardo L, Sabino V, Carratu MR, Cuomo V, Ferraro L. "Long-term effects on cortical glutamate release induced by prenatal exposure to the cannabinoid receptor agonist (R)-(+)-[2,3-dihydro-5-methyl-3-(4- morpholinyl-methyl)pyrrolo[1,2,3-de]-1,4-benzoxazin-6-yl]-1-naphthalenylmethanone: an *in vivo* microdialys study in the awake rat". *Neuroscience* **124**:367–375 (2004).

Arai A, Saito T, Hanai S, Sukigara S, Nabatame S, Otsuki T, Nakagawa E, Takahashi A, Kaneko Y, Kaido T, Saito Y, Sugai K, Sasaki M, Goto YI, Itoh M. "Abnormal maturation and differentiation of neocortical neurons in epileptogenic cortical malformation: Unique distribution of layer-specific marker cells of focal cortical dysplasia and hemimegalencephaly". *Brain Res* **1470**:89–97 (2012).

Argaw A, Duff G, Zabouri N, Cécyre B, Chainé N, Cherif H, Tea N, Lutz B, Ptito M, Bouchard JF."Concerted action of CB1 cannabinoid receptor and Deleted in Colorectal Cancer in axon guidance". *J Neurosci* **31**:1489–1499 (2011).

Aronica E, Boer K, Baybis M, Yu J, Crino P. "Co-expression of cyclin D1 and phosphorylated ribosomal S6 proteins in hemimegalencephaly". *Acta Neuropathol* **114**:287–293 (2007).

Aronica E, Crino P. "Epilepsy related to developmental tumors and Malformations of Cortical Development". *Neurotherapeutics* **11**:251–268 (2014).

Ascoli GA, Alonso-Nanclares L, Anderson SA, Barrionuevo G, Benavides-Piccione R, Burkhalter A, Buzsáki G, Cauli B, DeFelipe J, Fairén A, Feldmeyer D, Fishell G, Fregnac Y, Freund TF, Gardner D, Gardner EP, Goldberg JH, Helmstaedter M, Hestrin S, Karube F, Kisvárday ZF, Lambolez B, Lewis DA, Marín O, Markram H, Muñoz A, Packer A, Petersen CCH, Rockland KS, Rossier J, Rudy B, Somogyi P, Staiger JF, Gabor T, Thomson AM, Toledo-Rodríguez M, Wang Y, West DC, Yuste R. "Petilla terminology: nomenclature of features of GABAergic interneurons of the cerebral cortex". *Nat Rev Neurosci* **9**:557–568 (2008).

Bara A, Manduca A, Bernabeu A, Borsoi M, Serviado M, Lassalle O, Murphy M, Wager-Miller J, Mackie K, Pelissier-Alicot A-L, Trezza V, Manzoni OJ. "Sex-dependent effects of *in utero* cannabinoid exposure on cortical function". *eLife* **7**:e36234 (2018).

Barkovich AJ, Guerrini R, Kuzniecky RI, Jackson GD, Dobyns WB. "A developmental and genetic classification for malformations of cortical development: Update 2012". *Brain* **135**:1348–1369 (2012).

Barnes AP, Polleux F. "Establishment of axon-dendrite polarity in developing neurons". *Annu Rev Neurosci* **32**:347–381 (2009).

Bartolini G, Ciceri G, Marín O. "Integration of GABAergic interneurons into cortical cell assemblies: lessons from embryos and adults". *Neuron* **79**:849–864 (2013).

Baybis M, Yu J, Lee A, Golden JA, Weiner H, McKhann G, Aronica E, Crino P. "mTOR cascade activation distinguishes tubers from focal cortical dysplasia". *Ann Neurol* **56**:478–487 (2004).

Beggiato S, Borelli AC, Tomasini MC, Morgano L, Antonelli T, Tanganelli S, Cuomo V, Ferraro L. "Long-lasting alterations of hippocampal GABAergic neurotransmission in adult rats following perinatal Δ9-THC exposure". *Neurobiol Learn Mem* **139**:135–143 (2017).

Bellocchio L, Lafentre P, Cannich A, Cota D, Puente N, Grandes P, Chaouloff F, Piazza PV, Marsicano G. "Bimodal control of stimulated food intake by the endocannabinoid system". *Nat Neurosci* **13**:281–283 (2010).

Bergamaschi MM, Queiroz RHC, Chagas MHN, De Oliveira DCG, De Martinis BS, Kapczinski F, Quevedo J, Roesler R, Schröder N, Nardi AE, Martín-Santos R, Hallak JEC, Zuardi AW, Crippa JAS. "Cannabidiol reduces the anxiety induced by simulated public speaking in treatment-nave social phobia patients". *Neuropsychopharmacology* **36**:1219–1226 (2011).

Berghuis P, Dobszay MB, Wang X, Spano S, Ledda F, Sousa KM, Schulte G, Ernfors P, Mackie K, Paratcha G, Hurd YL, Harkany T. "Endocannabinoids regulate interneuron migration and morphogenesis by transactivating the TrkB receptor". *Proc Natl Acad Sci* **102**:19115–19120 (2005).

Berghuis P, Rajnicek AM, Morozov YM, Ross RA, Mulder J, Urbán GM, Monory K, Marsicano G, Matteoli M, Canty A, Irving AJ, Katona I, Yanagawa Y, Rakic P, Lutz B, Mackie K, Harkany T. "Hardwiring the brain: endocannabinoids shape neuronal connectivity". *Science* **316**:1212–1216 (2007).

Berrendero F, García-Gil L, Hernández ML, Romero J, Cebeira M, de Miguel R, Ramos JA, Fernández-Ruiz JJ. "Localization of mRNA expression and activation of signal transduction mechanisms for cannabinoid receptor in rat brain during fetal development". *Development* **125**:3179–3188 (1998).

Berrendero F, Sepe N, Ramos JA, Di Marzo V, Fernández-Ruiz JJ. "Analysis of cannabinoid receptor binding and mRNA expression and endogenous cannabinoid contents in the developing rat brain during late gestation and early postnatal period". *Synapse* **33**:181–191 (1999).

Biever A, Puighermanal E, Nishi A, David A, Panciatici C, Longueville S, Xirodimas D, Gangarossa G, Meyuhas O, Herve D, Girault JA, Valjent E. "PKA-dependent phosphorylation of ribosomal protein S6 does not correlate with translation efficiency in striatonigral and atriatopallidal medium-sized spiny neurons". *J Neurosci* **35**:4113–4130 (2015).

Blasco-Benito S, Moreno E, Seijo-Vila M, Tundidor I, Andradas A, Caffarel MM, Caro-Villalobos M, Urigüen L, Diez-Alarcia R, Moreno-Bueno G, Hernández L, Manso L, Homar-Ruano P, McCormick PJ, Bibic L, Bernadó-Morale C, Arribas J, Canals M, Casadó V, Canela EI, Guzmán M, Pérez-Gómez E, Sánchez C. "Therapeutic targeting of HER2–CB2 R heteromers in HER2-positive breast cancer". *Proc Natl Acad Sci* **116**:3863–3872 (2019).

Blasco-Benito S, Seijo-Vila M, Caro-Villalobos M, Tundidor I, Andradas C, García-Taboada E, Wade J, Smith S, Guzmán M, Pérez-Gómez E, Gordon M, Sánchez C. "Appraising the "entourage effect": antitumor action of a pure cannabinoid *versus* a botanical drug preparation in preclinical models of breast cancer". *Biochem Pharmacol* **157**:285–293 (2018).

Blázquez C, Chiarlone A, Sagredo O, Aguado T, Pazos MR, Resel E, Palazuelos J, Julien B, Salazar M, Börner C, Benito C, Carrasco C, Diez-Zaera M, Paoletti P, Díaz-Hernández M, Ruiz C, Sendtner M, Lucas JJ, de Yébenes JG, Marsicano G, Monory K, Lutz B, Romero J, Alberch J, Ginés S, Kraus J,Fernández-Ruiz, JJ, Galve-Roperh I, Guzmán M. "Loss of striatal type 1 cannabinoid receptors is a key pathogenic factor in Huntington's disease". *Brain* **134**:119–136 (2011).

Blázquez C, Chiarlone A, Bellocchio L, Resel E, Pruunsild P, García-Rincón D, Sendtner M, Timmusk T, Lutz B, Galve-Roperh I, Guzmán M. "The CB1 cannabinoid receptor signals striatal neuroprotection *via* a PI3K/Akt/mTORC1/BDNF pathway". *Cell Death Differ* **22**:1618–1629 (2015).

Blümcke I, Thom M, Aronica E, Armstrong DD, Vinters HV, Palmini A, Jacques TS, Avanzini G, Barkovich AJ, Battaglia G, Becker A, Cepeda C, Cendes F, Colombo N, Crino P, Cross JH, Delalande O, Dubeau F, Duncan J, Guerrini R, Kahane P, Mathern G, Najm I, Özkara Ç, Raybaud C, Represa A, Roper SN, Salamon N, Schulze-Bonhage A, Tassi L, Vezzani A, Spreafico R. "The clinicopathologic spectrum of focal cortical dysplasias: a consensus classification proposed by an *ad hoc* Task Force of the ILAE Diagnostic Methods Commission". *Epilepsia* **52**:158–174 (2011).

Blume LC, Patten T, Eldeeb K, Leone-Kabler S, Ilyasov AA, Keegan BM, O'Neal JE, Bass CE, Hantgan RR, Lowther WT, Selley DE, Howlett AC. "Cannabinoid receptor interacting protein 1a competition with β-Arrestin for CB1 receptor binding sites". *Mol Pharmacol* **91**:75–86 (2017).

Bonnin A, de Miguel R, Hernández ML, Ramos JA, Fernández-Ruiz JJ. "The prenatal exposure to δ9-tetrahydrocannabinol affects the gene expression and the activity of tyrosine hydroxylase during early brain development". *Life Sci* **56**:2177–2184 (1995).

Borrell V, Cárdenas A, Ciceri G, Galcerán J, Flames N, Pla R, Nóbrega-Pereira S, García-Frigola C, Peregrín S, Zhao Z, Ma L, Tessier-Lavigne M, Marín O. "Slit/Robo signaling modulates the proliferation of central nervous system progenitors". *Neuron* **76**:338–352 (2012).

Bravo-Ferrer I, Cuartero MI, Zarruk JG, Pradillo JM, Hurtado O, Romera VG, Díaz-Alonso J, García-Segura JM, Guzmán M, Lizasoain I, Galve-Roperh I, Moro MA. "Cannabinoid type-2 receptor drives neurogenesis and improves functional outcome after stroke". *Stroke* **48**:204–212.

Busquets-García A, Gomis-González M, Guegan T, Agustín-Pavón C, Pastor A, Mato S, Pérez-Samartín A, Matute C, de la Torre R, Dierssen M, Maldonado R, Ozaita A. "Targeting the endocannabinoid system in the treatment of fragile X syndrome". *Nat Med* **19**:603–607 (2013).

Buzsáki G. "Hippocampal sharp wave-ripple: a cognitive biomarker for episodic memory and planning". *Hippocampus* **25**:1073–1188 (2015).

Cameron RS, Rakic P. "Glial cell lineage in the cerebral cortex: a review and synthesis". *Glia* **4**:124–137 (1991).

Campolongo P, Trezza V, Cassano T, Gaetani S, Morgese MG, Ubaldi M, Soverchia L, Antonelli T, Ferraro L, Massi M, Ciccocioppo R, Cuomo V. "Perinatal exposure to delta-9-tetrahydrocannabinol causes enduring cognitive deficits associated with alteration of cortical gene expression and neurotransmission in rats". *Addict Biol* **12**:485–495 (2007).

Cass DK, Flores-Barrera E, Thomases DR, Vital WF, Caballero A, Tseng KY. "CB1 cannabinoid receptor stimulation during adolescence impairs the maturation of GABA function in the adult rat prefrontal cortex". *Mol Psychiatry* **19**:536–543 (2014).

Castillo PE. "Presynaptic LTP and LTD of excitatory and inhibitory synapses". *Cold Spring Harb Perspect Biol* **4**:a005728 (2012).

Castillo PE, Younts TJ, Chávez AE, Hashimotodani Y. "Endocannabinoid signaling and synaptic function". *Neuron* **76**:70–81 (2012).

Cepeda C, André VM, Levine MS, Salamon N, Miyata H, Vinters HV, Mathern GW. "Epileptogenesis in pediatric cortical dysplasia: the dysmature cerebral developmental hypothesis." *Epilepsy Behav* **9**:219–235 (2006).

Chalkiadaki K, Velli A, Kyriazidis E, Stavroulaki V, Vouvoutsis V, Chatzaki E, Aivaliotis M, Sidiropoulou K. "Development of the MAM model of schizophrenia in mice: sex similarities and differences of hippocampal and prefrontal cortical function". *Neuropharmacology* **144**:193–207 (2019).

Cheung AFP, Pollen AA, Tavare A, Deproto J, Molnár Z. "Comparative aspects of cortical neurogenesis in vertebrates". *J Anat* **211**:164–176 (2007).

Chiarlone A, Bellocchio L, Blázquez C, Resel E, Soria-Gómez E, Cannich A, Ferrero JJ, Sagredo O, Benito C, Romero J, Sánchez-Prieto J, Lutz B, Fernández-Ruiz J, Galve-Roperh I, Guzmán M. "A restricted population of CB1 cannabinoid receptors with neuroprotective activity". *Proc Natl Acad Sci* **111**:8257–8262 (2014).

Ciceri G, Dehorter N, Sols I, Huang ZJ, Maravall M, Marín O. "Lineage-specific laminar organization of cortical GABAergic interneurons". *Nat Neurosci* **16**:1199–1210 (2013).

Compagnucci C, Di Siena S, Bustamante MB, di Giacomo D, di Tommaso M, Maccarrone M, Grimaldi P, Sette C. "Type-1 (CB1) cannabinoid receptor promotes neuronal differentiation and maturation of neural stem cells". *PLoS One* **8**:e54271 (2013).

Copp AJ, Greene NDE, Murdoch JN. "The genetic basis of mammalian neurulation". *Nat Rev Genet* **4**:784–793 (2003).

Cravatt B, Lichtman AH. "The endogenous cannabinoid system and its role in nociceptive behavior". *J Neurobiol* **61**:149–160 (2004).

Crino P. "mTOR signaling in epilepsy: insights from malformations of cortical development". *Cold Spring Harb Perspect Med* **5**:a022442 (2015).

Curran HV, Freeman TP, Mokrysz C, Lewis DA, Morgan CJA, Parsons LH. "Keep off the grass? Cannabis, cognition and addiction". *Nat Rev Neurosci* **17**:293–306 (2016).

Cuttler C, Mischley LK, Sexton M. "Sex differences in cannabis use and effects: a cross-sectional survey of cannabis users". *Cannabis Cannabinoid Res* **1**:166–175 (2016).

D'Gama AM, Woodworth MB, Hossain AA, Bizzotto S, Hatem NE, LaCoursiere CM, Najm I, Ying Z, Yang E, Barkovich AJ, Kwiatkowski DJ, Vinters HV, Madsen JR, Mathern GW, Blümcke I, Poduri A, Walsh CA. "Somatic mutations activating the mTOR pathway in dorsal telencephalic progenitors cause a continuum of cortical dysplasias". *Cell Rep* **21**:3754–3766 (2017).

Davis MI, Ronesi J, Lovinger DM. "A predominant role for inhibition of the adenylate cyclase/protein kinase A pathway in ERK activation by cannabinoid receptor 1 in N1E-115 neuroblastoma cells". *J Biol Chem* **278**:48973–48980 (2003).

Day NL, Richardson GA."Prenatal marijuana use: epidemiology, methodologic issues, and infant outcome". *Clin Perinatol* **18**:77–91 (1991).

de Salas-Quiroga A, Díaz-Alonso J, García-Rincón D, Remmers F, Vega D, Gómez-Cañas M, Lutz B, Guzmán M, Galve-Roperh I. "Prenatal exposure to cannabinoids evokes long-lasting functional alterations by targeting CB1 receptors on developing cortical neurons". *Proc Natl Acad Sci* **112**:13693–13698 (2015).

DeFelipe J, López-Cruz PL, Benavides-Piccione R, Bielza C, Larrañaga P, Anderson S, Burkhalter A, Cauli B, Fairén A, Feldmeyer D, Fishell G, Fitzpatrick D, Freund TF, González-Burgos G, Hestrin S, Hill S, Hof PR, Huang J, Jones EG, Kawaguchi Y, Kisvárday Z, Kubota Y, Lewis DA, Marín O, Markram H, McBain CJ, Meyer HS, Monyer H, Nelson SB, Rockland K, Rossier J, Rubenstein JLR, Rudy B, Scanziani M, Shepherd GM, Sherwood CC, Staiger JF, Tamás G, Thomson A, Wang Y, Yuste R, Ascoli GA. "New insights into the classification and nomenclature of cortical GABAergic interneurons". *Nat Rev Neurosci* **14**:202–216 (2013).

del Pino I, Brotons-Mas JR, Marques-Smith A, Marighetto A, Frick A, Marín O, Rico B. "Abnormal wiring of CCK+ basket cells disrupts spatial information coding". *Nat Neurosci* **20**:784–792 (2017).

Díaz-Alonso J, Aguado T, de Salas-Quiroga A, Ortega Z, Guzmán M, Galve-Roperh I. "CB1 cannabinoid receptor-dependent activation of mTORC1/Pax6 signaling drives Tbr2 expression and basal progenitor expansion in the developing mouse cortex". *Cereb Cortex* **25**:2395–2408 (2015).

Díaz-Alonso J, Aguado T, Wu CS, Palazuelos J, Hofmann C, Garcez P, Guillemot F, Lu HC, Lutz B, Guzmán M, Galve-Roperh I. "The CB(1) cannabinoid receptor drives corticospinal motor neuron differentiation through the Ctip2/Satb2 transcriptional regulation axis". *J Neurosci* **32**:16651–16665 (2012).

Díaz-Alonso J, de Salas-Quiroga A, Paraíso-Luna J, García-Rincón D, Garcez P, Parsons M, Andradas C, Sánchez C, Guillemot F, Guzmán M, Galve-Roperh I. "Loss of cannabinoid CB1 receptors induces cortical migration malformations and increases seizure susceptibility". *Cereb Cortex* **27**:5303–5317 (2017).

Dimidschstein J, Passante L, Dufour A, van den Ameele J, Tiberi L, Hrechdakian T, Adams R, Klein R, Lie DC, Jossin Y, Vanderhaeghen P. "Ephrin-B1 controls the columnar distribution of cortical pyramidal neurons by restricting their tangential migration". *Neuron* **79**:1123–1135 (2013).

Dinieri JA, Wang X, Szutorisz H, Spano SM, Kaur J, Casaccia P, Dow-Edwards D, Hurd YL. "Maternal cannabis use alters ventral striatal dopamine D2 gene regulation in the offspring". *Biol Psychiatry* **70**:763–769 (2011).

Englund C, Fink A, Lau C, Pham D, Daza RAM, Bulfone A, Kowalczyk T, Hevner RF. "Pax6, Tbr2, and Tbr1 are expressed sequentially by radial glia, intermediate progenitor cells, and postmitotic neurons in developing neocortex". *J Neurosci* **25**:247–251 (2005).

Fernández-Ruiz JJ, Berrendero F, Hernández ML, Ramos JA. "The endogenous cannabinoid system and brain development". *Trends Neurosci* **23**:14–20 (2000).

Fernández-Ruiz JJ, Moro MA, Martínez-Orgado J. "Cannabinoids in neurodegenerative disorders and stroke/brain trauma: from preclinical models to clinical applications". *Neurotherapeutics* **12**:793–806 (2015).

Flames N, Marín O. "Developmental mechanisms underlying the generation of cortical interneuron diversity". *Neuron* **46**:377–381 (2005).

Foffani G, Uzcategui YG, Gal B, Menéndez de la Prida LM. "Reduced spike-timing reliability correlates with the emergence of fast ripples in the rat epileptic hippocampus". *Neuron* **55**:930–941 (2007).

Fried PA. "Marihuana use by pregnant women: neurobehavioral effects in neonates". *Drug Alcohol Depend* **6**:415–424 (1980).

Gal JS, Morozov YM, Ayoub AE, Chatterjee M, Rakic P, Haydar TF. "Molecular and morphological heterogeneity of neural precursors in the mouse neocortical proliferative zones". *J Neurosci* **26**:1045–1056 (2006).

Galve-Roperh I, Aguado T, Rueda D, Velasco G, Guzmán M. "Endocannabinoids: a new family of lipid mediators involved in the regulation of neural cell development". *Curr Pharm Des* **12**:2319–2325 (2006).

Galve-Roperh I, Chiurchiù V, Díaz-Alonso J, Bari M, Guzmán M, Maccarrone M. "Cannabinoid receptor signaling in progenitor/stem cell proliferation and differentiation". *Prog Lipid Res* **52**:633–650 (2013).

Galve-Roperh I, Rueda D, Gómez del Pulgar T, Velasco G, Guzmán M. "Mechanism of extracellular signal-regulated kinase activation by the CB(1) cannabinoid receptor". *Mol Pharmacol* **62**:1385–1392 (2002).

Gambardella A, Palmini A, Andermann F, Dubeau F, Da Costa JC, Quesney LF, Andermann E, Olivier A. "Usefulness of focal rhythmic discharges on scalp EEG of patients with focal cortical dysplasia and intractable epilepsy". *Electroencephalogr Clin Neurophysiol* **98**:243–249 (1996).

Giacoppo S, Bramanti P, Mazzon E. "Sativex in the management of multiple sclerosis-related spasticity: an overview of the last decade of clinical evaluation". *Mult Scler Relat Disord* **17**:22–31 (2017).

Gillespie AK, Jones EA, Lin YH, Karlsson MP, Kay K, Yoon SY, Tong LM, Nova P, Carr JS, Frank LM, Huang Y. "Apolipoprotein E4 Causes Age-Dependent Disruption of Slow Gamma Oscillations during Hippocampal Sharp-Wave Ripples". *Neuron* **90**:740–751 (2016).

Goffin K, van Paesschen W, van Laere K. "*In vivo* activation of endocannabinoid system in temporal lobe epilepsy with hippocampal sclerosis". *Brain* **134**:1033–1040 (2011).

Goldschmidt L, Day NL, Richardson GA. "Effects of prenatal marijuana exposure on child behavior problems at age 10". *Neurotoxicol Teratol* **22**:325–336 (2000).

Goldschmidt L, Richardson GA, Willford JA, Severtson SG, Day NL. "School achievement in 14-year-old youths prenatally exposed to marijuana". *Neurotoxicol Teratol* **34**:161–167 (2012).

Gómez O, Arévalo-Martín Á, García-Ovejero D, Ortega-Gutiérrez S, Cisneros JA, Almazán G, Sánchez-Rodríguez MA, Molina-Holgado F, Molina-Holgado E. "The constitutive production of the endocannabinoid 2-arachidonoylglycerol participates in oligodendrocyte differentiation". *Glia* **58**:1913–1927 (2010).

Götz M, Hartfuss E, Malatesta P. "Radial glial cells as neuronal precursors: a new perspective on the correlation of morphology and lineage restriction in the developing cerebral cortex of mice". *Brain Res Bull* **57**:777–788 (2002).

Govek EE, Hatten ME, van Aelst L. "The role of Rho GTPase proteins in CNS neuronal migration". *Dev Neurobiol* **71**:528–553 (2011).

Grant KS, Petroff R, Isoherranen N, Stella N, Burbacher TM. "Cannabis use during pregnancy: pharmacokinetics and effects on child development". *Pharmacol Ther* **182**:133–151 (2018).

Graus-Porta D, Blaess S, Senften M, Littlewood-Evans A, Damsky C, Huang Z, Orban P, Klein R, Schittny JC, Müller U. "β1-Class integrins regulate the development of laminae and folia in the cerebral and cerebellar cortex". *Neuron* **31**:367–379 (2001).

Greig LC, Woodworth MB, Galazo MJ, Padmanabhan H, Macklis JD. "Molecular logic of neocortical projection neuron specification, development and diversity". *Nat Rev Neurosci* **14**:755–769 (2013).

Guerrini R, Dobyns WB. "Malformations of cortical development: clinical features and genetic causes". *Lancet Neurol* **13**:710–726 (2014).

Guerrini R, Parrini E. "Neuronal migration disorders". *Neurobiol Dis* **38**:154–166 (2010).

Guggenhuber S, Alpár A, Chen R, Schmitz N, Wickert M, Mattheus T, Harasta AE, Purrio M, Kaiser N, Elphick MR, Monory K, Kilb W, Luhmann HJ, Harkany T, Lutz B, Klugmann M. "Cannabinoid receptor-interacting protein Crip1a modulates CB1 receptor signaling in mouse hippocampus". *Brain Struct Funct* **221**:2061–2074 (2016).

Gutiérrez SO, Casanova E, Goodenough S, Behl C, van der Stelt M, Eder M, Hermann H, Azad SC, Schutz G, Lutz B, Di Marzo V, Zieglgansberger W, Monory K, Cascio MG, Cannich A, Marsicano G, López-Rodríguez ML. "CB1 cannabinoid receptors and on-demand defense against excitotoxicity". *Science* **302**:84–88 (2003).

Hadjivassiliou G, Martinian L, Squier W, Blumcke I, Aronica E, Sisodiya SM, Thom M. "The application of cortical layer markers in the evaluation of cortical dysplasias in epilepsy". *Acta Neuropathol* **120**:517–528 (2010).

Hansen D V., Lui JH, Flandin P, Yoshikawa K, Rubenstein JL, Álvarez-Buylla A, Kriegstein AR. "Non-epithelial stem cells and cortical interneuron production in the human ganglionic eminences". *Nat Neurosci* **16**:1576–1587 (2013).

Harkany T, Guzmán M, Galve-Roperh I, Berghuis P, Devi LA, Mackie K. "The emerging functions of endocannabinoid signaling during CNS development". *Trends Pharmacol Sci* **28**:83–92 (2007).

Hartfuss E, Galli R, Heins N, Götz M. "Characterization of CNS precursor subtypes and radial glia". *Dev Biol* **229**:15–30 (2001).

Hartzell AL, Martyniuk KM, Brigidi GS, Heinz DA, Djaja NA, Payne A, Bloodgood BL. "NPAS4 recruits CCK basket cell synapses and enhances cannabinoid-sensitive inhibition in the mouse hippocampus". *eLife* **7**:e35927 (2018).

Hébert JM, Fishell G. "The genetics of early telencephalon patterning: some assembly required". *Nat Rev Neurosci* **9**:678–685 (2008).

Heng JIT, Chariot A, Nguyen L. "Molecular layers underlying cytoskeletal remodelling during cortical development". *Trends Neurosci* **33**:38–47 (2010).

Herkenham M, Lynn AB, Litrle MD, Johnsont MR, Melvin LS, Costa BRDE, Riceo KC. "Cannabinoid receptor localization in brain". *Proc Natl Acad Sci* **87**:1932–1936 (1990).

Hofman A, Jaddoe VWV, Mackenbach JP, Moll HA, Snijders RFM, Steegers EAP, Verhulst FC, Witteman JCM, Büller HA. "Growth, development and health from early fetal life until young adulthood: the Generation R Study". *Paediatr Perinat Epidemiol* **18**:61–72 (2004).

Howlett AC. "Cannabinoid inhibition of adenylate cyclase. Biochemistry of the response in neuroblastoma cell membranes". *Mol Pharmacol* **27**:429–436 (1985).

Howlett AC, Breivogel CS, Childers SR, Deadwyler SA, Hampson RE, Porrino LJ. "Cannabinoid physiology and pharmacology: 30 years of progress". *Neuropharmacology* **47**:345–358 (2004).

Hua T, Vemuri K, Pu M, Qu L, Han GW, Wu Y, Zhao S, Shui W, Li S, Korde A, Laprairie RB, Stahl EL, Ho JH, Zvonok N, Zhou H, Kufareva I, Wu B, Zhao Q, Hanson MA, Bohn LM, Makriyannis A, Stevens RC, Liu ZJ. "Crystal structure of the human cannabinoid receptor CB1". *Cell* **167**:750-762 (2016).

Hua T, Vemuri K, Nikas SP, Laprairie RB, Wu Y, Qu L, Pu M, Korde A, Jiang S, Ho JH, Han GW, Ding K, Li X, Liu H, Hanson MA, Zhao S, Bohn LM, Makriyannis A, Stevens R, Liu ZJ. "Crystal structures of agonist-bound human cannabinoid receptor CB1". *Nature* **547**:468–471 (2017).

Huang ZJ. "Toward a genetic dissection of cortical circuits in the mouse". *Neuron* **83**:1284–1302 (2014).

Iffland PH, Crino P. "Focal cortical dysplasia: gene mutations, cell signaling, and therapeutic implications". *Annu Rev Pathol Mech Dis* **12**:547–571 (2017).

Immer ANZ. "Altered gene expression in striatal projection neurons in CB1 cannabinoid receptor knockout mice". **96**:5786–5790 (1999).

Jansen LA, Mirzaa GM, Ishak GE, O'Roak BJ, Hiatt JB, Roden WH, Gunter SA, Christian SL, Collins S, Adams C, Rivière JB, St-Onge J, Ojemann JG, Shendure J, Hevner RF, Dobyns WB. "PI3K/AKT pathway mutations cause a spectrum of brain malformations from megalencephaly to focal cortical dysplasia". *Brain* **138**:1613–1628 (2015).

Jin K, Xie L, Kim SH, Parmentier-Batteur S, Sun Y, Mao XO, Childs J, Greenberg DA. "Defective adult neurogenesis in CB1 cannabinoid receptor knockout mice". *Mol Pharmacol* **66**:204–208 (2004).

Jin W, Brown S, Roche JP, Hsieh C, Celver JP, Kovoor A, Chavkin C, Mackie K. "Distinct domains of the CB1 cannabinoid receptor mediate desensitization and internalization". *J Neurosci* **19**:3773–3780 (1999).

Jordan JD, He JC, Eungdamrong NJ, Gomes I, Ali W, Nguyen T, Bivona TG, Philips MR, Devi LA, Iyengar R. "Cannabinoid Receptor-induced Neurite Outgrowth Is Mediated by Rap1 Activation through $G\alpha_{o/i}$-triggered proteasomal degradation of Rap1GAPII". *J Biol Chem* **280**:11413–11421 (2005).

Jutras-Aswad D, DiNieri JA, Harkany T, Hurd YL. "Neurobiological consequences of maternal cannabis on human fetal development and its neuropsychiatric outcome". *Eur Arch Psychiatry Clin Neurosci* **259**:395–412 (2009).

Kano M, Ohno-Shosaku T, Hashimotodani Y, Uchigashima M, Watanabe M. "Endocannabinoid-mediated control of synaptic transmission". *Physiol Rev* **89**:309–380 (2009).

Katona I, Freund TF. "Endocannabinoid signaling as a synaptic circuit breaker in neurological disease". *Nat Med* **14**:923–930 (2008).

Kaur R, Ambwani SR, Singh S. "Endocannabinoid system: a multi-facet therapeutic target". *Curr Clin Pharmacol* **11**:110–117 (2016).

Keimpema E, Barabas K, Morozov YM, Tortoriello G, Torii M, Cameron G, Yanagawa Y, Watanabe M, Mackie K, Harkany T. "Differential subcellular recruitment of monoacylglycerol lipase generates spatial specificity of 2-arachidonoyl glycerol signaling during axonal pathfinding". *J Neurosci* **30**:13992–14007 (2010).

Khatri D, Laroche G, Grant ML, Jones VM, Vetreno RP, Crews FT, Mukhopadhyay S. "Acute ethanol inhibition of adult hippocampal neurogenesis involves CB1 cannabinoid receptor signaling". *Alcohol Clin Exp Res* **42**:718–726 (2018).

Kim Y, Yang GR, Pradhan K, Venkataraju KU, Bota M, García del Molino LC, Fitzgerald G, Ram K, He M, Levine JM, Mitra P, Huang ZJ, Wang XJ, Osten P. "Brain-wide maps reveal stereotyped cell-type-based cortical architecture and subcortical sexual dimorphism". *Cell* **171**:456-469 (2017).

Kishimoto Y, Masanobu K. "Endogenous cannabinoid signaling through the CB1 receptor is essential for cerebellum-dependent discrete motor learning". *J Neurosci* **26**:8829–8837 (2006).

Klausberger T, Marton LF, O'Neill J, Huck JH, Dalezios Y, Fuentealba P, Suen WY, Papp E, Kaneko T, Watanabe M, Csicsvari J, Somogyi P. "Complementary roles of cholecystokinin- and parvalbumin-expressing GABAergic neurons in hippocampal network oscillations. *J Neurosci* **25**:9782–9793 (2005).

Klausberger T, Somogyi P. "Neuronal diversity and temporal dynamics: the unity of hippocampal circuit operations". *Science* **321**:53–57 (2008).

Kowalczyk T, Pontious A, Englund C, Daza RAM, Bedogni F, Hodge R, Attardo A, Bell C, Huttner WB, Hevner RF. "Intermediate neuronal progenitors (basal progenitors) produce pyramidal-projection neurons for all layers of cerebral cortex". *Cereb Cortex* **19**:2439–2450 (2009).

Kriegstein A, Álvarez-Buylla A. "The glial nature of embryonic and adult neural stem cells". *Annu Rev Neurosci* **32**:149–184 (2009).

Langston RF, Wood ER. "Associative recognition and the hippocampus: differential effects of hippocampal lesions on object-place, object-context and object-place-context memory". *Hippocampus* **20**:1139–1153 (2010).

Laporte SA, Scott MGH. "β-Arrestins: multitask scaffolds orchestrating the where and when in cell signalling" *Methods Mol Biol* **1957**:9-55 (2019).

Lauckner JE, Hille B, Mackie K. "The cannabinoid agonist WIN55,212-2 increases intracellular calcium *via* CB1 receptor coupling to $G_{q/11}$ G proteins". *Proc Natl Acad Sci* **102**:19144–19149 (2005).

Li G, Adesnik H, Li J, Long J, Nicoll RA, Rubenstein JLR, Pleasure SJ. "Regional distribution of cortical interneurons and development of inhibitory tone are regulated by Cxcl12/Cxcr4 signaling". *J Neurosci* **28**:1085–1098 (2008).

Lim JS, Kim W, Kang H, Kim SH, Park AH, Park EK, Cho Y, Kim S, Kim HM, Kim JA, Kim J, Rhee H, Kang S, Kim HD, Kim D, Kim D, Lee JH. "Brain somatic mutations in MTOR cause focal cortical dysplasia type II leading to intractable epilepsy". *Nat Med* **21**:395–400 (2015).

Lim L, Mi D, Llorca A, Marín O. "Development and functional diversification of cortical interneurons". *Neuron* **100**:294–313 (2018).

Ljungberg MC, Bhattacharjee MB, Lu Y, Armstrong DL, Yoshor D, Swann JW, Sheldon M, D'Arcangelo G. "Activation of mammalian target of rapamycin in cytomegalic neurons of human cortical dysplasia". *Ann Neurol* **60**:420–429 (2006).

López-Valero I, Saiz-Ladera C, Torres S, Hernández-Tiedra S, García-Taboada E, Rodríguez-Fornés F, Barba M, Dávila D, Salvador-Tormo N, Guzmán M, Sepúlveda JM, Sánchez-Gómez P, Lorente M, Velasco G. "Targeting glioma initiating cells with a combined therapy of cannabinoids and temozolomide". *Biochem Pharmacol* **157**:266–274 (2018).

Ludányi A, Eross L, Czirják S, Vajda J, Halász P, Watanabe M, Palkovits M, Maglóczky Z, Freund TF, Katona I. "Downregulation of the CB1 cannabinoid receptor and related molecular elements of the endocannabinoid system in epileptic human hippocampus." *J Neurosci* **28**:2976–2990 (2008).

Maccarrone M, Guzmán M, Mackie K, Doherty P, Harkany T. "Programming of neural cells by (endo)cannabinoids: from physiological rules to emerging therapies". *Nat Rev Neurosci* **15**:786–801 (2014).

Majolo F, Marinowic DR, Machado DC, Da Costa JC. "MTOR pathway in focal cortical dysplasia type 2: What do we know?". *Epilepsy Behav* **85**:157–163 (2018).

Malatesta P, Hartfuss E, Götz M. "Isolation of radial glial cells by fluorescent-activated cell sorting reveals a neuronal lineage". *Development* **127**:5253–5263 (2000).

Marín-Padilla M. "Cajal-Retzius cells and the development of the neocortex". *Trends Neurosci* **21**:64–71 (1998).

Marín O. "Cellular and molecular mechanisms controlling the migration of neocortical interneurons". *Eur J Neurosci* **38**:2019–2029 (2013).

Marín O, Müller U. "Lineage origins of GABAergic *versus* glutamatergic neurons in the neocortex". *Curr Opin Neurobiol* **26**:132–141 (2014).

Marín O, Rubenstein JLR. "A long, remarkable journey: tangential migration in the telencephalon". *Nat Rev Neurosci* **2**:780–790 (2001).

Marín O, Valdeolmillos M, Moya F. "Neurons in motion: same principles for different shapes?" *Trends Neurosci* **29**:655–661 (2006).

Maroso M, Szabo G, Kim HK, Alexander A, Bui A, Lee SH, Lutz B, Soltesz I. "Cannabinoid control of learning and memory through HCN channels". *Neuron* **89**:1059–1073 (2016).

Marroun H El, Hudziak JJ, Tiemeier H, Creemers H, Steegers EAP, Jaddoe VWV, Hofman A, Verhulst FC, van den Brink W, Huizink AC. "Intrauterine cannabis exposure leads to more aggressive behavior and attention problems in 18-month-old girls". *Drug Alcohol Depend* **118**:470–474 (2011).

Marsicano G, Lutz B. "Expression of the cannabinoid receptor CB1 in distinct neuronal subpopulations in the adult mouse forebrain". *Eur J Neurosci* **11**:4213–4225 (1999).

Marsicano G, Wotjak CT, Azad SC, Bisognok T, Rammes G, Casciok MG, Hermann H, Tang J, Hofmann C, Zieglgansberger W, Di Marzo V, Lutz B. "The endogenous cannabinoid system controls extinction of aversive memories". *Nature* **418**:530–534 (2002).

Martín R, Bajo-Grañeras R, Moratalla R, Perea G, Araque A. "Circuit-specific signaling in astrocyte-neuron networks in basal ganglia pathways". Science **349**:730–735 (2015).

Martynoga B, Drechsel D, Guillemot F. "Molecular control of neurogenesis: a view from the mammalian cerebral cortex". *Cold Spring Harb Perspect Biol* **4**:a008359 (2012).

Mato S, del Olmo E, Pazos A. "Ontogenetic development of cannabinoid receptor expression and signal transduction functionality in the human brain". *Eur J Neurosci* **17**:1747–1754 (2003).

Mechoulam R, Parker L. "The endocannabinoid system and the brain". *Annu Rev Psychol* **62**:21–47 (2013).

Mehmedic Z, Chandra S, Slade D, Denham H, Foster S, Patel AS, Ross SA, Khan IA, ElSohly MA "Potency trends of Δ9 -THC and other cannabinoids in confiscated cannabis preparations from 1993 to 2008". *J Forensic Sci* **55**:1209–1217 (2010).

Mereu G, Fa M, Ferraro L, Cagiano R, Antonelli T, Tattoli M, Ghiglieri V, Tanganelli S, Gessa GL, Cuomo V. "Prenatal exposure to a cannabinoid agonist produces memory deficits linked to dysfunction in hippocampal long-term potentiation and glutamate release". *Proc Natl Acad Sci* **100**:4915–4920 (2003).

Metna-Laurent M, Mondésir M, Grel A, Vallée M, Piazza PV. "Cannabinoid-induced tetrad in mice". *Curr Protoc Neurosci* **80**:9.59.1-9.59.10 (2017).

Meyuhas O. "Ribosomal protein S6 phosphorylation: four decades of research". *Int Rev Cell Mol Biol* **320**:41–73 (2015).

Mihalas AB, Elsen GE, Bedogni F, Daza RAM, Ramos-Laguna KA, Arnold SJ, Hevner RF. "Intermediate progenitor cohorts differentially generate cortical layers and require Tbr2 for timely acquisition of neuronal subtype identity". *Cell Rep* **16**:92–105 (2016).

Misson J, Takahashi T, Caviness VS. "Ontogeny of radial and other astroglial cells in murine cerebral cortex". *Glia* **4**:138–148 (1991).

Miyata T, Kawaguchi A, Okano H, Ogawa M. "Asymmetric inheritance of radial glial fibers by cortical neurons". *Neuron* **31**:727–741 (2001).

Miyoshi G, Fishell G. "GABAergic interneuron lineages selectively sort into specific cortical layers during early postnatal development". *Cereb Cortex* **21**:845–852 (2011).

Mizutani KI, Yoon K, Dang L, Tokunaga A, Gaiano N. "Differential Notch signalling distinguishes neural stem cells from intermediate progenitors". *Nature* **449**:351–355 (2007).

Molina-Holgado E, Vela JM, Arévalo-Martín A, Almazán G, Molina-Holgado F, Borrell J, Guaza C. "Cannabinoids promote oligodendrocyte progenitor survival: involvement of cannabinoid receptors and phosphatidylinositol-3 kinase/Akt signaling". *J Neurosci* **22**:9742–9753 (2002).

Molina-Holgado F, Rubio-Araiz A, García-Ovejero D, Williams RJ, Moore JD, Arévalo-Martín Á, Gómez-Torres O, Molina-Holgado E. "CB2 cannabinoid receptors promote mouse neural stem cell proliferation". *Eur J Neurosci* **25**:629–634 (2007).

Molyneaux BJ, Arlotta P, Menezes JRL, Macklis JD. "Neuronal subtype specification in the cerebral cortex". *Nat Rev Neurosci* **8**:427–437 (2007).

Monory K, Blaudzun H, Massa F, Kaiser N, Lemberger T, Schütz G, Wotjak CT, Lutz B, Marsicano G (2007) Genetic dissection of behavioural and autonomic effects of Δ9-tetrahydrocannabinol in mice. PLoS Biol 5:2354–2368 (2007).

Monory K, Massa F, Egertová M, Eder M, Blaudzun H, Westenbroek R, Kelsch W, Jacob W, Marsch R, During M, Klugmann M, Wölfel B, Dodt HU, Zieglgänsberger W, Wotjak CT, Mackie K, Elphick MR, Marsicano G, Lutz B. "The endocannabinoid system controls key epileptogenic circuits in the hippocampus". *Neuron* **51**:455–466 (2006).

Morcillo-Suárez C, Alegre J, Sangros R, Gazave E, de Cid R, Milne R, Amigo J, Ferrer-Admetlla A, Moreno-Estrada A, Gardner M, Casals F, Pérez-Lezaun A, Comas D, Bosch E, Calafell F, Bertranpetit J, Navarro A. "SNP analysis to results (SNPator): a web-based environment oriented to statistical genomics analyses upon SNP data". *Bioinformatics* **24**:1643–1644 (2008).

Morena M, Patel S, Bains JS, Hill MN. "Neurobiological interactions between stress and the endocannabinoid system". *Neuropsychopharmacology* **41**:80–102 (2016).

Moreno E, Chiarlone A, Medrano M, Puigdellívol M, Bibic L, Howell LA, Resel E, Puente N, Casarejos MJ, Perucho J, Botta J, Suelves N, Ciruela F, Ginés S, Galve-Roperh I, Casadó V, Grandes P, Lutz B, Monory K, Canela EI, Lluís C, McCormick PJ, Guzmán M. "Singular location and signaling profile of adenosine A2A-cannabinoid CB1 receptor heteromers in the dorsal striatum. *Neuropsychopharmacology* **43**:964–977 (2018).

Morris CV, Dinieri JA, Szutorisz H, Hurd YL. "Molecular mechanisms of maternal cannabis and cigarette use on human neurodevelopment". *Eur J Neurosci* **34**:1574–1583 (2011).

Moser MB, Rowland DC, Moser EI. "Place cells, grid cells, and memory". *Cold Spring Harb Perspect Biol* **7**:a021808 (2015).

Mountcastle VB. "The columnar organization of the neocortex". *Brain* **120**:701–722 (1997).

Mulder J, Aguado T, Keimpema E, Barabás K, Ballester Rosado CJ, Nguyen L, Monory K, Marsicano G, Di Marzo V, Hurd YL, Guillemot F, Mackie K, Lutz B, Guzmán M, Lu HC, Galve-Roperh I, Harkany T. "Endocannabinoid signaling controls pyramidal cell specification and long-range axon patterning". *Proc Natl Acad Sci* **105**:8760–8765 (2008).

Munro S, Thomas KL, Abu-Shaar M. "Molecular characterization of a peripheral receptor for cannabinoids". *Nature* **365**:61–65 (1993).

Nadarajah B, Brunstrom JE, Grutzendler J, Wong ROL, Pearlman AL. "Two modes of radial migration in early development of the cerebral cortex". *Nat Neurosci* **4**:143–150 (2001).

Najm I, Sarnat HB, Blümcke I. "The international consensus classification of focal cortical dysplasia – a critical update 2018". *Neuropathol Appl Neurobiol* **44**:18–31 (2018).

Navarro-Romero A, Vázquez-Oliver A, Gomis-González M, Garzón-Montesinos C, Falcón-Moya R, Pastor A, Martín-García E, Pizarro N, Busquets-García A, Revest JM, Piazza PV, Bosch F, Dierssen M, de la Torre R, Rodríguez-Moreno A, Maldonado R, Ozaita A. "Cannabinoid type-1 receptor blockade restores neurological phenotypes in two models for Down syndrome". *Neurobiol Dis* 125:92–106 (2019).

Nguyen L, Hippenmeyer S. Cellular and molecular control of neuronal migration. *Springer* (2014).

Noctor SC, Flint AC, Weissman TA, Dammerman RS, Kriegstein AR. "Neurons derived from radial glial cells establish radial units in neocortex". *Nature* **409**:714–720 (2001).

Noctor SC, Martínez-Cerdeño V, Ivic L, Kriegstein AR. "Cortical neurons arise in symmetric and asymmetric division zones and migrate through specific phases". Nat Neurosci **7**:136–144 (2004).

Noctor SC, Martínez-Cerdeño V, Kriegstein AR. "Distinct behaviors of neural stem and progenitor cells underlie cortical neurogenesis". *J Comp Neurol* **508**:28–44 (2008).

O'Connell BK, Gloss D, Devinsky O. "Cannabinoids in treatment-resistant epilepsy: a review". *Epilepsy Behav* **70**:341–348 (2017).

O'Leary DD, Sahara S. "Genetic regulation of arealization of the neocortex". *Curr Opin Neurobiol* **18**:90–100 (2008).

O'Leary DD, Chou SJ, Sahara S. "Area patterning of the mammalian cortex". *Neuron* **56**:252–269 (2007).

Ohno-Shosaku T, Tanimura A, Hashimotodani Y, Kano M. "Endocannabinoids and retrograde modulation of synaptic transmission". *Neuroscientist* **18**:119–132 (2012).

Ohtaka-Maruyama C, Okamoto M, Endo K, Oshima M, Kaneko N, Yura K, Okado H, Miyata T, Maeda N. "Synaptic transmission from subplate neurons controls radial migration of neocortical neurons". *Science* **360**:313–317 (2018).

Orlova KA, Tsai V, Baybis M, Heuer GG, Sisodiya S, Thom M, Strauss K, Aronica E, Storm PB, Crino P. "Early progenitor cell marker expression distinguishes type II from type I focal cortical dysplasias". *J Neuropathol Exp Neurol* **69**:850–863 (2010).

Osumi N, Shinohara H, Numayama-Tsuruta K, Maekawa M. "Concise review: Pax6 transcription factor contributes to both embryonic and adult neurogenesis as a multifunctional regulator". *Stem Cells* **26**:1663–1672 (2008).

Oudin MJ, Gajendra S, Williams G, Hobbs C, Lalli G, Doherty P. "Endocannabinoids regulate the migration of Subventricular Zone-derived neuroblasts in the postnatal brain". *J Neurosci* **31**:4000–4011 (2011).

Ozturk HM, Yetkin E, Ozturk S. "Synthetic cannabinoids and cardiac arrhythmia risk: review of the literature". *Cardiovasc Toxicol* **19**:191–197 (2019).

Palazuelos J, Ortega Z, Díaz-Alonso J, Guzmán M, Galve-Roperh I. "CB2 cannabinoid receptors promote neural progenitor cell proliferation *via* mTORC1 signaling". *J Biol Chem* **287**:1198–1209 (2012).

Pérez-Rosado A, Gómez M, Manzanares J, Ramos JA, Fernández-Ruiz JJ. "Changes in prodynorphin and POMC gene expression in several brain regions of rat fetuses prenatally exposed to Δ9-tetrahydrocannabinol". *Neurotox Res* **4**:211–218 (2002).

Pérez-Rosado A, Manzanares J, Fernández-Ruiz JJ, Ramos JA. "Prenatal Δ9-tetrahydrocannabinol exposure modifies proenkephalin gene expression in the fetal rat brain: sex-dependent differences". *Dev Brain Res* **120**:77–81 (2000).

Piazza PV, Cota D, Marsicano G. "The CB1 receptor as the cornerstone of exostasis". *Neuron* **93**:1252–1274 (2017).

Pijlman FTA, Rigter SM, Hoek J, Goldschmidt HMJ, Niesink RJM. "Strong increase in total delta-THC in cannabis preparations sold in Dutch coffee shops". *Addict Biol* **10**:171–180 (2005).

Pinky PD, Bloemer J, Smith WD, Moore T, Hong H, Suppiramaniam V, Reed MN. "Prenatal cannabinoid exposure and altered neurotransmission". *Neuropharmacology* **149**:181–194 (2019).

Piper BJ, Dekeuster RM, Beals ML, Cobb CM, Burchman CA, Perkinson L, Lynn ST, Nichols SD, Abess AT. "Substitution of medical cannabis for pharmaceutical agents for pain, anxiety, and sleep". *J Psychopharmacol* **31**:569–575 (2017).

Psychoyos D, Hungund B, Cooper T, Finnell RH. "A cannabinoid analogue of Δ9-tetrahydrocannabinol disrupts neural development in chick". *Birth Defects Res Part B - Dev Reprod Toxicol* **83**:477–488 (2008).

Puelles L, Kuwana E, Puelles E, Bulfone A, Shimamura K, Keleher J, Smiga S, Rubenstein JLR. "Pallial and subpallial derivatives in the embryonic chick and mouse telencephalon, traced by the expression of the genes Dlx-2, Emx-1, Nkx-2.1, Pax-6, and Tbr-1". *J Comp Neurol* **424**:409–438 (2000).

Puighermanal E, Busquets-García A, Maldonado R, Ozaita A. "Cellular and intracellular mechanisms involved in the cognitive impairment of cannabinoids". *Philos Trans R Soc B Biol Sci* **367**:3254–3263 (2012).

Puighermanal E, Marsicano G, Busquets-García A, Lutz B, Maldonado R, Ozaita A. "Cannabinoid modulation of hippocampal long-term memory is mediated by mTOR signaling". *Nat Neurosci* **12**:1152–1158 (2009).

Qian X, Shen Q, Goderie SK, He W, Capela A, Davis AA, Temple S. "Timing of CNS cell generation". *Neuron* **28**:69–80 (2000).

Quarta C, Bellocchio L, Mancini G, Mazza R, Cervino C, Braulke LJ, Fekete C, Latorre R, Nanni C, Bucci M, Clemens LE, Heldmaier G, Watanabe M, Leste-Lassere T, Maitre M, Tedesco L, Fanelli F, Reuss S, Klaus S, Srivastava RK, Monory K, Valerio A, Grandis A, de Giorgio R, Pasquali R, Nisoli E, Cota D, Lutz B, Marsicano G, Pagotto U. "CB1 signaling in forebrain and sympathetic neurons is a key determinant of endocannabinoid actions on energy balance". *Cell Metab* **11**:273–285 (2010).

Rakic P. "Mode of cell migration to the superficial layers of fetal monkey neocortex". *J Comp Neurol* **145**:61–83 (1972).

Rakic P. "Specification of cerebral cortical areas". *Science* **241**:170–176 (1988).

Ramón y Cajal S. "Comparative study of the sensory areas of the human cortex". *Clark University* (1899).

Raver SM, Keller A. "Permanent suppression of cortical oscillations in mice after adolescent exposure to cannabinoids: receptor mechanisms". *Neuropharmacology* **86**:161–173 (2014).

Reillo I, de Juan Romero C, García-Cabezas MÁ, Borrell V. "A role for intermediate radial glia in the tangential expansion of the mammalian cerebral cortex". *Cereb Cortex* **21**:1674–1694 (2011).

Riccio O, Hurni N, Murthy S, Vutskits L, Hein L, Dayer A. "Alpha2-adrenergic receptor activation regulates cortical interneuron migration". *Eur J Neurosci* **36**:2879–2887 (2012).

Ricos MG, Hodgson BL, Pippucci T, Saidin A, Ong YS, Heron SE, Licchetta L, Bisulli F, Bayly MA, Hughes J, Baldassari S, Palombo F, Santucci M, Meletti S, Berkovic SF, Rubboli G, Thomas PQ, Scheffer IE, Tinuper P, Geoghegan J, Schreiber AW, Dibbens LM. "Mutations in the mammalian target of rapamycin pathway regulators NPRL2 and NPRL3 cause focal epilepsy". *Ann Neurol* **79**:120–131 (2016).

Roland AB, Ricobaraza A, Carrel D, Jordan BM, Rico F, Simon A, Humbert-Claude M, Ferrier J, McFadden MH, Scheuring S, Lenkei Z. "Cannabinoid-induced actomyosin contractility shapes neuronal morphology and growth". eLife **3**:e03159 (2014).

Romero-Sandoval EA, Kolano AL, Alvarado-Vázquez PA. "Cannabis and cannabinoids for chronic pain". *Curr Rheumatol Rep* **19**:67 (2017).

Romero J, García-Palomero E, Berrendero F, García-Gil L, Hernández ML, Ramos JA, Fernández-Ruiz JJ. "Atypical location of cannabinoid receptors in white matter areas during rat brain development". *Synapse* **26**:317–323 (1997).

Rowitch DH, Kriegstein AR. "Developmental genetics of vertebrate glial-cell specification". *Nature* **468**:214–222 (2010).

Rubenstein JLR, Shimamura K, Martínez S, Puelles L. "Regionalization of the prosencephalic neural plate". *Annu Rev Neurosci* **21**:445–477 (1998).

Rubino T, Parolaro D. "Sexually dimorphic effects of cannabinoid compounds on emotion and cognition". *Front Behav Neurosci* **5**:64 (2011).

Saez TMMM, Aronne MP, Caltana L, Brusco AH. "Prenatal exposure to the CB1 and CB2 cannabinoid receptor agonist WIN 55,212-2 alters migration of early-born glutamatergic neurons and GABAergic interneurons in the rat cerebral cortex". *J Neurochem* **129**:637–648 (2014).

Sanchis-Segura C, Becker JB. "Why we should consider sex (and study sex differences) in addiction research". *Addict Biol* **21**:995–1006 (2016).

Sauer FC. "Mitosis in the neural tube". *J Comp Neurol* **62**:377–405 (1934).

Scheyer AF, Wager-Miller J, Pelissier-Alicot AL, Murphy MN, Mackie K, Manzoni OJ. "Maternal cannabinoid exposure during lactation alters the developmental trajectory of prefrontal cortex GABA-currents in offspring". *bioRxiv* :336735 (2018).

Shao Z, Yin J, Chapman K, Grzemska M, Clark L, Wang J, Rosenbaum DM. "High-resolution crystal structure of the human CB1 cannabinoid receptor". *Nature* **540**:602–606 (2016).

Shitamukai A, Konno D, Matsuzaki F. "Oblique radial glial divisions in the developing mouse neocortex induce self-renewing progenitors outside the germinal zone that resemble primate outer subventricular zone progenitors". *J Neurosci* **31**:3683–3695 (2011).

Sickmann HM, Patten AR, Morch K, Sawchuk S, Zhang C, Parton R, Szlavik L, Christie BR. "Prenatal ethanol exposure has sex-specific effects on hippocampal long-term potentiation". *Hippocampus* **24**:54–64 (2014).

Sidman RL, Rakic P. "Neuronal migration, with special reference to developing human brain: a review". *Brain Res* **62**:1–35 (1973).

Smith DR, Stanley CM, Foss T, Boles RG, McKernan K. "Rare genetic variants in the endocannabinoid system genes CNR1 and DAGLA are associated with neurological phenotypes in humans". *PLoS One* **12**:e0187926 (2017).

Soltesz I, Alger BE, Kano M, Lee SH, Lovinger DM, Ohno-Shosaku T, Watanabe M. "Weeding out bad waves: towards selective cannabinoid circuit control in epilepsy". *Nat Rev Neurosci* **16**:264–277 (2015).

Soltesz I, Losonczy A. "CA1 pyramidal cell diversity enabling parallel information processing in the hippocampus". *Nat Neurosci* **21**:484–493 (2018).

Soltys J, Yushak M, Mao-Draayer Y. "Regulation of neural progenitor cell fate by anandamide". *Biochem Biophys Res Commun* **400**:21–26 (2010).

Soria-Gómez E, Bellocchio L, Reguero L, Lepousez G, Martin C, Bendahmane M, Ruehle S, Remmers F, Desprez T, Matias I, Wiesner T, Cannich A, Nissant A, Wadleigh A, Pape HC, Chiarlone A, Quarta C, Verrier D, Vincent P, Massa F, Lutz B, Guzmán M, Gurden H, Ferreira G, Lledo PM, Grandes P, Marsicano G. "The endocannabinoid system controls food intake *via* olfactory processes". *Nat Neurosci* **17**:407–415 (2014).

Soriano E, del Río JA. "The cells of cajal-retzius: still a mystery one century after". *Neuron* **46**:389–394 (2005).

Stancik EK, Navarro-Quiroga I, Sellke R, Haydar TF. "Heterogeneity in ventricular zone neural precursors contributes to neuronal fate diversity in the postnatal neocortex". *J Neurosci* **30**:7028–7036 (2010).

Stanslowsky N, Jahn K, Venneri A, Naujock M, Haase A, Martin U, Frieling H, Wegner F. "Functional effects of cannabinoids during dopaminergic specification of human neural precursors derived from induced pluripotent stem cells". *Addict Biol* **22**:1329–1342 (2017).

Stark E, Roux L, Eichler R, Senzai Y, Royer S, Buzsáki G. "Pyramidal cell-interneuron interactions underlie hippocampal ripple oscillations". *Neuron* **83**:467–480 (2014).

Steindel F, Lerner R, Häring M, Ruehle S, Marsicano G, Lutz B, Monory K. "Neuron-type specific cannabinoid-mediated G protein signalling in mouse hippocampus". *J Neurochem* **124**:795–807 (2013).

Stella N. "Cannabinoid and cannabinoid-like receptors in microglia, astrocytes, and astrocytomas". *Glia* **58**:1017–1030 (2010).

Sullivan D, Csicsvari J, Mizuseki K, Montgomery S, Diba K, Buzsáki G. "Relationships between hippocampal sharp waves, ripples, and fast gamma oscillation: influence of dentate and entorhinal cortical activity". *J Neurosci* **31**:8605–8616 (2011).

Sun L, Tai L, Qiu Q, Mitchell R, Fleetwood-Walker S, Joosten EA, Cheung CW. "Endocannabinoid activation of CB1 receptors contributes to long-lasting reversal of neuropathic pain by repetitive spinal cord stimulation". *Eur J Pain* **21**:804–814 (2017).

Tabata H, Nakajima K. "Multipolar migration: the third mode of radial neuronal migration in the developing cerebral cortex". *J Neurosci* **23**:9996–10001 (2003).

Takahashi T, Nowakowski R, Caviness V. "Early ontogeny of the secondary proliferative population of the embryonic murine cerebral wall". *J Neurosci* **15**:6058–6068 (1995).

Takahashi T, Nowakowski R, Caviness V. "Cell cycle parameters and patterns of nuclear movement in the neocortical proliferative zone of the fetal mouse". *J Neurosci* **13**:820–833 (2018).

Tapia M, Domínguez A, Zhang W, del Puerto A, Ciorraga M, Benítez MJ, Guaza C, Garrido JJ. "Cannabinoid receptors modulate neuronal morphology and AnkyrinG density at the axon initial segment". *Front Cell Neurosci* **11**:5 (2017).

Tarabykin V, Stoykova A, Usman N, Gruss P. "Cortical upper layer neurons derive from the subventricular zone as indicated by Svet1 gene expression". *Development* **128**:1983–1993 (2001).

Tartaglia N, Bonn-Miller M, Hagerman R. "Treatment of fragile X syndrome with cannabidiol: a case series study and brief review of the literature". *Cannabis Cannabinoid Res* **4**:3–9 (2019).

Taverna E, Götz M, Huttner WB. "The cell biology of neurogenesis: toward an understanding of the development and evolution of the neocortex". *Annu Rev Cell Dev Biol* **30**:465–502 (2014).

Torii M, Hashimoto-Torii K, Levitt P, Rakic P. "Integration of neuronal clones in the radial cortical columns by EphA and ephrin-A signalling". *Nature* **461**:524–528 (2009).

Tortoriello G, Morris CV, Alpár A, Fuzik J, Shirran SL, Calvigioni D, Keimpema E, Botting CH, Reinecke K, Herdegen T, Courtney M, Hurd YL, Harkany T. "Miswiring the brain: Δ9-tetrahydrocannabinol disrupts cortical development by inducing an SCG10/stathmin-2 degradation pathway". *EMBO J* **33**:668–685 (2014).

Valero M, Averkin RG, Fernández-Lamo I, Aguilar J, López-Pigozzi D, Brotons-Mas JR, Cid E, Tamas G, Menéndez de la Prida LM. "Mechanisms for selective single-cell reactivation during offline sharp-wave ripples and their distortion by fast ripples". *Neuron* **94**:1234-1247 (2017).

Valero M, Cid E, Averkin RG, Aguilar J, Sánchez-Aguilera A, Viney TJ, Gómez-Domínguez D, Bellistri E, de la Prida LM. "Determinants of different deep and superficial CA1 pyramidal cell dynamics during sharp-wave ripples". *Nat Neurosci* **18**:1281–1290 (2015).

Valero M, de la Prida LM. "The hippocampus in depth: a sublayer-specific perspective of entorhinal-hippocampal function". *Curr Opin Neurobiol* **52**:107–114 (2018).

Vallée M, Vitiello S, Bellocchio L, Hébert-Chatelain E, Monlezun S, Martín-García E, Kasanetz F, Baillie GL, Panin F, Cathala A, Roullot-Lacarrière V, Fabre S, Hurst DP, Lynch DL, Shore DM, Deroche-Gamonet V, Spampinato U, Revest JM, Maldonado R, Reggio PH, Ross RA, Marsicano G, Piazza PV. "Pregnenolone can protect the brain from cannabis intoxication". *Science* **343**:94–98 (2014).

Vargish GA, Pelkey KA, Yuan X, Chittajallu R, Collins D, Fang C, McBain CJ. "Persistent inhibitory circuit defects and disrupted social behaviour following *in utero* exogenous cannabinoid exposure". *Mol Psychiatry* **22**:56–67 (2016).

Velasco G, Sánchez C, Guzmán M. "Towards the use of cannabinoids as antitumour agents". *Nat Rev Cancer* **12**:436–444 (2012).

Velasco G, Sánchez C, Guzmán M. "Anticancer mechanisms of cannabinoids". *Curr Oncol* **23**:S23–S32 (2016).

Vitalis T, Lainé J, Simon A, Roland A, Leterrier C, Lenkei Z. "The type 1 cannabinoid receptor is highly expressed in embryonic cortical projection neurons and negatively regulates neurite growth *in vitro*". *Eur J Neurosci* **28**:1705–1718 (2008).

Wang X, Dow-Edwards D, Anderson V, Minkoff H, Hurd YL. "Discrete opioid gene expression impairment in the human fetal brain associated with maternal marijuana use". *Pharmacogenomics J* **6**:255–264 (2006).

Wang X, Dow-Edwards D, Keller E, Hurd YL. "Preferential limbic expression of the cannabinoid receptor mRNA in the human fetal brain". *Neuroscience* **118**:681–694 (2003).

Wichterle H, Turnbull DH, Nery S, Fishell G, Álvarez-Buylla A. "*In utero* fate mapping reveals distinct migratory pathways and fates of neurons born in the mammalian basal forebrain". *Development* **128**:3759–3771 (2001).

Wilsch-Brauninger M, Peters J, Paridaen JTML, Huttner WB. "Basolateral rather than apical primary cilia on neuroepithelial cells committed to delamination". *Development* **139**:95–105 (2012).

Winterbottom EF, Moroishi Y, Halchenko Y, Armstrong DA, Beach PJ, Nguyen QP, Capobianco AJ, Ayad NG, Marsit CJ, Li Z, Karagas MR, Robbins DJ. "Prenatal arsenic exposure alters the placental expression of multiple epigenetic regulators in a sex-dependent manner". *Environ Heal* **18**:18 (2019).

Wu CS, Zhu J, Wager-Miller J, Wang S, O'Leary D, Monory K, Lutz B, Mackie K, Lu HC. "Requirement of cannabinoid CB(1) receptors in cortical pyramidal neurons for appropriate development of corticothalamic and thalamocortical projections". *Eur J Neurosci* **32**:693–706 (2010).

Yanagida M, Miyoshi R, Toyokuni R, Zhu Y, Murakami F. "Dynamics of the leading process, nucleus, and Golgi apparatus of migrating cortical interneurons in living mouse embryos". *Proc Natl Acad Sci* **109**:16737–16742 (2012).

Yao K, Duan Z, Zhou J, Li L, Zhai F, Dong Y, Wang X, Ma Z, Bian Y, Qi X, Li L. "Clinical and immunohistochemical characteristics of type II and type I focal cortical dysplasia". *Oncotarget* **7**:76415–76422 (2016).

Yeruva RR, Mekala HM, Sidhu M, Lippmann S. "Synthetic cannabinoids-"Spice" can induce a psychosis: a brief review". *Innov Clin Neurosci* **16**:31–32 (2019).

Young-Wolff KC, Tucker LY, Alexeeff S, Armstrong MA, Conway A, Weisner C, Goler N. "Trends in self-reported and biochemically tested marijuana use among pregnant females in California from 2009-2016". *JAMA* **318**:2490–2491 (2017).

Zimmer-Bensch G. "Diverse facets of cortical interneuron migration regulation – Implications of neuronal activity and epigenetics". *Brain Res* **1700**:160–169 (2018).

Zimmerman T, Maroso M, Beer A, Baddenhausen S, Ludewig S, Fan W, Vennin C, Loch S, Berninger B, Hofmann C, Korte M, Soltesz I, Lutz B, Leschik J. " Neural stem cell lineage-specific cannabinoid type-1 receptor regulates neurogenesis and plasticity in the adult mouse hippocampus". *Cer Cor* **28**;4454–4471 (2018).

Zurolo E, Iyer AM, Spliet WGM, van Rijen PC, Troost D, Gorter JA, Aronica E. "CB1 and CB2 cannabinoid receptor expression during development and in epileptogenic developmental pathologies". *Neuroscience* **170**:28–41 (2010).

# Addenda

## Participation in research articles

† ***Addendum* 1.** Blázquez C, Chiarlone A, Bellocchio L, Resel E, Pruunsild P, García-Rincón D, Sendtner M, Timmusk T, Lutz B, Galve-Roperh I, Guzmán M. "The $CB_1$ cannabinoid receptor signals striatal neuroprotection *via* a PI3K/Akt/MTORC1/BDNF pathway". *Cell Death Differ* **22**:1618–1629 (2015).

† ***Addendum* 2.** de Salas-Quiroga A*, Díaz-Alonso J*, García-Rincón D, Remmers F, Vega D, Gómez-Cañas M, Lutz B, Guzmán M, Galve-Roperh I. "Prenatal exposure to cannabinoids evokes long-lasting functional alterations by targeting $CB_1$ receptors on developing cortical neurons". *Proc Natl Acad Sci* **112**:13693–13698 (2015).

† ***Addendum* 3.** Díaz-Alonso J, de Salas-Quiroga A, Paraíso-Luna J, García-Rincón D, Garcez P, Parsons M, Andradas C, Sánchez C, Guillemot F, Guzmán M, Galve-Roperh I. "Loss of cannabinoid $CB_1$ receptors induces cortical migration malformations and increases seizure susceptibility". *Cereb Cortex* **27**:5303–5317 (2017).

† ***Addendum* 4.** García-Rincón D, Díaz-Alonso J, Paraíso-Luna J, Ortega Z, Aguareles J, de Salas-Quiroga A, Jou C, de Prada I, Martínez-Cerdeño V, Aronica E, Guzmán M, Pérez-Jiménez MA, Galve-Roperh I. "Contribution of altered endocannabinoid system to overactive mTORC1 signaling in focal cortical dysplasia". *Front Pharmacol* **9**:1508 (2019).

† ***Addendum* 5.** Aguareles J, Paraíso-Luna J, Palomares B, Bajo-Grañeras R, Navarrete C, Ruiz-Calvo A, García-Rincón D, García-Taboada E, Guzmán M, Muñoz E, Galve-Roperh I. "Oral administration of the cannabigerol derivative VCE-003.2 promotes subventricular zone neurogenesis and protects against mutant huntingtin-induced neurodegeneration". *Transl Neurodegener* **8**:9 (2019).

† de Salas-Quiroga A*, García-Rincón D*, Gómez-Domínguez D, Valero M, Paraíso-Luna J, Aguareles J, Simón S, Pujadas M, Muguruza C, Callado LF, Lutz B, Guzmán M, de la Prida LM, Galve-Roperh I. "Long-term hippocampal interneuronopathy drives sex-dimorphic spatial memory impairment induced by prenatal THC exposure". *Under review*.

OPEN

Cell Death and Differentiation (2015), 1–12

www.nature.com/cdd

# The $CB_1$ cannabinoid receptor signals striatal neuroprotection via a PI3K/Akt/mTORC1/BDNF pathway

C Blázquez[1,2], A Chiarlone[1,2], L Bellocchio[1,2], E Resel[1,2], P Pruunsild[3], D García-Rincón[1,2], M Sendtner[4], T Timmusk[3], B Lutz[5], I Galve-Roperh[1,2] and M Guzmán*[,1,2]

**The $CB_1$ cannabinoid receptor, the main molecular target of endocannabinoids and cannabis active components, is the most abundant G protein-coupled receptor in the mammalian brain. In particular, the $CB_1$ receptor is highly expressed in the basal ganglia, mostly on terminals of medium-sized spiny neurons, where it plays a key neuromodulatory function. The $CB_1$ receptor also confers neuroprotection in various experimental models of striatal damage. However, the assessment of the physiological relevance and therapeutic potential of the $CB_1$ receptor in basal ganglia-related diseases is hampered, at least in part, by the lack of knowledge of the precise mechanism of $CB_1$ receptor neuroprotective activity. Here, by using an array of pharmacological, genetic and pharmacogenetic (*designer receptor exclusively activated by designer drug*) approaches, we show that (1) $CB_1$ receptor engagement protects striatal cells from excitotoxic death via the phosphatidylinositol 3-kinase/Akt/mammalian target of rapamycin complex 1 pathway, which, in turn, (2) induces brain-derived neurotrophic factor (BDNF) expression through the selective activation of *BDNF* gene promoter IV, an effect that is mediated by multiple transcription factors. To assess the possible functional impact of the $CB_1$/BDNF axis in a neurodegenerative-disease context *in vivo*, we conducted experiments in the R6/2 mouse, a well-established model of Huntington's disease, in which the $CB_1$ receptor and BDNF are known to be severely downregulated in the dorsolateral striatum. Adeno-associated viral vector-enforced re-expression of the $CB_1$ receptor in the dorsolateral striatum of R6/2 mice allowed the re-expression of BDNF and the concerted rescue of the neuropathological deficits in these animals. Collectively, these findings unravel a molecular link between $CB_1$ receptor activation and BDNF expression, and support the relevance of the $CB_1$/BDNF axis in promoting striatal neuron survival.**
*Cell Death and Differentiation* advance online publication, 20 February 2015; doi:10.1038/cdd.2015.11

The $CB_1$ receptor is the most abundant G protein-coupled receptor in the mammalian brain.[1] This receptor is engaged by endocannabinoids, a family of prostanoid-like neural messengers, as well as by $\Delta^9$-tetrahydrocannabinol (THC), the main active component of the hemp plant *Cannabis sativa*.[1–3] Endocannabinoid signaling serves as a major feedback mechanism aimed at preventing excessive pre-synaptic activity, thereby tuning the functionality and plasticity of many synapses. In particular, the $CB_1$ receptor is very highly expressed in GABAergic terminals of the forebrain, where it mediates endocannabinoid-dependent inhibition of GABA release.[1]

In concert with this well-established neuromodulatory function, one of the most remarkable biological actions of the $CB_1$ receptor is to prevent neuronal death. This effect has been reported in many different animal models of acute brain damage and chronic neurodegeneration, and has raised hope about the possible clinical use of cannabinoids as neuroprotective drugs.[1,4–6] However, the assessment of the physiological relevance and therapeutic potential of the $CB_1$ receptor in neurological diseases is hampered, at least in part, by the lack of knowledge on the precise molecular mechanisms of $CB_1$ receptor neuroprotective activity.[5,7] It is well established that $CB_1$ receptor engagement inhibits excitotoxic neurotransmission by blunting pre-synaptic glutamate release, and this has been put forward as a major event underlying $CB_1$ receptor-mediated neuroprotection.[1,6,8,9] However, it is plausible that additional processes contribute to the neuroprotective activity of the $CB_1$ receptor. Specifically, studies conducted in the mouse and rat brain have reported a close association between $CB_1$ receptor activity and the expression of brain-derived neurotrophic factor (BDNF),[5,7] one of the master neurotrophins in the mammalian forebrain.[10] Moreover, acute

[1]Centro de Investigación Biomédica en Red sobre Enfermedades Neurodegenerativas (CIBERNED) and Instituto Ramón y Cajal de Investigación Sanitaria (IRYCIS), Madrid, Spain; [2]Department of Biochemistry and Molecular Biology I, School of Biology, Complutense University, and the Instituto Universitario de Investigación Neuroquímica (IUIN), Madrid, Spain; [3]Institute of Gene Technology, Tallinn University of Technology, Tallinn, Estonia; [4]Institute of Clinical Neurobiology, University of Würzburg, Würzburg, Germany and [5]Institute of Physiological Chemistry, University Medical Center of the Johannes Gutenberg University Mainz, Mainz, Germany
*Corresponding author: M Guzmán, Department of Biochemistry and Molecular Biology I, School of Biology, Complutense University, and the Instituto Universitario de Investigación Neuroquímica (IUIN), c/José Antonio Novais 2, Madrid 28040, Spain; Tel: +34 913944668; Fax: +34 913944672. E-mail: mgp@bbm1.ucm.es

**Abbreviations:** BDNF, brain-derived neurotrophic factor; CaMKII$\alpha$, calcium/calmodulin-dependent protein kinase II-$\alpha$; CaRF, calcium-responsive transcription factor; CNO, clozapine-*N*-oxide; CREB, cAMP response element-binding protein; Ct, threshold cycle; DARPP-32, dopamine- and cAMP-regulated phosphoprotein of 32 kDa; DREADD, designer receptor exclusively activated by designer drug; ERK, extracellular signal-regulated kinase; GAD-67, glutamic acid decarboxylase 67 kDa isoform; GFAP, glial fibrillary acidic protein; HD, Huntington's disease; JNK, c-Jun *N*-terminal kinase; MSN, medium-sized spiny neuron; mTORC1, mammalian target of rapamycin complex 1; NMDA, *N*-methyl-D-aspartate; NPAS4, neuronal PAS domain protein 4; PI3K, phosphatidylinositol 3-kinase; PKA, cAMP-dependent protein kinase; PSD-95, post-synaptic density protein 95; THC, $\Delta^9$-tetrahydrocannabinol; USF, upstream stimulatory factor

Received 15.7.14; revised 15.1.15; accepted 19.1.15; Edited by L Greene

intravenous administration of THC to healthy volunteers increases BDNF levels in the serum,[11] thus suggesting that a $CB_1$/BDNF connection could also exist in humans.

A putative $CB_1$/BDNF connection might be particularly relevant in the striatum, and influence their related motor disorders (e.g., Huntington's disease (HD) and Parkinson's disease), as, for example, (1) the $CB_1$ receptor is highly expressed in medium-sized spiny neurons (MSNs), the cells that constitute ~90% of total striatal neurons, and plays a key role in the control of motor behavior by basal ganglia circuitry;[4,12] (2) BDNF and its high-affinity receptor, TrkB, exert a pivotal function in MSN generation, survival and plasticity;[13–15] and (3) striatal $CB_1$ receptor,[16] BDNF[17] and TrkB[18] expression declines along disease progression in animal models of HD, and restoration of $CB_1$ receptor,[19] BDNF[20] or TrkB[21,22] function prevents HD-like neurodegeneration.

In spite of these concerted changes in $CB_1$ receptor activity and BDNF expression, no causative link between the two events has been defined yet. Hence, here we sought to establish a molecular connection between $CB_1$ receptor activation and BDNF expression in the striatum, and to assess the possible neuroprotective relevance of this putative $CB_1$/BDNF axis.

## Results

**The $CB_1$ receptor protects cultured striatal cells from excitoxicity via PI3K/Akt/mTORC1/BDNF.** The $CB_1$ cannabinoid receptor is a pleiotropic G protein-coupled receptor that modulates various pathways potentially involved in the control of cell survival such as phosphatidylinositol 3-kinase (PI3K)/Akt, mitogen-activated protein kinases (extracellular signal-regulated kinase (ERK), c-Jun *N*-terminal kinase (JNK) and p38) and cAMP/protein kinase A (PKA).[23] To study the mechanism of $CB_1$ receptor-mediated neuroprotection, we first used $STHdh^{Q7/Q7}$ mouse striatal neuroblasts, a widely used neuron-like cell line[24] that expresses functional $CB_1$ receptors.[19] Cells were incubated with two paradigmatic cannabinoid receptor agonists (THC, the major active ingredient of marijuana, and HU-210, a highly-potent synthetic derivative of THC) and evaluated how the aforementioned pathways were affected. Exposure of cells to cannabinoids led to a rapid (15 min) and transient (15–30 min) phosphorylation (activation) of Akt, which was followed by a transient (30 min) phosphorylation (activation) of ribosomal S6 protein, a canonical substrate of the Akt/mammalian target of rapamycin complex 1 (mTORC1) pathway (Figure 1a and Supplementary Figure S1a). This effect was dose dependent (Supplementary Figure S1b). In contrast, the phosphorylation status of ERK, JNK, p38 and PKA substrates was not changed by cannabinoids (Figure 1a).

These findings prompted us to test the involvement of the PI3K/Akt/mTORC1 pathway in $CB_1$ receptor-mediated neuroprotection. We used $STHdh^{Q7/Q7}$ cells exposed to the well-established excitotoxin *N*-methyl-D-aspartate (NMDA) because the $CB_1$ receptor is known to exert cytoprotection in that experimental system.[19] In agreement with some authors,[25,26] but, owing to unobvious reasons, in disagreement with others,[27] we could readily detect transcripts encoding NMDA receptor subunits in $STHdh^{Q7/Q7}$ cells (threshold cycle (Ct) values: NR1, 35; NR2A, 35; NR2B, 27; NR2C, 32; and NR2D, 34). These values support that NR2B and NR2C might be responsible for NMDA-induced responses in $STHdh^{Q7/Q7}$ cells, and that these cells express very low levels of other NMDA receptor subunits. Our $STHdh^{Q7/Q7}$ cells were sensitive to NMDA in a dose-dependent manner (Supplementary Figure S2). From these dose-dependency assays, which were similar to those previously reported by Xifro *et al.*,[26] we selected the standard dose of 1 mM NMDA for further experiments. THC and HU-210 rescued cells from 1-mM NMDA induced death, and blockade of PI3K (with wortmannin), Akt (with Akti-1/2) or mTORC1 (with rapamycin) abrogated cannabinoid-evoked cytoprotection (Figure 1b).

As BDNF plays a key protective role on MSNs, and an association between BDNF expression and $CB_1$ receptor function occurs in several pathophysiological settings,[5,7] we examined the possible involvement of BDNF in cannabinoid-induced neuroprotection. K252a, an inhibitor of the tyrosine kinase activity of the BDNF receptor TrkB, abrogated THC- and HU-210-induced neuroprotection (Figure 1c). A similar preventive effect was observed when *BDNF* or *TrkB* expression was silenced with specific siRNAs (which diminished total *BDNF* or *TrkB* mRNA levels to $29 \pm 10\%$ or $47 \pm 10\%$ of control siRNA-transfected cells, respectively; $n = 4–6$ experiments, $P < 0.01$; Figure 1d). Likewise, the involvement of the PI3K/Akt/mTORC1/BDNF axis in $CB_1$ receptor-evoked neuroprotection was also evident (1) when quinolinic acid instead of NMDA was used as excitotoxin (Supplementary Figure S3), and (2) when primary mouse striatal neurons (Ct values of NMDA receptor subunits: NR1, 28; NR2A, 31; NR2B, 26; NR2C, 32; and NR2D, 30) instead of $STHdh^{Q7/Q7}$ cells were used as cellular model (Figure 1e). Specifically, the protective effect of cannabinoids in those two experimental systems was prevented by the $CB_1$-selective antagonist SR141716 (rimonabant) or upon blockade of the PI3K/Akt/mTORC1/BDNF pathway (Supplementary Figure S3 and Figure 1e).

**The $CB_1$ receptor induces *BDNF* promoter IV via PI3K/Akt/mTORC1.** The *BDNF* gene consists of multiple promoters and 5′ untranslated exons, together with a common 3′ protein-coding exon. After transcription and splicing, one of the 5′ exons is joined to the single coding exon, therefore resulting in different *BDNF* mRNA forms but an identical BDNF protein.[28,29] To obtain direct evidence for the $CB_1$ receptor-mediated control of BDNF expression in $STHdh^{Q7/Q7}$ cells, we evaluated the effect of cannabinoids on the best characterized *Bdnf* gene promoters by using exon-specific qPCR primers. THC upregulated total *BDNF* transcripts ($Ct = 23$) and, specifically, exon IV-containing *BDNF* transcripts ($Ct = 27$; Figure 2a). Hence, *Bdnf* promoter IV was subsequently studied in further detail. THC-induced accumulation of exon IV-containing transcripts was mimicked by HU-210 and prevented by SR141716 (Figure 2b). As for cannabinoid-evoked neuroprotection (see above), blockade of the PI3K/Akt/mTORC1 pathway prevented the cannabinoid-induced increase of exon IV-containing transcripts (Figure 2b).

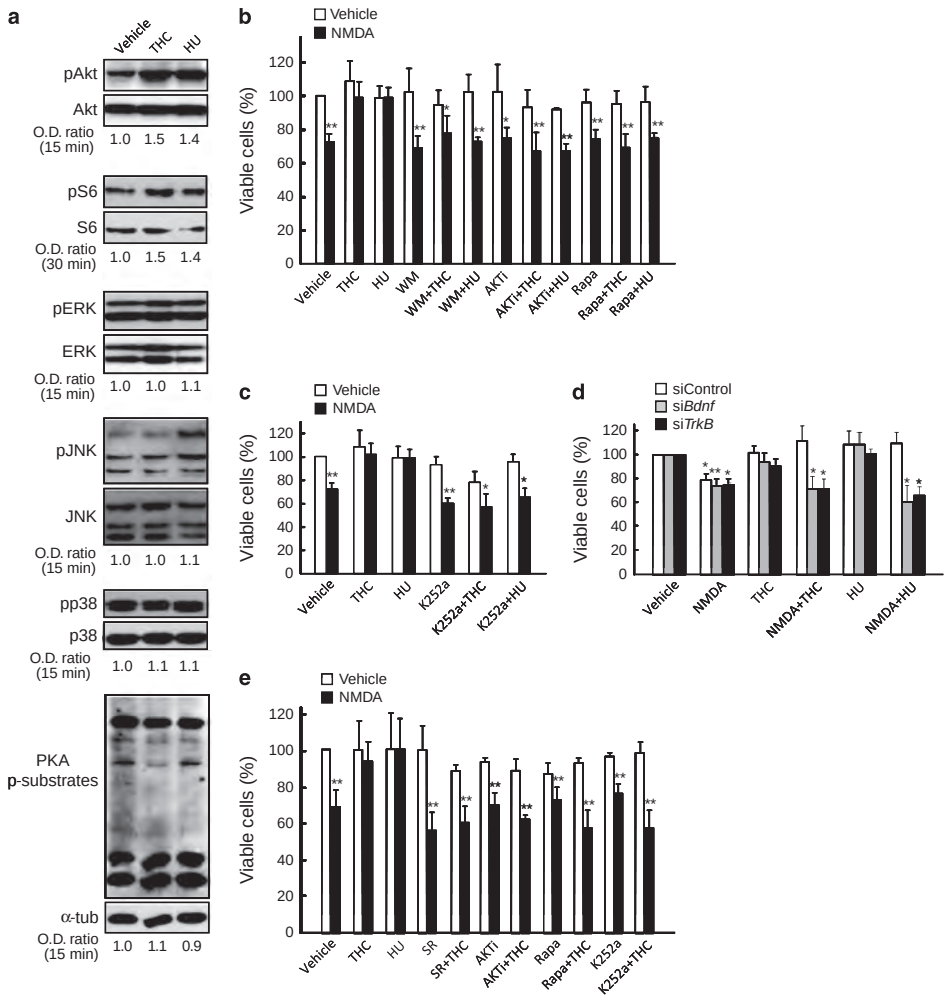


**Figure 1** The $CB_1$ receptor protects cultured striatal cells from NMDA-induced excitoxicity via PI3K/Akt/mTORC1/BDNF. (**a**) $STHdh^{Q7/Q7}$ cells were incubated for the times indicated with vehicle, 0.5-$\mu$M THC or 10-nM HU-210. Cells were lysed and western blot analyses were conducted. Quantification of mean optical density (O.D.) values relative to those of loading controls (respective total proteins, or $\alpha$-tubulin in the case of PKA phosphorylated substrates) as well as representative blots are shown ($n=3$–4 experiments). (**b**, **c**) $STHdh^{Q7/Q7}$ cells were preincubated for 5 h in Locke's solution with or without 1-mM NMDA together with vehicle, 0.5-$\mu$M THC, 10-nM HU-210, 0.2-$\mu$M wortmanin, 0.1-$\mu$M Akti-1/2, 30-nM rapamycin and/or 25-nM K252a, and subsequently incubated for 24 h in NMDA-free medium. Relative cell viability is shown ($n=6$–8 experiments). (**d**) $STHdh^{Q7/Q7}$ cells were transfected with a non-targeted siRNA or with siRNAs directed against *BDNF* or *TrkB*, and subsequently incubated for 5 h with or without NMDA, THC and/or HU-210 as in **b**. Relative cell viability is shown ($n=4$–6 experiments). (**e**) Primary mouse striatal neurons were incubated for 30 min in Locke's medium with or without 50-$\mu$M NMDA, together with vehicle, 0.3-$\mu$M THC, 10-nM HU-210, 0.25-$\mu$M SR141716, 0.1-$\mu$M Akti-1/2, 20-nM rapamycin and/or 10-nM K252a, and subsequently incubated for 2 h in NMDA-free medium. Relative cell viability is shown ($n=4$–6 experiments). Data were analyzed using ANOVA with *post hoc* Student-Newman-Keuls test. $^*P<0.05$ and $^{**}P<0.01$ from the corresponding vehicle-treated cells

We next used additional approaches to substantiate a $CB_1$ receptor-induced activation of *BDNF* promoter IV. (1) We transfected $STHdh^{Q7/Q7}$ cells with a construct that contains a human *BDNF* promoter IV fused to the luciferase reporter gene,[30] and found that promoter IV activity was enhanced by THC and HU-210, this effect being abrogated by blockade of Akt or mTORC1 (Figure 2c). (2) BDNF protein levels, as determined by ELISA in $STHdh^{Q7/Q7}$ cell-culture extracts, were also increased by THC and HU-210 in an Akt- and mTORC1-dependent manner (Figure 2d). (3) We isolated primary mouse striatal neurons and found that $CB_1$ receptor agonism increased both exon IV-containing (Ct = 29) and total *BDNF* transcripts (Ct = 27), as determined by qPCR (Figure 2e), as well as BDNF protein levels, as determined by western blot (Figure 2f; we were unable to reliably quantify BDNF by ELISA in neuron-culture supernatants). These neuron cultures had only ~5%

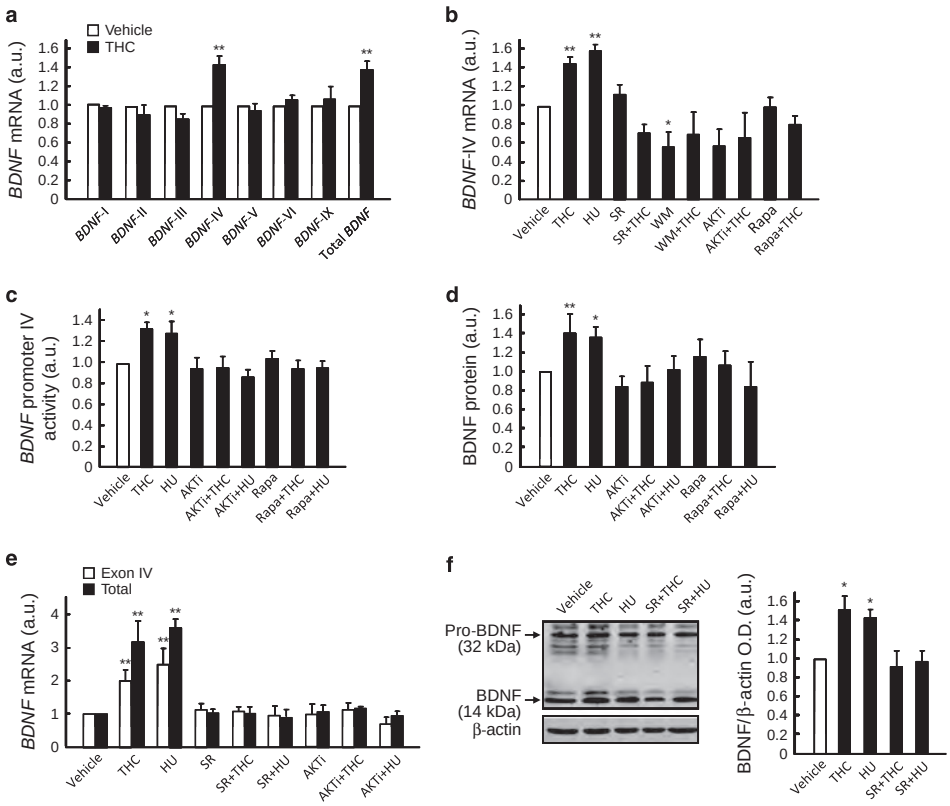


**Figure 2** The $CB_1$ receptor induces *BDNF* promoter IV via PI3K/Akt/mTORC1. (**a**) $STHdh^{Q7/Q7}$ cells were incubated for 15 h with vehicle or 0.5-$\mu$M THC and the levels of *BDNF* transcripts with the indicated 5′ exons were determined ($n=3$–4 experiments). (**b**) $STHdh^{Q7/Q7}$ cells were incubated for 15 h with vehicle or 0.5-$\mu$M THC, 10-nM HU-210, 0.25-$\mu$M SR141716, 0.2-$\mu$M wortmannin, 0.1-$\mu$M Akti-1/2 and/or 30-nM rapamycin, and the levels of *BDNF* transcripts containing exon IV were determined ($n=3$–4 experiments). (**c**) $STHdh^{Q7/Q7}$ cells were transfected with a construct harboring a 0.5-kb human *BDNF* promoter IV fused to the luciferase reporter gene and subsequently incubated for 15 h with 0.5-$\mu$M THC, 10-nM HU-210, 0.1-$\mu$M Akti-1/2 and/or 30-nM rapamycin. Relative promoter activity is shown ($n=4$–6 experiments). (**d**) $STHdh^{Q7/Q7}$ cells were incubated for 24 h with vehicle or 0.5-$\mu$M THC,10-nM HU-210, 0.1-$\mu$M Akti-1/2 and/or 30-nM rapamycin, and the levels of BDNF protein were determined ($n=3$–4 experiments). (**e**, **f**) Primary mouse striatal neurons were incubated with vehicle or 0.3-$\mu$M THC, 10-nM HU-210, 0.25-$\mu$M SR141716 and/or 0.1-$\mu$M Akti-1/2, and the levels of exon IV-containing and total *BDNF* transcripts (**e**; qPCR; 15-h incubation with the additions; $n=3$–4 experiments) as well as of BDNF protein were determined (**f**; western blot; 24-h incubation with the additions; $n=4$ experiments; quantification of mean ± S.E.M. optical density (O.D.) values relative to those of $\beta$-actin as well as a representative blot are shown). Data were analyzed using ANOVA with *post hoc* Student-Newman-Keuls test. $^*P<0.05$ and $^{**}P<0.01$ from the corresponding vehicle-treated cells

($n=3$ cultures) of contaminating glial fibrillary acidic protein (GFAP)-positive cells (assumed to be astroglia), and their content in BDNF/GFAP-double-positive cells relative to total BDNF-positive cells was negligible (Supplementary Figure S4). (4) We prepared mouse-brain organotypic cultures and found that THC increased striatal BDNF protein expression, as evidenced by western blot and immunofluorescence (Supplementary Figure S5).

**Multiple transcription factors are involved in the $CB_1$ receptor-mediated induction of *BDNF* promoter IV.** We next aimed at characterizing the specific regions of *BDNF* promoter IV involved in the $CB_1$ receptor-dependent control of gene transcription. For this purpose, $STHdh^{Q7/Q7}$ cells were transfected with *BDNF* promoter IV-luciferase reporter constructs containing mutations in *cis*-elements that control neuronal *BDNF* promoter IV upon different stimuli.[30,31] The cannabinoid-evoked activation of wild-type *BDNF* promoter IV was not evident when mutations were introduced in (1) bHLH-PAS transcription factor-response element (PasRE), to which neuronal PAS domain protein 4 (NPAS4)-aryl hydrocarbon receptor nuclear translocator 2 (ARNT2) dimers bind; (2) $Ca^{2+}$-response element 1 (CaRE1), to which calcium-responsive transcription factor (CaRF) binds; (3) upstream stimulatory factor-binding element (UBE), to which upstream stimulatory factors (USFs) bind; (4) cAMP/$Ca^{2+}$-response element (CRE), to which cAMP response element-binding protein (CREB) binds; (5) basic helix-loop-helix B2 (BHLHB2)-response element (BHLHB2-RE); and (6) conserved E-box element 2 (cEbox2; Figure 3a). Cannabinoid action on *BDNF* promoter IV was not affected when the NF$\kappa$B-response element (NF$\kappa$B-RE) was mutated (Figure 3a).

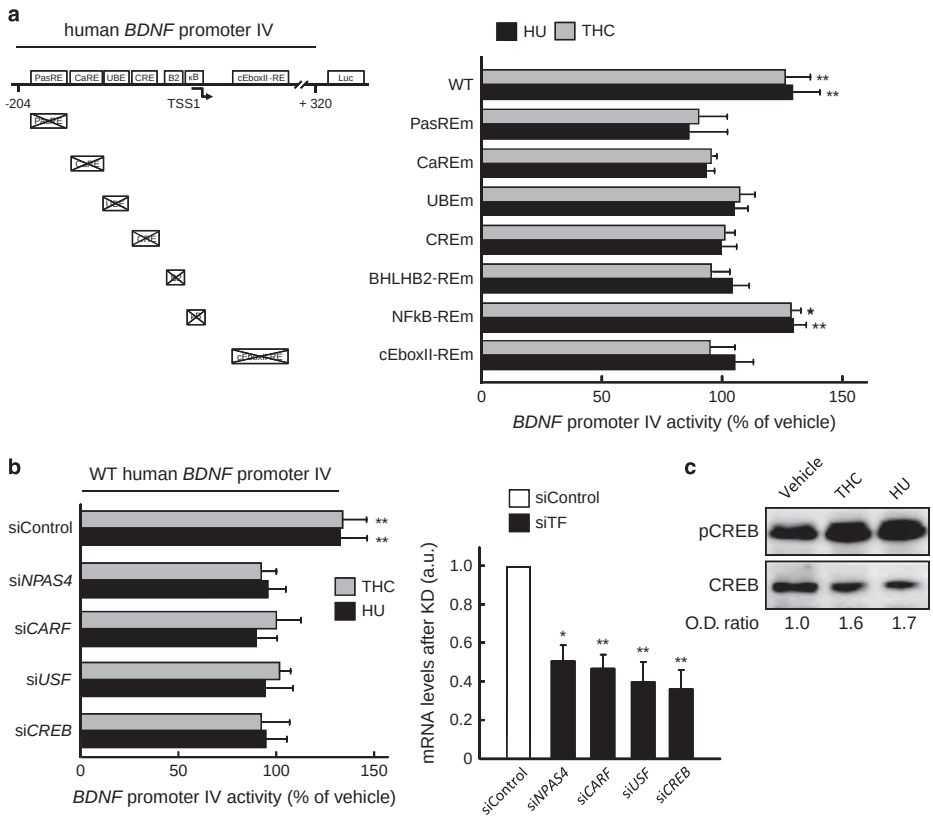


**Figure 3** Multiple transcription factors are involved in the $CB_1$ receptor-mediated induction of *BDNF* promoter IV. (**a**) $STHdh^{Q7/Q7}$ cells were transfected with a construct harboring a WT 0.5-kb human *BDNF* promoter IV fused to the luciferase reporter gene or with the same construct containing mutations (m) in the indicated response elements (RE). Cells were subsequently incubated for 15 h with vehicle, 0.5-$\mu$M THC or 10-nM HU-210. Promoter activity relative to vehicle incubations is shown ($n = 4$–6 experiments). (**b**) $STHdh^{Q7/Q7}$ cells were transfected with a non-targeted siRNA or siRNAs directed against the indicated transcription factors. After 24 h, they were transfected with the aforementioned WT *BDNF* promoter IV reporter construct, and, after an additional 24-h period, cells were incubated with vehicle, 0.5-$\mu$M THC or 10-nM HU-210 for 15 h. Left: promoter activity relative to vehicle incubations; right: knock-down (KD) efficacy of the siRNAs directed against the corresponding transcription factor (siTF; $n = 4$–6 experiments). Data were analyzed using unpaired Student's *t*-test. $^*P < 0.05$ and $^{**}P < 0.01$ from the corresponding vehicle-treated cells or siControl-transfected cells (**b**, left). (**c**) $STHdh^{Q7/Q7}$ cells were incubated for 30 min with vehicle, 0.5-$\mu$M THC or 10-nM HU-210, lysed and used for western blot analyses. Quantification of mean optical density (O.D.) values of pCREB relative to those of total CREB as well as a representative blot are shown ($n = 3$–4 experiments)

To evaluate the involvement of the best-defined transcription factors that bind to the aforementioned *BDNF* promoter IV regulatory elements, we silenced the expression of NPAS4, CaRF, USF and CREB with specific siRNAs and measured cannabinoid-evoked activation of the wild-type *BDNF* promoter IV. Knocking-down the expression of any of these transcription factors abrogated the cannabinoid-induced activation of *BDNF* promoter IV (Figure 3b), thus suggesting that all of them are necessary for the latter process to occur. Accordingly, CREB phosphorylation in its critical activatory S133 residue was enhanced by cannabinoid challenge (Figure 3c).

**$CB_1$ receptor antagonism attenuates BDNF upregulation induced by pharmacogenetic activation of striatal neurons.** To evaluate the relevance of the $CB_1$ receptor in the physiological control of striatal BDNF expression, we selectively manipulated MSN activity by the *designer receptor exclusively activated by designer drug* (DREADD) pharmacogenetic technique. This tool is based on the molecular evolution of muscarinic acetylcholine receptors, leading to a $G_q$ protein-coupled receptor with negligible affinity for the native agonist (acetylcholine) but to which the pharmacologically inert agonist clozapine-*N*-oxide (CNO) binds with high potency and efficacy,[32] thus allowing the remote control of neuronal activity in specific cell populations *in vivo*.[33]

First, we validated this experimental approach *in vitro*. $STHdh^{Q7/Q7}$ cells were nucleofected with a plasmid encoding a DREADD-$G_q$ (hM3Dq) fused to mCherry (or only mCherry) and subsequently treated with CNO (or vehicle). CNO-induced activation of hM3Dq led to an accumulation of both exon IV-containing and total *BDNF* transcripts, and SR141716

prevented this effect (Figure 4a). Next, we injected stereotactically C57BL/6J mice with a recombinant adeno-associated viral vector encoding hM3Dq-mCherry (or only mCherry) into the dorsolateral (motor) striatum (Figure 4b). The expression of the transgene was driven by the calcium/calmodulin-dependent protein kinase II-*α* (CaMKII*α*) promoter in order to confine it to MSNs and avoid other cell populations (e.g., interneurons and glia). Animals were subsequently treated with CNO (or vehicle) in conditions that evoke neuronal activation (one injection of CNO at 10 mg/kg body weight).[34] This procedure triggered the expression of exon IV-containing and total *BDNF* transcripts in the striatum *in situ*, and, of note, treatment with SR141716 (one injection at 1 mg/kg body weight) produced *per se* the opposite effect to CNO and attenuated the CNO-triggered upregulation of *BDNF* expression (Figure 4b).

**Pathophysiological relevance of $CB_1$ receptor-mediated striatal BDNF upregulation in HD.** To assess the functional impact of the $CB_1$/BDNF axis in a neurodegenerative-disease context *in vivo*, we used the R6/2 mouse, a well-established model of HD.[35] This devastating disease constitutes so far the best paradigm to study the neuroprotective role of the $CB_1$ receptor as this receptor is highly expressed in the basal ganglia by MSNs, the cells that constitute ~90% of total striatal neurons and primarily degenerate in HD, and plays a key role in the control of motor behavior, one of the processes that is typically affected in HD.[4,12] In addition, an early and remarkable downregulation of $CB_1$ receptor expression has been documented as one of the most characteristic neurochemical alterations of MSNs in HD animal models[36–38] and HD patients.[39,40] Moreover, we[19] and others[41] have provided genetic evidence for a neuroprotective role of the $CB_1$ receptor in HD mouse models.

To test whether this neuroprotective effect relies on BDNF signaling, we injected sterotactically 3.5- to 4-week-old R6/2 mice (or wild-type littermates) with a recombinant adeno-associated viral vector encoding $CB_1$ receptor (or empty vector)

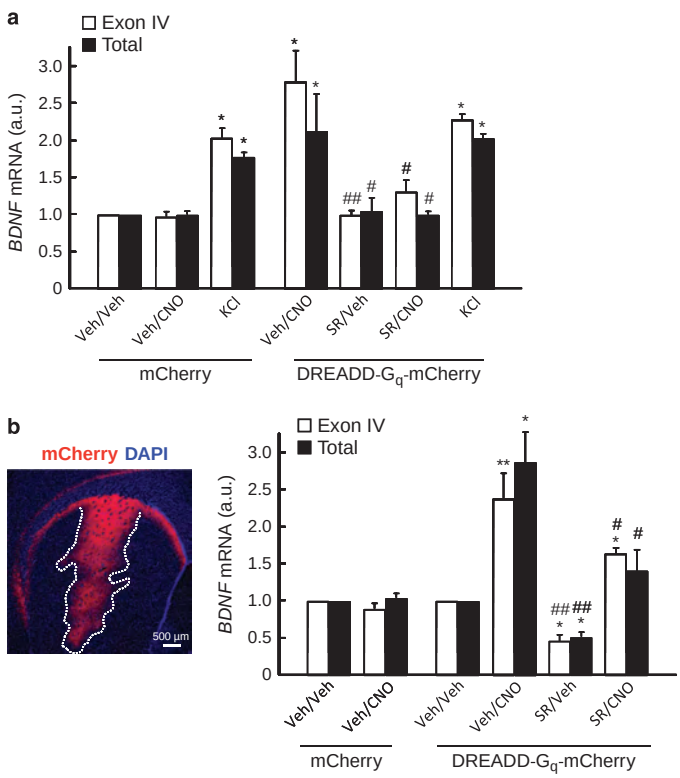


**Figure 4** $CB_1$ receptor antagonism attenuates BDNF upregulation induced by pharmacogenetic activation of striatal neurons. (**a**) STHdh$^{Q7/Q7}$ cells were nucleofected with a construct expressing hM3Dq-mCherry (or mCherry alone as control). Two days after, cells were treated with 50-$\mu$M CNO (or $H_2O$ as vehicle) plus 0.25-$\mu$M SR141716 (or 0.1% DMSO as vehicle) for 4 h, and the levels of exon IV-containing and total *BDNF* transcripts were determined by qPCR ($n = 3$–4 experiments). KCl (25 mM) was used as a control of activity-dependent *BDNF* expression upregulation. (**b**) Eight-week-old C57BL/6J mice were injected stereotactically into the dorsolateral striatum with a recombinant adeno-associated virus encoding hM3Dq-mCherry (or only mCherry as control) under the control of the CaMKII$\alpha$ promoter ($n = 6$–8 animals per group). Left: Example of a mouse brain injected with the mCherry construct. The site of infection in the striatum is outlined. Right: Levels of exon IV-containing and total *BDNF* transcripts in the dorsolateral striatum as determined by qPCR 4 h after i.p. injection of CNO (10 mg/kg body weight) with or without SR141716 (1 mg/kg body weight) or the corresponding vehicles. Data were analyzed using unpaired Student's *t*-test. $^{*}P < 0.05$ and $^{**}P < 0.01$ from the corresponding Veh/Veh group; $^{\#}P < 0.05$ and $^{\#\#}P < 0.01$ from the corresponding Veh/CNO group

into the dorsolateral striatum. This procedure allowed the subsequent re-expression of the $CB_1$ receptor (Figure 5a) as well as BDNF protein (Figure 5b), total *BDNF* mRNA (Figure 5c; Ct = 26) and exon IV-containing *BDNF* mRNA (Figure 5d; Ct = 29). Reactivation of the $CB_1$/BDNF axis also normalized the HD-like molecular-pathology profile of these animals, as determined by the recovered levels of the MSN marker dopamine- and cAMP-regulated phosphoprotein of 32 KDa (DARPP-32; Figure 6a; confirmation by stereological counting shown in Supplementary Figure S6), the *pan*-GABAergic-neuron marker glutamic acid decarboxylase 67 kDa isoform (GAD-67; Figure 6b), the post-synaptic marker post-synaptic density protein 95 (PSD-95; Figure 6c) and the mTORC1-activity marker phosphorylated (activated) ribosomal S6 protein (Figure 6d). In addition, $CB_1$ receptor re-expression rescued striatal atrophy, the main neuropathological hallmark of HD, as determined by MRI analysis (Figure 7). Cortical and hippocampal volumes, used as controls, were not significantly different in 8-week-old wild-type and R6/2 mice injected with $CB_1$ receptor-encoding or empty viral vectors (Supplementary Figure S7). (We note that overexpression of the $CB_1$ receptor in the striata of

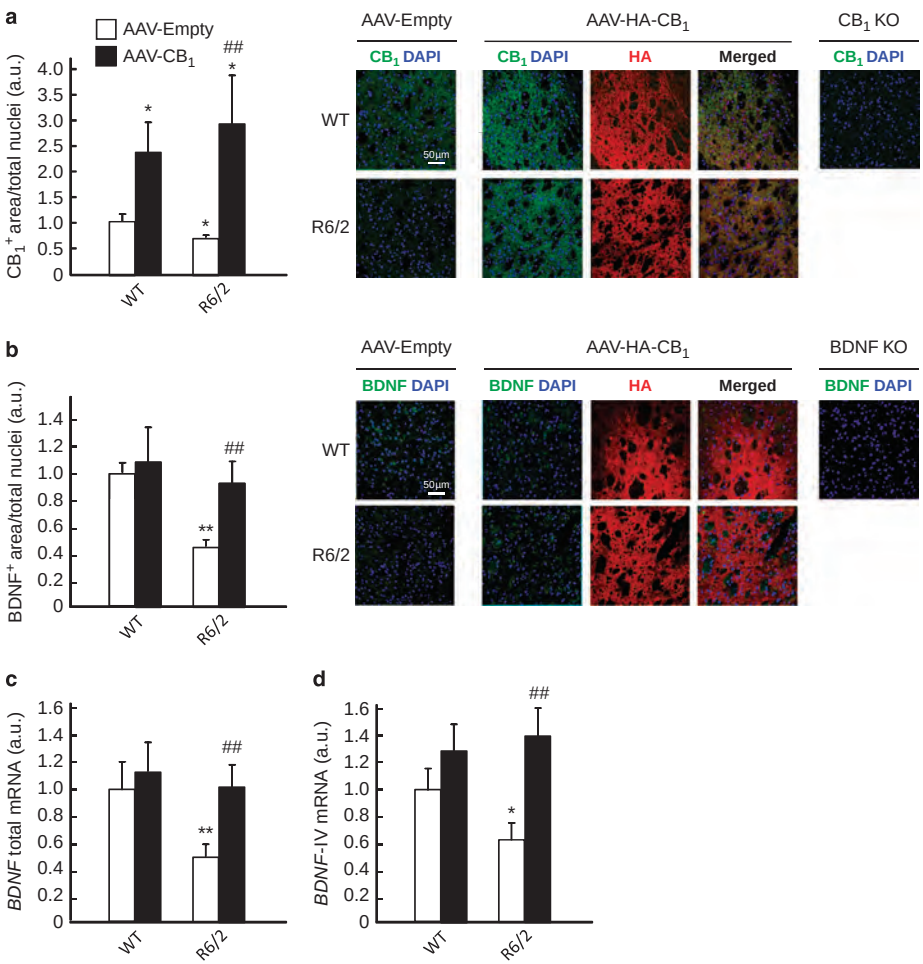


**Figure 5** Enforced re-expression of the $CB_1$ receptor rescues BDNF expression in the striata of R6/2 mice. R6/2 mice (3.5–4 weeks old) and WT littermates were injected stereotactically into the dorsolateral striatum with a recombinant adeno-associated virus (AAV) encoding HA-tagged $CB_1$ receptor or the empty vector as control ($n = 10$–$12$ animals per group). At week 8 of age, animals were killed for histological and qPCR analyses in the striatum. (**a**) $CB_1$ receptor immunoreactivity (relative values of $CB_1$ receptor-positive area/total cell nuclei). Slices from the dorsolateral striatum of $CB_1^{-/-}$ mice[70] were used as control of staining specificity. Representative images are shown. (**b**) BDNF immunoreactivity (relative values of BDNF-positive area/total cell nuclei). Slices from the dorsolateral striatum of neuron-specific, neurofilament L-conditional BDNF knockout (*Bdnf*$^{floxed/-}$;*Neff-Cre*$^{/+}$) mice (generated at Michael Sendtner's laboratory, University of Würzburg, Germany) were used as control of staining specificity. Representative images are shown. (**c**) Levels of total *BDNF* transcripts. (**d**) Levels of exon IV-containing *BDNF* transcripts. Data were analyzed using unpaired Student's *t*-test. $^{*}P < 0.05$ and $^{**}P < 0.01$ from the corresponding WT-empty group; $^{\#\#}P < 0.01$ from the corresponding R6/2-empty group

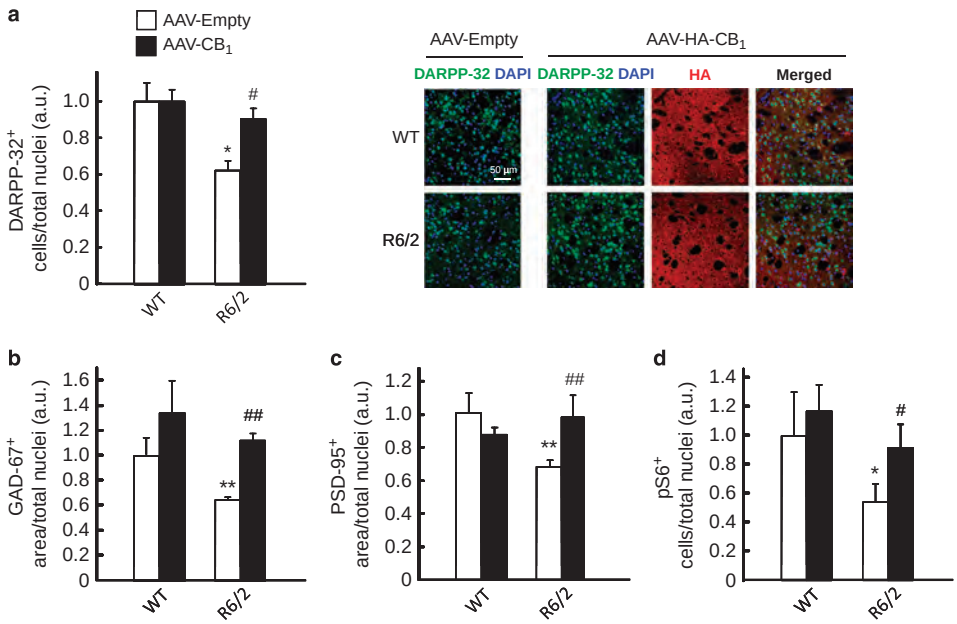


**Figure 6** Enforced re-expression of the $CB_1$ receptor rescues HD-like molecular-pathology markers in the striata of R6/2 mice. R6/2 mice (3.5–4 weeks old) and WT littermates were injected stereotactically into the dorsolateral striatum with a recombinant adeno-associated virus (AAV) encoding HA-tagged $CB_1$ receptor or the empty vector as control ($n = 10$–12 animals per group). At week 8 of age, animals were killed for histological analyses in the striatum. (**a**) DARPP-32 immunoreactivity (relative values of DARPP-32-positive cells/total cell nuclei). Representative images are shown. (**b**) GAD-67 immunoreactivity (relative values of GAD-67-positive area/total cell nuclei). (**c**) PSD-95 immunoreactivity (relative values of PSD-95-positive area/total cell nuclei). (**d**) Phospho-S6 immunoreactivity (relative values of pS6-positive cells/total cell nuclei). Data were analyzed using unpaired Student's *t*-test. $^{*}P < 0.05$ and $^{**}P < 0.01$ from the corresponding WT-empty group; $^{\#}P < 0.05$ and $^{\#\#}P < 0.01$ from the corresponding R6/2-empty group

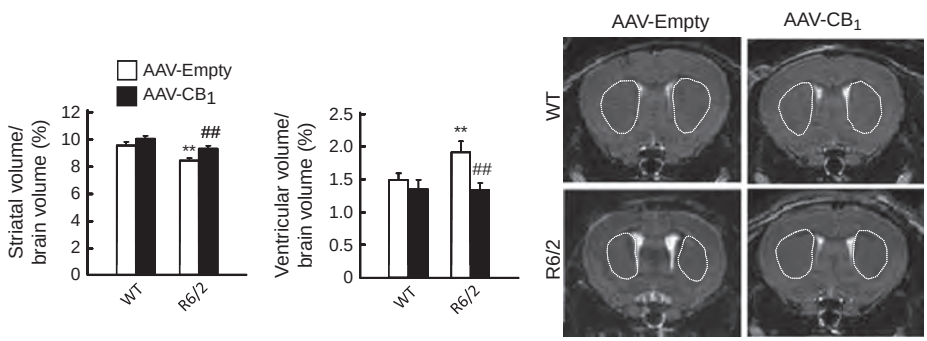


**Figure 7** Enforced re-expression of the $CB_1$ receptor rescues HD-like striatal atrophy in R6/2 mice. R6/2 mice (3.5–4 weeks old) and WT littermates were injected stereotactically into the dorsolateral striatum with a recombinant adeno-associated virus (AAV) encoding HA-tagged $CB_1$ receptor or empty vector as control ($n = 10$–12 animals per group). The volume of the striatum and lateral ventricles relative to total brain volume of 8-week-old animals is represented. Representative MRI pictures are shown. Striata are outlined. Data were analyzed using unpaired Student's *t*-test. $^{**}P < 0.01$ from the corresponding WT-empty group; $^{\#\#}P < 0.01$ from the corresponding R6/2-empty group

wild-type mice did not lead to a significant upregulation of BDNF or other markers of neuronal integrity/functionality. As MSNs express very large amounts of $CB_1$ receptors, it is conceivable that the $CB_1$ receptor-response system would be essentially saturated in the normal setting but not in conditions of restricted receptor function such as HD. In this regard, agonist-stimulated [$^{35}$S]GTPγS-binding studies have shown that when higher expression levels of $CB_1$ receptors occur, for example, in the striatum *versus* other brain regions,[42] in GABAergic *versus* glutamatergic terminals[43] or in $CB_1^{+/+}$ *versus* $CB_1^{+/-}$ mice,[44] the receptors couple with little efficacy to G proteins, thus making signaling in $CB_1$ highly expressing systems refractory to stimulation by mere increases in total receptor numbers.)

Finally, we analyzed a series of *post-mortem* human caudate-putamen samples for concerted changes in $CB_1$

receptor and BDNF immunoreactivity. In line with Zuccato and Cattaneo,[17] we found a significant reduction of $CB_1$ receptor-positive, BDNF-positive and $CB_1$/BDNF-double-positive neurons in HD patients compared to control subjects (Supplementary Figure S8a). Western blot analyses, which had previously shown a decrease in $CB_1$ receptor protein expression in caudate-putamen specimens of HD patients,[19] evidenced a parallel reduction of BDNF protein expression in those samples (Supplementary Figure S8b). This was associated to a concomitant decrease in the levels of pCREB (Supplementary Figure S8b), a key signaling marker of the $CB_1$/BDNF axis described above. These findings therefore suggest that a functional link between the $CB_1$ receptor and BDNF could also occur in the human brain.

## Discussion

Here we show that, in the mouse striatum, $CB_1$ receptor engagement upregulates BDNF expression, through which it can confer neuroprotection against excitotoxicity *in vitro* and mutant huntingtin-induced toxicity *in vivo*. On mechanistic grounds, this $CB_1$ receptor-mediated induction of *BDNF* gene expression relies on the activation of the PI3K/Akt/mTORC1 pathway, which, in turn, targets *BDNF* promoter IV, a promoter that is also responsive to various types of neuronal activity-related stimuli in the mouse, rat and human *BDNF* gene.[10,29,30] The induction of *BDNF* promoter IV evoked by the $CB_1$ receptor-mediated activation of the PI3K/Akt/mTORC1 pathway appears to be a complex process, as several responsive elements and transcription factors are involved. The observation that CREB is necessary for the $CB_1$ receptor-mediated induction of *BDNF* promoter IV fits with the pivotal role of this transcription factor in the regulation of BDNF action.[10,45] In fact, mice with a specific knock-in mutation in the CRE of *Bdnf* promoter IV display impaired sensory experience-induced expression of BDNF and defective development of cortical inhibitory circuits.[46] It is thus conceivable that the rapid and pleiotropic triggering of $Ca^{2+}$-, cAMP-, ERK- and/or Akt-related signals will converge in the immediate/early activation of CREB and CaRF, which, by binding to CRE[30] and CaRE1,[31,47] respectively, could initiate *BDNF* promoter IV transcription. Of note, and in line with our data, the $Ca^{2+}$ influx-dependent early activation of CRE/CaRE3 (via CREB) and CaRE1 (via CaRF) in the rat *BDNF* promoter IV is abrogated by genetic or pharmacological blockade of PI3K signaling.[31] Upon CREB and CaRF activation, at later time points other transcription factors, such as NPAS4 via PasRE,[30,48] could be important for sustaining the transcriptional activity of *BDNF* promoter IV under different conditions, including $CB_1$ receptor activation, as reported here.

The relation between $CB_1$ receptor activation and BDNF expression appears to be a region-specific process. Thus, this association has been clearly established in the mouse hippocampus by experiments involving $CB_1$ receptor gain of function ($CB_1$ receptor pharmacological agonism) and loss of function ($CB_1$ receptor genetic inactivation, $CB_1$ receptor pharmacological antagonism) conducted in various *in vitro* (tissue slices, cell cultures) and *in vivo* (whole mice) experimental systems.[8,49–54] In line with our present study in the mouse dorsolateral striatum, THC administration increased BDNF expression in the rat ventral striatum.[55] However, and in striking contrast with the hippocampus and the striatum, BDNF expression in the mouse cortex, which expresses high levels of the $CB_1$ receptor,[1] was unaffected by either THC administration[19,51] or $CB_1$ receptor genetic ablation,[19,52] while another study found only very marginal increases in BDNF levels in the medial prefrontal cortex and the frontoparietal cortex upon THC injection to rats.[55] Hence, albeit for hitherto unknown molecular reasons, BDNF expression seems to be much more refractory to $CB_1$ receptor activation in the cortex than in the striatum or hippocampus.

This zonation of the $CB_1$/BDNF axis in the brain is certainly relevant in the context of our findings because MSNs are known to receive BDNF from the cortex via the well-established corticostriatal pathway.[56] In addition, significant amounts of *BDNF* mRNA have been found in the striatum, thus indicating that striatal BDNF can also be produced *in situ*.[19,29,57,58] Moreover, our DREADD experiments, by allowing the remote and selective control of MSN activity, provide robust evidence for the activity-dependent production of BDNF in mouse MSNs *in vivo*. Further support to this notion comes from the findings that mutant huntingtin affects axonal transport of BDNF in striatal neurons but not in cortical neurons,[59] and that dopamine receptor heteromers control BDNF production by striatal neurons *in situ*.[60] All these observations do not downplay the corticostriatal pathway as a key source of BDNF for MSNs in the normal brain. For example, in our hands, significant amounts of *BDNF* transcripts are readily detected in the adult-mouse striatum, but their levels are lower than those found in the cortex (mRNA levels in the striatum relative to the cortex: total *BDNF*, $24 \pm 2\%$; *BDNF*-IV, $20 \pm 4\%$; $n = 8$ animals). However, it is likely that, under particular pathophysiological situations, BDNF production can increase in the striatum *in situ*, thereby complementing the bulk supply of BDNF from the cortex with a local –and thus spatially privileged- extra source of the neurotrophin for MSNs. The multiple lines of evidence provided by this study, together with the aforementioned lack of effect of $CB_1$ receptor activation on cortical BDNF expression, strongly support that the $CB_1$ receptor-mediated upregulation of striatal BDNF is a striatum-autonomous effect rather than the consequence of an enhanced anterograde supply of BDNF from the cortex. Nonetheless, the $CB_1$/BDNF connection in MSNs can be more complex and be accompanied, for example, by a reciprocal BDNF-dependent control of $CB_1$ receptor function.[61]

A key unanswered question in many neurodegenerative diseases is what precise factors dictate the selective damage of a particular neuronal population. Regarding HD, the disease has long been known to be caused by an expanded polyglutamine tract in the *N*-terminal domain of the huntingtin protein,[62] but the mechanisms by which MSNs are highly vulnerable to mutant huntingtin are still incompletely understood. We[19] and others[41] have provided genetic evidence for a neuroprotective role of the $CB_1$ receptor in two transgenic models of HD, which could open similar studies on other neurodegenerative diseases, such as Alzheimer's disease,[63–65] in which $CB_1$ receptor levels are known to be downregulated during disease state. Unfortunately, the precise relevance of $CB_1$ receptor and BDNF downregulation in HD pathology are not completely understood. For example, regarding the latter issue, Plotkin *et al*.[66] have recently shown

that, although reduced BDNF availability in the striatum may contribute to HD pathology,[17] a major pathogenic mechanism seems to rely on an aberrant BDNF signaling via p75 neurotrophin receptors located on indirect-pathway MSNs, which adds to the previously reported alterations of BDNF signaling via TrkB.[21,22] These possibilities notwithstanding, here we cogently show that, in the striatum of the R6/2 mouse *in vivo*, changes in $CB_1$ receptor expression parallel changes in the expression of BDNF and key markers of disease neuropathology, thus supporting the notion that BDNF may be a *bona fide* marker not only of HD neurodegeneration[17] but also of $CB_1$ receptor-evoked neuroprotection.

## Materials and Methods

**Animals.** Hemizygous male mice transgenic for exon 1 of the human huntingtin gene with a greatly expanded CAG tract (R6/2 mice; 155–175 CAG repeats)[35] and wild-type littermates were purchased from The Jackson Laboratory (Bar Harbor, ME, USA). C57BL/6J mice (Harlan, Barcelona, Spain) were used to obtain organotypic and cell cultures, as well as to conduct DREADD experiments. Animals were maintained as described.[19] All animal handling procedures were approved by the Complutense University Animal Research Committee in accordance with the directives of the European Commission.

**Cell cultures.** Conditionally, immortalized mouse striatal neuroblasts expressing wild-type huntingtin and infected with a defective retrovirus transducing the temperature-sensitive A58/U19 large T antigen (designated as $STHdh^{Q7/Q7}$ cells),[24] were grown at 33°C in DMEM supplemented with 10% fetal bovine serum, 1 mM sodium pyruvate, 2 mM L-glutamine and 400 $\mu$g/ml geneticin.

Primary striatal neurons were obtained from 2-day-old C57BL/6J mice using a papain dissociation system (Worthington, NJ, USA). Striata were dissected and cells were seeded on plates pre-coated with 0.1 mg/ml poly-D-lysine at 200 000 cells/$cm^2$ in the Neurobasal medium supplemented with B27 and GlutaMax (Gibco, Carlsbad, CA, USA).

**Cell viability.** $STHdh^{Q7/Q7}$ cells were transferred to a serum-free medium for 24 h and incubated for a further 5 h in home-made Locke's solution (154-mM NaCl, 5.6-mM KCl, 2.3-mM $CaCl_2$, 3.6-mM $NaHCO_3$, 5-mM HEPES (Lonza, Verviers, Belgium), 20-mM glucose and 10-$\mu$M glycine), supplemented or not with NMDA, together with the cannabinoid receptor agonists THC (The Health Concept, Richelbach, Germany) or HU-210 (Tocris, Bristol, UK), the PI3K inhibitor wortmannin (Sigma-Aldrich, Barcelona, Spain), the Akt inhibitor Akti-1/2 (Calbiochem, San Diego, CA, USA), the mTORC1 inhibitor rapamycin (Tecoland, Irvine, CA, USA), the tyrosine kinase inhibitor K252a (Calbiochem) or the respective vehicle (DMSO, 0.1–0.2% (v/v) final concentration). The medium was subsequently replaced by NMDA/serum-free DMEM supplemented with the corresponding drugs, and cell viability was determined after 24 h by the 3-(4,5-dimethylthiazol-2-yl)-2, 5-diphenyltetrazolium bromide (MTT) test.

Another set of $STHdh^{Q7/Q7}$ cell-viability experiments was conducted with quinolinic acid (Sigma-Aldrich) as neurotoxic agent. $STHdh^{Q7/Q7}$ cells were transferred to serum-free DMEM for 24 h and subsequently incubated in this medium, supplemented or not with quinolinic acid, together with THC, HU-210, the $CB_1$-selective antagonist SR141716 (rimonabant; kindly given by Sanofi-Aventis, Montpellier, France), Akti-1/2, rapamycin and K252a, or the respective vehicle (DMSO, 0.1–0.2% (v/v) final concentration) for 24 h. Cell viability was determined by the MTT test.

Primary C57/BL6J-mouse striatal neurons, grown for 2 days *in vitro*, were incubated for 30 min in the aforementioned Locke's solution, supplemented or not with NMDA, together with THC, HU-210, SR141716, Akti-1/2, rapamycin and K252a, or the respective vehicle (DMSO, 0.1–0.2% (v/v) final concentration). The medium was subsequently replaced by NMDA-free Neurobasal medium supplemented with B27 and GlutaMax (Gibco), plus the corresponding drugs, and cell viability was determined after 2 h by the MTT test.

**Cell transfection/nucleofection.** Cells were transfected transiently with an ON-TARGETplus SMARTpool m*Bdnf* siRNA (Re. L-042566-00) or m*TrkB* (= m*Ntrk2*) siRNA (Re. L-048017-00), or a non-targeted SMARTpool siRNA (Re. D-001810-10), using the DharmaFECT 1 transfection reagent (Thermo Fisher, Lafayette, CO, USA).

For the luciferase reporter assays, cells were transfected transiently with constructs expressing a 524-bp human *BDNF* promoter IV cloned into pGL4.15 (luc2P/Hygro), or the same promoter with mutated PasRE, CaRE, UBE, CRE, BHLHB2-RE, NFκB-RE or cEbox II sites also cloned into pGL4.15 (luc2P/Hygro), as described,[30] using Lipofectamine 2000 (Invitrogen, Madrid, Spain). For normalization, a renilla/pGL4.83 construct (driven by the thymidine kinase promoter) was cotransfected. Luciferase assays were performed with the Dual-Glo luciferase assay system (Promega Biotech Ibérica, Barcelona, Spain).

Other promoter activity experiments were conducted in cells transfected transiently with ON-TARGETplus SMARTpool m*Npas4* (Re. L-054722-01), m*Carf* (Re. L-051736-01), m*Usf1* (Ref. L-040656-00) or m*Creb1* (Re. L-040959-01) siRNAs, or the aforementioned non-targeted SMARTpool siRNA, using the DharmaFECT 1 transfection reagent (Thermo Fisher).

For DREADD experiments *in vitro*, cells were nucleofected with a construct expressing the hM3Dq receptor fused to mCherry (kindly provided by Bryan L Roth, University of North Carolina, Chapel Hill, NC, USA),[34] or mCherry alone as control vector, under the CAG promoter, by using an Amaxa mouse-neuron nucleofector kit (Lonza, Madrid, Spain). Cells were treated in the serum-free medium, 2 days after nucleofection, with CNO (or $H_2O$ as vehicle) plus SR141716 (or 0.1% DMSO as vehicle).

**Organotypic cultures.** Corticostriatal slices (300-$\mu$m thick) were obtained from adult (8 weeks old) C57/BL6J mice, and cultured under semidry conditions in the Neurobasal medium supplemented with B27 (1%), N2 (1%), glutamine (1%), penicillin/streptomycin (1%), Fungizone (1%; Gibco) and ciprofloxacin (5 $\mu$g/ml), as described.[19] Slices were incubated for 24 h with THC or vehicle (DMSO, 0.1% (v/v) final concentration) and subsequently fixed with formalin and processed in 15-$\mu$m sections, which were analyzed at equivalent regions of the rostral to caudal axis. Counting of BDNF and NeuN immunoreactivity (see below) was conducted in the dorsolateral striatum in a 1-in-6 series per slice.

**Real-time PCR.** RNA was isolated using TRIzol reagent or RNeasy (Invitrogen, Carlsbad, CA, USA). cDNA was obtained using Transcriptor (Roche, Basel, Switzerland). Real-time PCR (qPCR) assays were performed using the FastStart SYBR Green Master (Roche) and probes were obtained from the Universal Probe Library Set (Roche). The mRNA levels of the different *BDNF* exons were determined with previously described primers.[29,30] Other primers used are shown in Supplementary Table SI. Amplifications were run in a 7900 HT-Fast Real-time PCR system (Applied Biosystems, Foster City, CA, USA). Relative gene expression data were determined by the $2^{-\Delta\Delta Ct}$ method. Each value was adjusted to $\beta$-actin levels as reference.

**Viral vectors.** HA-tagged rat $CB_1$ cannabinoid receptor was subcloned in a rAAV expression vector with a CAG promoter by using standard molecular cloning techniques. Vectors were of an AAV1/AAV2-mixed serotype, and were generated by calcium phosphate transfection of HEK293T cells and subsequent purification as described.[67,68] R6/2 mice (3.5–4 weeks old) and their wild-type littermates were injected stereotactically with the viral vectors (in 1.5 $\mu$l PBS) into the dorsolateral striatum. Each animal received one bilateral injection at coordinates (to bregma): anteroposterior −0.5, lateral ±1.4, dorso-ventral −2.7. MRI analyses were conducted at 8 weeks of age. Mice were subsequently killed by intracardial perfusion and their brains were excised for immunofluorescence and qPCR analyses.

For DREADD experiments *in vivo*, 8-week-old male C57BL/6J animals were injected stereotactically with viral vectors expressing the hM3Dq receptor fused to mCherry (or mCherry as control) under a minimal CaMKII$\alpha$ promoter into the dorsolateral striatum as described before.[9] Six weeks after surgery, animals were injected with SR141716 (1 mg/kg body weight, i.p.) or vehicle (1% (v/v) DMSO in Tween 20 (Panreac, Barcelona, Spain)/saline (1 : 18, v/v)) and, 10 min later, with CNO (10 mg/kg body weight, i.p.) or vehicle (PBS). Animals were killed 4 h after the CNO injection, and their dorsolateral striata were quickly dissected on ice and frozen at −80°C for subsequent analyses.

**Western blot.** Western blot analysis was conducted with antibodies raised against phosphorylated Akt (1 : 1000; Cell Signaling, Danvers, MA, USA), total Akt (1 : 1000; Cell Signaling), phosphorylated S6 ribosomal protein (1 : 1000; Cell Signaling), total S6 ribosomal protein (1 : 1000; Cell Signaling), phosphorylated ERK (1 : 1000; Cell Signaling), total ERK (1 : 1000; Cell Signaling), phosphorylated JNK (1 : 1000; Cell Signaling), total JNK (1 : 1000; Cell Signaling), phosphorylated p38 (1 : 1000; Cell Signaling), total p38 (1 : 1000 Cell Signaling), PKA phosphorylated substrates (1 : 1000; Cell Signaling), phosphorylated CREB (1 : 1000, Cell Signaling), total CREB (1 : 1000, Cell Signaling), BDNF (1 : 1000, Santa Cruz Biotechnology, Santa Cruz, CA, USA), $\alpha$-tubulin (1 : 4000, Sigma-Aldrich) and $\beta$-actin (1 : 4000,

Sigma-Aldrich), following standard procedures. Specifically, samples from cell cultures, organotypic cultures and human *post-mortem* brains (obtained from the Banco de Tejidos para Investigación Neurológica, Madrid, Spain, as previously described)[19] were lysed in a buffer containing 50-mM Tris, 0.3% CHAPS, 1-mM EDTA, 1-mM EGTA, 50-mM NaF, 10-mM sodium $\beta$-glycerophosphate, 5-mM sodium pyrophosphate and 1-mM sodium orthovanadate (pH 7.5) supplemented with a protease inhibitor cocktail (Roche, Madrid, Spain), 0.1-mM PMSF and 1-$\mu$M microcystin. The running buffer consisted of 200-mM glycine, 25-mM Tris and 0.1% SDS (pH 8.3), and the transfer buffer contained 200-mM glycine, 25-mM Tris and 20% methanol (pH 8.3). Blots were incubated with Tris-buffered saline (20-mM Tris and 0.5-mM NaCl, pH 7.5)/Tween 20 (0.05%) supplemented with 1% bovine serum albumin. Densitometric analysis was performed with Quantity One software (Bio-Rad, Hercules, CA, USA).

**Immunomicroscopy (mouse samples).** Coronal free-floating sections (30 $\mu$m-thick) were obtained from paraformaldehyde-perfused mouse brains. Organotipic cultures were obtained as described before. Samples were incubated with antibodies against $CB_1$ cannabinoid receptor (1 : 500; Frontier Science, Hokkaido, Japan), HA (1 : 500, Roche), BDNF (1 : 300; generated at Michael Sendtner's laboratory, University of Würzburg, Germany),[19] DARPP-32 (1 : 1000; BD, Franklin Lakes, NJ, USA), GAD-67 (1 : 250; Chemicon, Temecula, CA, USA), PSD-95 (1 : 1000, Abcam, Cambridge, UK), phosphorylated S6 ribosomal protein (1 : 200; Cell Signaling) or NeuN (1 : 400; Chemicon), followed by staining with the corresponding highly cross-adsorbed Alexa Fluor 488, 594 or 647 antibodies (1 : 500; Molecular Probes, Leyden, The Netherlands).[19] GFAP was stained with an anti-GFAP-Cy3 antibody (1 : 1000, Sigma-Aldrich). Samples were subsequently incubated with DAPI (1 : 10 000, Roche) for 10 min, washed with PBS and mounted in Mowiol (Calbiochem, Madrid, Spain). Counting of brain sections was conducted in the caudate-putamen area in a 1-in-10 series per animal, ranging from bregma +1.5 mm to $-$0.5 mm coronal coordinates. Data were calculated as immunoreactive area per total cell nuclei, except for DARPP-32, phospho-S6 and NeuN, in which immunoreactive cells per total cell nuclei were counted. Confocal fluorescence images were acquired using TCS-SP2 software and a SP2 AOBS microscope (Leica, Wetzlar, Germany). Pixel quantification and co-localization were analyzed with ImageJ software (National Institutes of Health, Bethesda, MA, USA).

Stereological counting of the total number of DARPP-32-positive cells in the rAAV-infected region of the mouse dorsolateral striatum (Supplementary Figure S6) was performed in 30-$\mu$m-thick sections with the aforementioned DARPP-32/HA/DAPI staining conditions and within the aforementioned coronal coordinates using the optical fractionator method. A 1-in-8 series per animal was analyzed in an Olympus BX61 microscope (Olympus, Tokyo, Japan) with newCAST software (Visiopharm, Horsholm, Denmark). Volumes were calculated by applying the Cavalieri estimator. The frame area was set to 5625 $\mu m^2$ with a sampling interval of 240 $\mu$m at the *x* and *y* level, and the optical dissector constituting a 13-$\mu$m-thick fraction of the total section thickness. Results are expressed as number of DARPP-32-immunoreactive cells per $mm^3$ of rAAV-infected region. Gundersen's coefficient of error was always below 0.1.

**Immunomicroscopy (human samples).** Paraffin-embedded *post-mortem* 4-$\mu$m-thick brain sections containing caudate-putamen were provided by the Tissue Bank at Hospital Universitario Fundación Alcorcón (Madrid, Spain), and were obtained and handled following the ethical guidelines of that institution. Samples (four sections per individual) were obtained from HD donors (grades 3–4; $n = 9$; age (years old) and sex: 55♂, 47♀, 45♂, 45♂, 51♂, 51♀, 44♂, 77♀ and 49♂) and control subjects with no background of neuropsychiatric disease ($n = 7$; age (years old) and sex: 45♂, 62♀, 36♂, 74♂, 79♂, 75♀ and 69♂). For immunofluorescence analyses,[69] sections were incubated with anti-BDNF antibody (1 : 50; generated at Michael Sendtner's laboratory) and subsequently with Alexa Fluor 546 antibody (Molecular Probes). Samples were then incubated with anti-$CB_1$ cannabinoid receptor antibody (1 : 50; Affinity Bioreagents, Golden, CO, USA), followed by incubation with Alexa Fluor 488 antibody (Molecular Probes), and finally incubated with DAPI (1 : 10 000) for 10 min and washed with PBS. Then, sections were treated with 1% Sudan Black (Sigma-Aldrich) in 70% ethanol to quench endogenous autofluorescence and finally mounted in Mowiol.

**ELISA.** $STHdh^{Q7/Q7}$ cells were transferred to the serum-free medium and incubated with vehicle (DMSO, 0.1–0.2% (v/v) final concentration) or THC, HU-210, Akti-1/2 and rapamycin for 24 h as described above. BDNF protein levels were determined upon scraping the cell culture well and combining it with its medium by using a BDNF ELISA System (Promega Biotech Ibérica).

**Magnetic resonance imaging.** The volume of the striatum, ventricles, cortex (comprising somatosensory and motor areas) and hippocampus was measured by magnetic resonance imaging in a BIOSPEC BMT 47/40 (Bruker, Ettlingen, Germany) operating at 4.7 T as described.[19]

**Statistics.** Data are presented as mean $\pm$ S.E.M. Statistical comparisons were made by ANOVA with *post hoc* Student-Newman-Keuls test or by unpaired Student's *t*-test, as indicated in each figure legend.

## Conflict of Interest

The authors declare no conflict of interest.

**Acknowledgements**. This work was supported by Spanish Ministerio de Economía y Competitividad (Grant no. SAF2012-35759) and Comunidad de Madrid (Grant no. S2010/BMD-2308) to MG, as well as by Estonian Ministry of Education and Research (Grant no. 0140143, IUT 19-18), Estonian Science Foundation (Grant no. 8844) and Estonian Academy of Sciences to PP and TT. AC is supported by Ministerio de Economía y Competitividad (FPI Program). LB is supported by an EMBO Long-Term Fellowship. We are grateful to Andrés de la Rocha, Alba Revilla, Elena García-Taboada, Carmen Vázquez, Cristina Benito and Julián Romero for expert technical assistance, and to Ana Rebolledo for helping in the provision of human samples.

1. Katona I, Freund TF. Endocannabinoid signaling as a synaptic circuit breaker in neurological disease. *Nat Med* 2008; **14**: 923–930.
2. Gaoni Y, Mechoulam R. Isolation, structure and partial synthesis of an active constituent of hashish. *J Am Chem Soc* 1964; **86**: 1646–1647.
3. Piomelli D. The molecular logic of endocannabinoid signalling. *Nat Rev Neurosci* 2003; **4**: 873–884.
4. Fernandez-Ruiz J, Moreno-Martet M, Rodriguez-Cueto C, Palomo-Garo C, Gomez-Canas M, Valdeolivas S *et al.* Prospects for cannabinoid therapies in basal ganglia disorders. *Br J Pharmacol* 2011; **163**: 1365–1378.
5. Gowran A, Noonan J, Campbell VA. The multiplicity of action of cannabinoids: implications for treating neurodegeneration. *CNS Neurosci Ther* 2011; **17**: 637–644.
6. Shohami E, Cohen-Yeshurun A, Magid L, Algali M, Mechoulam R. Endocannabinoids and traumatic brain injury. *Br J Pharmacol* 2011; **163**: 1402–1410.
7. Galve-Roperh I, Aguado T, Palazuelos J, Guzman M. Mechanisms of control of neuron survival by the endocannabinoid system. *Curr Pharm Des* 2008; **14**: 2279–2288.
8. Marsicano G, Goodenough S, Monory K, Hermann H, Eder M, Cannich A *et al.* CB1 cannabinoid receptors and on-demand defense against excitotoxicity. *Science* 2003; **302**: 84–88.
9. Chiarlone A, Bellocchio L, Blazquez C, Resel E, Soria-Gomez E, Cannich A *et al.* A restricted population of $CB_1$ cannabinoid receptors with neuroprotective activity. *Proc Natl Acad Sci USA* 2014; **111**: 8257–8262.
10. Park H, Poo MM. Neurotrophin regulation of neural circuit development and function. *Nat Rev Neurosci* 2013; **14**: 7–23.
11. D'Souza DC, Pittman B, Perry E, Simen A. Preliminary evidence of cannabinoid effects on brain-derived neurotrophic factor (BDNF) levels in humans. *Psychopharmacology (Berl)* 2009; **202**: 569–578.
12. Kreitzer AC. Physiology and pharmacology of striatal neurons. *Annu Rev Neurosci* 2009; **32**: 127–147.
13. Ivkovic S, Ehrlich ME. Expression of the striatal DARPP-32/ARPP-21 phenotype in GABAergic neurons requires neurotrophins in vivo and in vitro. *J Neurosci* 1999; **19**: 5409–5419.
14. Rauskolb S, Zagrebelsky M, Dreznjak A, Deogracias R, Matsumoto T, Wiese S *et al.* Global deprivation of brain-derived neurotrophic factor in the CNS reveals an area-specific requirement for dendritic growth. *J Neurosci* 2010; **30**: 1739–1749.
15. Li Y, Yui D, Luikart BW, McKay RM, Rubenstein JL, Parada LF. Conditional ablation of brain-derived neurotrophic factor-TrkB signaling impairs striatal neuron development. *Proc Natl Acad Sci USA* 2012; **109**: 15491–15496.
16. Pazos MR, Sagredo O, Fernandez-Ruiz J. The endocannabinoid system in Huntington's disease. *Curr Pharm Des* 2008; **14**: 2317–2325.
17. Zuccato C, Cattaneo E. Brain-derived neurotrophic factor in neurodegenerative diseases. *Nat Rev Neurol* 2009; **5**: 311–322.
18. Gines S, Bosch M, Marco S, Gavalda N, Diaz-Hernandez M, Lucas JJ *et al.* Reduced expression of the TrkB receptor in Huntington's disease mouse models and in human brain. *Eur J Neurosci* 2006; **23**: 649–658.
19. Blazquez C, Chiarlone A, Sagredo O, Aguado T, Pazos MR, Resel E *et al.* Loss of striatal type 1 cannabinoid receptors is a key pathogenic factor in Huntington's disease. *Brain* 2011; **134**: 119–136.
20. Xie Y, Hayden MR, Xu B. BDNF overexpression in the forebrain rescues Huntington's disease phenotypes in YAC128 mice. *J Neurosci* 2010; **30**: 14708–14718.
21. Jiang M, Peng Q, Liu X, Jin J, Hou Z, Zhang J *et al.* Small-molecule TrkB receptor agonists improve motor function and extend survival in a mouse model of Huntington's disease. *Hum Mol Genet* 2013; **22**: 2462–2670.

22. Simmons DA, Belichenko NP, Yang T, Condon C, Monbureau M, Shamloo M *et al.* A small molecule TrkB ligand reduces motor impairment and neuropathology in R6/2 and BACHD mouse models of Huntington's disease. *J Neurosci* 2013; **33**: 18712–18727.
23. Pertwee RG, Howlett AC, Abood ME, Alexander SP, Di Marzo V, Elphick MR *et al.* International Union of Basic and Clinical Pharmacology. LXXIX. Cannabinoid receptors and their ligands: beyond $CB_1$ and $CB_2$. *Pharmacol Rev* 2010; **62**: 588–631.
24. Trettel F, Rigamonti D, Hilditch-Maguire P, Wheeler VC, Sharp AH, Persichetti F *et al.* Dominant phenotypes produced by the HD mutation in STHdh(Q111) striatal cells. *Hum Mol Genet* 2000; **9**: 2799–2809.
25. Gines S, Ivanova E, Seong IS, Saura CA, MacDonald ME. Enhanced Akt signaling is an early pro-survival response that reflects N-methyl-D-aspartate receptor activation in Huntington's disease knock-in striatal cells. *J Biol Chem* 2003; **278**: 50514–50522.
26. Xifro X, Garcia-Martinez JM, Del Toro D, Alberch J, Perez-Navarro E. Calcineurin is involved in the early activation of NMDA-mediated cell death in mutant huntingtin knock-in striatal cells. *J Neurochem* 2008; **105**: 1596–1612.
27. Marullo M, Valenza M, Leoni V, Caccia C, Scarlatti C, De Mario A *et al.* Pitfalls in the detection of cholesterol in Huntington's disease models. *PLoS Curr* 2012; **4**: e505886e9a1968.
28. Pruunsild P, Kazantseva A, Aid T, Palm K, Timmusk T. Dissecting the human BDNF locus: bidirectional transcription, complex splicing, and multiple promoters. *Genomics* 2007; **90**: 397–406.
29. Aid T, Kazantseva A, Piirsoo M, Palm K, Timmusk T. Mouse and rat BDNF gene structure and expression revisited. *J Neurosci Res* 2007; **85**: 525–535.
30. Pruunsild P, Sepp M, Orav E, Koppel I, Timmusk T. Identification of cis-elements and transcription factors regulating neuronal activity-dependent transcription of human BDNF gene. *J Neurosci* 2011; **31**: 3295–3308.
31. Zheng F, Zhou X, Luo Y, Xiao H, Wayman G, Wang H. Regulation of brain-derived neurotrophic factor exon IV transcription through calcium responsive elements in cortical neurons. *PLoS One* 2011; **6**: e28441.
32. Armbruster BN, Li X, Pausch MH, Herlitze S, Roth BL. Evolving the lock to fit the key to create a family of G protein-coupled receptors potently activated by an inert ligand. *Proc Natl Acad Sci USA* 2007; **104**: 5163–5168.
33. Lee HM, Giguere PM, Roth BL. DREADDs: novel tools for drug discovery and development. *Drug Discov Today* 2014; **19**: 469–473.
34. Alexander GM, Rogan SC, Abbas AI, Armbruster BN, Pei Y, Allen JA *et al.* Remote control of neuronal activity in transgenic mice expressing evolved G protein-coupled receptors. *Neuron* 2009; **63**: 27–39.
35. Mangiarini L, Sathasivam K, Seller M, Cozens B, Harper A, Hetherington C *et al.* Exon 1 of the HD gene with an expanded CAG repeat is sufficient to cause a progressive neurological phenotype in transgenic mice. *Cell* 1996; **87**: 493–506.
36. Denovan-Wright EM, Robertson HA. Cannabinoid receptor messenger RNA levels decrease in a subset of neurons of the lateral striatum, cortex and hippocampus of transgenic Huntington's disease mice. *Neuroscience* 2000; **98**: 705–713.
37. McCaw EA, Hu H, Gomez GT, Hebb AL, Kelly ME, Denovan-Wright EM. Structure, expression and regulation of the cannabinoid receptor gene (CB1) in Huntington's disease transgenic mice. *Eur J Biochem* 2004; **271**: 4909–4920.
38. Casteels C, Vandeputte C, Rangarajan JR, Dresselaers T, Riess O, Bormans G *et al.* Metabolic and type 1 cannabinoid receptor imaging of a transgenic rat model in the early phase of Huntington disease. *Exp Neurol* 2011; **229**: 440–449.
39. Richfield EK, Herkenham M. Selective vulnerability in Huntington's disease: preferential loss of cannabinoid receptors in lateral globus pallidus. *Ann Neurol* 1994; **36**: 577–584.
40. Glass M, Dragunow M, Faull RL. The pattern of neurodegeneration in Huntington's disease: a comparative study of cannabinoid, dopamine, adenosine and GABA(A) receptor alterations in the human basal ganglia in Huntington's disease. *Neuroscience* 2000; **97**: 505–519.
41. Mievis S, Blum D, Ledent C. Worsening of Huntington disease phenotype in CB1 receptor knockout mice. *Neurobiol Dis* 2011; **42**: 524–529.
42. Breivogel CS, Sim LJ, Childers SR. Regional differences in cannabinoid receptor/G-protein coupling in rat brain. *J Pharmacol Exp Ther* 1997; **282**: 1632–1642.
43. Steindel F, Lerner R, Haring M, Ruehle S, Marsicano G, Lutz B *et al.* Neuron-type specific cannabinoid-mediated G protein signalling in mouse hippocampus. *J Neurochem* 2013; **124**: 795–807.
44. Selley DE, Rorrer WK, Breivogel CS, Zimmer AM, Zimmer A, Martin BR *et al.* Agonist efficacy and receptor efficiency in heterozygous CB1 knockout mice: relationship of reduced CB1 receptor density to G-protein activation. *J Neurochem* 2001; **77**: 1048–1057.
45. Greer PL, Greenberg ME. From synapse to nucleus: calcium-dependent gene transcription in the control of synapse development and function. *Neuron* 2008; **59**: 846–860.
46. Hong EJ, McCord AE, Greenberg ME. A biological function for the neuronal activity-dependent component of Bdnf transcription in the development of cortical inhibition. *Neuron* 2008; **60**: 610–624.
47. Tao X, West AE, Chen WG, Corfas G, Greenberg ME. A calcium-responsive transcription factor, CaRF, that regulates neuronal activity-dependent expression of BDNF. *Neuron* 2002; **33**: 383–395.
48. Bloodgood BL, Sharma N, Browne HA, Trepman AZ, Greenberg ME. The activity-dependent transcription factor NPAS4 regulates domain-specific inhibition. *Nature* 2013; **503**: 121–125.
49. Derkinderen P, Valjent E, Toutant M, Corvol JC, Enslen H, Ledent C *et al.* Regulation of extracellular signal-regulated kinase by cannabinoids in hippocampus. *J Neurosci* 2003; **23**: 2371–2382.
50. Khaspekov LG, Brenz Verca MS, Frumkina LE, Hermann H, Marsicano G, Lutz B. Involvement of brain-derived neurotrophic factor in cannabinoid receptor-dependent protection against excitotoxicity. *Eur J Neurosci* 2004; **19**: 1691–1698.
51. Rubino T, Vigano D, Premoli F, Castiglioni C, Bianchessi S, Zippel R *et al.* Changes in the expression of G protein-coupled receptor kinases and beta-arrestins in mouse brain during cannabinoid tolerance: a role for RAS-ERK cascade. *Mol Neurobiol* 2006; **33**: 199–213.
52. Aso E, Ozaita A, Valdizan EM, Ledent C, Pazos A, Maldonado R *et al.* BDNF impairment in the hippocampus is related to enhanced despair behavior in $CB_1$ knockout mice. *J Neurochem* 2008; **105**: 565–572.
53. Beyer CE, Dwyer JM, Piesla MJ, Platt BJ, Shen R, Rahman Z *et al.* Depression-like phenotype following chronic CB1 receptor antagonism. *Neurobiol Dis* 2010; **39**: 148–155.
54. Ferreira-Vieira TH, Bastos CP, Pereira GS, Moreira FA, Massensini AR. A role for the endocannabinoid system in exercise-induced spatial memory enhancement in mice. *Hippocampus* 2014; **24**: 79–88.
55. Butovsky E, Juknat A, Goncharov I, Elbaz J, Eilam R, Zangen A *et al.* In vivo up-regulation of brain-derived neurotrophic factor in specific brain areas by chronic exposure to delta-9-tetrahydrocannabinol. *J Neurochem* 2005; **93**: 802–811.
56. Altar CA, Cai N, Bliven T, Juhasz M, Conner JM, Acheson AL *et al.* Anterograde transport of brain-derived neurotrophic factor and its role in the brain. *Nature* 1997; **389**: 856–860.
57. Timmusk T, Lendahl U, Funakoshi H, Arenas E, Persson H, Metsis M. Identification of brain-derived neurotrophic factor promoter regions mediating tissue-specific, axotomy-, and neuronal activity-induced expression in transgenic mice. *J Cell Biol* 1995; **128**: 185–199.
58. Canals JM, Marco S, Checa N, Michels A, Perez-Navarro E, Arenas E *et al.* Differential regulation of the expression of nerve growth factor, brain-derived neurotrophic factor, and neurotrophin-3 after excitotoxicity in a rat model of Huntington's disease. *Neurobiol Dis* 1998; **5**: 357–364.
59. Her LS, Goldstein LS. Enhanced sensitivity of striatal neurons to axonal transport defects induced by mutant huntingtin. *J Neurosci* 2008; **28**: 13662–13672.
60. Hasbi A, Fan T, Alijaniaram M, Nguyen T, Perreault ML, O'Dowd BF *et al.* Calcium signaling cascade links dopamine D1-D2 receptor heteromer to striatal BDNF production and neuronal growth. *Proc Natl Acad Sci USA* 2009; **106**: 21377–21382.
61. De Chiara V, Angelucci F, Rossi S, Musella A, Cavasinni F, Cantarella C *et al.* Brain-derived neurotrophic factor controls cannabinoid $CB_1$ receptor function in the striatum. *J Neurosci* 2010; **30**: 8127–8137.
62. The Huntington's Disease Collaborative Research Consortium A novel gene containing a trinucleotide repeat that is expanded and unstable on Huntington's disease chromosomes. *Cell* 1993; **72**: 971–983.
63. Benito C, Nunez E, Tolon RM, Carrier EJ, Rabano A, Hillard CJ *et al.* Cannabinoid $CB_2$ receptors and fatty acid amide hydrolase are selectively overexpressed in neuritic plaque-associated glia in Alzheimer's disease brains. *J Neurosci* 2003; **23**: 11136–11141.
64. Ramirez BG, Blazquez C, Gomez del Pulgar T, Guzman M, de Ceballos ML. Prevention of Alzheimer's disease pathology by cannabinoids: neuroprotection mediated by blockade of microglial activation. *J Neurosci* 2005; **25**: 1904–1913.
65. Bedse G, Romano A, Cianci S, Lavecchia AM, Lorenzo P, Elphick MR *et al.* Altered expression of the $CB_1$ cannabinoid receptor in the triple transgenic mouse model of Alzheimer's disease. *J Alzheimers Dis* 2014; **40**: 701–712.
66. Plotkin JL, Day M, Peterson JD, Xie Z, Kress GJ, Rafalovich I *et al.* Impaired TrkB receptor signaling underlies corticostriatal dysfunction in Huntington's disease. *Neuron* 2014; **83**: 178–188.
67. Monory K, Massa F, Egertova M, Eder M, Blaudzun H, Westenbroek R *et al.* The endocannabinoid system controls key epileptogenic circuits in the hippocampus. *Neuron* 2006; **51**: 455–466.
68. Guggenhuber S, Monory K, Lutz B, Klugmann M. AAV vector-mediated overexpression of $CB_1$ cannabinoid receptor in pyramidal neurons of the hippocampus protects against seizure-induced excitoxicity. *PLoS One* 2010; **5**: e15707.
69. Benito C, Romero JP, Tolon RM, Clemente D, Docagne F, Hillard CJ *et al.* Cannabinoid $CB_1$ and $CB_2$ receptors and fatty acid amide hydrolase are specific markers of plaque cell subtypes in human multiple sclerosis. *J Neurosci* 2007; **27**: 2396–2402.
70. Marsicano G, Wotjak CT, Azad SC, Bisogno T, Rammes G, Cascio MG *et al.* The endogenous cannabinoid system controls extinction of aversive memories. *Nature* 2002; **418**: 530–534.



Supplementary Information accompanies this paper on Cell Death and Differentiation website (http://www.nature.com/cdd)

# Prenatal exposure to cannabinoids evokes long-lasting functional alterations by targeting $CB_1$ receptors on developing cortical neurons

Adán de Salas-Quiroga[a,b,c,1], Javier Díaz-Alonso[a,b,c,1,2], Daniel García-Rincón[a,b,c], Floortje Remmers[d], David Vega[a,c], María Gómez-Cañas[a,b,e], Beat Lutz[d], Manuel Guzmán[a,b,c], and Ismael Galve-Roperh[a,b,c,3]

[a]Centro de Investigación Biomédica en Red sobre Enfermedades Neurodegenerativas (CIBERNED), 28049 Madrid, Spain; [b]Instituto de Investigación Sanitaria Ramón y Cajal (IRYCIS), 28034 Madrid, Spain; [c]Department of Biochemistry and Molecular Biology I, Complutense University, 28040 Madrid, Spain; [d]Institute of Physiological Chemistry, University Medical Center of the Johannes Gutenberg University Mainz, 55128 Mainz, Germany; and [e]Department of Biochemistry and Molecular Biology III, Complutense University, 28040 Madrid, Spain

Edited by Leslie Lars Iversen, University of Oxford, Oxford, United Kingdom, and approved September 16, 2015 (received for review August 3, 2015)

**The $CB_1$ cannabinoid receptor, the main target of $\Delta^9$-tetrahydrocannabinol (THC), the most prominent psychoactive compound of marijuana, plays a crucial regulatory role in brain development as evidenced by the neurodevelopmental consequences of its manipulation in animal models. Likewise, recreational cannabis use during pregnancy affects brain structure and function of the progeny. However, the precise neurobiological substrates underlying the consequences of prenatal THC exposure remain unknown. As $CB_1$ signaling is known to modulate long-range corticofugal connectivity, we analyzed the impact of THC exposure on cortical projection neuron development. THC administration to pregnant mice in a restricted time window interfered with subcerebral projection neuron generation, thereby altering corticospinal connectivity, and produced long-lasting alterations in the fine motor performance of the adult offspring. Consequences of THC exposure were reminiscent of those elicited by $CB_1$ receptor genetic ablation, and $CB_1$-null mice were resistant to THC-induced alterations. The identity of embryonic THC neuronal targets was determined by a Cre-mediated, lineage-specific, $CB_1$ expression-rescue strategy in a $CB_1$-null background. Early and selective $CB_1$ reexpression in dorsal telencephalic glutamatergic neurons but not forebrain GABAergic neurons rescued the deficits in corticospinal motor neuron development of $CB_1$-null mice and restored susceptibility to THC-induced motor alterations. In addition, THC administration induced an increase in seizure susceptibility that was mediated by its interference with $CB_1$-dependent regulation of both glutamatergic and GABAergic neuron development. These findings demonstrate that prenatal exposure to THC has long-lasting deleterious consequences in the adult offspring solely mediated by its ability to disrupt the neurodevelopmental role of $CB_1$ signaling.**

cannabis | $CB_1$ cannabinoid receptor | corticospinal | neurodevelopment | seizures

Recreational cannabis consumption during pregnancy can exert deleterious consequences in the progeny, including anxiety, depression, psychosis risk, and cognitive and social impairments (1, 2). In the last two decades, important advances in our understanding of the endocannabinoid system have paved the way to elucidate the particular neurobiological substrates responsible for some cannabinoid-induced neurological alterations in adult animals and humans (3). The currently accepted scenario is that the $CB_1$ cannabinoid receptor ($CB_1R$), the main target of marijuana-derived cannabinoids, is located presynaptically and, upon engagement by endocannabinoids [2-arachidonoylglycerol (2-AG) and anandamide], can act as a key neuromodulatory and plasticity-tuning signaling platform at many different mature synapses (4). In fact, $CB_1R$ constitutes one of the most abundant and functionally relevant G protein-coupled receptors in several regions of the adult mammalian brain (3, 4).

Manipulation of $CB_1R$ function in animal models, either directly or indirectly, by modulating 2-AG or anandamide levels through the main endocannabinoid-synthesizing [diacylglycerol lipase (DAGL) α/β] or degrading enzymes [monoacylglycerol lipase (MAGL) and fatty acid amide hydrolase (FAAH)], influences key processes of forebrain development, including (*i*) progenitor cell expansion and neurogenesis, (*ii*) neuronal and glial specification, and (*iii*) axonal pathfinding (5–7). Alterations of these developmental processes may conceivably underlie the functional deficits observed in the offspring upon prenatal exposure to THC. A crucial role has been assigned to $CB_1R$ in the development of long-range axonal connectivity by regulating corticofugal axon navigation and fasciculation (8, 9). In particular, $CB_1R$ is essential for subcerebral projection neuron development, as it regulates the appropriate balance between the transcription factors Ctip2 and Satb2 (10), which is responsible for corticospinal motor neuron (CSMN) specification (11).

In this study, we modeled prenatal cannabis consumption in mice to identify the particular neurodevelopmental substrates responsible for cannabinoid-induced functional alterations that

## Significance

**Marijuana is the most commonly used illicit drug, and its consumption constitutes a serious health concern. The psychoactivity of the plant is exerted by its cannabinoid constituents, especially $\Delta^9$-tetrahydrocannabinol (THC), which acts by engaging $CB_1$ cannabinoid receptors. Despite the large knowledge accumulated on how THC affects the adult brain, its molecular and functional impact on neuronal development remains obscure. This study demonstrates that remarkable detrimental consequences of embryonic THC exposure on adult-brain function, which are evident long after THC withdrawal, are solely due to the impact of THC on $CB_1$ receptors located on developing cortical neurons. Our findings thus delineate the risk of cannabis consumption during pregnancy and contribute to identify precise neuronal lineages targeted by prenatal THC exposure.**

Author contributions: A.d.S.-Q., J.D.-A., M.G., and I.G.-R. designed research; A.d.S.-Q., J.D.-A., D.G.-R., F.R., D.V., and M.G.-C. performed research; F.R. and B.L. contributed new reagents/analytic tools; A.d.S.-Q., J.D.-A., D.G.-R., F.R., B.L., M.G., and I.G.-R. analyzed data; and A.d.S.-Q., J.D.-A., F.R., B.L., M.G., and I.G.-R. wrote the paper.

The authors declare no conflict of interest.

This article is a PNAS Direct Submission.

[1]A.d.S.-Q. and J.D.-A. contributed equally to this work.

[2]Present address: Department of Cellular and Molecular Pharmacology, University of California, San Francisco, CA 94143.

[3]To whom correspondence should be addressed. Email: igr@quim.ucm.es.

This article contains supporting information online at www.pnas.org/lookup/suppl/doi:10.1073/pnas.1514962112/-/DCSupplemental.

remain overt in adult animals. Administration of THC was conducted during a restricted embryonic time window, coinciding with the active period of glutamatergic neuron generation in the telencephalon (11). To unequivocally assess the role of $CB_1R$ signaling in THC-induced alterations, we used $CB_1R$-deficient mice, which were resistant to THC-induced developmental effects. Next, by using a Cre-mediated, lineage-specific, $CB_1R$ expression-rescue strategy in a $CB_1R$-null background, we were able to selectively rescue the deficits in CSMN development of $CB_1R$-deficient mice and, in turn, fully restore the susceptibility to THC-induced motor alterations in adulthood. We also found that embryonic THC exposure induced an increase in seizure susceptibility that was mediated by $CB_1R$ present in developing dorsal telencephalic pyramidal neurons and forebrain GABAergic neurons. Hence, targeting $CB_1R$ with the most prominent marijuana-derived psychoactive compound in a particular neuronal population and time frame during embryonic development can evoke remarkable long-lasting neurological alterations.

## Results

**Prenatal THC Exposure Interferes with Cortical Projection Neuron Development.** To investigate the impact of prenatal THC exposure on cortical development and to avoid the confounding influence that the cannabinoid could exert during very early gestational stages (12, 13), we administered one daily i.p. injection of THC or its vehicle to pregnant wild-type mice from E12.5 to E16.5. To minimize potential $CB_1R$ off-targets, a low dose of THC (3 mg/kg) was used. Of note, maternal and neonate body weight was unaffected by THC treatment, thus indicating that the dose used did not induce deleterious effects on general physical status. As the $CB_1R$ is essential for CSMN specification (10), the effects of embryonic THC exposure on the developing cortex were first assessed by quantifying the generation of subcerebral projection neurons. Confocal immunofluorescence analysis of Ets-related protein 81 (ER81), a bona fide marker of subcerebral projection neurons (11), was performed in the treated offspring at P20. $ER81^+$ neurons were decreased in THC-exposed animals compared with their vehicle-treated controls (Fig. 1 *A* and *B*). The impact of THC on CSMN development was also analyzed at the level of corticospinal axon projections. For this purpose, we performed fluorescent retrograde labeling (Red RetroBeads) from the cervical spinal cord to unequivocally identify CSMNs (14) (Fig. 1*C*). Red-labeled somata in deep cortical layer V were shown to express ER81, thus confirming the validity of ER81 as an appropriate marker of CSMNs (Fig. 1*D*). We also found a significant reduction in the number of labeled CSMN somata in THC-treated mice compared with their controls, pointing to an alteration of CSMN development and subcerebral connectivity (Fig. 1 *E* and *F*).

**Prenatal THC Exposure Induces Long-Lasting Alterations in Skilled Motor Function and Seizure Susceptibility.** To examine the functional consequences of the impaired subcerebral projection neuron development induced by prenatal cannabinoid exposure, we first used the skilled reaching test, which allows the dissection of CSMN-dependent motor function as reflected by the ability to retrieve a pellet of palatable food with a forelimb through a narrow slit (15). To rule out potential unspecific developmental alterations in the offspring owing to maternal care induced by THC administration (16), we used $CB_1^{-/-}$ females, devoid of the behavioral impact of THC, which were mated with heterozygous $CB_1^{+/-}$ males. Therefore, we analyzed skilled motor function in the $CB_1^{+/-}$ and $CB_1^{-/-}$ offspring. $CB_1^{+/-}$ mice have been shown to exhibit an increased efficacy of agonist-induced G protein-coupled receptor signaling, which becomes comparable to that of wild-type $CB_1^{+/+}$ mice, thus supporting the validity of this experimental approach (17). THC-exposed $CB_1^{+/-}$ animals showed a significant impairment in skilled motor function compared with their vehicle-treated counterparts (Fig. 2*A*). Remarkably, $CB_1^{-/-}$ mice, which consistently with our previous report showed an impairment in this task compared with their vehicle-treated $CB_1^{+/-}$ littermates (10), did not suffer from any worsening in their skilled motor performance upon THC exposure (Fig. 2*A*). Importantly, neither the number of trials (Fig. 2*B*) nor the success in unskilled conditions was changed among groups, ruling out generalized motivational or unspecific motor alterations in the observed skilled motor deficits. Corticospinal function was also assessed with the staircase test, and again, a decreased performance was evident in THC-exposed $CB_1^{+/-}$ mice compared with their vehicle-treated controls (Fig. 2*C*). In addition, $CB_1^{-/-}$ control mice performed worse than their $CB_1^{+/-}$ littermates, and THC treatment did not significantly worsen their ability to reach the pellets. Control quantifications of unskilled reaching did not show significant differences among groups (Fig. 2*D*). Altogether, these data demonstrate the $CB_1R$ dependency of embryonic THC-evoked motor alterations.

Developmental THC administration induces alterations in synaptic connectivity and plasticity (18, 19), but its long-lasting functional consequences remain largely unknown. Therefore, we analyzed whether seizure susceptibility was affected in the adult offspring of THC-administered pregnant mice by using a pentylenetetrazole (PTZ) administration paradigm. Of note, latency to seizures was significantly decreased in prenatally THC-exposed $CB_1^{+/-}$ mice compared with their vehicle-treated counterparts (Fig. 2*E*; 31.8 ± 1.4 and 37.0 ± 1.3 min, respectively; $P < 0.01$).

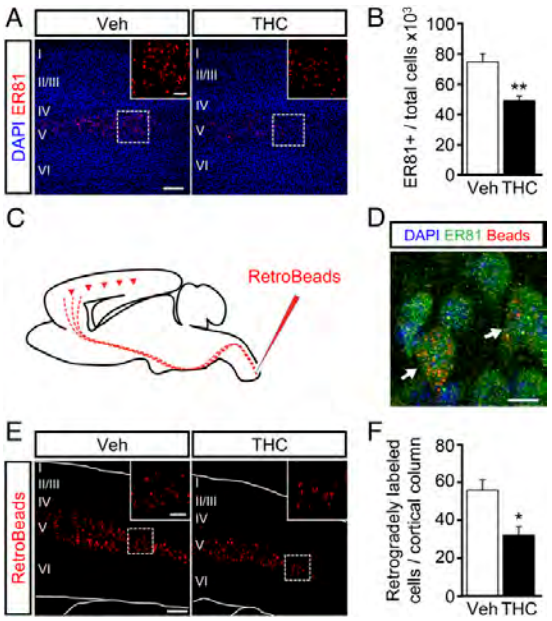


**Fig. 1.** Embryonic THC exposure impairs subcerebral projection neuron development. (*A*) Subcerebral projection neurons in embryonically vehicle- and THC-administered mice at P15 were stained with an anti-ER81 antibody ($n$ = 7 and 5, respectively). (*B*) ER81+ cell number was quantified and referred to the total cell number (DAPI) per cortical column. (*C*) CSMNs were labeled by injecting retrogradelly transported red fluorescent beads (RetroBeads) in the cervical spinal cord at P10. (*D*) Representative image showing RetroBead colocalization with the subcerebral projection neuron marker ER81. (*E*) Representative images of retrogradelly labeled somata in cortical layer V at P15. (*F*) RetroBead-labeled somata per cortical column were quantified in vehicle- and THC-exposed mice ($n$ = 5 and 4, respectively). *$P < 0.05$, **$P < 0.01$ vs. vehicle-treated mice. [Scale bar, (*A* and *E*) 200 μm (*Insets*, 60 μm) and (*D*) 10 μm.]

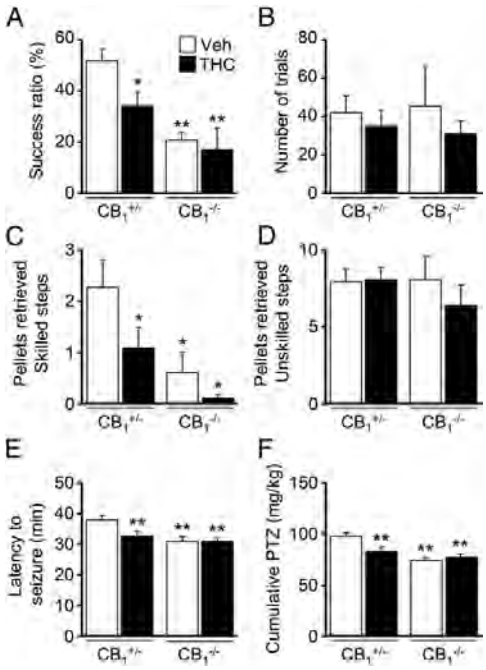


**Fig. 2.** Embryonic THC exposure impairs corticospinal motor function. (*A* and *B*) The skilled pellet-reaching test was evaluated in adult $CB_1^{+/-}$ and $CB_1^{-/-}$ littermates prenatally exposed to vehicle or THC from E12.5 to E16.5. The success ratio of pellets retrieved in the skilled paradigm (*A*) and the total number of trials performed (*B*) were quantified [$n = 11$ and 8 ($CB_1^{+/-}$ vehicle- and THC-treated mice, respectively); $n = 6$ and 4 ($CB_1^{-/-}$ vehicle- and THC-treated mice, respectively)]. (*C* and *D*) Mice were subjected to the staircase pellet-reaching test, and the sum of pellets retrieved from skilled steps (from four to eight) was compared between vehicle- and THC-administered mice (*C*). As a control, the number of pellets reached in unskilled steps 1–3 was calculated (*D*) [$n = 8$ and 12 ($CB_1^{+/-}$ vehicle- and THC-treated mice, respectively); $n = 5$ and 3 ($CB_1^{-/-}$ vehicle- and THC-treated mice, respectively)]. (*E* and *F*) THC- and vehicle-treated $CB_1^{+/-}$ and $CB_1^{-/-}$ mice were subjected to a PTZ administration paradigm. Latency to tonic-clonic seizure appearance after the first PTZ injection (*E*) and the cumulative dose of PTZ required (*F*) were calculated [$n = 15$ and 18 ($CB_1^{+/-}$ vehicle- and THC-treated mice, respectively); $n = 13$ and 11 ($CB_1^{-/-}$ vehicle- and THC-treated mice, respectively)]. $^*P < 0.05$, $^{**}P < 0.01$ vs. vehicle-treated $CB_1^{+/-}$ mice.

Consequently, a reduced PTZ cumulative dose was required to induce generalized seizures in the THC-treated offspring (Fig. 2*F*; THC vs. vehicle, $81.3 \pm 4.1$ and $96.0 \pm 3.5$ mg/kg, respectively; $P < 0.01$). This effect of prenatal cannabinoid administration was reminiscent of the adult $CB_1^{-/-}$ mice phenotype, which displays increased seizure susceptibility in the kainic acid model (20, 21). Importantly, we found no further enhancement of PTZ susceptibility in THC-treated $CB_1^{-/-}$ mice with respect to their vehicle-treated counterparts, thus confirming the $CB_1R$ specificity of THC action (Fig. 2*F*; THC vs. vehicle, $30.2 \pm 0.7$ and $30.1 \pm 1.0$ min, respectively). Overall, the neuronal and functional analyses of prenatally THC-administered mice showed a similar phenotype to $CB_1R$-null mice, thus indicating that embryonic THC exposure interferes with the neurodevelopmental role of $CB_1R$ signaling.

**Prenatal THC Exposure Transiently Impairs $CB_1R$ Signaling.** We next analyzed the consequences of prenatal THC administration on $CB_1R$ expression. $CB_1R$ protein levels, as determined by Western blot, were significantly down regulated in THC-treated embryonic brains at E17.5 compared with controls (Fig. 3 *A* and *C*). Notably, at a perinatal stage (P2.5), $CB_1R$ levels returned to those of the vehicle condition (Fig. 3 *B* and *D*), indicating that $CB_1Rs$ are altered only transiently in our embryonic THC-exposure paradigm. The presence of functional plasma membrane-exposed $CB_1R$ was next analyzed by the binding of the radioactively labeled $CB_1R$ agonist [$^3$H]CP-55,940. A reduced cannabinoid binding was observed in the brains of THC-treated embryos at E17.5 (Fig. 3 *E* and *G*), and its values recovered to the level of vehicle-treated animals at P2.5 (Fig. 3 *F* and *H*). Overall, these findings support that embryonic THC administration transiently disrupts appropriate $CB_1R$ function in the developing brain.

**Neuronal Lineage-Specific $CB_1R$ Reexpression Selectively Rescues the Behavioral Traits of Embryonic THC Exposure.** To unequivocally determine the neuronal identity of embryonic THC-exposure actions, we made use of a Cre-mediated, lineage-specific, embryonic $CB_1R$ expression-rescue strategy in a $CB_1R$-null background (Stop-$CB_1$ mice) (21). The selective expression of $CB_1R$ in dorsal telencephalic glutamatergic neurons (Glu-$CB_1$-RS mice) was achieved by expressing Cre under the regulatory elements of the Nex gene (21). In addition, we rescued $CB_1R$ expression in forebrain GABAergic neurons (GABA-$CB_1$-RS mice) by using the Dlx5/6-Cre mouse line (20). As a control, a global $CB_1R$ expression

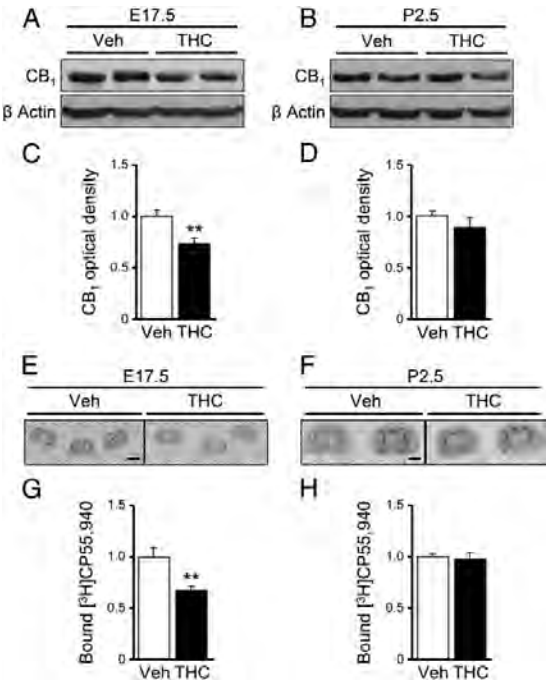


**Fig. 3.** Embryonic THC exposure transiently down-regulates $CB_1Rs$. (*A–D*) $CB_1R$ protein levels were determined by Western blot in brain samples at E17.5 (*A* and *C*) and P2.5 (*B* and *D*) after THC or vehicle administration from E12.5 to E16.5. The optical density of the $CB_1R$ band was quantified and normalized to β-actin [$n = 9$ and 6 (E17.5 vehicle- and THC-treated brain samples, respectively); $n = 7$ and 7 (P2.5 vehicle- and THC-treated brain samples, respectively)]. (*E–H*) Radiolabeled CP-55,940 binding was quantified in coronal brain sections at E17.5 (*E* and *G*) and P2.5 (*F* and *H*) [$n = 4$ and 6 (E17.5 vehicle- and THC-treated brains, respectively); $n = 8$ and 8 (P2.5 vehicle- and THC-treated brains, respectively)]. $^{**}P < 0.01$ vs. vehicle-treated mice. (Scale bar, 2 mm.)

rescue approach driven by EIIa-Cre ($CB_1$-RS) was also used (21). Characterization of $CB_1R$ expression by immunofluorescence was performed in the different mouse lines. In a Stop-$CB_1$ mice-only background, a nonspecific signal was detected, whereas in Glu-$CB_1$-RS and GABA-$CB_1$-RS animals, $CB_1R$ immunoreactivity was observed with a distinctive pattern of expression (Fig. 4 *A–C*). Glu-$CB_1$-RS mice at P2.5 revealed a significant $CB_1R$ expression in descending corticofugal axons, whereas in GABA-$CB_1$-RS mice a prominent $CB_1R$ expression was observed in the immature hippocampal formation (Fig. 4 *A*, *A1–A4*). Cortical $CB_1R$ expression at P20 in Glu-$CB_1$-RS mice appeared as scarce immunopositive puncta, in agreement with the low expression of the receptor in mature projection neurons (4), whereas most $CB_1R$ expression corresponded to GABAergic neurons (Fig. 4 *B*, *B1–B4*). Double immunofluorescence with VGLUT1 and VGAT, presynaptic markers of glutamatergic and GABAergic terminals, respectively, confirmed the selectivity of the $CB_1R$ expression-rescue strategy (Fig. 4*C*). Thus, in Glu-$CB_1$-RS mice, the small puncta of $CB_1R$ did not colocalize with VGAT immunoreactivity, in agreement with their presynaptic location in glutamatergic neurons (Fig. 4*C*).

To assess the reestablishment of the neurobiological substrate of THC-induced alterations, we quantified the number of ER81-positive cells in cortical layer V. Remarkably, in vehicle-treated Glu-$CB_1$-RS mice, the number of deep-layer ER81-positive cells per cortical column was significantly rescued compared with Stop-$CB_1$ animals (96.8 ± 6.6 and 71.7 ± 4.9, respectively; $P < 0.05$), and in concert, Glu-$CB_1$-RS mice gained susceptibility to THC-induced impairment of subcerebral projection-neuron development (73.2 ± 5.5; $P < 0.05$ vs. vehicle-treated Glu-$CB_1$-RS mice).

Once the lineage selectivity of the $CB_1R$ expression-rescue strategy at the cellular level was proved, we investigated the functional impact of embryonic THC exposure in adulthood. THC or vehicle was administered to pregnant mice coming from crosses of Stop-$CB_1$ with Nex-Cre (Glu-$CB_1$-RS) or Dlx5/6-Cre (GABA-$CB_1$-RS) animals, and their respective offspring were analyzed at an adult age. $CB_1R$ reexpression in Glu-$CB_1$-RS mice, but not in GABA-$CB_1$-RS mice, rescued the skilled motor deficits of Stop-$CB_1$ mice as assessed by both the skilled-reaching test (Fig. 5*A*) and the staircase test (Fig. 5*B*). Global rescue of $CB_1R$ expression in $CB_1$-RS mice also abolished the skilled motor deficits observed in Stop-$CB_1$ mice. Overall, $CB_1R$ expression rescue in dorsal telencephalic glutamatergic neurons is necessary and sufficient to confer THC susceptibility to corticospinal motor function.

Finally, we also analyzed PTZ-induced seizure susceptibility in the various $CB_1R$ expression-rescued mice. Stop-$CB_1$ mice showed a seizure-prone phenotype that was fully restored when the $CB_1R$ was expressed systemically in $CB_1$-RS mice, whereas seizure susceptibility was partially restored in both Glu-$CB_1$-RS and GABA-$CB_1$-RS (Fig. 5 *C* and *D*; latency to seizures in THC-treated mice, Glu-$CB_1$-RS vs. $CB_1$-RS, 34.0 ± 5.0 and 42.7 ± 2.2 min, respectively, $P < 0.05$; GABA-$CB_1$-RS vs. $CB_1$-RS, 33.6 ± 2.2 and 42.7 ± 2.2 min, respectively, $P < 0.05$; cumulative PTZ dose, Glu-$CB_1$-RS vs. $CB_1$-RS, 90.0 ± 10 and 106.6 ± 5.1 mg/kg, respectively, $P < 0.05$; GABA-$CB_1$-RS vs. $CB_1$-RS, 87.2 ± 6.6 mg/kg and 106.6 ± 5.1 mg/kg, respectively, $P < 0.01$). Notably, upon THC administration, only $CB_1$-RS mice showed increases in seizure latency and PTZ cumulative dose, whereas no significant differences were found among Stop-$CB_1$, Glu-$CB_1$-RS, and GABA-$CB_1$-RS mice (Fig. 5 *C* and *D*). These findings support the notion that prenatal $CB_1R$ signaling in both glutamatergic and GABAergic cell lineages is required for the appropriate balance of neuronal activity.

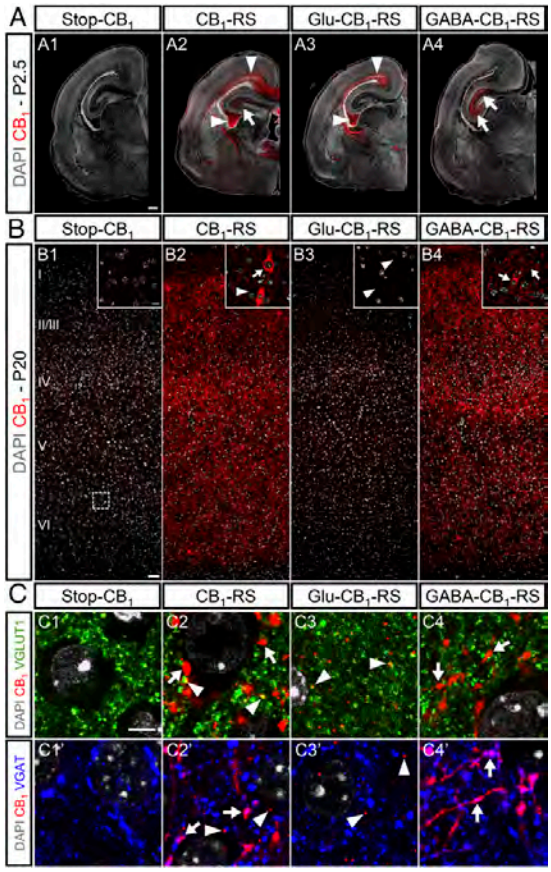


**Fig. 4.** Characterization of selective $CB_1R$ expression rescue in dorsal glutamatergic neurons and forebrain GABAergic neurons. (*A*) Immunofluorescence analysis of $CB_1R$ reexpression driven by Nex (Glu-$CB_1$-RS) (*A3*), Dlx5/6 (GABA-$CB_1$-RS) (*A4*), or EIIa ($CB_1$-RS) (*A2*) promoters in Stop-$CB_1$ mice (*A1*) was performed in P2.5 coronal brain sections. (*B*) Cortical $CB_1R$ expression analysis in the same mouse strains was performed at P20 (*B1–B4*). (*C*) Double immunofluorescence was performed with anti-$CB_1$ antibody combined with anti-VGLUT1 (*C1–C4*) or anti-VGAT (*C1′–C4′*) antibodies. Arrowheads point to the glutamatergic $CB_1R$ signal, which is abundant in pyramidal neuron fibers at P2.5 (*A*) and to scarce immunopositive puncta corresponding to glutamatergic (VGLUT1-positive) terminals at P20 (*B* and *C*). Arrows point to the abundant $CB_1R$ signal corresponding to GABAergic (VGAT-positive) neurons within the hippocampal formation at P2.5 (*A*) and the mature cortex at P20 (*B* and *C*). [Scale bars, (*A*) 200 μm, (*B*) 50 μm (*Inset*, 10 μm), and (*C*) 5 μm.]

## Discussion

The present study reveals that embryonic THC exposure exerts long-lasting consequences in the offspring owing to a transient disruption of $CB_1R$ signaling that impedes the adequate temporally and spatially confined function of the receptor in cortical neuron development. Remarkably, the deleterious consequences of prenatal THC exposure in the progeny are independent of the classical neuromodulatory role of $CB_1R$ signaling in the adult brain and emerge exclusively as a consequence of the transient disruption of physiological $CB_1R$ signaling during prenatal development, when synaptic neuronal activity is not yet established. These findings provide previously unidentified preclinical evidence for the risk of cannabis consumption during pregnancy. Cannabis is, by far, the most commonly consumed illicit drug during pregnancy in Western countries, and therefore its use

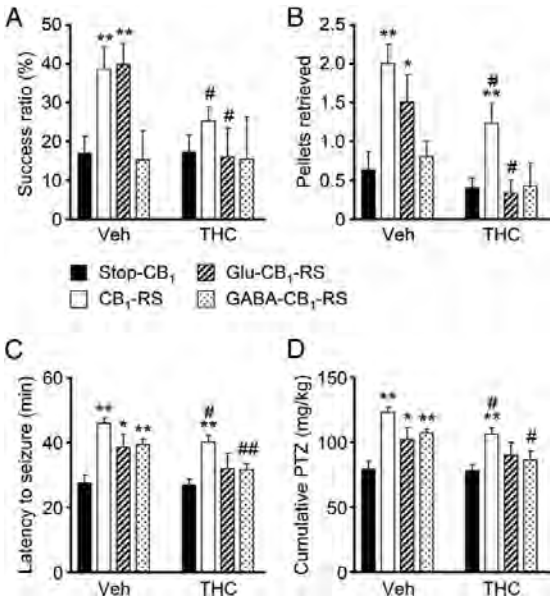


**Fig. 5.** Selective $CB_1R$ expression rescue restores functional alterations and reestablishes THC susceptibility in Stop-$CB_1$ mice. (*A* and *B*) Skilled motor activity was assessed by the skilled pellet-reaching (*A*) and staircase (*B*) tests in adult $CB_1R$-rescued mice [$n = 15$ and 15 (Stop-$CB_1$ vehicle- and THC-treated mice, respectively); $n = 20$ and 17 ($CB_1$-RS vehicle- and THC-treated mice, respectively); $n = 9$ and 6 (Glu-$CB_1$-RS vehicle- and THC-treated mice, respectively); $n = 5$ and 7 (GABA-$CB_1$-RS vehicle- and THC-treated mice, respectively)]. (*C* and *D*) Seizure susceptibility to subconvulsive doses of PTZ was determined. Latency to seizures (*C*) and the cumulative dose of PTZ required (*D*) are shown [$n = 13$ and 19 (Stop-$CB_1$ vehicle- and THC-treated mice, respectively); $n = 18$ and 19 ($CB_1$-RS vehicle- and THC-treated mice, respectively); $n = 9$ and 5 (Glu-$CB_1$-RS vehicle- and THC-treated mice, respectively); $n = 9$ and 8 (GABA-$CB_1$-RS vehicle- and THC-treated mice, respectively)]. $^{*}P < 0.05$, $^{**}P < 0.01$ vs. corresponding Stop-$CB_1$ mice; $^{\#}P < 0.05$, $^{\#\#}P < 0.01$ vs. corresponding vehicle-treated group.

constitutes a considerable public health issue (1, 2, 16). Over the last few decades, longitudinal studies on human cohorts (1, 2), as well as research using animal models (22), have addressed the impact of early cannabinoid exposure in adulthood. The majority of these studies suggest that early cannabinoid exposure sensitizes the CNS to cognitive impairments, increases the risk of neuropsychiatric disorders such as schizophrenia and anxiety, induces motor alterations, and enhances drug-addiction susceptibility (23–25). Our findings show that exposure to low doses of THC in a narrow temporal window during prenatal development negatively impacts mouse cortical development, and this, in turn, has long-term functional consequences on the mature offspring. Specifically, we unequivocally identify the pool of $CB_1R$ located on developing cortical glutamatergic neurons as the sole reason for the deficits in corticospinal function induced by embryonic THC exposure.

The $CB_1R$ plays a pivotal neurodevelopmental role by transducing information from the endocannabinoid ligands present in the neurogenic niche into the coordination of the intrinsic developmental program of developing neurons (6, 26). In agreement, early developmental exposure of chicken embryos to a THC analog (27) and genetic manipulation of the $CB_1R$-interacting protein CRIP1 (28) have been shown to disrupt the appropriate balance of transcription factors that intrinsically drive neuronal development. Thus, $CB_1R$ signaling refines the molecular, laminar, and hodological identity of projection neurons in the pre- and postnatal cerebral cortex (5, 6). The present findings support that THC can act as a functional suppressor of $CB_1R$ signaling, as restricted exposure to THC interferes with developmental $CB_1R$ function in a transient but functionally impacting manner. Therefore, prenatal cannabinoid exposure recapitulates the long-term structural and functional deficits in corticospinal connectivity previously demonstrated in $CB_1R$-knockout mice (10). The susceptibility of axonal connectivity to embryonic $CB_1R$ loss of function (present report) may persist at later developmental stages in critically susceptible areas, as it has been demonstrated that THC consumption in adolescents can also result in axonal connectivity deficits (29). Nevertheless, in another study, daily marijuana consumption did not induce volumetric changes in several brain areas (30).

Our findings are in partial agreement with a previous study reporting that chronic prenatal THC administration alters neuronal connectivity by disrupting cytoskeletal dynamics in motile axons. Specifically, prolonged THC administration (E5.5 to E17.5) was shown to disrupt cannabinoid signaling by interfering with 2-AG–metabolizing enzymes, MAGL, and DAGL, but did not induce $CB_1R$ desensitization (18). In that study, the functional consequences of chronic prenatal THC administration on axonal projections were not determined. Manipulation of endocannabinoid levels in perinatal stages by chronic pharmacological inhibition of FAAH, the main anandamide-degrading enzyme, induced depressive and cognitive impairment traits, despite the fact that no specific neuronal development alterations could be demonstrated (9). On the other hand, pharmacological inhibition of MAGL increased 2-AG levels and induced axon fasciculation alterations by interfering with Slit2/Robo1 signaling, but the functional consequences of these actions remain unknown (31). Other studies have also shown that perinatal cannabinoid administration induces cognitive deficits that can be linked to neuronal transmission adaptations, particularly plasticity of glutamatergic neuron activity (19, 25, 32, 33) and aberrant synaptic organization (18, 34). In humans, prenatal cannabis exposure interferes with executive function (2) and increases children's depressive symptoms when excluding identified covariate factors such as maternal tobacco use, education, and child composite IQ (35). Moreover, prenatal cannabis exposure interferes with prefrontal cortex-mediated response inhibition as revealed by functional MRI, which may reflect delayed cortical maturation (36). Thus, whereas it is already known that postnatal cannabinoid exposure has negative consequences on neurological functions in the adult brain (1), this study unveils long-lasting functional neuronal alterations induced by restricted prenatal cannabinoid administration that can be unequivocally ascribed to specific developing neuronal lineages. Notably, our findings reveal a direct impact of THC exposure on the developing embryo that does not rely on indirect consequences of maternal programming and that is evident without the requirement of a second hit, as proposed for cannabis-induced risk of psychosis (16). In any case, translating the long-term implications of developmental cannabis exposure into humans requires a very stringent control of confounding factors (37, 38), and this is more important when analyzing cognitive and psychiatric traits than merely determining plastic adaptations of neuronal activity or drug abuse sensitivity.

In addition to corticospinal motor function alterations, embryonic THC exposure increased seizure susceptibility in adult mice, even when $CB_1Rs$ return to normal levels shortly after cessation of THC exposure. The neuromodulatory role of $CB_1R$ in the mature brain exerts overall an anticonvulsant action (4). In addition, great interest has recently emerged in the potential application of cannabis preparations enriched in cannabidiol for the management of pediatric epilepsy disorders such as Dravet and Gaston–Leroux syndromes (39). However, results presented herein demonstrate that THC interferes with the developmental role of $CB_1R$ signaling and induces a proepileptogenic neural

circuitry configuration independently of its neuromodulatory role in the adult brain. Our $CB_1R$ expression-rescue experiments show that the THC-induced increase in PTZ-evoked seizure susceptibility relies on alterations not only of projection neurons but also of GABAergic neurons. Further investigations are required to underscore the potential contribution of these and perhaps other neuronal lineages targeted by prenatal cannabinoid exposure. In any event, our preclinical observations support that although cannabis preparations can exert anticonvulsive actions in children and adults, they can also enhance the risk of seizures by suppressing $CB_1R$ signaling in the developing brain, thus raising a note of caution that might be considered when the potential therapeutic uses of cannabinoid-based medicines are defined and regulated for pregnant women.

## Materials and Methods

**THC Administration.** Ultrapure THC (≥99% HPLC; THC Pharm) was administered i.p. to pregnant female mice at a final dose of 3 mg/kg for 5 consecutive days from E12.5 to E16.5.

**Cellular Analyses and Behavioral Determinations.** CSMN immunofluorescence and retrograde labeling analyses were performed at P20. Skilled motor function (skilled-reaching and staircase) tests were carried out in 2-month-old mice prenatally exposed to THC or its vehicle. Seizure susceptibility was assessed by injecting PTZ (22.5 mg/kg) every 10 min until generalized seizures occurred.

**$CB_1R$ Biochemical Characterization.** $CB_1R$ levels were analyzed by Western blot as well as binding of radiolabeled CP-55,940 in E17.5- and P2.5-treated brain samples.

**Genetic $CB_1R$ Rescue.** $CB_1R$ expression rescue was performed in Stop-$CB_1$ mice by using Nex-Cre, Dlx5/6-Cre, and EIIa-Cre–driven recombination (20, 21). Immunohistological characterization of different $CB_1R$-rescue mice was performed in P2.5 and P20 brain samples. Corticospinal motor function as well as seizure susceptibility were assessed in THC- and vehicle-treated 2-month-old $CB_1R$-rescue mice.

**Animals.** Experimental designs and procedures were approved by the Complutense University Animal Research Committee in accordance with the European Commission regulations. All efforts were made to minimize the number of animals and their suffering throughout the experiments.

Additional experimental procedures are described in *SI Materials and Methods*.

**ACKNOWLEDGMENTS.** We thank Elena García-Taboada and Eva Resel for technical assistance, Abel Sánchez for statistical analyses guidance, Luigi Bellochio for behavioral determinations advice, and the rest of our lab members for a stimulating scientific and intellectual environment. This work was supported by Instituto de Salud Carlos III Grant PI12-00919 (to I.G-R.), German Research Foundation Grant SFB-TRR 58 (to B.L.), Ministerio de Economía y Competitividad Grant SAF2012-35759 (to M.G.), Comunidad de Madrid Grant S2011/BMD-2336 (to I.G.-R.), and Fundación Alicia Koplowitz (to I.G.-R.). J.D.-A., A.d.S.-Q., and D.G.-R. are supported by predoctoral fellowships from Fondo de Investigaciones Sanitarias; Ministerio de Educación, Cultura y Deportes Formación del Profesorado Universitario (FPU) Program; and Complutense University, respectively.

1. Volkow ND, Baler RD, Compton WM, Weiss SRB (2014) Adverse health effects of marijuana use. *N Engl J Med* 370(23):2219–2227.
2. Fried PA, Smith AM (2001) A literature review of the consequences of prenatal marihuana exposure. An emerging theme of a deficiency in aspects of executive function. *Neurotoxicol Teratol* 23(1):1–11.
3. Mechoulam R, Parker LA (2013) The endocannabinoid system and the brain. *Annu Rev Psychol* 64:21–47.
4. Soltesz I, et al. (2015) Weeding out bad waves: Towards selective cannabinoid circuit control in epilepsy. *Nat Rev Neurosci* 16(5):264–277.
5. Maccarrone M, Guzmán M, Mackie K, Doherty P, Harkany T (2014) Programming of neural cells by (endo)cannabinoids: From physiological rules to emerging therapies. *Nat Rev Neurosci* 15(12):786–801.
6. Díaz-Alonso J, Guzmán M, Galve-Roperh I (2012) Endocannabinoids via $CB_1$ receptors act as neurogenic niche cues during cortical development. *Philos Trans R Soc Lond B Biol Sci* 367(1607):3229–3241.
7. Reisenberg M, Singh PK, Williams G, Doherty P (2012) The diacylglycerol lipases: Structure, regulation and roles in and beyond endocannabinoid signalling. *Philos Trans R Soc Lond B Biol Sci* 367(1607):3264–3275.
8. Mulder J, et al. (2008) Endocannabinoid signaling controls pyramidal cell specification and long-range axon patterning. *Proc Natl Acad Sci USA* 105(25):8760–8765.
9. Wu C-S, et al. (2010) Requirement of cannabinoid CB(1) receptors in cortical pyramidal neurons for appropriate development of corticothalamic and thalamocortical projections. *Eur J Neurosci* 32(5):693–706.
10. Díaz-Alonso J, et al. (2012) The CB(1) cannabinoid receptor drives corticospinal motor neuron differentiation through the Ctip2/Satb2 transcriptional regulation axis. *J Neurosci* 32(47):16651–16665.
11. Molyneaux BJ, Arlotta P, Menezes JR, Macklis JD (2007) Neuronal subtype specification in the cerebral cortex. *Nat Rev Neurosci* 8(6):427–437.
12. Galve-Roperh I, et al. (2013) Cannabinoid receptor signaling in progenitor/stem cell proliferation and differentiation. *Prog Lipid Res* 52(4):633–650.
13. Wang H, Dey SK (2006) Roadmap to embryo implantation: Clues from mouse models. *Nat Rev Genet* 7(3):185–199.
14. Arlotta P, et al. (2005) Neuronal subtype-specific genes that control corticospinal motor neuron development in vivo. *Neuron* 45(2):207–221.
15. Tomassy GS, et al. (2010) Area-specific temporal control of corticospinal motor neuron differentiation by COUP-TFI. *Proc Natl Acad Sci USA* 107(8):3576–3581.
16. Calvigioni D, Hurd YL, Harkany T, Keimpema E (2014) Neuronal substrates and functional consequences of prenatal cannabis exposure. *Eur Child Adolesc Psychiatry* 23(10):931–941.
17. Selley DE, et al. (2001) Agonist efficacy and receptor efficiency in heterozygous CB1 knockout mice: Relationship of reduced CB1 receptor density to G-protein activation. *J Neurochem* 77(4):1048–1057.
18. Tortoriello G, et al. (2014) Miswiring the brain: Δ9-tetrahydrocannabinol disrupts cortical development by inducing an SCG10/stathmin-2 degradation pathway. *EMBO J* 33(7):668–685.
19. Mereu G, et al. (2003) Prenatal exposure to a cannabinoid agonist produces memory deficits linked to dysfunction in hippocampal long-term potentiation and glutamate release. *Proc Natl Acad Sci USA* 100(8):4915–4920.
20. Monory K, et al. (2006) The endocannabinoid system controls key epileptogenic circuits in the hippocampus. *Neuron* 51(4):455–466.
21. Ruehle S, et al. (2013) Cannabinoid CB1 receptor in dorsal telencephalic glutamatergic neurons: Distinctive sufficiency for hippocampus-dependent and amygdala-dependent synaptic and behavioral functions. *J Neurosci* 33(25):10264–10277.
22. Schneider M (2009) Cannabis use in pregnancy and early life and its consequences: Animal models. *Eur Arch Psychiatry Clin Neurosci* 259(7):383–393.
23. Szutorisz H, et al. (2014) Parental THC exposure leads to compulsive heroin-seeking and altered striatal synaptic plasticity in the subsequent generation. *Neuropsychopharmacology* 39(6):1315–1323.
24. Sonon KE, Richardson GA, Cornelius JR, Kim KH, Day NL (2015) Prenatal marijuana exposure predicts marijuana use in young adulthood. *Neurotoxicol Teratol* 47:10–15.
25. Rubino T, et al. (2015) Adolescent exposure to THC in female rats disrupts developmental changes in the prefrontal cortex. *Neurobiol Dis* 73:60–69.
26. Butti E, et al. (2012) Subventricular zone neural progenitors protect striatal neurons from glutamatergic excitotoxicity. *Brain* 135(Pt 11):3320–3335.
27. Psychoyos D, Hungund B, Cooper T, Finnell RH (2008) A cannabinoid analogue of Δ9-tetrahydrocannabinol disrupts neural development in chick. *Birth Defects Res B Dev Reprod Toxicol* 83(5):477–488.
28. Zheng X, Suzuki T, Takahashi C, Nishida E, Kusakabe M (2015) cnrip1 is a regulator of eye and neural development in Xenopus laevis. *Genes Cells* 20(4):324–339.
29. Zalesky A, et al. (2012) Effect of long-term cannabis use on axonal fibre connectivity. *Brain* 135(Pt 7):2245–2255.
30. Weiland BJ, et al. (2015) Daily marijuana use is not associated with brain morphometric measures in adolescents or adults. *J Neurosci* 35(4):1505–1512.
31. Alpár A, et al. (2014) Endocannabinoids modulate cortical development by configuring Slit2/Robo1 signalling. *Nat Commun* 5:4421.
32. Campolongo P, et al. (2007) Perinatal exposure to delta-9-tetrahydrocannabinol causes enduring cognitive deficits associated with alteration of cortical gene expression and neurotransmission in rats. *Addict Biol* 12(3-4):485–495.
33. Antonelli T, et al. (2005) Prenatal exposure to the CB1 receptor agonist WIN 55,212-2 causes learning disruption associated with impaired cortical NMDA receptor function and emotional reactivity changes in rat offspring. *Cereb Cortex* 15(12):2013–2020.
34. Bernard C, et al. (2005) Altering cannabinoid signaling during development disrupts neuronal activity. *Proc Natl Acad Sci USA* 102(26):9388–9393.
35. Gray KA, Day NL, Leech S, Richardson GA (2005) Prenatal marijuana exposure: Effect on child depressive symptoms at ten years of age. *Neurotoxicol Teratol* 27(3):439–448.
36. Smith AM, Fried PA, Hogan MJ, Cameron I (2004) Effects of prenatal marijuana on response inhibition: An fMRI study of young adults. *Neurotoxicol Teratol* 26(4):533–542.
37. Rogeberg O (2013) Correlations between cannabis use and IQ change in the Dunedin cohort are consistent with confounding from socioeconomic status. *Proc Natl Acad Sci USA* 110(11):4251–4254.
38. Volkow ND, Baler R (2015) Beliefs modulate the effects of drugs on the human brain. *Proc Natl Acad Sci USA* 112(8):2301–2302.
39. Devinsky O, et al. (2014) Cannabidiol: Pharmacology and potential therapeutic role in epilepsy and other neuropsychiatric disorders. *Epilepsia* 55(6):791–802.

**Cerebral Cortex Advance Access published October 6, 2016**

OXFORD

*Cerebral Cortex*, 2016; 1–15

**doi: 10.1093/cercor/bhw309**
Original Article

ORIGINAL ARTICLE

# Loss of Cannabinoid $CB_1$ Receptors Induces Cortical Migration Malformations and Increases Seizure Susceptibility

Javier Díaz-Alonso[1,2,6,*], Adán de Salas-Quiroga[1,2,*], Juan Paraíso-Luna[1,2,†], Daniel García-Rincón[1,2,†], Patricia P. Garcez[3,7], Maddy Parsons[4], Clara Andradas[1,5], Cristina Sánchez[1,5], François Guillemot[3], Manuel Guzmán[1,2], and Ismael Galve-Roperh[1,2]

[1]Department of Biochemistry and Molecular Biology I, Instituto Ramón y Cajal de Investigación Sanitaria (IRYCIS), and Instituto Universitario de Investigación Neuroquímica (IUIN), Complutense University, 28040 Madrid, Spain, [2]Centro de Investigación Biomédica en Red sobre Enfermedades Neurodegenerativas (CIBERNED), 28049 Madrid, Spain, [3]The Francis Crick Institute, Mill Hill Laboratory, The Ridgeway, London NW7 1AA, UK, [4]Randall Division of Cell and Molecular Biophysics, King's College London, London SE1 1UL, UK, [5]Instituto de Investigación Sanitaria Hospital 12 de Octubre, 28041 Madrid, Spain, [6]Current address: Department of Cellular and Molecular Pharmacology, University of California, San Francisco, CA 94158, USA, and [7]Current address: Instituto de Ciências Biomédicas, Universidade Federal do Rio de Janeiro, 21941-902 Rio de Janeiro, RJ, Brazil

[*] Co-first authors

[†]J.P.-L. and D.G.-R. have contributed equally to this work
Address correspondence to Javier Díaz-Alonso and Ismael Galve-Roperh, Instituto Ramón y Cajal de Investigación Sanitaria (IRYCIS), Department of Biochemistry and Molecular Biology I, and Instituto Universitario de Investigación Neuroquímica (IUIN), Complutense University, 28040 Madrid, Spain. Email: javier.diazalonso@ucsf.edu (J.D.-A.) / igr@quim.ucm.es (I.G.-R.)

J.D.-A. and I.G.-R. conceived the project. J.D.-A., A.d.S.-Q., M.G.-P., and I.G.-R. designed the experiments, with help from P.G., M.P., C.S., and F.G. J.D.-A. and A.d.S.-Q. performed most of the experiments, with help from M.P., C.A., J.P.-L., and D.G.-R. J.D.-A., A.d.S.-Q., P.G., M.P., C.S., F.G., M.G., and I.G.-R. interpreted data and J.D.-A., A.d.S.-Q., M.G., and I.G.-R. wrote the manuscript. All authors discussed the results and commented on the manuscript.



## Abstract

Neuronal migration is a fundamental process of brain development, and its disruption underlies devastating neurodevelopmental disorders. The transcriptional programs governing this process are relatively well characterized. However, how environmental cues instruct neuronal migration remains poorly understood. Here, we demonstrate that the cannabinoid $CB_1$ receptor is strictly required for appropriate pyramidal neuron migration in the developing cortex. Acute silencing of the $CB_1$ receptor alters neuronal morphology and impairs radial migration. Consequently, $CB_1$ siRNA-electroporated mice display cortical malformations mimicking subcortical band heterotopias and increased seizure susceptibility in adulthood. Importantly, rescuing the $CB_1$ deficiency-induced radial migration arrest by knockdown of the GTPase protein RhoA restored the hyperexcitable neuronal network and seizure susceptibility. Our findings show that $CB_1$ receptor/RhoA signaling regulates pyramidal neuron migration, and that deficient $CB_1$ receptor signaling may contribute to

cortical development malformations leading to refractory epilepsy independently of its canonical neuromodulatory role in the adult brain.

**Key words:** endocannabinoid system, epileptogenesis, radial migration, small GTPases, subcortical band heterotopia

## Introduction

During development, cortical projection neurons are generated in the ventricular and subventricular zones (VZ/SVZ), 2 proliferative niches that surround the lateral ventricles. After exiting cell cycle, pyramidal neurons undergo radial migration toward the cortical plate (CP) to finally occupy their corresponding cortical layer. Proper migration of neurons is essential as it establishes the basis for the subsequent wiring of the cortical circuitry. Not surprisingly, brain organization abnormalities emerge as a consequence of disrupted neuronal migration, which can have devastating consequences on adult brain function, including mental retardation, cognitive disorders, and epilepsy. Double cortex syndrome or subcortical band heterotopia (SBH) is a type of migration disorder consisting in heterotopic accumulations of cortical neurons within the subcortical white matter (WM) (Valiente and Marín 2010; Barkovich et al. 2012). SBH is believed to increase seizure susceptibility by causing focal hyperexcitability of cortical areas directly connected with the subcortical lesions (Shafi et al. 2015).

Pyramidal neuron migration requires the adoption of different morphologies along their transition through the various cortical compartments (Noctor et al. 2004). Actin filaments and microtubules control complementary aspects of neuronal migration. Overall, the actin cytoskeleton plays an essential role in cell polarization and leading process extension, while the microtubular network is fundamental for nucleokinesis. Nowadays, we know a number of genes encoding cytoskeletal or cytoskeleton-associated proteins, such as TUBA1A, Doublecortin (DCX) Lissencephaly-1 (LIS 1), and FilaminA, whose mutations underlie severe human malformations of cortical development (MCDs), including SBH, X-linked periventricular heterotopia (PH) and lissencephaly (Barkovich et al. 2012). Additionally, Rho GTPases are crucial regulators of actin cytoskeleton dynamics (Heasman and Ridley 2008) and therefore, several members of this protein family play a pivotal role in neuronal migration (Govek et al. 2011; Azzarelli et al. 2014a). Specifically, Rac1 and Cdc42 modulate different phases of cortical neuron migration in a cell-autonomous fashion (Konno et al. 2005), while RhoA exerts a key non-cell autonomous contribution to pyramidal neuron migration, its expression being required in radial glial cells but not in migrating neurons (Cappello et al. 2012). The inactivation of RhoA emerges as a critical requirement for the polarization of cortical projection neurons during migration, and different cell-autonomous and extrinsic factors converge in RhoA inhibition to promote migration (Hand et al. 2005; Nguyen et al. 2006; Pacary et al. 2011; Tang et al. 2014; Azzarelli et al. 2014b). How promigratory extracellular signals modulate the intrinsic regulators responsible for neuronal migration is beginning to be understood. Semaphorins, by acting through PlexinB2 receptors, modulate RhoA activity to favor a promigratory cytoskeletal configuration (Azzarelli et al. 2014b). Some G protein-coupled receptors (GPCRs), such as the $GABA_B$ receptor (Bony et al. 2013) and the serotonin 5-$HT_6$ receptor, also promote radial migration of pyramidal neurons, in the latter case in a ligand-independent manner (Jacobshagen et al. 2014). Other GPCRs have been associated with neuronal migration disorders, for example GPR56 with polymicrogyria, but their mechanism of action remains unknown (Piao et al. 2004).

The cannabinoid $CB_1$ receptor is a GPCR physiologically engaged by a family of lipid ligands, the endocannabinoids (eCBs), among which 2-arachidonoylglicerol (2-AG) and N-arachidonoylethanolamine (anandamide) are the best characterized. Besides its well-known neuromodulatory role mediating retrograde suppression of neuronal activity at adult synaptic terminals (Soltesz et al. 2015), the $CB_1$ receptor plays several roles during CNS development. The $CB_1$ receptor is expressed in the developing cerebral cortex, where it controls the proliferation and phenotype of cortical neural precursor cells (Díaz-Alonso et al. 2014), the specification of pyramidal neurons (Díaz-Alonso et al. 2012), and axon guidance and synaptogenesis (Mulder et al. 2008; Vitalis et al. 2008; Keimpema et al. 2010; Argaw et al. 2011). In addition, the $CB_1$ receptor regulates neuronal migration in the embryonic brain (Mulder et al. 2008), and eCB signaling promotes migration of newborn neurons along the rostral migratory stream in the postnatal mouse brain (Oudin et al. 2011). However, the molecular mechanisms and pathophysiological implications of $CB_1$ receptor signaling-mediated regulation of pyramidal neuron migration remain unknown. Given that cannabis is the most widely used illicit drug during pregnancy (Jutras-Aswad et al. 2009), deciphering how its main molecular target—the $CB_1$ receptor—signals in the developing brain is critical for understanding the neurobiological processes potentially affected in the fetus upon cannabis consumption during pregnancy.

In this study, we performed transient siRNA-mediated $CB_1$ receptor knockdown in newborn pyramidal neurons to reveal the impact of developmentally restricted, short-term $CB_1$ receptor loss of function in their migration. We observed a migration arrest that led to profound and long-lasting alterations in cortical neuron positioning, including SBH. Consequently, seizure susceptibility was increased in adult mice. Biochemical and cellular analyses showed that loss of $CB_1$ receptor function led to an abnormal RhoA protein accumulation in newborn pyramidal neurons, thereby disrupting the morphology of migrating cells. Remarkably, migration deficits elicited by loss of $CB_1$ receptor function were fully rescued by RhoA knockdown. Collectively, our findings pave the way toward a better understanding of the physiological role of eCB signaling in brain development, and provide relevant molecular mechanistic insights into human MCDs caused by altered neuronal migration.

## Materials and Methods

### Materials

pCAG-DAGL expression vector and $CB_1$ receptor in situ hybridization (ISH) probes (sense and antisense) were kindly provided by Prof. Pat Doherty (Wolfson Age Research Center, London, UK) and Prof. Beat Lutz (Johannes Gutemberg University, Mainz, Germany), respectively.

### Animals

Experimental designs and procedures were approved by the Complutense University Animal Research Committee in accordance with the European Commission regulations. All efforts were made to minimize the number of animals and their suffering throughout the experiments. $CB_1^{-/-}$, Nex-$CB_1^{-/-}$ and Dlx5/6-$CB_1^{-/-}$ colony-founding mice were provided by Prof B. Lutz (Johannes Gutemberg University, Mainz, Germany). Mouse embryonic tissues were obtained upon timed mating as assessed by vaginal plug observation (E0.5).

### Immunofluorescence and Confocal Microscopy

Cell proliferation was determined after intraperitoneal bromodeoxyuridine (BrdU) injection (50 μg/g body weight) of pregnant females at E14.5. Coronal embryonic and postnatal brain slices (14 and 30 μm thick, respectively) were processed as previously described (Palazuelos et al. 2009; Díaz-Alonso et al. 2012). Immunofluorescence was performed, after blockade with 5% goat serum, by overnight incubation at 4°C with the indicated primary antibodies (see Supplementary Information).

### In Situ Hybridization

Coronal sections (20 μm) of E16.5 and E17.5 embryonic mouse brains were obtained and processed for ISH as described (Díaz-Alonso et al. 2012) using antisense and sense $CB_1$ riboprobes (Marsicano and Lutz 1999). Further details are provided in Supplementary Information.

### In Utero Electroporation

The indicated siRNAs or expression constructs (see Supplementary Information) were electroporated at a final concentration of 10 μM or 1 μg/μl, respectively, into the lateral ventricle of E13.5 or E14.5 embryos as described previously (Pacary et al. 2011). All electroporations shown include a constitutive GFP overexpression plasmid (pCAG-GFP) to allow proper visualization.

### Explant Migration Assays

Cortical explants were prepared from E14.5 embryonic forebrain slices. Briefly, small cortical fragments of about 400 μm were dissected with scalpel and incubated for 1 h in Minimum Essential Medium Eagle EMEM (Lonza) containing 10% FBS, 1% glucose at 37°C in 5% $CO_2$. COS7 cell aggregates transfected with the indicated expression vectors (see Supplementary Information) were prepared by diluting a pellet of transfected cells with Matrigel (BD) in a 1:1 proportion. After jellification, cell aggregates were cut with a scalpel in small cubes of ~600 μm. Subsequently, cortical explants were placed in a Matrigel 3-dimensional matrix facing the corresponding COS7-transfected cell aggregates. Cocultures were maintained in Neurobasal culture medium (Gibco), supplemented with N2 (Millipore) and B-27 (Invitrogen) for 72 h, and then fixed. Cell migration from the explants was analyzed in 4 quadrants by quantification of cell nuclei counterstained with DAPI, and the proximal/distal ratio with respect to the corresponding cell aggregate was calculated.

### RhoA Activity Measurement

Dorsal telencephali from E17.5 Nex-$CB_1^{-/-}$ and $CB_1^{f/f}$ littermates were carefully dissected and directly processed for active RhoA quantification with the G-LISA kit (Cytoskeleton Inc.), following the manufacturer's instructions.

### Susceptibility to PTZ

Mice were placed in Plexiglas cages and monitored by an experimenter blinded to their treatment and genotype. PTZ (Sigma-Aldrich) was dissolved in 0.9% saline and administered intraperitoneally to mice at P60 at a concentration of 22.5 mg/kg every 10 min until generalized seizures occurred. Seizure severity was monitored as described (Manent et al. 2009; de Salas-Quiroga et al. 2015). Mice placed in Plexiglas cages were injected with the PTZ-containing solution every 10 min, with consecutive injections of PTZ until generalized seizures occurred. This was considered the end of the experiment. All the procedure was video-recorded and analyzed later by an experimenter blinded to the experimental groups, who determined the precise moment of generalized seizure onset. There was no statistically significant difference in weight or sex ratio between the different groups of mice.

### Statistical Analysis

Results shown represent the means ± SEM, and the number of independent experiments or biological samples is indicated in every case. Statistical analyses were performed by Student–Newman–Keuls post hoc test.

Experimental procedures are further described in Supplementary Methods. That section includes a detailed description of animal procedures, antibodies employed for immunofluorescence and confocal microscopy, ISH, sequences of siRNAs and constructs employed in in utero electroporation (IUE) and explant migration assays, adherent cortical progenitor cell culture, quantitative PCR, immunoblot assays and data analysis and statistics.

## Results

### Acute Cannabinoid $CB_1$ Receptor Knockdown Blocks Radial Migration

To evaluate the role of the $CB_1$ receptor in neuronal migration, we initially confirmed $CB_1$ receptor expression in the developing cortex at E17.5. $CB_1$ receptor mRNA and protein show a gradient with increased levels in postmitotic compartments of the developing cortex, that is, the intermediate zone (IZ) and the CP (Supplementary Fig. 1A–C), suggesting that $CB_1$ receptor expression is upregulated in newborn pyramidal neurons after cell cycle exit and radial migration initiation (Mulder et al. 2008; Díaz-Alonso et al. 2014). We also explored the presence of $CB_1$ receptor in developing pyramidal neurons by combining $CB_1$ ISH with Satb2 immunofluorescence (Supplementary Fig. 1A, right panel). Confocal analysis further confirmed $CB_1$ receptor protein expression in immature $Satb2^+$ pyramidal neurons in E17.5 embryonic cortices, a large proportion of which are undergoing radial migration at this developmental stage (Supplementary Fig. 1C). During development, the $CB_1$ protein is enriched in axons of immature pyramidal neurons (Supplementary Fig. 1C) (Berrendero et al. 1999; Mulder et al. 2008), making extremely difficult to estimate the contribution of somatic $CB_1$ immunostaining in migrating neurons to the

overall staining. Thus, to recapitulate $CB_1$ receptor expression in migrating pyramidal neurons, we used ISH of $CB_1$ receptor transcripts in GFP-positive cells in E16.5 embryonic cortices subjected to IUE at E14.5 (Supplementary Fig. 1B). As developing GABAergic interneurons also express $CB_1$ receptor (Berghuis et al. 2007; Morozov et al. 2009), to unequivocally assess the presence of $CB_1$ receptor in pyramidal neurons we took advantage of the Dlx5/6-driven forebrain GABAergic neuron-selective $CB_1$-deficient mice (Monory et al. 2007). Thus, in Dlx5/6-$CB_1^{-/-}$ embryonic cortices, $CB_1$ immunostaining was hardly distinguishable from their $CB_1^{f/f}$ littermates (Supplementary Fig. 1D), while in the developing hippocampus a clear reduction of $CB_1$ receptor expression was evident. Overall, these results confirm the expression of $CB_1$ in radially migrating pyramidal neurons, in addition to its presence in developing interneurons (Berghuis et al. 2007; Morozov et al. 2009).

We then assessed the cell-autonomous role of $CB_1$ receptor signaling in pyramidal neuron migration during cortical development. To this end, we acutely knocked down the $CB_1$ receptor in radially migrating neurons at E14.5 by IUE of a pool of siRNAs directed against 4 sequences of the $CB_1$ receptor mRNA (hereafter $CB_1$ siRNA) together with a GFP expression construct, and subsequently analyzed the distribution of radially migrating cells at different time points. In our hands, transfection of cortical cells with this siRNA pool reduces $CB_1$ receptor expression by 50% (Díaz-Alonso et al. 2014). $CB_1$ receptor knockdown significantly impaired newborn pyramidal cell migration (Fig. 1A–C). Remarkably, after either 2 days (Supplementary Fig. 2A,B) or 3 days (Fig. 1A,B) in utero we observed a reduced colonization of the CP by $CB_1$-knockdown cells that, instead, appeared stacked in the IZ and the VZ/SVZ. Moreover, when we restricted our analyses to the cells that had reached the CP we also found a significant delay in $CB_1$ siRNA-electroporated cells, that were less abundant in upper cortical layers of the cortex, to which E14.5-born neurons are committed to migrate (Greig et al. 2013) (Fig. 1C). We confirmed that acute $CB_1$ receptor silencing impairs radial migration by using additional strategies: both a $CB_1$ short-hairpin RNA (shRNA, not shown) and Cre recombinase electroporation of $CB_1^{f/f}$ embryos (Supplementary Fig. 2C,D) impaired migration of cortical projection neurons at very similar extents than siRNA-mediated $CB_1$ knockdown.

To invade the CP, migrating neurons must undergo a morphological switch from their characteristic multipolar shape, adopted to explore the SVZ and IZ environment, to a bipolar morphology, which enables their radial glial-aided migration in the CP (Heng et al. 2008; Pacary et al. 2011). siRNA-mediated $CB_1$ knockdown increased the number of primary neurites in cultured E14.5 cortical neurons (Supplementary Fig. 2E–G). Hence, we analyzed whether silencing of $CB_1$ receptors affects the morphology of migrating neurons in vivo. We quantified the number of $GFP^+$ cells with >2 primary processes in the CP of control siRNA and $CB_1$ siRNA-transfected brains, and found a 2-fold increase in the proportion of cells with this aberrant morphology in $CB_1$ siRNA-electroporated cortices (Fig. 1D,E), thereby indicating that radial migration blockade occurs concurrently with an impairment of the multipolar to bipolar transition.

## Transient $CB_1$ Receptor Knockdown Long-Lastingly Impairs Pyramidal Neuron Migration and Generates SBH

To assess whether $CB_1$-knockdown cells suffer from a transient delay in their radial migration and finally reach the appropriate cortical layer if given enough time, as is the case following the silencing of other cell migration regulators (Creppe et al. 2009;

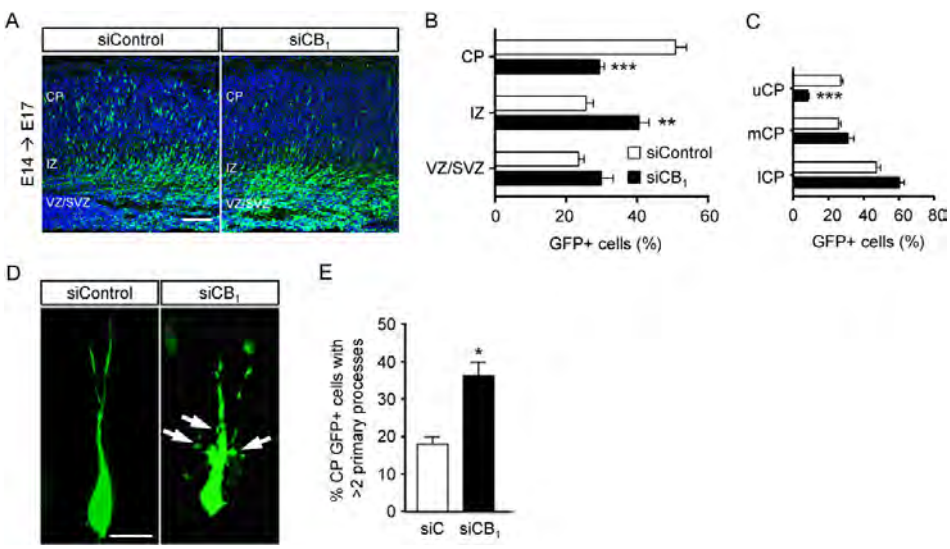


**Figure 1.** Cannabinoid $CB_1$ receptor knockdown impairs pyramidal neuron migration. (A–C) Analysis of the migration of cortical neurons electroporated in utero with $CB_1$ siRNA or a control siRNA together with a GFP expression plasmid at E14.5 and analyzed 3 days later, at E17.5. Representative images are shown (A). The distribution of $GFP^+$ cells in the VZ/SVZ, IZ, and CP of the developing cerebral cortex in both conditions was quantified (B). The migration of targeted cells within the CP (uCP, upper CP; mCP, median CP; lCP, lower CP) was also analyzed (C). (D,E) The morphology of CP migrating cells was analyzed, and we quantified the proportion of cells with >2 primary processes. Arrows point to abnormal primary processes in $CB_1$-knockdown cells. $n$ = at least 3 different embryos from different litters per condition. Graphs represent mean ± SEM. $^*P < 0.05$; $^{**}P < 0.01$; $^{***}P < 0.001$. Scale bars: (A) 100 μm; (D) 10 μm.

Manent et al. 2009), we extended our IUE experiments until early postnatal life (P2 and P10), when the siRNA is no longer active. In P2 brains, the migration arrest observed upon $CB_1$ expression manipulation was still present (Fig. 2A,B), thus confirming that temporally restricted $CB_1$ receptor loss of function compromises radial migration of newborn neurons in the developing cortex. In P10 brains, we observed a greater proportion of $GFP^+$ cells in the upper layers of $CB_1$ siRNA-

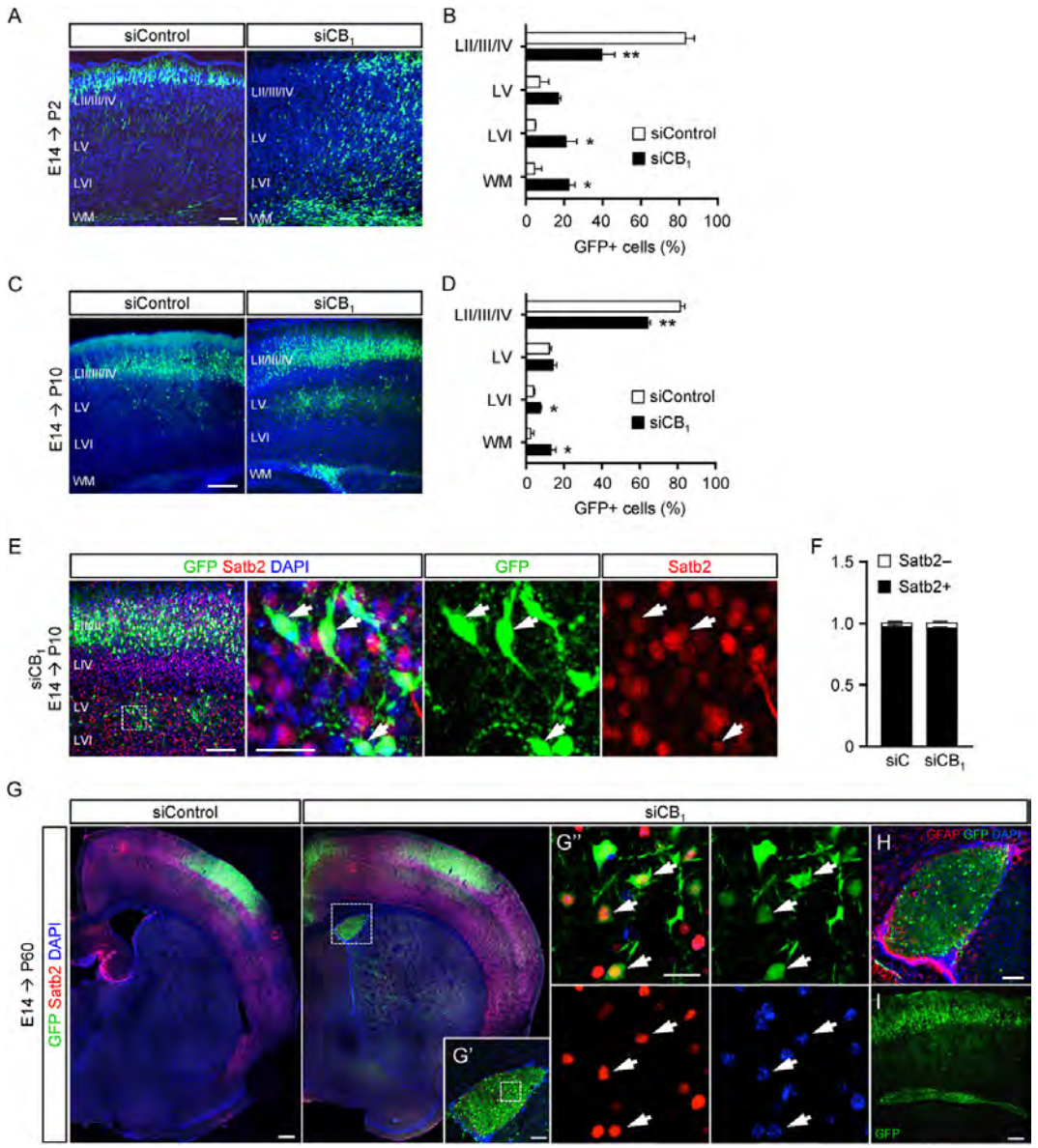


**Figure 2.** Transient $CB_1$ receptor knockdown generates long-lasting aberrant neuronal positioning and SBH. (*A*,*B*) Migration analysis of cortical neurons electroporated in utero with $CB_1$ siRNA or a control siRNA together with a GFP expression plasmid at E14.5 and analyzed at P2. Electroporated cell distribution was analyzed in the indicated cortical layers and WM. (*C*,*D*) Brains electroporated at E14.5 were analyzed as above at P10. (*E*,*F*) Migration-arrested $GFP^+$ cells from electroporated P10 brains were stained with the callosal projection neuron marker Satb2. The specification of targeted cells was quantified in control and $CB_1$ siRNA-electroporated cortices (*F*). (*G*) Subcortical accumulations of pyramidal neurons were evident in $CB_1$ siRNA-electroporated brains at P60. (*G'*, *G''''*) Detail of the expression of the callosal projection neuron marker Satb2 in SBH. Arrows point to $Satb2^+$ $GFP^+$ cells. (*H*) The SBH nature of the lesions was confirmed by the identification of a glial GFAP-immunoreactive capsule around the ectopic cell accumulations. (*I*) Example of an SBH-like lesion in another P60 $CB_1$ siRNA-electroporated brain. $n$ = at least 3 different embryos from different litters per condition. Graphs represent mean ± SEM. $^*P < 0.05$; $^{**}P < 0.01$. Scale bars: (*A*,*E*) 100 μm (insets, 20 μm); (*C*) 200 μm; (*G'*,*H*) 200 μm; (*G''''*) 25 μm; (*I*) 100 μm.

electroporated cortices, although we consistently found GFP$^+$ cells in deep cortical layers. Remarkably, we also found accumulations of GFP$^+$ cells stacked in the WM of $CB_1$-knockdown brains (Fig. 2C,D). siRNA-electroporated mice that develop until young adults (P60) were assessed for the definitive positioning of transfected cells. Strikingly, we still found subcortical accumulations of GFP$^+$ neurons in 6 out of 9 $CB_1$ siRNA-electroporated brains (Fig. 2G–I).

We next determined the identity of GFP$^+$ $CB_1$-knockdown cells at postnatal stages. Cells found in deep cortical layers of $CB_1$ siRNA-transfected brains at P10 were immunoreactive for the callosal projection neuron specification marker Satb2 (Alcamo et al. 2008) (Fig. 2E,F). We found that virtually all GFP$^+$ cells in the subcortical heterotopias at P60 were also immunopositive for Satb2 (Fig. 2G–G""), even though the expression of this transcriptional regulator in the telencephalon is normally confined to the cerebral cortex (Alcamo et al. 2008). This observation indicates that migration-arrested cells retain their corresponding callosal specification program even in ectopic locations. We then asked about the nature of the ectopic neuronal accumulations found in $CB_1$ siRNA-transfected brains. SBH can be distinguished from PH because neuronal accumulations are surrounded by a glial capsule in SBH but not in PH. Hence, we stained samples from $CB_1$ siRNA-electroporated P60 brains for the astrocytic marker GFAP and confirmed that the neuronal accumulations correspond to the SBH type (Fig. 2H).

We then explored whether the observed $CB_1$ receptor-dependent promotion of radial migration was unique of E14.5-born cells. To this end, we performed IUE at E13.5 and conducted analyses 3 days later (Supplementary Fig. 2H,I). Similarly to our previous manipulations at E14.5, when targeting E13.5-born cells an overall delay in GFP$^+$ cell migration was observed in $CB_1$-knockdown brains after 3 days in utero. Furthermore, delayed radial migration was still present at P2 in $CB_1^{f/f}$ neurons electroporated at E13.5 with a Cre recombinase expression vector (Supplementary Fig. 2C,D).

## The $CB_1$ Receptor Promotes Radial Migration of Postmitotic Pyramidal Neurons

The $CB_1$ receptor plays an active role in the regulation of cortical progenitor cell proliferation and identity (Mulder et al. 2008; Díaz-Alonso et al. 2014). Hence, we determined whether the observed $CB_1$ receptor-dependent promotion of pyramidal neuron migration involves $CB_1$ receptors located on cortical progenitor cells. To test this possibility, we electroporated a Cre recombinase-encoding construct driven by the postmitotic neuron-specific promoter Dcx in E14.5 $CB_1^{f/f}$ embryos, and analyzed the position of targeted cells at E17.5 (Fig. 3A–C). A clear migration defect was evident upon $CB_1$ receptor ablation exclusively in postmitotic neurons. Importantly, this manipulation also affected the morphology of migrating GFP$^+$ cells (Fig. 3D,E). Moreover, we tested whether postmitotic $CB_1$ receptor ablation results in a transient or permanent migration impairment by allowing the electroporated embryos to develop until P2. Although many of the electroporated cells were found in the

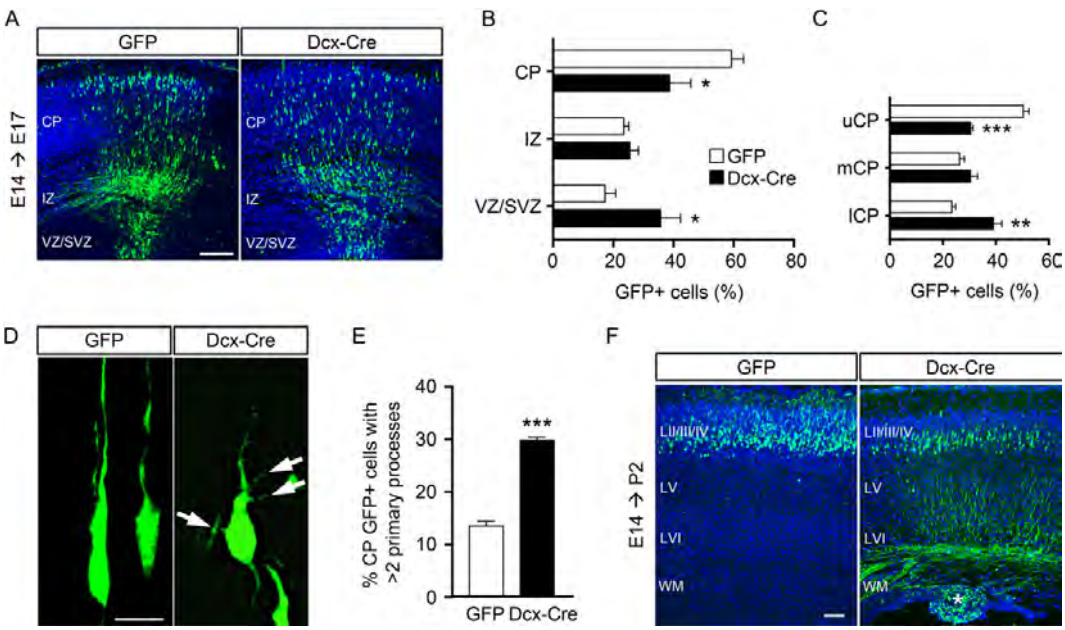


**Figure 3.** $CB_1$ receptor signaling promotes radial migration postmitotically. (A–C) Migration of cortical neurons was analyzed in E17.5 $CB_1^{f/f}$ embryos electroporated in utero at E14.5 with Dcx-Cre expression vector, to ablate the $CB_1$ receptor in postmitotic neurons, or GFP as a control (see Materials and Methods). The distribution of GFP$^+$ cells along the developing cerebral cortex in E17.5 is indicated in (B). Quantification of the migration of targeted cells within the CP is shown (C). (D, E) The morphology of migrating cells was analyzed in the CP, and the proportion of cells with >2 processes was quantified. Arrows point to abnormal primary processes in $CB_1$-deficient cells. (F) Migration analysis of cortical neurons electroporated in utero with Dcx-Cre or GFP at E14.5 and analyzed at P2. In Dcx-Cre-transfected cortices, heterotopic GFP$^+$ cell accumulations were consistently found in subcortical areas (asterisk). $n$ = at least 3 different embryos from different litters per condition. Graphs represent mean ± SEM. Scale bars: (A, F) 100 μm; (D) 10 μm. *P < 0.05; **P < 0.01; ***P < 0.001.

upper cortical layers at this stage, we consistently found accumulations of Dcx-Cre$^+$ cells ectopically located in the WM (Fig. 3F). These observations demonstrate that $CB_1$ receptor signaling promotes radial migration in postmitotic neurons independently of the pyramidal precursor cell pool.

We sought for additional support to the postmitotic nature of the $CB_1$ receptor promigratory role by analyzing the migration of postmitotic neurons in $CB_1^{-/-}$ embryos. Constitutively null mutation of $CB_1$ receptors has been shown to affect several aspects of pyramidal neuron development (Mulder et al. 2008), although its precise impact on radial migration remains unclear. Thus, we performed birthdate labeling experiments in $CB_1$-knockout embryos and control littermates by administering BrdU at E14.5 followed by double immunofluorescence for BrdU and Ki67 at E16.5 in order to discard cells that were still proliferating. BrdU$^+$Ki67$^-$ cells, that is, the cells that had exited cell cycle between E14.5 and E16.5, were significantly delayed in their radial migration in $CB_1^{-/-}$ embryos when compared to WT littermates (Supplementary Fig. 3A,B).

As the $CB_1$ receptor is known to trigger prosurvival mechanisms in neurons (Galve-Roperh et al. 2008), we assessed whether its knockdown interferes with neuronal migration by affecting cell viability. Hence, we analyzed the apoptosis marker cleaved caspase-3 in cortices subjected to IUE with the $CB_1$ siRNA. We did not find significant differences in apoptotic cells in the developing cortex of $CB_1$ siRNA-electroporated and control siRNA-electroporated cortices (Supplementary Fig. 3C). Likewise, no differences were observed by TUNEL staining in $CB_1$ siRNA-electroporated versus control cortices (Supplementary Fig. 3D), thus ruling out a contribution of neuronal survival in the promigratory effect of the $CB_1$ receptor.

## The eCBs 2-AG and Anandamide Act as Chemoattractant Cues for Newborn Pyramidal Neurons

To better understand the mechanism of $CB_1$ receptor-driven neuronal migration, we first investigated the ability of endogenous cannabinoid ligands to modulate pyramidal neuron migration. We prepared E14.5 dorsal telencephalic explants and exposed them to a confined source of eCBs. Diacylglycerol lipase alpha (DAGLα) is the key enzyme involved in 2-AG synthesis, and mice lacking this enzyme show impaired eCB-mediated neuromodulation and compromised adult neurogenesis (Gao et al. 2010). Neurons arising from cortical explants showed a marked preference to migrate toward DAGLα-overexpressing COS7 cells when compared with control, GFP-transfected cells (Fig. 4A,B). Importantly, this effect was blocked by the $CB_1$ receptor antagonist SR141716. Anandamide biosynthesis is mainly achieved through the action of *N*-acylphosphatidylethanolamine-hydrolyzing phospholipase D (NAPE-PLD). Likewise, the migration of neurons from cortical explants was favored toward COS7 cells overexpressing NAPE-PLD, this effect being also blocked by SR141716. Thus, both eCBs promote pyramidal neuron migration by acting through $CB_1$ receptors.

The aforementioned observations could be explained by two alternative mechanisms: eCBs might either promote neuronal motility and/or instruct the directionality of neuronal migration. To dissect these 2 processes, we overexpressed DAGLα in utero at E14.5 to disrupt the gradient of eCBs, and analyzed neuronal migration at E17.5. DAGLα-overexpressing cells showed a mild though significant migration delay compared with GFP-electroporated cells, thus suggesting that blurring the cortical eCB gradient misleads neuronal migration (Fig. 4B). We then evaluated the non-cell autonomous consequences of disturbing the cortical gradient of 2-AG on the subsequent waves of migrating neurons. Thus, we injected BrdU 12 h after DAGLα electroporation to label proliferating cells, and then tracked their migration at E17.5. BrdU-labeled cells accumulated aberrantly in the VZ of DAGLα-electroporated brains, where DAGLα-overexpressing cells were most abundant (Fig. 4C–E), thus indicating that abnormally high levels of 2-AG in the apical side of the cortex prevent proper newborn neuron migration. These findings suggest that eCBs may act as spatially regulated cues for the adequate migration of pyramidal neurons in the developing cortex.

## $CB_1$ Receptor Signaling Promotes RhoA Degradation in Migrating Pyramidal Neurons

Several signaling pathways involved in the regulation of neuronal migration converge in the modulation of the activity of the small GTPase protein RhoA (Cappello et al. 2012; Pacary et al. 2013; Azzarelli et al. 2014b). Given the morphological alterations found in $CB_1$-deficient migrating cells described above, and the previous evidence suggesting a functional link between $CB_1$ receptor signaling and RhoA activity in both neuronal (Berghuis et al. 2007) and non-neural (Nithipatikom et al. 2012; Mai et al. 2015) cells, we hypothesized that the promigratory effect of the $CB_1$ receptor in newborn pyramidal cells relies on the modulation of this pathway. To investigate whether $CB_1$ receptor signaling regulates RhoA activity in vivo, we measured the amount of GTP-bound RhoA in cortical tissue extracts from E17.5 embryos, when a large proportion of neurons are undergoing migration. We employed dorsal telencephalic glutamatergic neuron-specific $CB_1$ receptor knockouts (Nex-$CB_1^{-/-}$) to determine the regulation of RhoA activity by $CB_1$ signaling specifically in postmitotic cortical pyramidal neurons (Díaz-Alonso et al. 2012). We found that active RhoA levels were increased by 2-fold in E17.5 Nex-$CB_1^{-/-}$ cortices compared with their $CB_1^{f/f}$ littermates (Fig. 5A), suggesting that $CB_1$ receptor signaling dampens RhoA activity in migrating pyramidal neurons. This observation indicates that in Nex-$CB_1^{-/-}$ cortical tissue either the active fraction of RhoA is increased and/or there is an accumulation of total RhoA protein. Hence, we examined total RhoA protein levels by western blot and also found a 2-fold increase in Nex-$CB_1^{-/-}$ tissue extracts compared with their $CB_1^{f/f}$ littermates (Fig. 5B), thus indicating that $CB_1$ inactivation in postmitotic pyramidal neurons leads to an accumulation of RhoA protein rather than to an increase in the active fraction of RhoA. We subsequently analyzed RhoA expression in those samples by qPCR and found no significant difference (Supplementary Fig. 4A), suggesting that $CB_1$ receptor signaling likely controls RhoA at a post-translational level rather than by regulating its gene transcription. The mRNA expression levels of other Rho-family members involved in neuronal migration, RhoB, Rac1, and Cdc42, were not affected either by $CB_1$ receptor ablation (Supplementary Fig. 4A).

To determine whether acute $CB_1$ receptor knockdown strategy also modifies RhoA protein levels, we performed ex vivo electroporation of $CB_1$ siRNA or control siRNA together with GFP into E14.5-mouse embryonic dorsal telencephalon, and maintained dissociated cortical cells for 4 days in vitro (DIV). In agreement with knockout mice-derived tissue, RhoA immunoreactivity was increased in $CB_1$ siRNA-transfected compared with control siRNA-transfected GFP$^+$ cells (Fig. 5C,D).

It has been recently reported that RhoA expression in pyramidal neurons is largely dispensable for their migration, and that its overactivation results in radial migration arrest

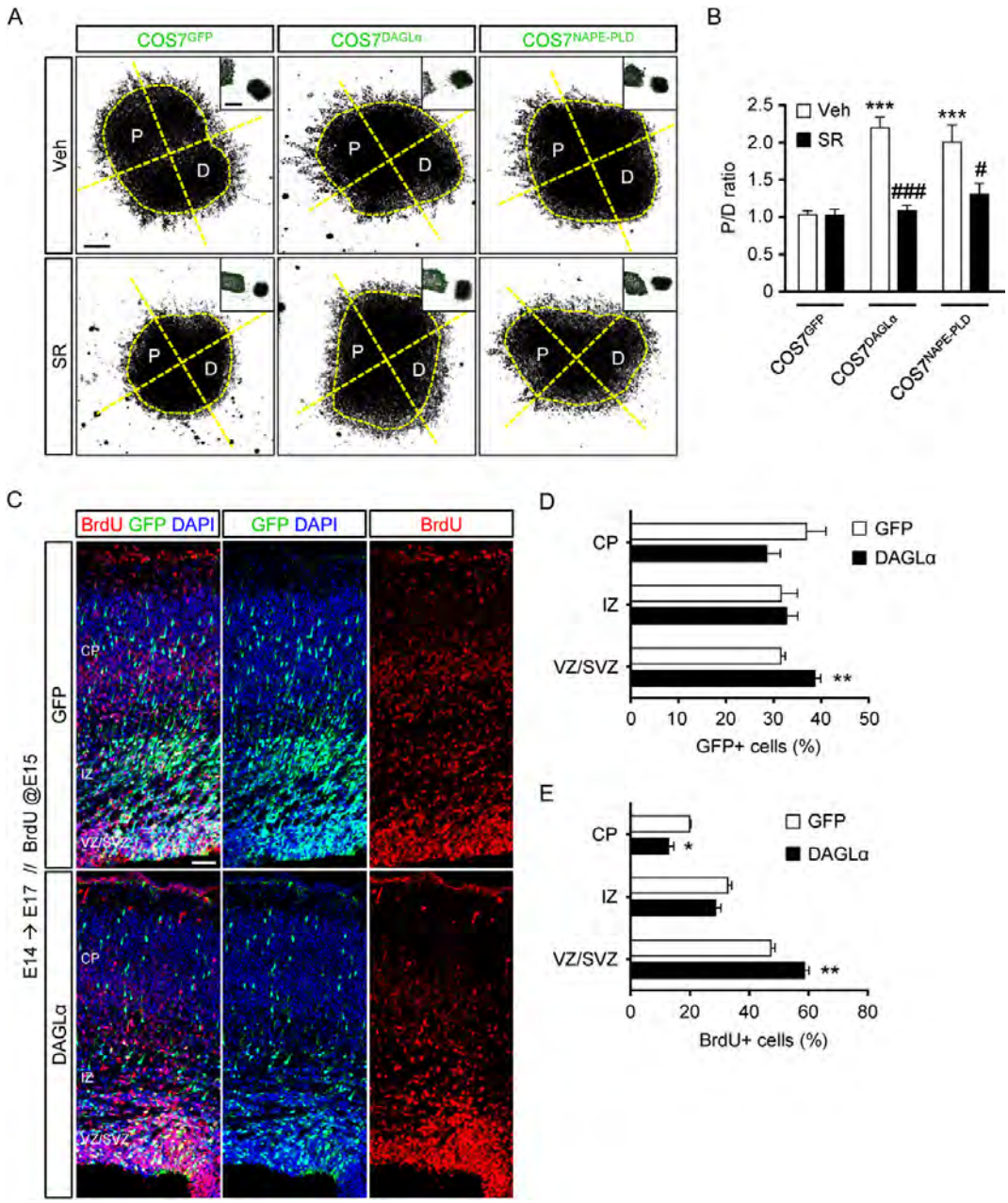


**Figure 4.** The eCBs 2-AG and AEA act as promigratory cues for newborn cortical neurons. (*A*) Representative images of pyramidal neuronal migration assays from E14.5 cortical explants in response to DAGLα-, NAPE-PLD-, or mock (GFP)-transfected COS7 cells. (*B*) The promigratory action of eCBs was quantified by determining the ratio of neurons in the proximal and distal (P/D) quadrants. The involvement of $CB_1$ receptors was determined by including in the medium the $CB_1$ antagonist SR141716 (SR, 10 μM) or vehicle. $n = 3$ independent experiments with at least 5 explants per condition. (*C–E*) Migration analysis of cortical neurons electroporated in utero with pCAG-DAGLα together with a GFP expression or a control pCAG-GFP plasmid at E14.5 and analyzed at E17.5. BrdU was injected 12 h after IUE to label the subsequent migrating cells. Representative images are shown. Quantification of $GFP^+$ cell distribution in the indicated cortical compartments is shown (*D*). Analysis of BrdU-labeled cells at E17.5 (*E*). $n$ = at least 3 different embryos from different litters per condition. Graphs represent mean ± SEM. $^*P < 0.05$; $^{**}P < 0.01$ (Student's t-test). $^{***}P < 0.001$ versus GFP/Vehicle-treated slices of GFP-electroporated embryos; $^{\#}P < 0.05$; $^{\#\#\#}P < 0.001$ versus the corresponding vehicle-treated explants. Scale bars: (*A*) 100 μm; inset 500 μm; (*C*) 100 μm.

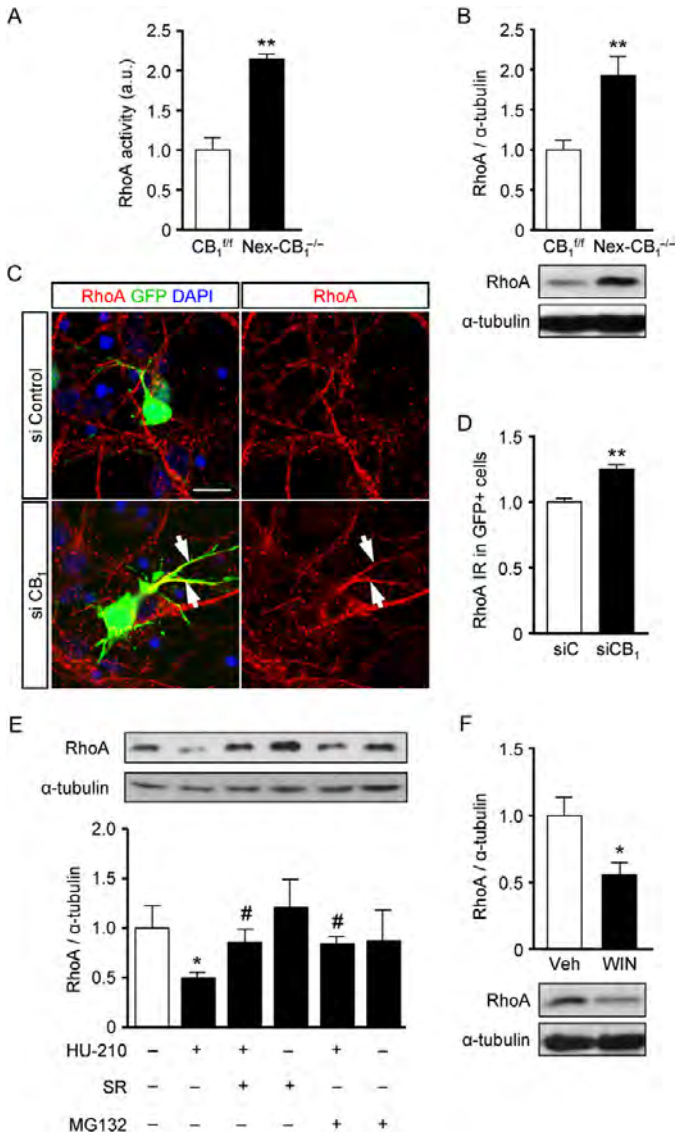


**Figure 5.** $CB_1$ signaling controls RhoA protein levels in pyramidal neurons. (*A*) Analysis of RhoA activity levels in $CB_1^{f/f}$ and Nex-$CB_1^{-/-}$ E17.5 embryonic cortices. (*B*) RhoA protein levels were determined by western blot in cortical tissue in E17.5 Nex-$CB_1^{-/-}$ and $CB_1^{f/f}$ littermates. Loading control was performed with anti α-tubulin antibody. (*C*, *D*) Analysis of RhoA levels in E14.5 primary cortical neurons electroporated with a $CB_1$ siRNA or a control siRNA and maintained in differentiating conditions for 4 DIV. Mean RhoA immunoreactivity (IR) fluorescence intensity was calculated in the $GFP^+$ area. Arrows point to RhoA-enriched processes in $CB_1$-knockdown cells. $n = 3$ independent experiments with at least 100 $GFP^+$ cells from 6 imaging fields per experiment. (*E*) RhoA protein levels were determined by western blot upon pharmacological manipulation with HU-210 (50 nM) for 6 h in primary differentiating CPCs. In addition, CPCs were incubated in the presence of the $CB_1$ receptor antagonist SR (1 μM) and with the proteasome inhibitor MG132 (10 μM). (*F*) RhoA protein levels were determined by western blot in cortical samples from E17.5 embryos exposed to the $CB_1$ agonist WIN55,212-2 (5 mg/kg) or its vehicle for 6 h. $n$ = at least 3 different embryos per genotype or treatment. Graphs represent mean ± SEM. $^*P < 0.05$; $^{**}P < 0.01$; $^{\#}P < 0.05$ versus HU-210-treated cells. Scale bar: 25 μm.

(Pacary et al. 2011; Cappello et al. 2012). This is consistent with the expression pattern of RhoA in the developing cortex, which shows a clear downregulation of RhoA in migrating neurons compared with cortical progenitors (Azzarelli et al. 2014a). We designed an experimental approach aimed at recapitulating the cellular context of migrating pyramidal neurons to study how $CB_1$ signaling affects RhoA levels. Thus, we obtained adherent cortical progenitor cell (CPC) cultures, which can be differentiated into cortical neurons by changing the medium and withdrawing growth factors (see Supplementary Methods).

Characterization of CPC cultures (Supplementary Fig. 5A–E) revealed their appropriateness to model the cellular context of a migrating cortical neuron. As expected, neuronal differentiation reduced nestin and Pax6 expression, while increasing the expression of the neuronal marker Tuj1 and the $CB_1$ receptor. RhoA expression also decreased with differentiation, mirroring the abrupt downregulation that occurs during pyramidal neuron maturation in vivo. To evaluate whether $CB_1$ receptor manipulation during this process affects RhoA protein levels, we stimulated $CB_1$ signaling in differentiating CPCs with the cannabinoid agonist HU-210 and observed that $CB_1$ receptor activation led to a decrease in total RhoA protein levels compared with vehicle-treated CPCs (Fig. 5E). Noteworthy, HU-210-induced reduction of RhoA levels was prevented by SR141716. Differentiating CPCs were also co-incubated with HU-210 and the proteasome inhibitor MG132, and HU-210-induced regulation of RhoA levels was abolished (Fig. 5E). These results indicate that $CB_1$ receptor signaling promotes proteasomal degradation of RhoA in newborn pyramidal neurons.

We also evaluated whether pharmacological stimulation of the $CB_1$ receptor affects RhoA protein levels in developing cortical neurons in vivo. We administered the cannabinoid agonist WIN55,212-2 or its vehicle to pregnant females in gestational day 17 and embryos were collected 6 h later. Cannabinoid administration resulted in the reduction of RhoA protein levels (0.55 ± 0.08 vs. vehicle-treated RhoA levels) in embryonic cortical extracts (Fig. 5F), without affecting the expression of RhoA, RhoB, Cdc42, or Rac1 (Supplementary Fig. 4B). Considering that RhoB is highly expressed during cortical development, its homology, and function redundancy with RhoA, we also analyzed RhoB protein levels upon $CB_1$ receptor genetic and pharmacological manipulation. RhoB levels were increased in Nex-$CB_1$-deficient mice cortical extracts, while WIN55,212-2 administration in vivo and HU-210 treatment of CPCs decreased RhoB levels (Supplementary Fig. 6).

## RhoA Downregulation Is Sufficient to Rescue $CB_1$ Receptor Knockdown-Induced Migration Arrest

The aforementioned findings indicate that $CB_1$ receptor silencing leads to RhoA protein accumulation in newborn pyramidal neurons. To test whether this effect underlies the migration impairment in $CB_1$ siRNA-electroporated cells, we co-electroporated a RhoA-directed shRNA together with the $CB_1$ siRNA. The efficacy of the RhoA shRNA to decrease RhoA expression has previously been demonstrated (Pacary et al. 2011). As shown in Figure 6, knocking-down RhoA fully rescued $CB_1$ silencing-induced migration arrest, and restored both the distribution of $GFP^+$ cells along the different cortical compartments (VZ/SVZ, IZ, and CP; Fig. 6B) and the adequate positioning of the cells within the CP (Fig. 6C). This observation provides evidence for the notion that RhoA accumulation upon $CB_1$ knockdown underlies the impairment of neuronal migration. Cofilin is a downstream effector of RhoA that promotes actin filament disassembly. Since F-actin depolymerization is required for neuronal migration as it allows the continuous dynamic recycling of actin cytoskeleton, we tested the ability of a nonphosphorylatable form of cofilin ($cofilin^{S3A}$, Pacary et al. 2011), which constitutively depolymerizes F-actin to rescue $CB_1$ receptor knockdown-evoked migration arrest. Expression of $cofilin^{S3A}$ rescued the si$CB_1$-induced cell migration blockade as quantified by IUE experiments from E14 to E17 (Fig. 6A–C). These

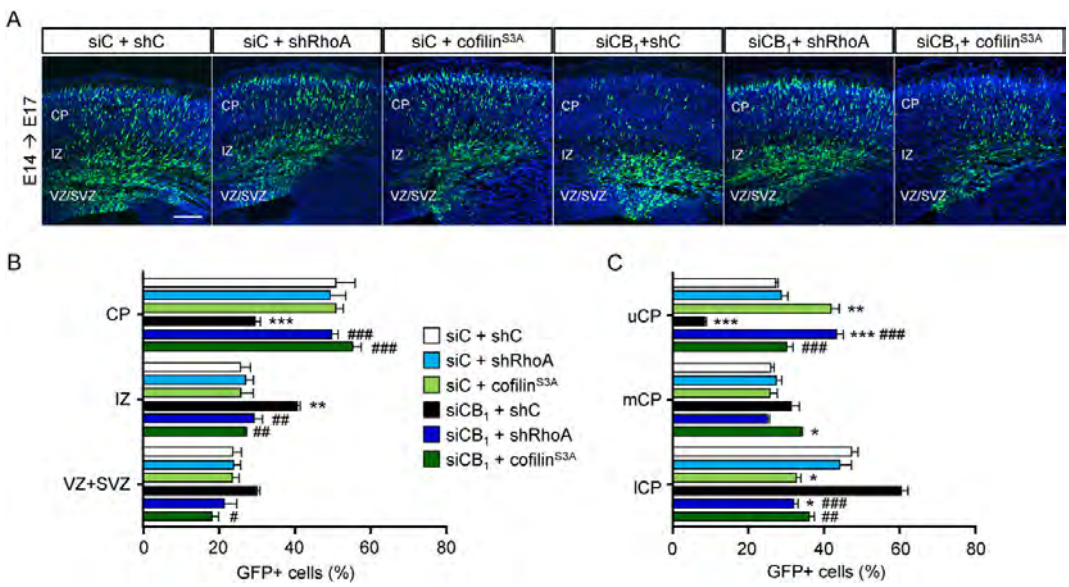


**Figure 6.** RhoA knockdown or expression of nonphosphorylatable cofilin rescues $CB_1$ silencing-induced migration arrest. (*A*, *B*) Migration analysis of cortical neurons electroporated in utero with a control siRNA or $CB_1$ siRNA together or not with a RhoA shRNA or a plasmid encoding a nonphosphorylatable form of cofilin [$cofilin^{S3A}$] and a GFP expression plasmid at E14.5 and analyzed 3 days later, at E17.5. Representative images are shown for the different conditions (*A*). $GFP^+$ cell distribution in the indicated developing cortical areas and within the CP was quantified (*B*, *C*). $n$ = at least 3 different embryos from different litters per condition. Graphs represent mean ± SEM. $^*P < 0.05$; $^{**}P < 0.01$; $^{***}P < 0.001$ versus siRNA control-electroporated brains; $^{\#}P < 0.05$; $^{\#\#}P < 0.01$; $^{\#\#\#}P < 0.001$ versus $CB_1$ siRNA-electroporated brains. Scale bar: 100 μm.

findings indicate that RhoA accumulation in $CB_1$-deficient cells compromises neuronal migration by altering actin cytoskeleton dynamics.

### Neuronal Migration Arrest Induced by $CB_1$ Receptor Knockdown Increases Seizure Susceptibility in Adulthood

We next examined whether the rescue of radial migration by RhoA downregulation results in a correct neuronal positioning in the adult cerebral cortex. Electroporated embryos that developed until P60 were analyzed for the distribution of $GFP^+$ cells. We found that the majority of $CB_1$ siRNA-electroporated brains showed SBH, while normal neuronal lamination and SBH were absent in brains co-electroporated with the RhoA shRNA (Fig. 7A). Taken together, these findings demonstrate that preventing RhoA accumulation rescues the migration defects caused by $CB_1$ receptor silencing. Similarly to human MCDs, experimentally induced ectopic accumulations of cortical neurons are aberrantly wired to the cortical circuitry, thus leading to an overall increased susceptibility to seizures (Manent et al. 2009; Feliciano et al. 2011). We studied whether migration deficits caused by in utero $CB_1$ receptor knockdown sensitize the offspring to seizures induced by the convulsant pentylenetetrazol (PTZ). We administered subconvulsive doses of PTZ intraperitoneally every 10 min to young adult (P60) mice, and measured the latency and cumulative dose of PTZ necessary for generalized seizures to occur. PTZ susceptibility was significantly increased in $CB_1$ siRNA-electroporated mice, as shown by the reduced threshold for generalized seizures. Noteworthy, the rescue of $CB_1$ siRNA-induced neuronal migration arrest achieved by shRhoA co-electroporation also prevented the increased seizure susceptibility (Fig. 7B,C). RhoA knockdown alone did not significantly alter PTZ susceptibility. These observations indicate that developmental alterations generated by transient $CB_1$ receptor silencing in migrating pyramidal neurons decrease seizure threshold in adult offspring, and that the rescue of neuronal migration induced by simultaneous RhoA downregulation normalizes seizure susceptibility.

## Discussion

Overall, this study reveals an unprecedented pivotal role of the cannabinoid $CB_1$ receptor signaling in the adequate migration and positioning of cortical pyramidal neurons, which dysfunction can trigger profound long-lasting alterations in brain function. It has been long assumed that adult $CB_1$-deficient mice have increased seizure susceptibility owing to the loss of eCB-dependent retrograde suppression of glutamate release from excitatory terminals (Katona and Freund 2008; Soltesz et al. 2015). Of note, our study adds to this classical view by demonstrating that developmentally restricted loss of $CB_1$ receptor function also increases seizure susceptibility, likely by causing aberrant positioning of cortical neurons, thus conceivably affecting their wiring and sensitizing the resulting circuitry to epileptogenesis.

Neuronal migration is largely dependent on the dynamic regulation of the cytoskeleton (Valiente and Marín 2010). Actin cytoskeleton remodeling plays a fundamental role in this process, and the control of RhoA activity is a common feature of different promigratory pathways (Hand et al. 2005; Nguyen et al. 2006; Pacary et al. 2011; Tang et al. 2014; Azzarelli et al. 2014b). The expression pattern of RhoA in the developing cortex, with high abundance in the VZ/SVZ and very low—if any—levels in the IZ and CP (Azzarelli et al. 2014a), suggests that this protein is dispensable for pyramidal neuron migration, as

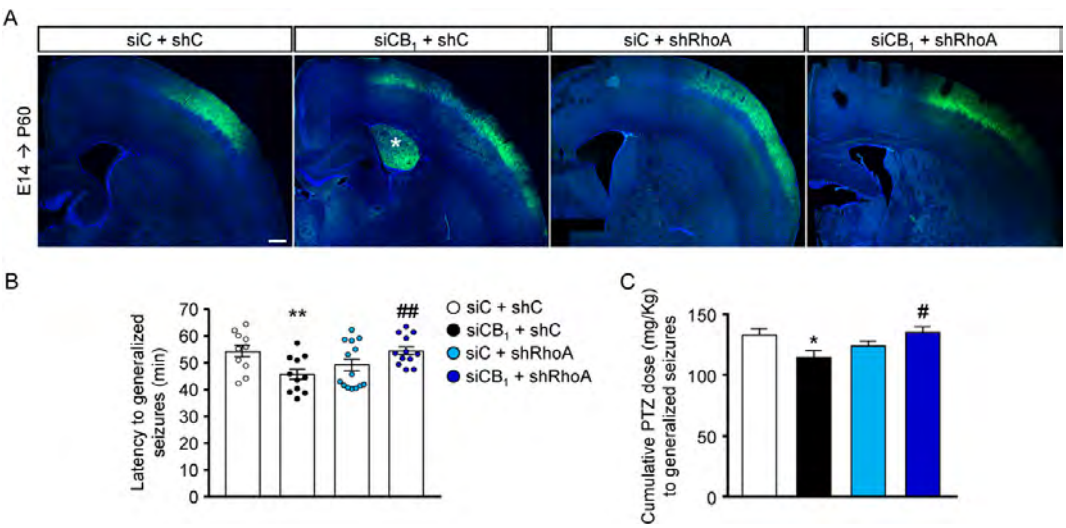


**Figure 7.** Transient $CB_1$ receptor knockdown in migrating pyramidal neurons increases seizure susceptibility in adulthood. (*A*) Representative images of $GFP^+$ cells in adult mice (P60) subjected to IUE at E14.5 with $CB_1$ or control siRNA together with RhoA or control shRNA . $GFP^+$ cell accumulation within the subcortical WM in $CB_1$ siRNA/shControl condition is indicated (asterisk). (*B*, *C*) P60 mice subjected to IUE at E14.5 with $CB_1$ or control siRNAs combined with RhoA or control shRNAs as above were injected i.p. with PTZ (22.5 mg/kg) every 10 min until generalized seizures occurred. The mean latency to the occurrence of generalized seizures is represented (*B*) and the cumulative PTZ dose necessary for the onset of generalized seizures was calculated (*C*). $n = 10–14$ mice per group. Graphs represent mean ± SEM. $^*P < 0.05$; $^{**}P < 0.01$ versus siRNA control-electroporated mice; $^{\#}P < 0.05$; $^{\#\#}P < 0.01$; versus $CB_1$ siRNA-electroporated brains. Scale bar: 200 μm.

demonstrated in a recent report (Cappello et al. 2012). RhoA ubiquitination and degradation plays an important role in the regulation of neuronal cell morphology (Bryan et al. 2005; Tian et al. 2011) and affects cancer cell migration (Nethe and Hordijk 2010). However, to the best of our knowledge, this is the first study that identifies a specific role of the proteasomal degradation of RhoA in the promotion of neuronal migration. Our findings are in agreement with the involvement of the small GTPase Rac1 degradation in cancer cell migration (Oberoi et al., 2012). Taking into account the complementary expression pattern of both the $CB_1$ receptor and RhoA in the developing cortex, it is conceivable that $CB_1$-mediated RhoA degradation ensures a complete clearance of the remaining RhoA protein in newborn neurons to allow their migration. Our results are also in line with previous findings supporting that the actin cytoskeleton is a major target of $CB_1$ signaling in developing neurons (Berghuis et al. 2007; Oudin et al. 2011; Roland et al. 2014; Njoo et al. 2015). In addition, $CB_1$ receptor activation can reduce RhoB protein levels (Supplementary Fig. 6), and therefore we cannot exclude a potential contribution of this related GTPase in $CB_1$ receptor-dependent neuronal migration.

We found that the migration defects caused by $CB_1$ receptor silencing affect more a subset of the targeted $GFP^+$ cells. This might be related to the unequal knockdown efficacy among targeted cells and/or to the heterogeneity of a neuronal population in their capacity to compensate the loss of a given promigratory mechanism. Similarly, in humans, MCDs frequently affect only relatively small neuronal populations, even when caused by germline mutations (Lim and Crino 2013). Interestingly, a recent study supports that the migration deficits caused by Dcx shRNA are due to off-target effects of such manipulation onto endogenous miRNAs (Baek et al. 2014). In line with this notion, the specificity of our $CB_1$ receptor genetic knockdown strategy and its consequences on radial migration blockade are validated by the comparable phenotypes observed when using $CB_1$ siRNA, $CB_1$ shRNA, and Cre-mediated ablation of the $CB_1$ receptor in $CB_1^{f/f}$ mice. Noteworthy, the severe migration defects observed upon acute $CB_1$ receptor knockdown are notably subtler upon constitutive $CB_1$ receptor loss (Supplementary Fig. 3A,B). This is most likely due to compensatory mechanisms occurring in germline or lineage-specific knockout mice, as also occurs for other migration regulatory proteins such as Dcx (Bai et al. 2003), amyloid precursor protein (Young-Pearse et al. 2007), and EF-hand domain-containing protein 1 (de Nijs et al. 2009).

A wide variety of neurodevelopmental diseases are caused by the disruption of neuronal migration. Understanding the biological mechanisms responsible for a finely tuned corticogenesis emerges as a key requisite for the elaboration of rational therapeutic strategies for the consequences of MCDs, including epileptogenesis and neuropsychiatric disorders. Noteworthy, a genetic origin has been identified for some human diseases caused by neuronal migration alterations, and the genes identified in such diseases correspond, in most cases, to cytoskeletal or cytoskeleton-regulatory proteins (Lim and Crino 2013). Therefore, the implications of the malfunctioning of the eCB system in the origin of neurodevelopmental diseases caused by cell migration defects are exciting perspectives for future research. Of note, evidences in the literature associate gene alterations (i.e., copy number variations) and gene polymorphisms of some of the eCB system elements *CNR1*, *DAGLA*, *NAPEPLD*, *ABHD12*, or *CNRIP1*, with the occurrence of human diseases, such as autism spectrum disorders, intellectual disability, or the polyneuropathy, hearing loss, ataxia, retinitis pigmentosa and cataract syndrome named as PHARC (Fiskerstrand et al. 2010; Blankman et al. 2013; Bragin et al. 2014). Particularly, the $CB_1$ receptor encoding *CNR1* gene has even put forward as a strong autism-related candidate gene, given the increased status of de novo mutations in this gene in samples from a cohort of 2588 autistic patients (Girirajan et al. 2013) or the strikingly high probability of *CNR1* haploinsufficiency (Huang et al. 2010). In agreement with these indications, $CB_1$ receptor signaling regulates the neuronal identity transcriptional factor axis Ctip2-Satb2 (Díaz-Alonso et al. 2012) that together with Tbr1 is responsible for neuronal connectivity deficits that associate with mental retardation and autism (Carpentier et al. 2013; Deriziotis et al. 2014; Huang et al. 2014).

Alterations of multiple cellular mechanisms frequently converge in the pathogenesis of MCDs, and an unbalanced activity of $CB_1$ receptor signaling can affect cortical development by interfering with several processes in addition to neuronal migration (Díaz-Alonso et al. 2012). While SBH is most frequently originated from abnormal neuronal migration, some neocortical heterotopias are associated with ectopic progenitor cell divisions (Kielar et al. 2014). $CB_1$ receptor signaling controls the activity of the phosphatidylinositol-3-kinase/mammalian target of rapamycin complex 1 pathway, both in neuronal precursors (Díaz-Alonso et al. 2014) and in mature neurons (Puighermanal et al. 2009), and the deregulation of this signaling route is at the origin of some focal MCDs, in particular tuberous sclerosis, type 2 focal cortical dysplasia, and megalencephaly (Lim and Crino 2013).

Beyond genetic alterations in elements of the cannabinoid signaling machinery, environmental insults can affect $CB_1$ receptor-dependent neuronal migration. In particular, prenatal exposure to the cannabinoids present in marijuana has been shown to affect fetal development in both mice and humans (Hurd et al. 2005; Jutras-Aswad et al. 2009; Tortoriello et al. 2014). Although detrimental consequences in executive function have been reported in studies following children from mothers that smoked marijuana (Fried 2002), the neurobiological substrate of these changes remains unknown. Altered $CB_1$ receptor signaling induced by long half-life phytocannabinoids may eventually interfere with neuronal migration, as previously shown for synthetic cannabinoids (Saez et al. 2014). Likewise, gestational cannabinoid exposure may disturb cortical laminarization and cause changes in social behavior and cognition (Díaz-Alonso et al. 2012; Carpentier et al. 2013; de Salas-Quiroga et al. 2015). Cannabinoids have a great potential as medicines owing to the broad distribution of their receptor targets throughout the body, together with their high safety and fair tolerability (Pertwee 2012). In particular, cannabidiol, the most relevant nonpsychoactive phytocannabinoid, has recently received a huge attention as a promising pharmacologic tool for the management of pediatric epilepsies such as the Dravet and Gaston-Leroux syndromes (Devinsky et al. 2014). However, as our study and other pieces of evidence support (Maccarrone et al. 2014), cannabis intake, for both therapeutic and recreational use, must be exquisitely controlled if not absolutely discouraged during pregnancy in order to avoid interferences with the crucial role played by the $CB_1$ receptor during brain development.

## Supplementary Material

Supplementary material can be found at: http://www.cercor.oxfordjournals.org/

## Funding

This study was funded (to I.G.-R.) by Instituto de Salud Carlos III (#PI15-0310; Plan Estatal de I+D+i 2013-2016) and cofinanced by the European Development Regional Fund "A way to achieve Europe" (ERDF), Comunidad de Madrid (BMD2011-2336 to I.G.-R.), and Spanish Ministerio de Economía y Competitividad (MINECO/FEDER; grants SAF2012-35759 and SAF2015-64945-R to M.G.). J.D.-A. was supported by a PFIS program fellowship cofinanced by the European Social Fund "El FSE invierte en tu futuro" (ESF) and by a FEBS short-term fellowship. A.d.S.-Q., J.P.-L., and D.G.-R. were supported by Ministerio de Educación, Cultura y Deporte (FPU program), Neurostem BMD2011-2336, Complutense University fellowship (DG-R).

## Notes

We are indebted to Eva Resel, Elena García-Taboada, and David Vega for their excellent support, Verona Villar-Cerviño for assistance in explant migration assays, and to members of the Galve-Roperh, Guzmán and Guillemot laboratories for critical suggestions to the manuscript and creating an inspiring scientific environment. *Conflict of Interest*: None declared.

## References

Alcamo EA, Chirivella L, Dautzenberg M, Dobreva G, Fariñas I, Grosschedl R, McConnell SK. 2008. Satb2 regulates callosal projection neuron identity in the developing cerebral cortex. Neuron. 57:364–377.

Argaw A, Duff G, Zabouri N, Cécyre B, Chainé N, Cherif H, Tea N, Lutz B, Ptito M, Bouchard J-F. 2011. Concerted action of CB1 cannabinoid receptor and deleted in colorectal cancer in axon guidance. J Neurosci. 31:1489–1499.

Azzarelli R, Kerloch T, Pacary E. 2014a. Regulation of cerebral cortex development by Rho GTPases: insights from in vivo studies. Front Cell Neurosci. 8:445.

Azzarelli R, Pacary E, Garg R, Garcez P, van den Berg D, Riou P, Ridley AJ, Friedel RH, Parsons M, Guillemot F. 2014b. An antagonistic interaction between PlexinB2 and Rnd3 controls RhoA activity and cortical neuron migration. Nat Commun. 5:3405.

Baek ST, Kerjan G, Bielas SL, Lee JE, Fenstermaker AG, Novarino G, Gleeson JG. 2014. Off-target effect of doublecortin family shRNA on neuronal migration associated with endogenous microRNA dysregulation. Neuron. 82:1255–1262.

Bai J, Ramos RL, Ackman JB, Thomas AM, Lee R V, LoTurco JJ. 2003. RNAi reveals doublecortin is required for radial migration in rat neocortex. Nat Neurosci. 6:1277–1283.

Barkovich AJ, Guerrini R, Kuzniecky RI, Jackson GD, Dobyns WB. 2012. A developmental and genetic classification for malformations of cortical development: Update 2012. Brain. 135:1348–1369.

Berghuis P, Rajnicek AM, Morozov YM, Ross RA, Mulder J, Urban GM, Monory K, Marsicano G, Matteoli M, Canty A, et al. 2007. Hardwiring the brain: endocannabinoids shape neuronal connectivity. Science. 316:1212–1216.

Berrendero F, Sepe N, Ramos JA, Di Marzo V, Fernández-Ruiz JJ. 1999. Analysis of cannabinoid receptor binding and mRNA expression and endogenous cannabinoid contents in the developing rat brain during late gestation and early postnatal period. Synapse. 33:181–191.

Blankman JL, Long JZ, Trauger SA, Siuzdak G, Cravatt BF. 2013. ABHD12 controls brain lysophosphatidylserine pathways that are deregulated in a murine model of the neurodegenerative disease PHARC. Proc Natl Acad Sci U S A. 110:1500–1505.

Bony G, Szczurkowska J, Tamagno I, Shelly M, Contestabile A, Cancedda L. 2013. Non-hyperpolarizing GABAB receptor activation regulates neuronal migration and neurite growth and specification by cAMP/LKB1. Nat Commun. 4:1800.

Bragin E, Chatzimichali EA, Wright CF, Hurles ME, Firth HV, Bevan AP, Swaminathan GJ. 2014. DECIPHER: database for the interpretation of phenotype-linked plausibly pathogenic sequence and copy-number variation. Nucleic Acids Res. 42:D993–D1000.

Bryan B, Cai Y, Wrighton K, Wu G, Feng XH, Liu M. 2005. Ubiquitination of RhoA by Smurf1 promotes neurite outgrowth. FEBS Lett. 579:1015–1019.

Cappello S, Böhringer CRJ, Bergami M, Conzelmann KK, Ghanem A, Tomassy GS, Arlotta P, Mainardi M, Allegra M, Caleo M, et al. 2012. A radial glia-specific role of RhoA in double cortex formation. Neuron. 73:911–924.

Carpentier PA, Haditsch U, Braun AE, Cantu A V., Moon HM, Price RO, Anderson MP, Saravanapandian V, Ismail K, Rivera M, et al. 2013. Stereotypical alterations in cortical patterning are associated with maternal illness-induced placental dysfunction. J Neurosci. 33:16874–16888.

Creppe C, Malinouskaya L, Volvert ML, Gillard M, Close P, Malaise O, Laguesse S, Cornez I, Rahmouni S, Ormenese S, et al. 2009. Elongator controls the migration and differentiation of cortical neurons through acetylation of alpha-tubulin. Cell. 136:551–564.

de Nijs L, Léon C, Nguyen L, LoTurco JJ, Delgado-Escueta AV, Grisar T, Lakaye B. 2009. EFHC1 interacts with microtubules to regulate cell division and cortical development. Nat Neurosci. 12:1266–1274.

de Salas-Quiroga A, Díaz-Alonso J, García-Rincón D, Remmers F, Vega D, Gómez-Cañas M, Lutz B, Guzmán M, Galve-Roperh I. 2015. Prenatal exposure to cannabinoids evokes long-lasting functional alterations by targeting CB $_1$ receptors on developing cortical neurons. Proc Natl Acad Sci. 112:201514962.

Deriziotis P, O'Roak BJ, Graham SA, Estruch SB, Dimitropoulou D, Bernier RA, Gerdts J, Shendure J, Eichler EE, Fisher SE. 2014. De novo TBR1 mutations in sporadic autism disrupt protein functions. Nat Commun. 5:4954.

Devinsky O, Cilio MR, Cross H, Fernandez-Ruiz J, French J, Hill C, Katz R, Di Marzo V, Jutras-Aswad D, Notcutt WG, et al. 2014. Cannabidiol: Pharmacology and potential therapeutic role in epilepsy and other neuropsychiatric disorders. Epilepsia. 55:791–802.

Díaz-Alonso J, Aguado T, de Salas-Quiroga A, Ortega Z, Guzmán M, Galve-Roperh I. 2014. CB1 cannabinoid receptor-dependent activation of mTORC1/Pax6 signaling drives Tbr2 expression and basal progenitor expansion in the developing mouse cortex. Cereb Cortex. 210:1–14.

Díaz-Alonso J, Aguado T, Wu C-S, Palazuelos J, Hofmann C, Garcez P, Guillemot F, Lu H-C, Lutz B, Guzmán M, et al. 2012. The CB(1) cannabinoid receptor drives corticospinal motor neuron differentiation through the Ctip2/Satb2 transcriptional regulation axis. J Neurosci. 32:16651–16665.

Feliciano DM, Su T, Lopez J, Platel J-C, Bordey A. 2011. Single-cell Tsc1 knockout during corticogenesis generates tuber-like lesions and reduces seizure threshold in mice. J Clin Invest. 121:1596–1607.

Fiskerstrand T, H'mida-Ben Brahim D, Johansson S, M'zahem A, Haukanes BI, Drouot N, Zimmermann J, Cole AJ, Vedeler C, Bredrup C, et al. 2010. Mutations in ABHD12 cause the

neurodegenerative disease PHARC: an inborn error of endocannabinoid metabolism. Am J Hum Genet. 87:410–417.
Fried PA. 2002. Conceptual issues in behavioral teratology and their application in determining long-term sequelae of prenatal marihuana exposure. J Child Psychol Psychiatry Allied Discip. 43:81–102.
Galve-Roperh I, Aguado T, Palazuelos J, Guzmán M. 2008. Mechanisms of control of neuron survival by the endocannabinoid system. Curr Pharm Des. 14:2279–2288.
Gao Y, Vasilyev DV, Goncalves MB, Howell FV, Hobbs C, Reisenberg M, Shen R, Zhang M-Y, Strassle BW, Lu P, et al. 2010. Loss of retrograde endocannabinoid signaling and reduced adult neurogenesis in diacylglycerol lipase knockout mice. J Neurosci. 30:2017–2024.
Girirajan S, Dennis MY, Baker C, Malig M, Coe BP, Campbell CD, Mark K, Vu TH, Alkan C, Cheng Z, et al. 2013. Refinement and discovery of new hotspots of copy-number variation associated with autism spectrum disorder. Am J Hum Genet. 92:221–237.
Govek E-E, Hatten ME, Van Aelst L. 2011. The role of Rho GTPase proteins in CNS neuronal migration. Dev Neurobiol. 71:528–553.
Greig LC, Woodworth MB, Galazo MJ, Padmanabhan H, Macklis JD. 2013. Molecular logic of neocortical projection neuron specification, development and diversity. Nat Rev Neurosci. 14:755–769.
Hand R, Bortone D, Mattar P, Nguyen L, Heng JI, Guerrier S, Boutt E, Peters E, Barnes AP, Parras C, et al. 2005. Phosphorylation of Neurogenin2 specifies the migration properties and the dendritic morphology of pyramidal neurons in the neocortex. Neuron. 48:45–62.
Heasman SJ, Ridley AJ. 2008. Mammalian Rho GTPases: new insights into their functions from in vivo studies. Nat Rev Mol Cell Biol. 9:690–701.
Heng JI, Nguyen L, Castro DS, Zimmer C, Wildner H, Armant O, Skowronska-Krawczyk D, Bedogni F, Matter JM, Hevner R, et al. 2008. Neurogenin 2 controls cortical neuron migration through regulation of Rnd2. Nature. 455:114–118.
Huang N, Lee I, Marcotte EM, Hurles ME. 2010. Characterising and predicting haploinsufficiency in the human genome. PLoS Genet. 6:e1001154.
Huang TN, Chuang HC, Chou WH, Chen CY, Wang HF, Chou SJ, Hsueh YP. 2014. Tbr1 haploinsufficiency impairs amygdalar axonal projections and results in cognitive abnormality. Nat Neurosci. 17:240–247.
Hurd Y, Wang X, Anderson V, Beck O, Minkoff H, Dow-Edwards D. 2005. Marijuana impairs growth in mid-gestation fetuses. Neurotoxicol Teratol. 27:221–229.
Jacobshagen M, Niquille M, Chaumont-Dubel S, Marin P, Dayer A. 2014. The serotonin 6 receptor controls neuronal migration during corticogenesis via a ligand-independent Cdk5-dependent mechanism. Development. 141:3370–3377.
Jutras-Aswad D, DiNieri JA, Harkany T, Hurd YL. 2009. Neurobiological consequences of maternal cannabis on human fetal development and its neuropsychiatric outcome. Eur Arch Psychiatry Clin Neurosci. 259:395–412.
Katona I, Freund TF. 2008. Endocannabinoid signaling as a synaptic circuit breaker in neurological disease. Nat Med. 14: 923–930.
Keimpema E, Barabas K, Morozov YM, Tortoriello G, Torii M, Cameron G, Yanagawa Y, Watanabe M, Mackie K, Harkany T. 2010. Differential subcellular recruitment of monoacylglycerol lipase generates spatial specificity of 2-arachidonoyl glycerol signaling during axonal pathfinding. J Neurosci. 30: 13992–14007.
Kielar M, Tuy FPD, Bizzotto S, Lebrand C, de Juan Romero C, Poirier K, Oegema R, Mancini GM, Bahi-Buisson N, Olaso R, et al. 2014. Mutations in Eml1 lead to ectopic progenitors and neuronal heterotopia in mouse and human. Nat Neurosci. 17:923–933.
Konno D, Yoshimura S, Hori K, Maruoka H, Sobue K. 2005. Involvement of the phosphatidylinositol 3-kinase/rac1 and cdc42 pathways in radial migration of cortical neurons. J Biol Chem. 280:5082–5088.
Lim KC, Crino PB. 2013. Focal malformations of cortical development: New vistas for molecular pathogenesis. Neuroscience. 252:262–276.
Maccarrone M, Guzmán M, Mackie K, Doherty P, Harkany T. 2014. Programming of neural cells by (endo)cannabinoids: from physiological rules to emerging therapies. Nat Rev Neurosci. 15:786–801.
Mai P, Tian L, Yang L, Wang L, Yang L, Li L. 2015. Cannabinoid receptor 1 but not 2 mediates macrophage phagocytosis by G(α)i/o /RhoA/ROCK signaling pathway. J Cell Physiol. 230:1640–1650.
Manent J-B, Wang Y, Chang Y, Paramasivam M, LoTurco JJ. 2009. Dcx reexpression reduces subcortical band heterotopia and seizure threshold in an animal model of neuronal migration disorder. Nat Med. 15:84–90.
Marsicano G, Lutz B. 1999. Expression of the cannabinoid receptor CB1 in distinct neuronal subpopulations in the adult mouse forebrain. Eur J Neurosci. 11:4213–4225.
Monory K, Blaudzun H, Massa F, Kaiser N, Lemberger T, Schütz G, Wotjak CT, Lutz B, Marsicano G. 2007. Genetic dissection of behavioural and autonomic effects of Delta(9)-tetrahydrocannabinol in mice. PLoS Biol. 5:e269.
Morozov YM, Torii M, Rakic P. 2009. Origin, early commitment, migratory routes, and destination of cannabinoid type 1 receptor-containing interneurons. Cereb Cortex. 19 (Suppl 1):i78–i89.
Mulder J, Aguado T, Keimpema E, Barabás K, Ballester Rosado CJ, Nguyen L, Monory K, Marsicano G, Di Marzo V, Hurd YL, et al. 2008. Endocannabinoid signaling controls pyramidal cell specification and long-range axon patterning. Proc Natl Acad Sci U S A. 105:8760–8765.
Nethe M, Hordijk PL. 2010. The role of ubiquitylation and degradation in RhoGTPase signalling. J Cell Sci. 123:4011–4018.
Nguyen L, Besson A, Heng JI, Schuurmans C, Teboul L, Parras C, Philpott A, Roberts JM, Guillemot F. 2006. P27Kip1 independently promotes neuronal differentiation and migration in the cerebral cortex. Genes Dev. 20:1511–1524.
Nithipatikom K, Gomez-Granados AD, Tang AT, Pfeiffer AW, Williams CL, Campbell WB. 2012. Cannabinoid receptor type 1 (CB1) activation inhibits small GTPase RhoA activity and regulates motility of prostate carcinoma cells. Endocrinology. 153:29–41.
Njoo C, Agarwal N, Lutz B, Kuner R. 2015. The cannabinoid receptor CB1 interacts with the WAVE1 complex and plays a role in actin dynamics and structural plasticity in neurons. PLOS Biol. 13:e1002286.
Noctor SC, Martínez-Cerdeño V, Ivic L, Kriegstein AR. 2004. Cortical neurons arise in symmetric and asymmetric division zones and migrate through specific phases. Nat Neurosci. 7:136–144.
Oberoi TK, Dogan T, Hocking JC, Scholz RP, Mooz J, Anderson CL, Karreman C, Meyer zu Heringdorf D, Schmidt G, Ruonala M, et al. 2012. IAPs regulate the plasticity of cell migration by directly targeting Rac1 for degradation. EMBO J. 31:14–28..

Oudin MJ, Gajendra S, Williams G, Hobbs C, Lalli G, Doherty P. 2011. Endocannabinoids regulate the migration of subventricular zone-derived neuroblasts in the postnatal brain. J Neurosci. 31:4000–4011.

Pacary E, Azzarelli R, Guillemot F. 2013. Rnd3 coordinates early steps of cortical neurogenesis through actin-dependent and -independent mechanisms. Nat Commun. 4:1635.

Pacary E, Heng J, Azzarelli R, Riou P, Castro D, Lebel-Potter M, Parras C, Bell DM, Ridley AJ, Parsons M, et al. 2011. Proneural transcription factors regulate different steps of cortical neuron migration through Rnd-mediated inhibition of RhoA signaling. Neuron. 69:1069–1084.

Palazuelos J, Aguado T, Pazos MR, Julien B, Carrasco C, Resel E, Sagredo O, Benito C, Romero J, Azcoitia I, et al. 2009. Microglial CB2 cannabinoid receptors are neuroprotective in Huntington's disease excitotoxicity. Brain. 132:3152–3164.

Pertwee RG. 2012. Targeting the endocannabinoid system with cannabinoid receptor agonists: pharmacological strategies and therapeutic possibilities. Philos Trans R Soc B Biol Sci. 367:3353–3363.

Piao X, Hill RS, Bodell A, Chang BS, Basel-Vanagaite L, Straussberg R, Dobyns WB, Qasrawi B, Winter RM, Innes AM, et al. 2004. G protein-coupled receptor-dependent development of human frontal cortex. Science. 303:2033–2036.

Puighermanal E, Marsicano G, Busquets-Garcia A, Lutz B, Maldonado R, Ozaita A. 2009. Cannabinoid modulation of hippocampal long-term memory is mediated by mTOR signaling. Nat Neurosci. 12:1152–1158.

Roland AB, Ricobaraza A, Carrel D, Jordan BM, Rico F, Simon A, Humbert-Claude M, Ferrier J, McFadden MH, Scheuring S, et al. 2014. Cannabinoid-induced actomyosin contractility shapes neuronal morphology and growth. Elife. 3:e03159.

Saez TMM, Aronne MP, Caltana L, Brusco AH. 2014. Prenatal exposure to the CB1 and CB2 cannabinoid receptor agonist WIN 55,212-2 alters migration of early-born glutamatergic neurons and GABAergic interneurons in the rat cerebral cortex. J Neurochem. 129:637–648.

Shafi MM, Vernet M, Klooster D, Chu CJ, Boric K, Barnard ME, Romatoski K, Westover MB, Christodoulou JA, Gabrieli JD, et al. 2015. Physiological consequences of abnormal connectivity in a developmental epilepsy. Ann Neurol. 77:487–503.

Soltesz I, Alger BE, Kano M, Lee S-H, Lovinger DM, Ohno-Shosaku T, Watanabe M. 2015. Weeding out bad waves: towards selective cannabinoid circuit control in epilepsy. Nat Rev Neurosci. 16:264–277.

Tang J, Ip JPK, Ye T, Ng Y-P, Yung W-H, Wu Z, Fang W, Fu AKY, Ip NY. 2014. Cdk5-Dependent Mst3 Phosphorylation and Activity Regulate Neuronal Migration through RhoA Inhibition. J Neurosci. 34:7425–7436.

Tian M, Bai C, Lin Q, Lin H, Liu M, Ding F, Wang H-R. 2011. Binding of RhoA by the C2 domain of E3 ligase Smurf1 is essential for Smurf1-regulated RhoA ubiquitination and cell protrusive activity. FEBS Lett. 585:2199–2204.

Tortoriello G, Morris C V, Alpar A, Fuzik J, Shirran SL, Calvigioni D, Keimpema E, Botting CH, Reinecke K, Herdegen T, et al. 2014. Miswiring the brain: Δ9-tetrahydrocannabinol disrupts cortical development by inducing an SCG10/stathmin-2 degradation pathway. EMBO J. 33:668–685.

Valiente M, Marín O. 2010. Neuronal migration mechanisms in development and disease. Curr Opin Neurobiol. 20:68–78.

Vitalis T, Lainé J, Simon A, Roland A, Leterrier C, Lenkei Z. 2008. The type 1 cannabinoid receptor is highly expressed in embryonic cortical projection neurons and negatively regulates neurite growth in vitro. Eur J Neurosci. 28:1705–1718.

Young-Pearse TL, Bai J, Chang R, Zheng JB, LoTurco JJ, Selkoe DJ. 2007. A critical function for beta-amyloid precursor protein in neuronal migration revealed by in utero RNA interference. J Neurosci. 27:14459–14469.

frontiers in Pharmacology

ORIGINAL RESEARCH
published: 09 January 2019
doi: 10.3389/fphar.2018.01508

# Contribution of Altered Endocannabinoid System to Overactive mTORC1 Signaling in Focal Cortical Dysplasia

*Daniel García-Rincón[1,2], Javier Díaz-Alonso[1,2], Juan Paraíso-Luna[1,2], Zaira Ortega[1,2], José Aguareles[1,2], Adán de Salas-Quiroga[1,2], Cristina Jou[3], Inmaculada de Prada[4], Verónica Martínez-Cerdeño[5], Eleonora Aronica[6,7], Manuel Guzmán[1,2], María Ángeles Pérez-Jiménez[4] and Ismael Galve-Roperh[1,2]**

[1] Instituto Ramón y Cajal de Investigación Sanitaria, Department of Biochemistry and Molecular Biology and Instituto Universitario de Investigación Neuroquímica, Complutense University, Madrid, Spain, [2] Centro de Investigación Biomédica en Red sobre Enfermedades Neurodegenerativas, Madrid, Spain, [3] Departamento de Anatomía Patológica, Hospital Sant Joan de Déu, Barcelona, Spain, [4] Hospital Infantil Universitario Niño Jesús, Madrid, Spain, [5] Institute for Pediatric Regenerative Medicine, Shriners Hospital for Children of Northern California and Department of Pathology and Laboratory Medicine, School of Medicine, University of California, Davis, Sacramento, CA, United States, [6] Amsterdam UMC, Department of (Neuro)Pathology, Amsterdam Neuroscience, University of Amsterdam, Amsterdam, Netherlands, [7] Stichting Epilepsie Instellingen Nederland, Heemstede, Netherlands

OPEN ACCESS

**Edited by:**
*Luis F. Callado,*
*Universidad del País Vasco, Spain*

**Reviewed by:**
*Allyn C. Howlett,*
*Wake Forest School of Medicine, United States*
*Emmanuel Valjent,*
*Center for the National Scientific Research (CNRS), France*

***Correspondence:**
*Ismael Galve-Roperh*
*igr@quim.ucm.es*

**Specialty section:**
*This article was submitted to Neuropharmacology, a section of the journal Frontiers in Pharmacology*

**Received:** *18 September 2018*
**Accepted:** *10 December 2018*
**Published:** *09 January 2019*

**Citation:**
*García-Rincón D, Díaz-Alonso J, Paraíso-Luna J, Ortega Z, Aguareles J, de Salas-Quiroga A, Jou C, de Prada I, Martínez-Cerdeño V, Aronica E, Guzmán M, Pérez-Jiménez MÁ and Galve-Roperh I (2019) Contribution of Altered Endocannabinoid System to Overactive mTORC1 Signaling in Focal Cortical Dysplasia. Front. Pharmacol. 9:1508. doi: 10.3389/fphar.2018.01508*

Alterations of the PI3K/Akt/mammalian target of rapamycin complex 1 (mTORC1) signaling pathway are causally involved in a subset of malformations of cortical development (MCDs) ranging from focal cortical dysplasia (FCD) to hemimegalencephaly and megalencephaly. These MCDs represent a frequent cause of refractory pediatric epilepsy. The endocannabinoid system -especially cannabinoid $CB_1$ receptor- exerts a neurodevelopmental regulatory role at least in part via activation of mTORC1 signaling. Therefore, we sought to characterize the possible contribution of endocannabinoid system signaling to FCD. Confocal microscopy characterization of the $CB_1$ receptor expression and mTORC1 activation was conducted in FCD Type II resection samples. FCD samples were subjected to single nucleotide polymorphism screening for endocannabinoid system elements, as well as $CB_1$ receptor gene sequencing. Cannabinoid $CB_1$ receptor levels were increased in FCD with overactive mTORC1 signaling. $CB_1$ receptors were enriched in phospho-S6-positive cells including balloon cells (BCs) that co-express aberrant markers of undifferentiated cells and dysplastic neurons. Pharmacological regulation of $CB_1$ receptors and the mTORC1 pathway was performed in fresh FCD-derived organotypic cultures. HU-210-evoked activation of $CB_1$ receptors was unable to further activate mTORC1 signaling, whereas $CB_1$ receptor blockade with rimonabant attenuated mTORC1 overactivation. Alterations of the endocannabinoid system may thus contribute to FCD pathological features, and blockade of cannabinoid signaling might be a new therapeutic intervention in FCD.

**Keywords: cannabinoid, $CB_1$ receptor, malformation of cortical development, corticogenesis, neural progenitor, cannabinoid, mTORC1, mammalian target of rapamycin**

**Abbreviations:** CAT, chloramphenicol acetyltransferase; DAGL, diacylglycerol lipase; ECS, endocannabinoid system; FAAH, fatty acid amide hydrolase; FCD, focal cortical dysplasia; MAGL, monoacylglycerol lipase; MCD, malformation of cortical development; mTORC1, mammalian target of rapamycin complex 1; TSC, tuberous sclerosis complex.

## INTRODUCTION

Malformations of cortical development are associated with refractory epilepsy in children and young adults (Iffland and Crino, 2017). These alterations are originated by the disruption of key processes during brain development, such as neural progenitor cell proliferation or neuronal migration. Within MCD, some types of FCD and TSC are associated with overactivation of the mTORC1 signaling pathway (Aronica and Crino, 2014; Najm et al., 2018). TSC has a clear genetic origin on loss-of-function mutations of mTORC1 signaling regulators such as TSC1/TSC2 (hamartin–tuberin), which leads to the overactivation of mTORC1. Whereas the origin of the different FCD subtypes is still unclear, recent research has demonstrated the involvement of alterations of the PI3K/Akt/mTORC1 pathway particularly in FCD Type II (Jansen et al., 2015; Lim et al., 2015; D'Gama et al., 2017). Characteristic features of FCD Type II are the presence of balloon cells (BCs) and cytomegalic neurons with overactive mTORC1 signaling (usually revealed by the phosphorylation of one of its canonical targets, the ribosomal protein S6). Hence, FCD Type II cases are distinguishable at the molecular level from FCD Type I by the overactivation of mTORC1 signaling. FCD Type II cases are also distinguishable from Type I cases by the expression of undifferentiated cell markers in BCs that suggests a developmental origin (Orlova et al., 2010). Thus, this subtype of FCDs and hemimegalencephaly are known to be originated in the dorsal telencephalic progenitors and excitatory projection neuron lineage (D'Gama et al., 2017; Iffland et al., 2018). Further investigation on the mechanisms responsible for the epileptogenic network is required for the development of novel therapeutic strategies aimed to manage FCDs.

The ECS, and especially the cannabinoid $CB_1$ receptor, exerts an essential neuromodulatory role in the adult brain via the retrograde lipid messengers 2-arachidonoylglycerol and anandamide (Soltesz et al., 2015). In addition, $CB_1$ receptors are expressed during human cortical development (Mato et al., 2003; Wang et al., 2003). During early stages in brain development, endocannabinoids act as neural cell fate regulatory cues, and the $CB_1$ receptor is coupled to activation of the mTORC1 pathway, which allows the control of neural progenitor identity and pyramidal neuron generation (Díaz-Alonso et al., 2015). Cannabinoid signaling regulates long-range axon projection (Mulder et al., 2008; Argaw et al., 2011; Díaz-Alonso et al., 2012), but also local microcircuits and interneuron development (Berghuis et al., 2005, 2007). Moreover, $CB_1$ receptors are required for proper radial migration during cortical development, and their genetic inactivation induces brain hyperexcitability (Díaz-Alonso et al., 2017). Interestingly, transient loss of $CB_1$ receptor function (induced by pharmacological down-regulation or small-interfering RNA) during embryonic development exerts long-lasting alterations in cortical development that result in increased seizure susceptibility in the adult offspring (de Salas-Quiroga et al., 2015; Díaz-Alonso et al., 2017). $CB_1$ receptors are expressed in FCD (Zurolo et al., 2010), but their functional relevance is unclear. Thus, here we sought to investigate the potential contribution of aberrant cannabinoid signaling to FCD developmental pathogenesis.

## MATERIALS AND METHODS

### Human Samples

The FCD cases included in this study were obtained from the archives of the Departments of Neuropathology of the Academic Medical Center (University of Amsterdam, Netherlands), the University Medical Center in Utrecht (Netherlands), Hospital Infantil Niño Jesús (Madrid, Spain) and Biobanc de l'Hospital Infantil Sant Joan de Déu per a la Investigació (Barcelona, Spain) integrated in the Spanish Biobank Network of ISCIII. A total of 30 surgical specimens (10 FCD Type I and 20 FCD Type II), resected from patients undergoing surgery for intractable epilepsy, were examined (**Table 1**). Tissue was obtained and used in accordance with the Declaration of Helsinki and informed consent was obtained for the use of brain tissue and for access to medical records for research purposes. All cases were reviewed

**TABLE 1 |** Clinical features of cortical development alterations in patients analyzed in this study.

| Patient | Age range at surgery (years) | Duration of epilepsy (years) | Diagnosis | Location | Engel's class |
|---|---|---|---|---|---|
| 1 | 10 ≤ 15 | 8 | FCD Ia | Parietal | II |
| 2 | 15 ≤ 20 | 10 | FCD Ia | Frontal | I |
| 3 | >20 | 16 | FCD Ia | Temporal | I |
| 4 | 15 ≤ 20 | 11 | FCD Ia | Frontal | I |
| 5 | >20 | 17 | FCD Ia | Temporal | I |
| 6 | 15 ≤ 20 | 12 | FCD Ia | Frontal | II |
| 7 | 0 ≤ 5 | 4 | FCD Ia | Temporal | I |
| 8 | 0 ≤ 5 | 3 | FCD Ia | Frontal | I |
| 9 | 0 ≤ 5 | 1.5 | FCD Ia | Multilobar | IV |
| 10 | 0 ≤ 5 | 2 | FCD Ia | Frontal | I |
| 11 | >20 | 21 | FCD IIb | Temporal | I |
| 12 | >20 | 18 | FCD IIb | Temporal | I |
| 13 | >20 | 19 | FCD IIb | Frontal | I |
| 14 | 15 ≤ 20 | 9 | FCD IIb | Temporal | I |
| 15 | 10 ≤ 15 | 10 | FCD IIb | Frontal | I |
| 16 | 0 ≤ 5 | 5 | FCD IIb | Multilobar | II |
| 17 | 5 ≤ 10 | 5 | FCD IIb | Multilobar | III |
| 18 | 5 ≤ 10 | 7.5 | FCD IIb | Frontal | II |
| 19 | 0 ≤ 5 | 0.5 | FCD IIb | Multilobar | III |
| 20 | 15 ≤ 20 | 17 | FCD IIb | Multilobar | II |
| 21 | 0 ≤ 5 | 0.5 | FCD IIb | Multilobar | II |
| 22 | >20 | 21 | FCD IIb | Multilobar | III |
| 23 | 0 ≤ 5 | 2.5 | FCD IIb | Temporal | I |
| 24 | 10 ≤ 15 | 15 | FCD IIb | Parietal | II |
| 25 | 10 ≤ 15 | 6 | FCD IIb | Occipital | I |
| 26 | 5 ≤ 10 | 5 | FCD IIb | Frontal | I |
| 27 | 0 ≤ 5 | 0.5 | FCD IIa | Occipital | II |
| 28 | 5 ≤ 10 | 5 | FCD IIa | Temporal | I |
| 29 | 5 ≤ 10 | 5 | FCD IIa | Multilobar | I |
| 30 | 0 ≤ 5 | 3 | FCD IIb | Frontal | I |

by the corresponding neuropathologist and the diagnosis was confirmed according to ILAE classification system (Blümcke et al., 2011; Najm et al., 2018). Control brains from patients that were not diagnosed with neurologic disorders were also employed [*n = 6;* age (years): 53; 40; 34; 21; 51; 25; 58]. Formalin-fixed, paraffin-embedded tissue (one representative paraffin block per case containing the complete lesion or the largest part of the lesion resected at surgery) was sectioned at 6 μm and mounted on pre-coated glass slides (Star Frost, Waldemar Knittel GmbH, Barunschweig, Germany). Sections of all specimens were processed for hematoxylin eosin, luxol fast blue and Nissl stainings and neuronal and glial markers for classification and selection.

## FCD Neuronal and Organotypic Cultures

Focal cortical dysplasia derived organotypic cultures were obtained as described (Eugène et al., 2014). In brief, resection tissue derived from refractory epilepsy surgery of FCD Type II patients was sliced at 300 μm. Slices were cultured on a transwell semiporous membrane for 7 days and subjected to pharmacological regulation. After incubation, slices were fixed and sectioned for immunofluorescence characterization. Alternatively, proteins were extracted after cell lysis in a buffer containing 50 mM Tris, 0.1% Triton X-100, 1 mM ethylenediaminetetraacetic acid, 1 mM ethylene glycol tetraacetic acid, 50 mM NaF, 10 mM sodium b-glicerophosphate, 5 mM sodium pyrophosphate and 1 mM sodium orthovanadate (pH 7.5) supplemented with a protease inhibitor cocktail (Roche, Basel, Switzerland), 0.1 mM phenylmethane-sulphonylfluoride, 0.1% β-mercaptoethanol and 1 μM microcystin for Western blot analyses.

## $CB_1$ Receptor Promoter Transcriptional Assays

Embryonic carcinoma P19 cells were employed in reporter assays as previously described (Díaz-Alonso et al., 2015). Cells were transfected transiently with a construct encoding the −3016 to +142 sequence (referring to the first nucleotide of exon 1) of the human $CB_1$ receptor gene promoter fused to the CAT reporter gene (ph$CB_1$-3016-CAT) (Blázquez et al., 2011). The reporter gene construct was based on the pBLCAT2/pBLCAT3 system, in which the thymidine kinase minimal promoter was replaced for the human $CB_1$ receptor promoter upstream of CAT. CAT activity was subsequently analyzed by ELISA following manufacturer's instructions (Roche, distributed by Sigma #11363727001, Madrid, Spain).

## Immunofluorescence Microscopy

P19 carcinoma cells, organotypic brain slices and FCD samples were fixed and immunofluorescence performed. After blockade with 5% goat serum, overnight incubation at 4°C with the indicated primary antibodies was performed: polyclonal guinea pig anti-$CB_1$ receptor (1:500, Frontier Institute, Japan), polyclonal rabbit anti-phosphoS235/S236-S6 ribosomal protein (1:100) and polyclonal rabbit anti-phosphoS240/S244-S6 ribosomal protein (1:800; Cell Signaling Technology, Barcelona, Spain) and monoclonal mouse anti-c-Myc (1:500; Sigma, Madrid, Spain). Specificity of $CB_1$ immunoreactivity was confirmed with an additional polyclonal anti-$CB_1$ antibody (kindly donated by K. Mackie, Indiana University, Bloomington, IN, United States). The appropriate anti-mouse, rat, guinea pig, and rabbit highly cross-adsorbed AlexaFluor 488, AlexaFluor 546, AlexaFluor 594, and AlexaFluor 647 secondary antibodies (Invitrogen, Carlsbad, CA, United States) were used. Confocal fluorescence images were acquired by using both Leica TCS-SP2 and LAS-X software (Wetzlar, Germany) with a SP2 or a SP8 microscope, respectively, with three passes by Kalman filter and a 1024 × 1024 or a 2048 × 2048 collection box, respectively. Immunofluorescence data were obtained in a blind manner by an independent observer and sample code remained unsealed during the whole data processing and analysis. mTORC1 activation status and $CB_1$ immunoreactivity were quantified in a minimum of 500 cells for each FCD patient or control sample. Immunoreactivity was measured using Fiji (ImageJ) software establishing a threshold to measure only specific signal. The resulting binary mask was then used along the built-in measure function to acquire the total integrated gray density among all the pixels inside the binary mask overlayed on top of the original image. The obtained value was then referred to the number of $DAPI^+$ cell nuclei present in the optic field. For *in vitro* studies, P19 cells ($n$ = 6 independent experiments) and FCD organotypic cultures ($n$ = 4 independent FCD cases) were quantified.

## Western Blot Assays

Equal amount of protein samples were electrophoretically separated and transferred to PVDF membranes. After blocking with 5% BSA, membranes were incubated overnight at 4°C with anti-phosphoS235/S236-S6 ribosomal protein (1:1000), anti-phosphoS240/S244-S6 ribosomal protein (1:1000), anti-$CB_1$ (1:500) or anti-β-actin (1:5000) primary antibodies. PVDF membranes were then incubated with the corresponding secondary antibodies coupled to horseradish peroxidase. Optical density of the specific immunoreactive band was quantified with Fiji software. The values of pS6 were normalized to those of β-actin in the same membranes.

## DNA Single Nucleotide Polymorphisms Analyses and Sequencing

Genomic DNA was obtained by standard methods and Sequenom SNP analyses were performed by Centro Nacional de Genotipado (CEGEN-PRB2 USC node, Santiago de Compostela, Spain) using the iPlex® Gold chemistry and MassARRAY platform, according to manufacturer's instructions (Sequenom, San Diego, CA, United States). Genotyping assays were designed using the Sequenom MassARRAY Assay Designer 4.1 software. SNPs were genotyped in three assays, PCR reactions were set up in a 5 μl volume and contained 20 ng of template DNA, 1× PCR buffer, 2 mM $MgCl_2$, 500 μM dNTPs and 1 U/reaction of PCR enzyme. A pool of PCR primers (Metabion, Steinkirchen, Germany) was made at a final concentration of each primer of 100 nM. The thermal cycling conditions for the reaction

consisted on an initial denaturation step at 94°C for 2 min, followed by 45 cycles of 94°C for 30 s, 56°C for 30 s and 72°C for 1 min, and a final extension step of 72°C for 1 min. PCR products were treated with 0.5 U shrimp alkaline phosphatase, followed by enzyme inactivation to neutralize unincorporated dNTPs.

The iPLEX GOLD reactions were set up in a final 9 μl volume and contained 0.222x iPLEX buffer Plus, 1x iPLEX termination mix and 1x iPLEX enzyme. An extension primer mix (Metabion) was made to give a final concentration of each primer between 0.52 μM and 1.57 μM. The thermal cycling conditions for the reaction included an initial denaturation step at 94°C for 30 s, followed by 40 cycles of 94°C for 5 s, with an internal five cycles loop at 52°C for 5 s and 80°C for 5 s, followed by a final extension step of 72°C for 3 min. The iPLEX Gold reaction products were desalted, dispensed onto a 384 Spectrochip II using an RS1000 Nanodispenser and spectra were acquired using the MA4 mass spectrometer, followed by manual inspection of spectra by trained personnel using MassARRAY Typer software, version 4.0. All assays were performed in 384-well plates, including negative controls and a trio of Coriell samples (Na10830, Na10831, and Na12147) for quality control. Seven samples were tested in duplicate and they were 100% concordant. Genomic DNA sequencing of the $CB_1$ receptor gene coding exon was performed by the Sanger method under standard conditions by Secugen (Madrid, Spain).

## Data and Statistical Analyses

Results shown represent the means ± SEM, and the number of experiments is indicated in every case. Statistical analysis was performed with GraphPad Prism 6.07 (GraphPad Software, La Jolla, CA, United States) using one-way ANOVA. A *post hoc* analysis by the Student–Newman–Keuls test was made (**Table 2**). Disease-Genotype association test was performed by the SNPator online tool (Morcillo-Suarez et al., 2008) to examine genotype and allele frequencies between patients and controls. *P*-values of $<0.05$ were regarded as statistically significant.

**TABLE 2 |** Statistical analyses.

| Figure | Comparison | Statistic value | Significance |
|---|---|---|---|
| **Figure 1A** | One-way ANOVA | $F = 22.57$ | **** |
| | FCDI vs. Co | $q = 1.930$ | ns |
| | FCDII vs. Co | $q = 7.833$ | **** |
| | FCDII vs. FCDI | $q = 7.005$ | **** |
| **Figure 1B** | One-way ANOVA | $F = 24.87$ | **** |
| | FCDI vs. Co | $q = 1.013$ | ns |
| | FCDII vs. Co | $q = 8.856$ | **** |
| | FCDII vs. FCDI | $q = 7.271$ | **** |
| **Figure 1C** | One-way ANOVA | $F = 24.87$ | **** |
| | FCDI vs. Co | $q = 0.7072$ | ns |
| | FCDII vs. Co | $q = 7.399$ | **** |
| | FCDII vs. FCDI | $q = 8.187$ | **** |
| **Figure 3A** | One-way ANOVA | $F = 8.749$ | ** |
| | RHEB vs. pCAG-GFP | $q = 4.450$ | ** |
| | shTSC2 vs. shCo | $q = 5.700$ | ** |
| **Figure 3B** | One-way ANOVA | $F = 2.917$ | * |
| | Tbr2 vs. GFP | $q = 5.083$ | ** |
| **Figure 5A** | One-way ANOVA | $F = 16.77$ | *** |
| | RAPA vs. VEH | $q = 7.675$ | *** |
| | RAPA vs. HU-210 | $q = 6.139$ | ** |
| **Figure 5B** | One-way ANOVA | $F = 7.305$ | *** |
| | HU-210 vs. VEH | $q = 0.2946$ | ns |
| | SR1 vs. VEH | $q = 4.164$ | * |
| | RAPA vs. VEH | $q = 5.153$ | ** |
| | HU-210 + SR1 vs. VEH | $q = 5.208$ | ** |

*One-way ANOVA followed by Student–Newman–Keuls post hoc test. Statistical significance ****$p < 0.0001$; ***$p < 0.001$; **$p < 0.01$; *$p < 0.05$; ns, non-significant.*

# RESULTS

## $CB_1$ Cannabinoid Receptor Expression in FCD Is Associated With Overactive mTORC1 Pathway

To assess the pathophysiological relevance of $CB_1$ receptor signaling in MCD we analyzed $CB_1$ receptor immunoreactivity in control and dysplastic brain areas (**Figure 1**). FCD cases ($n = 30$) were included with a mean patient age of 11.4 years and a male/female distribution of $n = 18$ and 12, respectively (**Table 1**). Double immunofluorescence analysis with anti-phospho-S6 (recognizing the phosphoS240/S244 sites) and anti-$CB_1$ antibodies confirmed the selective overactivation of the mTORC1 pathway in FCD Type II but not FCD Type I samples (**Figures 1A,B**). Quantification of $CB_1$ immunoreactivity revealed that receptor expression is notably enriched in the dysplastic areas of FCD Type II when compared with control brain tissue, but not in FCD Type I (**Figures 1A,C**). A more detailed analysis of double immunofluorescence images showed that $CB_1$-positive cells largely colocalized with phospho-S6 immunoreactivity in FCD Type II, and $CB_1{}^{+}pS6^{+}$ cells were highly enriched in the dysplastic areas when compared to control cortical tissue (**Figure 1D**). Equivalent findings of $CB_1$ enrichment in phospho-S6-positive cells were reproduced when using as alternative readout, anti phosphoS235/S236-S6 antibody (**Supplementary Figure 1**). Moreover, the intensity of phospho-S6 immunoreactivity was selectively increased when comparing FCD Type II and I ($1.61 \pm 0.14$ versus $1.00 \pm 0.07$, respectively; $p < 0.05$, $n = 4$). Next, we analyzed $CB_1$ receptor expression in BCs and dysplastic neurons based in morphological characterization and mTORC1 overactivation (**Figure 2A**). This indicated that $2.43 \pm 0.92$ and $0.57 \pm 0.29$% of total $CB_1$ tissue immunoreactivity corresponded to these cell subpopulations, respectively. FCD Type II is characterized by the expression of undifferentiated markers in BC including Sox2, Oct4, Pax6, Tbr1, Otx1, and others (Hadjivassiliou et al., 2010; Orlova et al., 2010; Arai et al., 2012; Yao et al., 2016). Thus, we analyzed the expression of $CB_1$ receptors in FCD Type II neurons together with undifferentiated-cell markers. Whereas in FCD Type II sparse c-Myc-positive cells could be detected, this was never the case in the FCD Type I samples. Importantly, c-Myc-positive cells

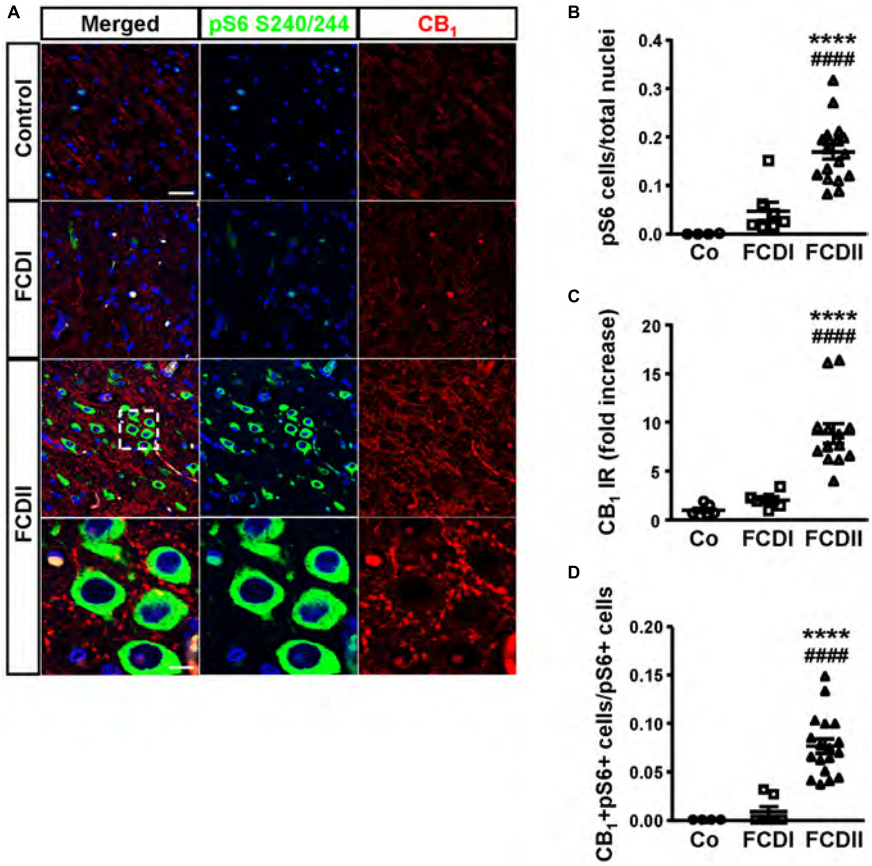


**FIGURE 1 |** The $CB_1$ receptor is enriched in focal cortical dysplasia (FCD) Type II in cells with overactive mTORC1 signaling. **(A)** Representative immunofluorescence images showing the presence of $CB_1$ receptors in samples from Type I and II FCD and control brains, revealed with an anti-$CB_1$ antibody (red). Cells with over-active mTORC1 signaling are stained with phospho-$S6_{Ser240/244}$ antibody (green). High magnification images of $CB_1$ receptor expression associated with mTORC1 overactivation in FCD Type II are shown. **(B,C)** Phospho-$S6^+$ cells and $CB_1$ receptor immunoreactivity (IR) were quantified in the dysplastic area and referred to total cell number (DAPI counterstaining). Control, FCD Type I and FCD Type II cases (**B**, $n = 4$, 7 and 18, respectively; **C**, $n = 6$, 8, 13). **(D)** $CB_1{}^+$ phospho-$S6^+$ double-labeled cells were quantified and referred to total $pS6^+$ cells. Control, FCD Type I and FCD Type II cases ($n = 4$, 7, and 18, respectively). Statistical comparison versus control samples, $^{****}p < 0.0001$; statistical comparison versus FCD Type I samples, $^{\#\#\#\#}p < 0.0001$. Scale bar 45 μm, insets, 10 μm.

expressed $CB_1$ receptors and showed active mTORC1 signaling ($pS6^+$) (**Figure 2B**). Hence, in FCD Type II we determined that 72.74 ± 11.04% c-Myc-positive cells were also phospho-S6 positive.

## $CB_1$ Cannabinoid Receptor Expression Is Not Induced by mTORC1 Signaling

To determine if $CB_1$ receptor enrichment in FCD lesions was a cause or a consequence of mTORC1 overactivation we analyzed if this signaling pathway can regulate $CB_1$ receptor expression. P19 cells were transfected with a plasmid encoding a constitutively active mutant of the mTORC1 upstream activator Rheb (RhebQ64L) or a Tsc2 specific short-hairpin RNA coding plasmid (shTSC2). In these conditions, as compared to control cells, mTORC1 pathway activity increased as evidenced by the strong increase of $pS6^+$ immunoreactive cells (**Figure 3A**). However, under the same conditions of overactive mTORC1 signaling, $CB_1$ receptor protein levels were not induced (**Figure 3B**). We also performed $CB_1$ promoter transcriptional assays by co-transfection with a CAT gene reporter in frame with a minimal *CNR1* promoter (Blázquez et al., 2011). Again, in cells with overactive mTORC1 pathway $CB_1$ promoter activity was not induced (**Figure 3C**). As a control of the sensitivity of this assay, P19 cells were transfected with the intermediate progenitor transcription factor Tbr2 (Eomes). The $CB_1$ promoter has several putative Tbr2-binding sites [**Table 3**, Matinspector (Genomatix)],

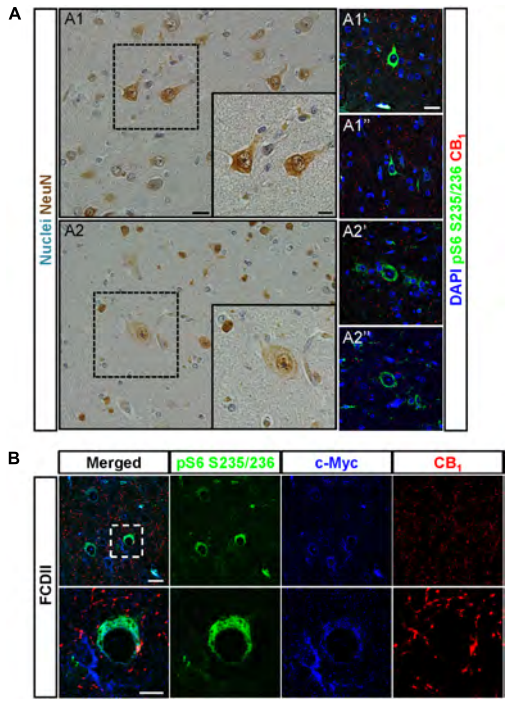


**FIGURE 2 |** $CB_1$ receptors are present in undifferentiated cells. **(A)** Dysplastic neurons **(A1,A1′,A1′′)** and balloon cells **(A2,A2′,A2′′)** were identified based in morphological criteria in hematoxylin/eosin sections stained with NeuN antibody **(A1,A2)**. $CB_1$ receptor expression and mTORC1 activity status were analyzed by immunofluorescence with $CB_1$ and phospho-S6 antibodies, respectively **(A1′,A1′′,A2′,A2′′)**. **(B)** Representative immunofluorescence images showing the presence of $CB_1$ receptor (red) in FCD Type II brain cells labeled with the undifferentiated cell marker c-Myc (blue) and active mTORC1 signaling phospho-$S6^+$ cells (green). High magnification insets are shown (lower panels). Scale bar: 25 μm, insets, 10 μm.

and its expression was indeed sufficient to increase $CB_1$ promoter reporter activity (**Figure 3C**), but failed to increase protein levels (**Figure 3B**). In summary, these results indicate that the increased $CB_1$ receptor levels in FCD are not a direct consequence of an overactive mTORC1 pathway.

## Genetic Characterization of the Endocannabinoid System in FCD

The observation that $CB_1$ receptor levels are increased in the dysplastic cells of FCD Type II cases prompted us to expand the analyses to other elements of the ECS that may contribute to cannabinoid signaling deregulation. Genomic DNA and messenger RNA from the FCD collection were obtained. Real time PCR expression analysis confirmed increased levels of $CB_1$ receptor transcripts in FCD Type II versus control brain extracts (**Table 4**), further supporting the results obtained at the protein level by immunofluorescence characterization (**Figure 1**). Transcript levels of other elements of the ECS [DAGL alpha and beta isoforms, MAGL, FAAH and *N*-acyl phosphatidylethanolamine phospholipase D (NAPE-PLD)] were also quantified and no differences were observed (**Table 4**). To further characterize if cannabinoid signaling alterations may contribute to overactive mTORC1 in FCD Type II, we performed single nucleotide polymorphism (SNP) analysis of various genes of the ECS including the $CB_1$ receptor, DAGL alpha and beta, MAGL, FAAH and $CB_2$ receptor (**Supplementary Table 1**). A total 48 SNPs of the ECS were selected, based on previous evidences that point to their potential involvement in different nervous system disorders. Genotype disease association analysis revealed the existence of three polymorphisms in the *DAGLA* gene differentially expressed in FCD Type II versus control specimens (**Table 5**). The rest of SNPs analyzed for *CNR1*, *DAGLB*, *MAGL*, *FAAH*, and *CNR2* did not show any difference between pathologic samples and controls. To further investigate the potential involvement of $CB_1$ receptors in FCD we sequenced the *CNR1* gene exon in the FCD and control genomic DNA samples. *CNR1* exon 1 sequencing revealed normal wild-type sequence in most samples and only rs1049353 SNP (c.1359G>A; p.Thr453) was identified with similar distribution among dysplastic and control DNA.

In summary, these results suggest that the DAGLα-evoked generation of the endocannabinoid 2-AG might be altered in FCD Type II and can contribute to its etiopathology. However, the exact contribution of endocannabinoid tone alterations in MCD would require more complex genetic studies to identify its potential association with the origin of the disease.

## $CB_1$ Cannabinoid Receptor Crosstalk With the mTORC1 Pathway in FCD Resections

Additional specimens derived from surgical resection for intractable epilepsy were analyzed *ex vivo* for mechanistic studies. 3T magnetic resonance imaging (MRI), fluorodeoxyglucose (FDG)-PET scan, scalp electroencephalography (EEG) recording and invasive neurophysiological studies were employed to identify the origin of epileptic seizures (**Figure 4A**). Representative images of one case prior and after surgery are shown. In this particular patient, a 5-year-old male, a small FCD Type II involving the left rolandic region and superior frontal gyrus (arrowheads, **Figure 4A**) was associated with daily focal motor seizures and *Epilepsia Partialis Continua* involving the left arm and the face. Scalp EEG analyses revealed continuous focal epileptiform discharges (arrowhead, **Figure 4B**) in accordance with a hypermetabolic FDG-PET focus. Intracraneal EEG exploration of the dysplastic lesion, using a combination of subdural electrodes and depth electrodes, better defined a characteristic EEG pattern, indicative of FCD. This characteristic EEG pattern shows continuous repetitive burst of epileptiform activity turning into focal EEG ictal patterns (arrowhead, **Figure 4C**), in association with the onset of clinical seizure signs. After tailored resection of the epileptogenic zone, 1 year follow-up after surgery revealed a seizure-free clinical status,

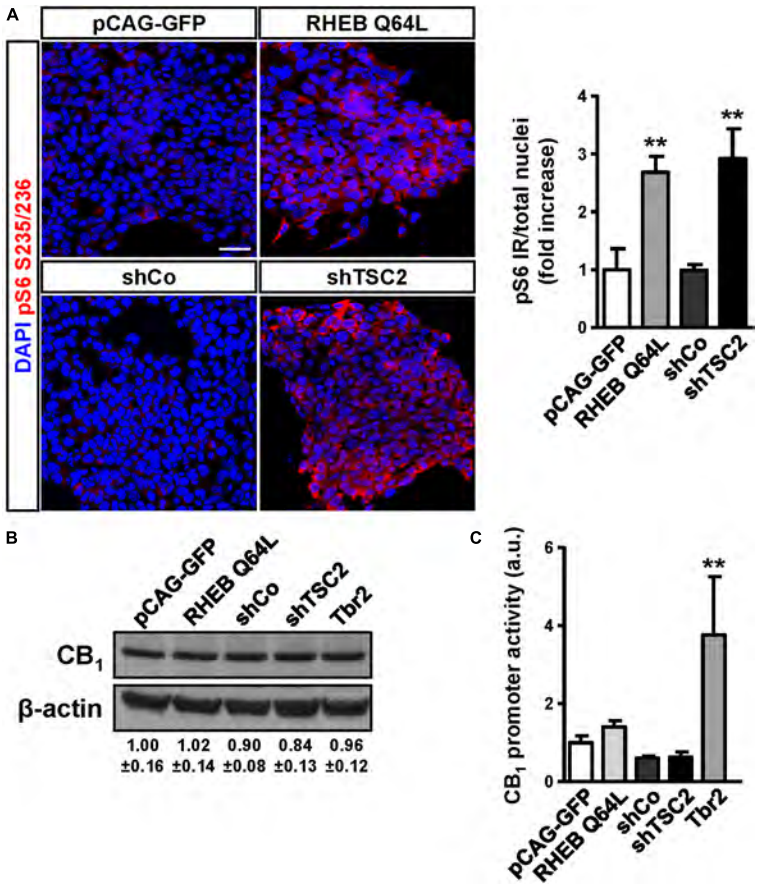


**FIGURE 3 |** The mTORC1 pathway does not regulate $CB_1$ receptor expression. **(A)** Characterization of mTORC1 activation in P19 cells after transfection with the Rheb constitutive active mutant Q64L, shTSC2, a scrambled shRNA encoding vector (shCo), or GFP encoding plasmid. mTORC1 activation was analyzed by means of phospho-S6-positive cells quantification. Scale bar: 50 μm. **(B)** Western blot analysis of $CB_1$ receptor levels in the same conditions as above. Representative immunoblot luminograms for $CB_1$ and β-actin as loading control are shown and quantification is provided (mean ± SEM, $n = 3$). **(C)** $CB_1$ receptor promoter activity was analyzed using a CAT construct 24 h after transfection ($n = 6$). Statistical comparison versus the corresponding control samples, $^{**}p < 0.01$.

MRI and EEG showed absence of the lesion and normalization of hyperexcitability.

Considering the regulatory role of $CB_1$ receptors in cortical progenitor cell identity via mTORC1 signaling (Díaz-Alonso et al., 2015), we next sought to investigate the impact of the receptor in FCD-derived neurons. We obtained FCD Type II organotypic cultures derived from fresh resections that were maintained for 7 days *in vitro* and subjected to pharmacological manipulation. Quantification of phospho-S6 immunoreactivity revealed that $CB_1$ receptor activation with the cannabinoid agonist HU-210 was without effect on mTORC1 activation, whereas the mTORC1 inhibitor rapamycin was effective in reducing mTORC1 overactivation (**Figure 5A**). Western blot analysis confirmed that $CB_1$ receptor agonism did not influence mTORC1 activation, whereas the $CB_1$ inverse agonist SR141716 (rimonabant), as well as rapamycin, reduced mTORC1 activation as assessed by phosphoS240/244-S6 levels (**Figure 5B**). Equivalent results were obtained with the alternative phosphoS235/236-S6 antibody (**Supplementary Figure 2**). Overall, these results indicate that inhibition, but not activation of the $CB_1$ receptor, may tune the overactive mTORC1 pathway found in FCD Type II dysplastic brain.

## DISCUSSION

In the present study, we characterized the expression and function of the ECS to assess its potential contribution to the

**TABLE 3 |** Putative Tbr2 (Eomes) binding sites in the Cnr1 locus identified using MatInspector software.

| Species | Gene location | Binding site position | | Strand | Matrix similarity |
|---|---|---|---|---|---|
| | | Start | End | | |
| Human | 6q15 | 88164872 | 88164900 | + | 0.941 |
| | | 88166737 | 88166765 | + | 0.963 |
| | | 88166645 | 88166673 | + | 0.989 |
| | | 88166554 | 88166568 | + | 0.902 |
| | | 88168289 | 88168317 | + | 0.99 |
| Mouse | 4A5 | 33936594 | 33936608 | – | 0.896 |
| | | 33925880 | 33925908 | + | 0.901 |
| | | 33944561 | 33944589 | – | 0.999 |

**TABLE 4 |** Endocannabinoid system elements analyzed by qPCR in FCD Type II and control samples.

| Transcript | Condition | Mean | SEM | Significance |
|---|---|---|---|---|
| $CB_1$ | Control | 1.00 | 0.2397 | * |
| | FCDII | 33.70 | 5.3080 | |
| DAGLα | Control | 1.00 | 0.0004 | ns |
| | FCDII | 0.45 | 0.1286 | |
| DAGLβ | Control | 1.00 | 0.0106 | ns |
| | FCDII | 0.84 | 0.2274 | |
| MAGL | Control | 1.00 | 0.0005 | ns |
| | FCDII | 0.88 | 0.3061 | |
| NAPE-PLD | Control | 1.00 | 0.0264 | ns |
| | FCDII | 0.72 | 0.1176 | |
| FAAH | Control | 1.00 | 0.0182 | ns |
| | FCDII | 0.36 | 0.1910 | |

*Statistical comparison versus control tissue *$p < 0.05$. $CB_1$ transcript ($n = 4$ and 22, control and FCDII), other endocannabinoid system elements ($n = 4$ and 8 control and FCDII).*

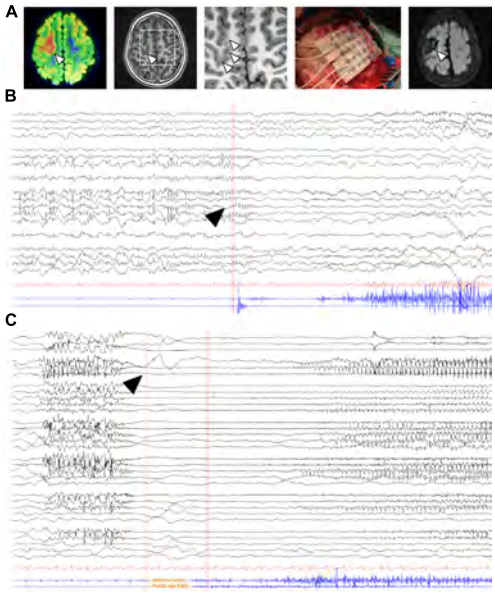


**FIGURE 4 |** EEG characterization of a representative FCD case subject to surgery. **(A)** FDG-PET scan co-registered with 3T MRI of a 5-year-old child affected by a "malignant rolandic epilepsy" with daily motor seizures and *Epilepsia Partialis Continua*. Hypermetabolic FDG-PET focus (arrowheads). Small focal cortical dysplasia involving the left rolandic region and superior frontal gyrus (arrowhead) and MRI 1 year after epilepsy surgery. **(B,C)** Scalp and intracraneal EEG recording, respectively, of the previous patient, using a combination of subdural electrodes and depth electrodes, prior resection of the epileptogenic zone. Arrowheads, indicate epileptiform activity.

etiopathology of MCDs, in particular FCD Type II. Our results reveal a striking increase in $CB_1$ receptor expression levels in FCD Type II, and this enrichment occurs in neurons with overactive mTORC1 signaling. In addition, characterization of genomic DNA in the dysplastic brain resections showed an enrichment of three SNPs in the *DAGLA* gene in FCD Type II versus controls. The SNPs analyzed in other ECS element genes did not show any difference between groups. In addition, sequencing of the *CNR1* coding exon did not reveal any SNP or mutation differentially present in FCD Type II versus control brains.

Presynaptic $CB_1$ receptors engaged by retrograde endocannabinoid messengers constitute an efficient regulatory mechanism of excessive neurotransmitter release. Hence, endocannabinoid signaling is a crucial pathway controlling neuronal activity and its activation or blockade modulates seizures and epilepsy development (Soltesz et al., 2015). Patients of temporal lobe epilepsy have decreased $CB_1$ receptor expression (Ludányi et al., 2008; Goffin et al., 2011). Likewise, selective loss of function of presynaptic $CB_1$ receptors in projection neuron populations of the mouse brain results in an imbalance of the excitatory/inhibitory tone and a higher susceptibility to seizures (Monory et al., 2006). Thus, the enrichment in $CB_1$ receptor expression in FCD lesions could represent a compensatory mechanism to attenuate the imbalance of excitatory/inhibitory neuronal activity. In addition, gene expression assays indicate that, at least for the $hCB_1$ receptor promoter employed (−3016 to +142 bp sequence), is not directly induced by overactive mTORC1 pathway, indicating that other signaling events control $CB_1$ receptor expression in this context.

SNPs analyses and genomic DNA sequencing of the *CNR1* exon did not reveal any mutation associated with FCD Type II. Alternatively, the potential involvement of 2-AG metabolism in FCD Type II is suggested by the existence of a selective enrichment in three SNPs of the *DAGLA* gene. The impact of the *DAGLA* SNPs found in our study in 2AG production or DAGL regulation, is yet unknown as they correspond to non-coding regions. Nevertheless *DAGLA* transcript levels were slightly reduced in FCD when compared to control tissue. These results are in agreement with a recent study that found *DAGLA* polymorphisms associated with neurodevelopmental disorders and seizures (Smith et al., 2017), while $CB_1$ receptor associated with pain sensitivity, sleep, memory or anxiety, but not seizures. $CB_1$ receptors are coupled to the mTORC1 signaling pathway

**TABLE 5 |** SNPs analyzed in Focal cortical dysplasia Type II and control brain genomic DNA extracts.

| SNP | Alleles | Major allele homozygous (%) | | Heterozygous (%) | | Minor allele homozygous (%) | | Disease association |
|---|---|---|---|---|---|---|---|---|
| | Major/Minor | Controls | FCD | Controls | FCD | Controls | FCD | |
| rs806365 | C/T | 20.0 | 36.4 | 70.0 | 45.4 | 10.0 | 18.2 | |
| rs7766029 | T/C | 20.0 | 31.8 | 50.0 | 54.5 | 30.0 | 13.6 | |
| rs806366 | T/C | 40.0 | 31.8 | 40.0 | 31.8 | 20.0 | 36.4 | |
| rs806368 | T/C | 60.0 | 54.5 | 20.0 | 36.4 | 20.0 | 9.0 | |
| rsl2720071 | A/G | 60.0 | 86.4 | 40.0 | 13.6 | 0.0 | 0.0 | |
| rs4707436 | G/A | 60.0 | 59.1 | 30.0 | 40.9 | 10.0 | 0.0 | |
| rsl049353 | G/A | 80.0 | 68.2 | 10.0 | 31.8 | 10.0 | 0.0 | |
| rs806369 | C/T | 60.0 | 45.5 | 30.0 | 40.9 | 10.0 | 13.6 | |
| rs2023239 | T/C | 60.0 | 63.6 | 40.0 | 36.4 | 0.0 | 0.0 | |
| rsl535255 | T/G | 70.0 | 63.6 | 30.0 | 36.4 | 0.0 | 0.0 | |
| rs806379 | A/T | 30.0 | 18.2 | 60.0 | 77.3 | 10.0 | 4.5 | |
| rs9444584 | C/T | 60.0 | 54.5 | 30.0 | 45.5 | 10.0 | 0.0 | |
| rs9450898 | C/T | 70.0 | 63.6 | 30.0 | 36.4 | 0.0 | 0.0 | |
| rs806380 | A/G | 60.0 | 54.5 | 30.0 | 40.9 | 10.0 | 4.5 | |
| rs6454674 | T/G | 40.0 | 63.6 | 40.0 | 31.8 | 20.0 | 4.5 | |
| rs2180619 | A/G | 30.0 | 31.8 | 50.0 | 45.5 | 20.0 | 22.7 | |
| rs4963304 | G/A | 10.0 | 68.2 | 50.0 | 31.8 | 40.0 | 0.0 | * |
| rs7931563 | T/G | 50.0 | 40.9 | 50.0 | 40.9 | 0.0 | 18.2 | |
| rs7942387 | C/A | 90.0 | 100.0 | 10.0 | 0.0 | 0.0 | 0.0 | |
| rsl98430 | C/T | 30.0 | 77.3 | 40.0 | 22.7 | 30.0 | 0.0 | * |
| rsl98444 | T/C | 40.0 | 4.5 | 60.0 | 45.5 | 0.0 | 50.0 | * |
| rs34365114 | G/A | 100.0 | 95.5 | 0.0 | 4.5 | 0.0 | 0.0 | |
| rsl44674730 | C/T | 100.0 | 100.0 | 0.0 | 0.0 | 0.0 | 0.0 | |
| rsl43650244 | AAA/- | 90.0 | 100.0 | 10.0 | 0.0 | 0.0 | 0.0 | |
| rsl87296513 | C/T | 100.0 | 100.0 | 0.0 | 0.0 | 0.0 | 0.0 | |
| rs3813518 | G/A | 50.0 | 77.3 | 50.0 | 18.2 | 0.0 | 4.5 | |
| rs3813517 | A/G | 100.0 | 95.5 | 0.0 | 4.5 | 0.0 | 0.0 | |
| rs836559 | C/G | 10.0 | 36.4 | 40.0 | 45.4 | 50.0 | 18.2 | |
| rs2303361 | T/C | 40.0 | 72.8 | 30.0 | 22.7 | 30.0 | 4.5 | |
| rs76802560 | G/T | 100.0 | 100.0 | 0.0 | 0.0 | 0.0 | 0.0 | |
| rs6801421 | G/A | 90.0 | 63.6 | 10.0 | 36.4 | 0.0 | 0.0 | |
| rs72969613 | C/T | 100.0 | 100.0 | 0.0 | 0.0 | 0.0 | 0.0 | |
| rs4881 | A/G | 70.0 | 81.8 | 20.0 | 18.2 | 10.0 | 0.0 | |
| rsll5970931 | A/G | 100.0 | 100.0 | 0.0 | 0.0 | 0.0 | 0.0 | |
| rs932816 | G/A | 80.0 | 50.0 | 20.0 | 45.5 | 0.0 | 4.5 | |
| rs4141964 | G/A | 30.0 | 40.9 | 30.0 | 40.9 | 40.0 | 18.2 | |
| rs324420 | C/A | 30.0 | 59.1 | 50.0 | 22.7 | 20.0 | 18.2 | |
| rs324419 | G/A | 80.0 | 81.8 | 20.0 | 18.2 | 0.0 | 0.0 | |
| rs2295632 | C/A | 30.0 | 54.5 | 40.0 | 27.3 | 30.0 | 18.2 | |
| rsl2029329 | G/C | 30.0 | 54.5 | 40.0 | 27.3 | 30.0 | 18.2 | |
| rsl2744386 | C/T | 10.0 | 31.8 | 70.0 | 50.0 | 20.0 | 18.2 | |
| rsll30321 | A/G | 20.0 | 27.3 | 80.0 | 54.5 | 20.0 | 18.2 | |
| rsll06 | G/C | 20.0 | 27.3 | 80.0 | 54.5 | 20.0 | 18.2 | |
| rs2229579 | C/T | 70.0 | 63.6 | 30.0 | 27.3 | 0.0 | 9.1 | |
| rs2501431 | A/G | 20.0 | 27.3 | 80.0 | 54.5 | 20.0 | 18.2 | |
| rs41311993 | G/T | 100.0 | 100.0 | 0.0 | 0.0 | 0.0 | 0.0 | |
| rs35761398 | CC/TT | 20.0 | 23.8 | 80.0 | 57.2 | 20.0 | 19.0 | |
| rs2501432 | C/T | 20.0 | 27.3 | 80.0 | 54.5 | 20.0 | 18.2 | |

*Major and minor allele's distribution in control and focal cortical dysplasia (FCD) Type II. Disease association *$p < 0.05$.*

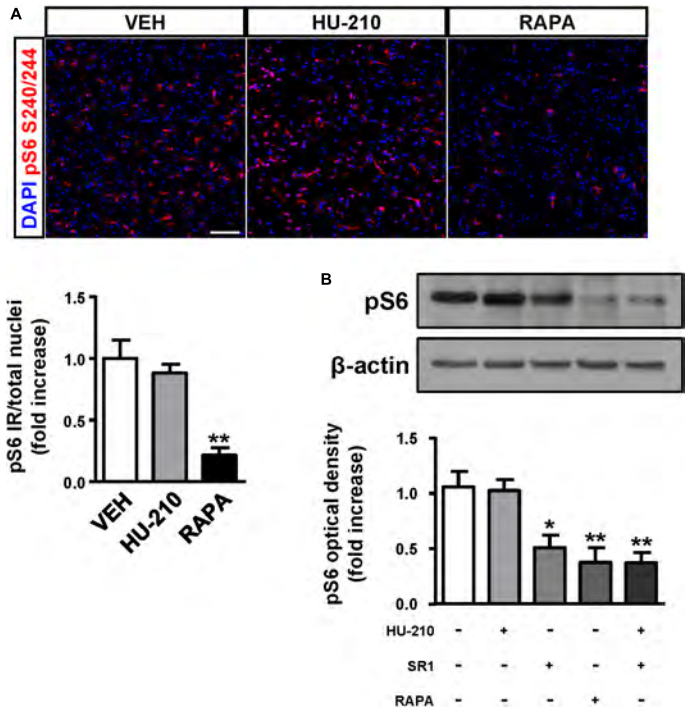


**FIGURE 5 |** $CB_1$ receptors blockade attenuates mTORC1 overactivation in FCD organotypic cultures. Organotypic cultures of FCD resections were cultured 7 days *in vitro* and exposed to the $CB_1$ receptor agonist HU-210 (1 μM), and rapamycin (1 μM) 90 min. **(A)** Representative images of immunofluorescence characterization with phospho-$S6_{S240/244}$ antibody were quantified and phosphoS6 immunoreactivity was referred to the total number of cells revealed by DAPI counterstaining. **(B)** Western blot analysis of phospho-$S6_{S240/244}$ levels was performed in slice extracts after 90 min incubation with HU-210 alone or together with SR141716 (25 μM), SR141716 or rapamycin ($n$ = 4 experiments). Statistical comparison *versus* vehicle samples, $^*p < 0.05$; $^{**}p < 0.01$. Scale bar: 80 μm.

at early stages of neocortex formation (Díaz-Alonso et al., 2015) as well as in the adult brain (Puighermanal et al., 2009). We therefore analyzed $CB_1$ receptor downstream signaling in FCD-derived organotypic slices. The $CB_1$ agonist HU-210 was unable to further increase mTORC1 activation, reflecting that the pathway is already overactive. Remarkably, the $CB_1$ inverse agonist rimonabant was efficient in reducing phospho-S6 levels. This is of interest, as dampening overactive $CB_1$ receptor activity with rimonabant in other settings as the Fmr1 knockout mice efficiently decreases exacerbated mTORC1 activity and symptoms (Busquets-Garcia et al., 2013). Thus, these results point to a basal cannabinoid signaling tone that sustains exacerbated mTORC1 activity in FCD Type II. The ribosomal S6 protein is regulated by phosphorylation at multiple sites (Meyuhas, 2015). S6 phosphorylation at Ser240/244 is selectively mediated by S6K1/2 providing a better readout of mTORC1 upstream activation, while Ser235/236 phosphorylation is regulated by different signaling pathways (cAMP/PKA, casein kinase 1, MAPK-activated protein kinase-1 and mTORC1/S6K1/2). Initial studies revealed increased levels of phosphoS235/236-S6 protein in FCD and TSC (Baybis et al., 2004; Aronica et al., 2007). More recently, somatic mutations of MTOR signaling pathway and other upstream regulators PI3K/Akt, TSC1, TSC2, DEPDC5 have been demonstrated in FCD Type II (Jansen et al., 2015; Lim et al., 2015; Ricos et al., 2016). Hence, phosphorylation of S6 protein by different mechanisms may have different functional consequences in FCD and may differ among neural cell types (Ljungberg et al., 2006; Biever et al., 2015). Considering the finding that $CB_1$ receptor antagonism attenuates the phosphorylation of the ribosomal S6 protein at different amino acids (Ser235/236 and Ser240/244) it can be predicted that different $CB_1$ downstream signaling effectors: cyclic AMP-mediated and cAMP-independent (PI3K/Akt-mediated) contribute to its regulation. Hence, regulation of cannabinoid signaling constitutes and attractive target for various mTOR-associated disorders and symptoms -the so-called "mTORopathies". Cannabidiol, a non-psychotomimetic cannabinoid with multiple targets, marketed as Epidiolex (GW Pharma), has demonstrated its efficacy as antiepileptic drug in refractory epilepsy including TSC, Dravet and Lennox-Gastaut syndromes, and is under clinical trial for FCDs (Devinsky et al., 2015; Hess et al., 2016; Thiele et al., 2018).

Interestingly, FCD type II is believed to be originated from the dorsal telencephalic progenitor cell compartment and their excitatory neuronal progeny (D'Gama et al., 2017). Noteworthy, in mTORopathies experimental models of MCDs unbalanced deep and upper layer neuronal development occurs as consequence of aberrant expression of neural fate determinants. Hence, a contribution of $CB_1$ receptor signaling to neural precursor alterations responsible for FCD Type II cannot be excluded. The consequences of $CB_1$ receptor activity during development and later in the adult brain can be intrinsically different. During embryonic development, $CB_1$ receptor controls radial glial to intermediate progenitor cell transition via mTORC1 signaling (Díaz-Alonso et al., 2015), and later, at postmitotic stages, tunes deep cortical neuronal differentiation (Mulder et al., 2008; Díaz-Alonso et al., 2012). Thus, $CB_1$ receptor activity during embryonic stages controls progenitor proliferation and neuronal differentiation, and alterations in cannabinoid signaling have the potential to evoke long-term neuronal plasticity and abnormalities underlying FCD neuronal hyperexcitability. In animal models, conditional ablation of the $CB_1$ receptor during embryonic development results in increased RhoA levels, ectopic neuron accumulations and increased seizure susceptibility (Díaz-Alonso et al., 2017). Noteworthy, RhoA knockdown prevents brain hyperexcitability and projection neuron alterations induced by $CB_1$ receptor ablation. Therefore, either hyper- or hypoactive endocannabinoid signaling during cortical development can be responsible for neuronal differentiation and positioning deficits contributing to MCDs. Later, in adult brain, when neuronal activity is established, the neuromodulatory function of the ECS takes place. The precise consequences of $CB_1$ receptor activity in the hyperexcitability neuronal circuit of the dysplastic brain remain unknown. Among other mechanisms involved in FCD, decreased hyperpolarization-activated non-specific cation currents contribute to pyramidal layer V hyperexcitability (Albertson et al., 2011). Interestingly, a particular pool of somatodendritic $CB_1$ receptors can regulate Ih currents and this explains in turn some of the cognitive consequences of $CB_1$ signaling (Maroso et al., 2016).

This study highlights the pathological implications of altered developmental cannabinoid signaling in refractory epilepsy. Characterization of epileptogenic FCD tissue from palliative surgery and dysplastic-derived organotypic cultures indicates that increased $CB_1$ receptor signaling may constitute a compensatory mechanism to counteract FCD Type II hyperexcitability, and its antagonism can dampen mTORC1 overactivation. We anticipate that in the near future new genetic linkage association analyses using larger cohorts of patients with pediatric epilepsy could provide further support to cannabinoid signaling deregulation as a causal mechanism underlying refractory epilepsy.

## ETHICS STATEMENT

This study was carried out in accordance with the recommendations of "Hospital Universitario Niño Jesús Madrid, Ethic committee" with written informed consent from all subjects. All subjects gave written informed consent in accordance with the Declaration of Helsinki. The protocol was approved by the "Ethic committee of Hospital Universitario Niño Jesús Madrid".

## AUTHOR CONTRIBUTIONS

DG-R, JD-A, ZO, AdS-Q, JP-L, JA, and CJ obtained the samples, processed them, and performed the experiments. IdP, VM-C, EA, and MP-J were in charge of resection handling and determination of the dysplastic areas that were analyzed. MG, MP-J, and IG-R designed the study, analyzed the data, and wrote the manuscript.

## FUNDING

This study was funded by Instituto de Salud Carlos III (#PI15-0310 #PI18-00941, Plan Estatal de I+D+i to IG-R) and co-financed by the European Development Regional Fund "A way to achieve Europe" (EDRF), Spanish Ministerio de Economía y Competitividad (co-funded by the EDRF in the Framework of the Operative Program "Reinforcement of Research, Technological Development and Innovation" RTC-2015-3364-1 to IG-R and MINECO/FEDER, grant SAF2015-64945-R to MG). EA is supported by EPISTOP (grant 603291). JD-A was supported by a PFIS program fellowship co-financed by the European Social Fund "El FSE invierte en tu futuro" (ESF). DG-R, AdS-Q, JP-L, and JA were supported by Fundación Tatiana Pérez de Guzmán el Bueno (DG-R) and Ministerio de Educación, Cultura y Deporte (FPU program), respectively. The genotyping service was carried out at CEGEN-PRB2-ISCIII, it is supported by grant PT13/0001, ISCIII-SGEFI / FEDER.

## SUPPLEMENTARY MATERIAL

The Supplementary Material for this article can be found online at: https://www.frontiersin.org/articles/10.3389/fphar.2018.01508/full#supplementary-material

## REFERENCES

Albertson, A. J., Yang, J., and Hablitz, J. J. (2011). Decreased hyperpolarization-activated currents in layer 5 pyramidal neurons enhances excitability in focal cortical dysplasia. *J. Neurophysiol.* 106, 2189–2200. doi: 10.1152/jn.00164.2011

Arai, A., Saito, T., Hanai, S., Sukigara, S., Nabatame, S., Otsuki, T., et al. (2012). Abnormal maturation and differentiation of neocortical neurons in epileptogenic cortical malformation: unique distribution of layer-specific marker cells of focal cortical dysplasia and hemimegalencephaly. *Brain Res.* 1470, 89–97. doi: 10.1016/j.brainres.2012.06.009

Argaw, A., Duff, G., Zabouri, N., Cécyre, B., Chainé, N., Cherif, H., et al. (2011). Concerted action of CB1 cannabinoid receptor and deleted in colorectal cancer in axon guidance. *J. Neurosci.* 31, 1489–1499. doi: 10.1523/JNEUROSCI.4134-09.2011

Aronica, E., Boer, K., Baybis, M., Yu, J., and Crino, P. (2007). Co-expression of cyclin D1 and phosphorylated ribosomal S6 proteins in hemimegalencephaly. *Acta Neuropathol.* 114, 287–293. doi: 10.1007/s00401-007-0225-6

Aronica, E., and Crino, P. B. (2014). Epilepsy related to developmental tumors and malformations of cortical development. *Neurotherapeutics* 11, 251–268. doi: 10.1007/s13311-013-0251-0

Baybis, M., Yu, J., Lee, A., Golden, J. A., Weiner, H., McKhann, G., et al. (2004). mTOR cascade activation distinguishes tubers from focal cortical dysplasia. *Ann. Neurol.* 56, 478–487. doi: 10.1002/ana.20211

Berghuis, P., Dobszay, M. B., Wang, X., Spano, S., Ledda, F., Sousa, K. M., et al. (2005). Endocannabinoids regulate interneuron migration and morphogenesis by transactivating the TrkB receptor. *Proc. Natl. Acad. Sci. U.S.A.* 102, 19115–19120. doi: 10.1073/pnas.0509494102

Berghuis, P., Rajnicek, A. M., Morozov, Y. M., Ross, R. A., Mulder, J., Urban, G. M., et al. (2007). Hardwiring the brain: endocannabinoids shape neuronal connectivity. *Science* 316, 1212–1216. doi: 10.1126/science.1137406

Biever, A., Puighermanal, E., Nishi, A., David, A., Panciatici, C., Longueville, S., et al. (2015). PKA-dependent phosphorylation of ribosomal protein S6 does not correlate with translation efficiency in striatonigral and striatopallidal medium-sized spiny neurons. *J. Neurosci.* 35, 4113–4130. doi: 10.1523/JNEUROSCI.3288-14.2015

Blázquez, C., Chiarlone, A., Sagredo, O., Aguado, T., Pazos, M. R., Resel, E., et al. (2011). Loss of striatal type 1 cannabinoid receptors is a key pathogenic factor in huntington's disease. *Brain* 134, 119–136. doi: 10.1093/brain/awq278

Blümcke, I., Thom, M., Aronica, E., Armstrong, D. D., Vinters, H. V., Palmini, A., et al. (2011). The clinicopathologic spectrum of focal cortical dysplasias: a consensus classification proposed by an ad hoc task force of the ILAE diagnostic methods commission. *Epilepsia* 52, 158–174. doi: 10.1111/j.1528-1167.2010.02777.x

Busquets-Garcia, A., Gomis-González, M., Guegan, T., Agustín-Pavón, C., Pastor, A., Mato, S., et al. (2013). Targeting the endocannabinoid system in the treatment of fragile X syndrome. *Nat. Med.* 19, 603–607. doi: 10.1038/nm.3127

de Salas-Quiroga, A., Díaz-Alonso, J., García-Rincón, D., Remmers, F., Vega, D., Gómez-Cañas, M., et al. (2015). Prenatal exposure to cannabinoids evokes long-lasting functional alterations by targeting CB 1 receptors on developing cortical neurons. *Proc. Natl. Acad. Sci.* 112, 13693–13698. doi: 10.1073/pnas.1514962112

Devinsky, O., Marsh, E., Friedman, D., Thiele, E., Laux, L., Sullivan, J., et al. (2015). Cannabidiol in patients with treatment-resistant epilepsy: an open-label interventional trial. *Lancet Neurol.* 15, 270–278. doi: 10.1016/S1474-4422(15)00379-8

D'Gama, A. M., Woodworth, M. B., Hossain, A. A., Bizzotto, S., Hatem, N. E., LaCoursiere, C. M., et al. (2017). Somatic mutations activating the mTOR pathway in dorsal telencephalic progenitors cause a continuum of cortical dysplasias. *Cell Rep.* 21, 3754–3766. doi: 10.1016/j.celrep.2017.11.106

Díaz-Alonso, J., Aguado, T., de Salas-Quiroga, A., Ortega, Z., Guzmán, M., and Galve-Roperh, I. (2015). CB1 cannabinoid receptor-dependent activation of mTORC1/Pax6 signaling drives Tbr2 expression and basal progenitor expansion in the developing mouse cortex. *Cereb. Cortex* 25, 2395–2408. doi: 10.1093/cercor/bhu039

Díaz-Alonso, J., Aguado, T., Wu, C.-S., Palazuelos, J., Hofmann, C., Garcez, P., et al. (2012). The CB(1) cannabinoid receptor drives corticospinal motor neuron differentiation through the Ctip2/Satb2 transcriptional regulation axis. *J. Neurosci.* 32, 16651–16665. doi: 10.1523/JNEUROSCI.0681-12.2012

Díaz-Alonso, J., De Salas-Quiroga, A., Paraíso-Luna, J., García-Rincón, D., Garcez, P. P., Parsons, M., et al. (2017). Loss of cannabinoid cb1receptors induces cortical migration malformations and increases seizure susceptibility. *Cereb. Cortex* 27, 5303–5317. doi: 10.1093/cercor/bhw309

Eugène, E., Cluzeaud, F., Cifuentes-Diaz, C., Fricker, D., Le Duigou, C., Clemenceau, S., et al. (2014). An organotypic brain slice preparation from adult patients with temporal lobe epilepsy. *J. Neurosci. Methods* 235, 234–244. doi: 10.1016/j.jneumeth.2014.07.009

Goffin, K., Van Paesschen, W., and Van Laere, K. (2011). In vivo activation of endocannabinoid system in temporal lobe epilepsy with hippocampal sclerosis. *Brain* 134, 1033–1040. doi: 10.1093/brain/awq385

Hadjivassiliou, G., Martinian, L., Squier, W., Blumcke, I., Aronica, E., Sisodiya, S. M., et al. (2010). The application of cortical layer markers in the evaluation of cortical dysplasias in epilepsy. *Acta Neuropathol.* 120, 517–528. doi: 10.1007/s00401-010-0686-x

Hess, E. J., Moody, K. A., Geffrey, A. L., Pollack, S. F., Skirvin, L. A., Bruno, P. L., et al. (2016). Cannabidiol as a new treatment for drug-resistant epilepsy in tuberous sclerosis complex. *Epilepsia* 7, 1617–1624. doi: 10.1111/EPI.13499

Iffland, P. H., Baybis, M., Barnes, A. E., Leventer, R. J., Lockhart, P. J., and Crino, P. B. (2018). DEPDC5 and NPRL3 modulate cell size, filopodial outgrowth, and localization of mTOR in neural progenitor cells and neurons. *Neurobiol. Dis.* 114, 184–193. doi: 10.1016/j.nbd.2018.02.013

Iffland, P. H., and Crino, P. B. (2017). Focal cortical dysplasia: gene mutations, cell signaling, and therapeutic implications. *Annu. Rev. Pathol. Mech. Dis.* 12, 547–571. doi: 10.1146/annurev-pathol-052016-100138

Jansen, L. A., Mirzaa, G. M., Ishak, G. E., O'Roak, B. J., Hiatt, J. B., Roden, W. H., et al. (2015). PI3K/AKT pathway mutations cause a spectrum of brain malformations from megalencephaly to focal cortical dysplasia. *Brain* 138, 1613–1628. doi: 10.1093/brain/awv045

Lim, J. S., Kim, W. I., Kang, H. C., Kim, S. H., Park, A. H., Park, E. K., et al. (2015). Brain somatic mutations in MTOR cause focal cortical dysplasia type II leading to intractable epilepsy. *Nat. Med.* 21, 395–400. doi: 10.1038/nm.3824

Ljungberg, M. C., Bhattacharjee, M. B., Lu, Y., Armstrong, D. L., Yoshor, D., Swann, J. W., et al. (2006). Activation of mammalian target of rapamycin in cytomegalic neurons of human cortical dysplasia. *Ann. Neurol.* 60, 420–429. doi: 10.1002/ana.20949

Ludányi, A., Eross, L., Czirják, S., Vajda, J., Halász, P., Watanabe, M., et al. (2008). Downregulation of the CB1 cannabinoid receptor and related molecular elements of the endocannabinoid system in epileptic human hippocampus. *J. Neurosci.* 28, 2976–2990. doi: 10.1523/JNEUROSCI.4465-07.2008

Maroso, M., Szabo, G. G., Kim, H. K., Alexander, A., Bui, A. D., Lee, S. H., et al. (2016). Cannabinoid control of learning and memory through HCN Channels. *Neuron* 89, 1059–1073. doi: 10.1016/j.neuron.2016.01.023

Mato, S., Del Olmo, E., and Pazos, A. (2003). Ontogenetic development of cannabinoid receptor expression and signal transduction functionality in the human brain. *Eur. J. Neurosci.* 17, 1747–1754. doi: 10.1046/j.1460-9568.2003.02599.x

Meyuhas, O. (2015). Ribosomal protein S6 phosphorylation. *Int. Rev. Cell Mol. Biol.* 320, 41–73. doi: 10.1016/bs.ircmb.2015.07.006

Monory, K., Massa, F., Egertová, M., Eder, M., Blaudzun, H., Westenbroek, R., et al. (2006). The Endocannabinoid system controls key epileptogenic circuits in the hippocampus. *Neuron* 51, 455–466. doi: 10.1016/j.neuron.2006.07.006

Morcillo-Suarez, C., Alegre, J., Sangros, R., Gazave, E., de Cid, R., Milne, R., et al. (2008). SNP analysis to results (SNPator): a web-based environment oriented to statistical genomics analyses upon SNP data. *Bioinformatics* 24, 1643–1644. doi: 10.1093/bioinformatics/btn241

Mulder, J., Aguado, T., Keimpema, E., Barabás, K., Ballester Rosado, C. J., Nguyen, L., et al. (2008). Endocannabinoid signaling controls pyramidal cell specification and long-range axon patterning. *Proc. Natl. Acad. Sci. U.S.A.* 105, 8760–8765. doi: 10.1073/pnas.0803545105

Najm, I. M., Sarnat, H. B., and Blümcke, I. (2018). Review: the international consensus classification of focal cortical dysplasia - a critical update 2018. *Neuropathol. Appl. Neurobiol.* 44, 18–31. doi: 10.1111/nan.12462

Orlova, K. A., Tsai, V., Baybis, M., Heuer, G. G., Sisodiya, S., Thom, M., et al. (2010). Early progenitor cell marker expression distinguishes type II from type I focal cortical dysplasias. *J. Neuropathol. Exp. Neurol.* 69, 850–863. doi: 10.1097/NEN.0b013e3181eac1f5

Puighermanal, E., Marsicano, G., Busquets-Garcia, A., Lutz, B., Maldonado, R., and Ozaita, A. (2009). Cannabinoid modulation of hippocampal long-term memory is mediated by mTOR signaling. *Nat. Neurosci.* 12, 1152–1158. doi: 10.1038/nn.2369

Ricos, M. G., Hodgson, B. L., Pippucci, T., Saidin, A., Ong, Y. S., Heron, S. E., et al. (2016). Mutations in the mammalian target of rapamycin pathway regulators NPRL2 and NPRL3 cause focal epilepsy. *Ann. Neurol.* 79, 120–131. doi: 10.1002/ana.24547

Smith, D. R., Stanley, C. M., Foss, T., Boles, R. G., and McKernan, K. (2017). Rare genetic variants in the endocannabinoid system genes CNR1 and DAGLA are associated with neurological phenotypes in humans. *PLoS One* 12:e0187926. doi: 10.1371/journal.pone.0187926

Soltesz, I., Alger, B. E., Kano, M., Lee, S.-H., Lovinger, D. M., Ohno-Shosaku, T., et al. (2015). Weeding out bad waves: towards selective cannabinoid circuit control in epilepsy. *Nat. Rev. Neurosci.* 16, 264–277. doi: 10.1038/nrn3937

Thiele, E. A., Marsh, E. D., French, J. A., Mazurkiewicz-Beldzinska, M., Benbadis, S. R., Joshi, C., et al. (2018). Cannabidiol in patients with seizures associated with lennox-gastaut syndrome (GWPCARE4): a randomised, double-blind, placebo-controlled phase 3 trial. *Lancet* 391, 1085–1096. doi: 10.1016/S0140-6736(18)30136-3

Wang, X., Dow-Edwards, D., Keller, E., and Hurd, Y. L. (2003). Preferential limbic expression of the cannabinoid receptor mRNA in the human fetal brain. *Neuroscience* 118, 681–694. doi: 10.1016/S0306-4522(03)00020-4

Yao, K., Duan, Z., Zhou, J., Li, L., Zhai, F., Dong, Y., et al. (2016). Clinical and immunohistochemical characteristics of type II and type I focal cortical dysplasia. *Oncotarget* 7, 76415–76422. doi: 10.18632/oncotarget.13001

Zurolo, E., Iyer, A. M., Spliet, W. G. M., Van Rijen, P. C., Troost, D., Gorter, J. A., et al. (2010). CB1 and CB2 cannabinoid receptor expression during development and in epileptogenic developmental pathologies. *Neuroscience* 170, 28–41. doi: 10.1016/j.neuroscience.2010.07.004

**Conflict of Interest Statement:** The authors declare that the research was conducted in the absence of any commercial or financial relationships that could be construed as a potential conflict of interest.

Aguareles et al. Translational Neurodegeneration (2019) 8:9
https://doi.org/10.1186/s40035-019-0148-x

Translational Neurodegeneration

RESEARCH Open Access

# Oral administration of the cannabigerol derivative VCE-003.2 promotes subventricular zone neurogenesis and protects against mutant huntingtin-induced neurodegeneration

José Aguareles[1,2,3], Juan Paraíso-Luna[1,2,3], Belén Palomares[4,5,6], Raquel Bajo-Grañeras[1,2,3], Carmen Navarrete[7], Andrea Ruiz-Calvo[1,2,3], Daniel García-Rincón[1,2,3], Elena García-Taboada[1,2,3], Manuel Guzmán[1,2,3], Eduardo Muñoz[4,5,6] and Ismael Galve-Roperh[1,2,3*]

## Abstract

**Background:** The administration of certain cannabinoids provides neuroprotection in models of neurodegenerative diseases by acting through various cellular and molecular mechanisms. Many cannabinoid actions in the nervous system are mediated by $CB_1$ receptors, which can elicit psychotropic effects, but other targets devoid of psychotropic activity, including $CB_2$ and nuclear PPARγ receptors, can also be the target of specific cannabinoids.

**Methods:** We investigated the pro-neurogenic potential of the synthetic cannabigerol derivative, VCE-003.2, in striatal neurodegeneration by using adeno-associated viral expression of mutant huntingtin *in vivo* and mouse embryonic stem cell differentiation *in vitro*.

**Results:** Oral administration of VCE-003.2 protected striatal medium spiny neurons from mutant huntingtin-induced damage, attenuated neuroinflammation and improved motor performance. VCE-003.2 bioavailability was characterized and the potential undesired side effects were evaluated by analyzing hepatotoxicity after chronic treatment. VCE-003.2 promoted subventricular zone progenitor mobilization, increased doublecortin-positive migrating neuroblasts towards the injured area, and enhanced effective neurogenesis. Moreover, we demonstrated the proneurogenic activity of VCE-003.2 in embryonic stem cells. VCE-003.2 was able to increase neuroblast formation and striatal-like CTIP2-mediated neurogenesis.

**Conclusions:** The cannabigerol derivative VCE-003.2 improves subventricular zone-derived neurogenesis in response to mutant huntingtin-induced neurodegeneration, and is neuroprotective by oral administration.

**Keywords:** Cannabinoid, Huntingtin, Neurodegeneration, Neurogenesis, PPAR

* Correspondence: igr@quim.ucm.es
[1]Instituto Ramón y Cajal de Investigación Sanitaria (IRYCIS), Ctra. Colmenar Viejo, km, 9100 Madrid, Spain
[2]Departamento de Bioquímica y Biología Molecular and Instituto Universitario de Investigación Neuroquímica, Universidad Complutense, Madrid, Spain
Full list of author information is available at the end of the article

## Background

Huntington's disease (HD) is a monogenic neurodegenerative disease produced by the expression of mutant huntingtin (htt) protein with expanded glutamine repeats in the N-terminal portion of the protein [1]. Mutant htt expression induces striatal atrophy and medium spiny neuron (MSN) death, which is responsible for the characteristic motor symptoms of the disease. The length of the polyglutamine tract expansion in the htt gene, higher than 40 repeats, is closely associated with disease onset. Hence, although HD neurodegeneration occurs in adult brain, mutant htt expression is also known to interfere with normal neurodevelopment at several levels. Mutant huntingtin interferes with the activity of various transcription factors (GSX2+, ASCL1+, ISLT1+, NKX2.1) that are essential in controlling cortical and striatal neurogenesis [2, 3]. Among others, mutant huntingtin decreases NeuroD1 activity, a transcription factor that acts as a major confluence node of different neurodevelopmental gene pathways [3]. Mutant huntingtin also alters the mode of division of subventricular zone (SVZ) progenitors by influencing mitotic spindle orientation, that in turn controls asymmetric cell division and neurogenesis [4]. Moreover, mutant huntingtin expression interferes with projection neuron migration as normal huntingtin regulates Rab11-mediated N-cadherin trafficking [5].

Certain cannabinoids, the main active compounds of *Cannabis sativa*, and their endogenous counterparts 2-arachidonoylglycerol and anandamide exert symptomatic relief in various neurodegenerative and neuroinflammatory conditions [6]. Neuroprotection in mouse HD models as induced by $\Delta^9$-tetrahydrocannabinol (THC), the most abundant bioactive compound of *Cannabis sativa*, occurs at least in part in a cell-autonomous manner via the $CB_1$ receptor [7]. Unfortunately, considering that $CB_1$ receptor levels notably diminish at early stages of HD [8–10], and that $CB_1$ receptor agonists produce undesired psychoactive effects [11], the development of clinical treatments based on $CB_1$-receptor acting cannabinoids constitutes an extremely complicated task. Hence, investigating the potential use of cannabinoids other than THC, with different pharmacological profiles, constitutes an interesting research area for the development of new candidate molecules with reduced unwanted actions. Cannabigerol (CBG) is a non-psychoactive cannabinoid that has been tested as a candidate molecule for pharmacological therapies in HD experimental models [12]. CBG via the nuclear receptor peroxisome proliferator-activated receptor-γ (PPARγ) alleviates motor symptoms, neuroinflammation and neurodegeneration in murine models of HD based on either striatal neurotoxicity (3-nitropropionic acid injection model) or transgenic expression of human mutant huntingtin exon 1 (R6/2 model) [12]. Of interest, thiazolidinedione-induced PPARγ activation is neuroprotective against mutant huntingtin-induced cell death and reduce huntingtin aggregates in the brain [13]. In order to improve the pharmacological profile of CBG, chemical modifications were introduced, leading to the CBG quinone derivatives VCE-003 and VCE-003.2 [14, 15]. VCE-003.2 ([2-(3,7-dimethyl-octa-2, 6-dienyl)-6-ethylamino-3-hydroxy-5-pentyl-(1,4) benzoquinone]), an aminoquinone derivative of CBG, improves the pharmacological profile of VCE-003 by eliminating the characteristic side effects of potent PPARγ activators. Fundamentally, VCE-003.2 is neuroprotective in the quinolinic acid-administration model of HD and increases neural progenitor survival [14]. In the present study, we evaluated the neuroprotective efficacy of oral VCE-003.2 administration. Noteworthy, oral VCE-003.2 was neuroprotective against mutant huntingtin-induced damage, and also improved SVZ-derived neurogenesis. Overall, these findings provide further support to the neuroprotective and anti-inflammatory activities of VCE-003.2, and suggests its potential as a disease-modifying agent, considering its ability to improve the endogenous neurogenic response.

## Methods

### Cell culture and reagents

All reagents, unless indicated, were from Sigma-Aldrich (St. Louis, MO, USA). The synthesis and structure of VCE-003.2 were previously described [14, 15]. Mouse embryonic teratocarcinoma P19 were cultured in high-glucose DMEM (Invitrogen) supplemented with 10% fetal bovine serum and 1% penicillin/streptomycin. P19 cells were plated in 24-well plates and transfected with Lipofectamine 2000 reagent according to the manufacture's protocol (Invitrogen). Twenty-four hours post transfection, cells were collected for RNA extraction or luciferase assay determinations. P19 neurosphere formation assay was performed using dissociated P19 cells cultured in high-glucose DMEM (Invitrogen) supplemented with 5% of fetal bovine serum and 0. 5 μM retinoic acid. Twenty-four hours later the mean neurosphere size was quantified. Luciferase construct with the MAR sequence A4 of the Ctip2 promoter was kindly provided (R. Grosschedl, Max-Planck-Institute of Immunobiology and Epigenetics, Freiburg, Germany).

### Mouse embryonic stem cell differentiation

R1 mouse embryonic stem (mES) cell line was grown on gelatin 0.1%, in Knockout DMEM supplemented with 20% Knockout Serum Replacement, 1000 U ml-1 of LIF, 0.1 mM of non-essential amino acids, 2 mM ultraglutamine, 50 U ml-1 of penicillin and streptomycin and 0.1 mM of 2-mercaptoethanol. Cells were then differentiated at low density in Defined Default Medium (DDM) containing DMEM/F12 + GlutaMAX supplemented with N2 supplement (1×), 5 mM of Hepes Buffer, 0.1 mM of

non-essential amino acids, 1 mM of sodium pyruvate, 2.5 mg ml-1 of AlbuMax-I, 30 mM of D-Glucose, 0.1 mM of non-essential amino acids, 0.1 mM of 2-mercaptoethanol, 50 U ml-1 of penicillin and streptomycin for 12 days. The cells were then plated on polylysine/laminin-coated dishes in 50% DDM and 50% Neurobasal/B27 containing Neurobasal supplemented with B27 (1×), 2 mM of Ultraglutamine and 50 U ml-1 of penicillin and streptomycin for 9 days.

### Luciferase transcriptional assays

To study CTIP2 transcriptional activity P19 cells were seeded in 24-well plates and transiently co-transfected with the luciferase reporter vector MARS-A4-luc [16] using Roti-Fect (Carl Roth, Karlsruhe, Germany) following the manufacturer's instructions. To correct for transfection efficacy, 100 ng *Renilla* luciferase (pRL-CMV) was also cotransfected. After stimulation, the luciferase activities were quantified using Dual-Luciferase Assay (Promega, Madison, WI, USA).

### Mutant huntingtin-induced neurodegeneration

Male C57BL/6 N mice (10 weeks old) were housed under standard conditions (12-h light/dark cycle) in groups with access to food and water *ad libitum*. All experiments were performed in accordance with European Union guidelines and approved by the Animal Research Ethics Committee of Complutense and Córdoba University. Procedures were designed to minimize the number of animals used and their suffering. Constructs expressing CFP-tagged human huntingtin exon 1 harboring a pathogenic polyQ tract of 94 CAG repeats or a normal, non-pathogenic polyQ tract of 16 CAG repeats (kindly provided by Dr. José J. Lucas, Severo Ochoa Molecular Biology Center, Madrid, Spain) were employed using an AAV1/AAV2 mixed serotype, generated by polyethyleneimine transfection of HEK293T cells and subsequent purification in iodixanol gradient. Vectors were injected stereotactically (in 3 μl PBS) into the dorsal striatum in a bilateral manner at coordinates (mm to bregma): antero-posterior + 0.5, lateral ±2.5, dorso-ventral − 3.5 as previously described [17]. VCE-003.2 (10 mg/kg) or vehicle (sesame oil) were orally administered once daily (Fig. 1), and for neurogenesis experiments BrdU (100 mg/kg) was administered i.p. twice daily on the first week after viral injection. RotaRod test was conducted prior to drug injections to avoid acute effects of the compounds under investigation. RotaRod started at 4 rpm, with an acceleration rate of 6 rpm/min until either maximum speed is reached or the mouse falls from the apparatus. Maximum time assay was 10 min. Basal RotaRod performance was determined 6 days prior to striatal injury in 3 consecutive days with 3 trials/day (30 min of rest between each trial), and groups with equivalent motor function were assigned. RotaRod test was performed during 3 consecutive days prior to sacrifice and plasma was obtained for peripheral biomarker analyses. All experiments included a minimum of 6 mice per condition. The precise number of animals analyzed in each experiment is indicated in the corresponding figure legends.

### Gene expression

Total RNA was isolated from striate using the Qiagen RNeasy Lipid kit (Qiagen, Germany). Total RNA (1 μg) was retrotranscribed using the iScript cDNA Synthesis Kit and the cDNA analyzed by real-time PCR using the iQTM SYBR Green Supermix and a CFX96 Real-time PCR Detection System (Bio-Rad; Hercules, CA, USA). The HPRT gene was used to standardize mRNA expression in each sample. Gene expression was quantified using the $2^{-\Delta\Delta Ct}$ method and the percentage of relative expression against controls (untreated cells or mice) was

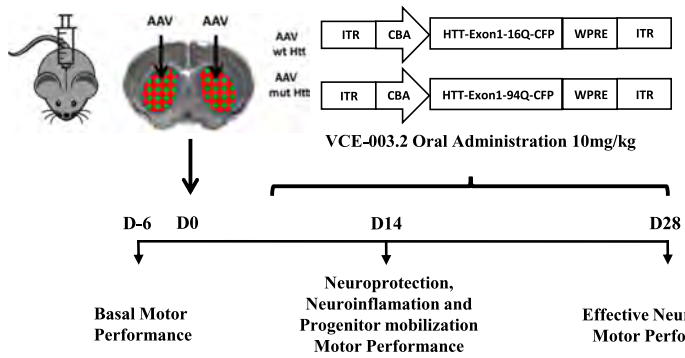


**Fig. 1** Experimental design for pharmacological manipulation and characterization of in vivo model of Huntington's disease based on adeno-associated viral expression of mutant huntingtin exon1

represented. The primers used in this study were: IL-6; forward: 5'GAACAACGATGATGCACTTGC3'; reverse: 5'TCCAGGTAGCTATGGTACTCC3'; TNFα; forward: 5'AGAGGCACTCCC CCAAAAGA-3; reverse: CGAT CACCCCGAAGTTCCCATT.

### Pharmacokinetics

Six-week old male Sprague Dawley rats (Janvier Labs, France) were located in the rodent area of Eurofins ADME Bioanalyses (Vergèze, France) and housed under standard conditions (12-h light/dark cycle) in groups with access to food and water *ad libitum*. Each animal was identified by an ear tag and examined for general health and welfare. Process, treatment and euthanasia were conducted according to the current procedures in use at Eurofins ADME Bioanalyses. Animals were treated with a single intravenous bolus of VCE-003.2 (10 mg/Kg in DMSO) or with oral VCE-003.2 (50 mg/Kg in sesame oil). At the prescribed times, blood (0.5 ml) was collected using a capillary tube and plasma frozen at − 20 °C until analysis. After 24 h, the animals were anesthetized and perfused with 20 mL of saline solution directly into the heart to extract the maximal blood sample from the brain. Plasma samples (100 μl) were mixed with 300 μl of acetonitrile and after protein precipitation, analysis of VCE-003.2 content was performed using LC-MS/MS (3 animals per each time point). For brain samples, the tissues were homogenized with an Ultra-turrax® using UHQ water (1/1, *w*/w). 100 μl of each homogenate was mixed with 300 μl of acetonitrile and the mixture centrifuged for 5 min at 25,000 g. Brain homogenate supernatants were directly measured by LC-MS/MS. Previous studies have shown that there are not significant differences between mice and rats in the main pharmacokinetic parameters of different cannabinoids, including CBG [18]. As the dose used here was different between i.v. and oral routes of administration, bioavailability was calculated taking into account the dose as follows: [AUCt (oral)/dose (oral)]/[AUCt(i.v.)/dose(i.v.)].

### Proteome array

Plasma samples from wild-type and mutant huntingtin-expressing C57BL/6 N mice were pooled ($n = 6$ animals per group) and analyzed for cytokine and adipokine expression. The Proteome Profiler Mouse XL Cytokine Array and the Proteome Profiler Mouse Adipokine Array (R&D Systems) were used according to the manufacturer's protocols to obtain protein expression profiles using 100 μl plasma samples. Spot density was determined using Quick Spots image analysis software (R&D Systems).

### Immunofluorescence and confocal microscopy

Free floating coronal brain slices (30 μm) were processed as previously described [17]. In brief, after blocking with 10% goat serum, brain sections were incubated with the indicated primary antibodies followed by secondary antibody incubation (2 h at room temperature). The appropriate mouse, rat and rabbit highly cross-adsorbed AlexaFluor 488, AlexaFluor 594 and AlexaFluor 647 secondary antibodies (1:500; Molecular Probes, Leyden, The Netherlands) were used. Samples were subsequently incubated with DAPI (1:5000, Roche) for 10 min, washed with PBS and mounted in Mowiol. All immunofluorescence data were obtained in a blinded manner by independent observers in a minimum of 6 correlative slices, from 1-in-10 series located between − 0.4 to + 1.6 mm to bregma. The lateral SVZ zone was delineated by using DAPI-counterstained cell nuclei, and analyses were performed in the upper dorsal tier, in which positively-labelled cells and immunoreactivity were quantified not beyond 100 μm of the SVZ. Confocal fluorescence images were acquired by using LAS-X software (Wetzlar, Germany) and SP8 microscope with 2 passes by Kalman filter, a 1024X1024 collection box, and pinhole AU 1. Double-labelled positive cells (GFAP/Ki-67 and BrdU/NeuN cells) were counted at a magnification of 40×. Cells were quantified within a 20 × 20 μm counting frame, which randomly sampled within a 122.8 × 68.9 μm counting grid. Cells that contacted the lateral or upper exclusion plane were excluded. The total number of cells counted was divided by the number of sampled counting frames and multiplied by its size to obtain the density of positive cells. Co-localization was confirmed by orthogonal projection of 18 z-stack files (1-μm each), and data were expressed as cells/mm$^2$. Neurodegeneration and glial activation was determined by dopamine- and cAMP-regulated phosphoprotein of 32 kDa mouse anti-DARPP32 (1:500 BD Transduction Laboratories, Lexington, KY), rabbit anti-Iba-1 (1:500 Wako Pure Chemical, Osaka, Japan) and mouse anti-GFAP-Cy3 (1:500 Sigma, St. Louis, MO) immunostaining, and quantified with Image-J software designed by the National Institutes of Health (NIH; Bethesda, MD, USA). Neurogenesis and SVZ-progenitor mobilization were characterized by immunofluorescence with rat anti-CTIP2 antibodies (1:500 Abcam, Cambridge, United Kingdom). Rabbit anti-Doublecortin (1:1000 from Abcam), rat anti-BrdU (1:250 from Abcam) and mouse anti-NeuN (1:500 from Chemicon) antibodies, or rabbit anti-GFAP and rabbit anti-Ki67 (1:400 from Invitrogen and 1:500 from ThermoScientific).

### Statistical analysis

*In vitro* data are expressed as mean ± S.D. and *in vivo* results are represented as mean ± SEM. Data were subjected

to Kolmogorov-Smirnov normality test and then, differences were analyzed by one-way ANOVA followed by Tukey post hoc test. $P < 0.05$ was considered significant. Statistical analysis was performed using GraphPad Prism version 5.01 and is shown in figure legends. Images were analyzed and quantified using the ImageJ.

## Results

### VCE-003.2 exerts a pro-neurogenic effect *in vitro*

To investigate the pro-neurogenic potential of VCE-003.2 we analyzed its influence in ES-neuronal differentiation. The R1 line of mouse ES cells was treated with VCE-003.2 during neural differentiation for 21 days and we assessed CTIP2-positive striatal MSN differentiation [19]. Immunofluorescence quantification revealed that VCE-003.2 increased the number of CTIP2-positive cells as well as doublecortin immunoreactivity (Fig. 2a-b). Next, using neuralized mouse embryonic teratocarcinoma P19 cells, we performed CTIP2 transcriptional activity assays by transfecting a luciferase reporter construct (A4-Mar) corresponding to one of the regulatory MARS sequences of the CTIP2 promoter. VCE-003.2 promoted neuronal-like differentiation as revealed by CTIP2 reporter activation (Fig. 2c). Furthermore, using a P19 neurosphere formation assay, VCE-003.2 generated larger neurospheres than vehicle-treated cells (367.90 ± 15.20 μm and 268.70 ± 9.20 μm, respectively; Fig. 2d). These results support a pro-neurogenic action of VCE-003.2 on neural stem cell differentiation.

### Pharmacokinetics and bioavailability of VCE-003.2

As VCE-003.2 was previously shown to exert a neuroprotective action in preclinical HD models, and considering its pro-neurogenic profile, we evaluated the pathophysiological impact and potential therapeutic value of VCE-003.2 after oral administration. Pharmacokinetic analyses were performed in rats after oral administration of VCE-003.2 (50 mg/kg) dissolved in sesame oil. Plasma VCE-003.2 levels peaked at 8 h (Tmax) and then slowly declined to basal levels. Oral VCE-003.2 resulted in 13.8% bioavailability and after 24 h the concentration of the compound in the brain was similar upon oral or i.v. treatment (Table 1). We also investigated some critical ADME/Tox parameters. By using human liver microsomes we found that VCE-003.2 undergoes a rapid intrinsic clearance *in vitro*, which was similar to the parental compound CBG (Additional file 1). Moreover, VCE-003.2 did not inhibit significantly the activity of relevant cytochrome P450 isoforms (Additional file 2). We also determined the potential hepatotoxicity of chronic VCE-003.2 administration by hematoxylin-eosin staining. VCE-003.2- and vehicle-treated mouse-derived livers did not show any evidence of fibrosis, steatosis, vacuolization, ballooning or inflammation (data not shown). In addition, VCE-003.2 administration did not inhibit hERG channel activity, suggesting a potential lack of cardiotoxicity (Additional file 3), and it was not genotoxic as assessed by AMES assays (Additional file 4). We also determined the impact of VCE-003.2 administration on peripheral biomarkers by quantifying the levels of cytokines and other soluble mediators. Viral infection lead to changes in various neuroinflammation biomarkers, notably C-reactive protein and pentraxins 2, 3 were increased by htt94Q and these changes were reverted by VCE-003.2 treatment (Additional file 5). These data indicate that mutant huntingtin induces a process of neuroinflammation that results in the release of soluble factors that can be quantified in plasma and normalized by VCE-003.2 oral administration.

### Oral administration of VCE-003.2 attenuates neuroinflammation and is neuroprotective in a viral model of mutant huntingtin expression

To evaluate the neuroprotective profile of oral VCE-003.2 administration, a viral model of HD was employed [20] in which wild-type mice were subjected to bilateral intrastriatal injection of adeno-associated virus (AAV) expressing either exon 1 of human pathogenic huntingtin with a polyQ tract of 94 CAG repeats, or a normal, non-pathogenic huntingtin with a polyQ tract of 16 CAG repeats (AAV-htt16Q and AAV-htt94Q, respectively), and treated with VCE-003.2 (10 mg/kg/day). Whereas expression of (exon1)-huntingtin-16Q during 14 days did not affect motor coordination, mutant huntingtin-94Q decreased RotaRod latency to fall (Fig. 3a). Motor impairment in htt94Q mice was accompanied by profound activation of microglial cells, as evidenced by Iba1 confocal immunofluorescence, in the area surrounding the infection site (Fig. 3b). Mice treated with VCE-003.2 performed better in the RotaRod test than their vehicle-treated AAV-htt94Q counterparts, and showed reduced microglial activation (Fig. 3a-b). Furthermore, VCE-003.2 administration prevented htt94Q-induced MSN degeneration as evidenced by DARPP-32 and NeuN immunofluorescence (Fig. 4a-b). These results are in line with previous findings on the neuroprotective ability of VCE-003.2 in toxin-based models of neurodegeneration [14, 21] and expand its potential clinical profile since oral administration was as effective as i.p. delivery. Likewise, oral VCE-003.2 administration was also neuroprotective and anti-inflammatory in the 3-NP model of striatal neurodegeneration (Additional file 6).

### Oral administration of VCE-003.2 promotes striatal neurogenesis

The neuroprotective action of oral VCE-003.2 and its pro-neurogenic impact *in vitro* prompted us to investigate if this compound could contribute to striatal

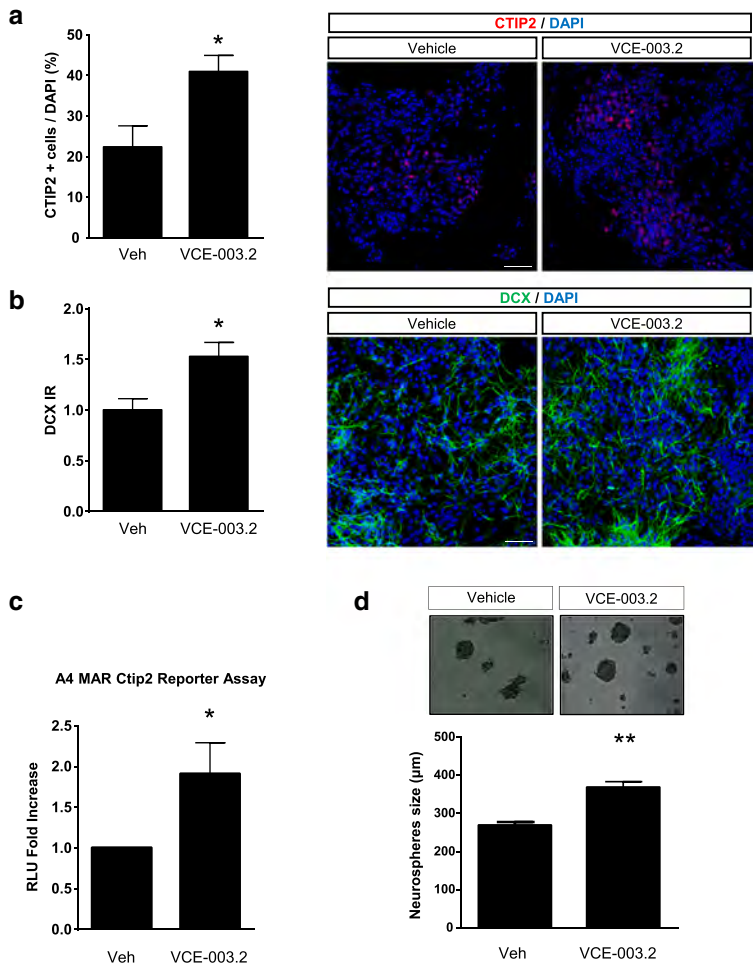


**Fig. 2** VCE-003.2 exerts a pro-neurogenic effect in vitro. **a-b** Mouse embryonic stem cells (R1 line) were treated with Vehicle, VCE-003.2 (500 nM) during neural differentiation for 21 days. Representative immunofluorescence images and quantification of CTIP2- and doublecortin-positive cells is shown ($n = 3$). **c** Luciferase reporter assay of the A4-MARS sequence of the CTIP2 locus was performed 24 h after P19 cell transfection under neuronal differentiation conditions and subject to pharmacological regulation as above. **d** P19 neurosphere formation assay was performed by culturing the cells for 24 h in the presence of Vehicle or VCE-003.2. Statistics: Unpaired t-test vs Vehicle **a** * $p < 0.05$; t = 2.82; df = 4; 95% Confidence interval (CI) = 0.3149 to 36.85; $R^2 = 0.66$. **b** * $p < 0.05$; t = 2.91; df = 4; 95% CI = 0.02 to 1.03; $R^2 = 0.67$. **c** * $p < 0.05$; t = 2.87; df = 5; 95% CI = 0.09 to 1.72; $R^2 = 0.62$. **d** ** < 0.01 t = 5.91; df = 362; 95% CI = 66.20 to 132.20; R2 = 0.08. Scale bar, 50 µm

**Table 1** Pharmacokinetic parameters of VCE-003.2. Pharmacokinetic parameters of VCE-003.2 in plasma following a single intravenous (i.v.) (10 mg/kg) and oral (50 mg/kg) dose in Sprague Dawley rats

| Compound | Route | Cmax (ng/mL) | Tmax (h) | AUCt ng/mL*h) | Bioavailability | Brain Concentration (24 h) (ng/mL) |
|---|---|---|---|---|---|---|
| VCE-003.2 | IV | 83160 | 0.08 | 475094.96 | | 93.7 ± 37.7 |
| VCE-003.2 | ORAL | 20266.67 | 8 | 327154.14 | 13.77% | 86.8 ± 34.0 |

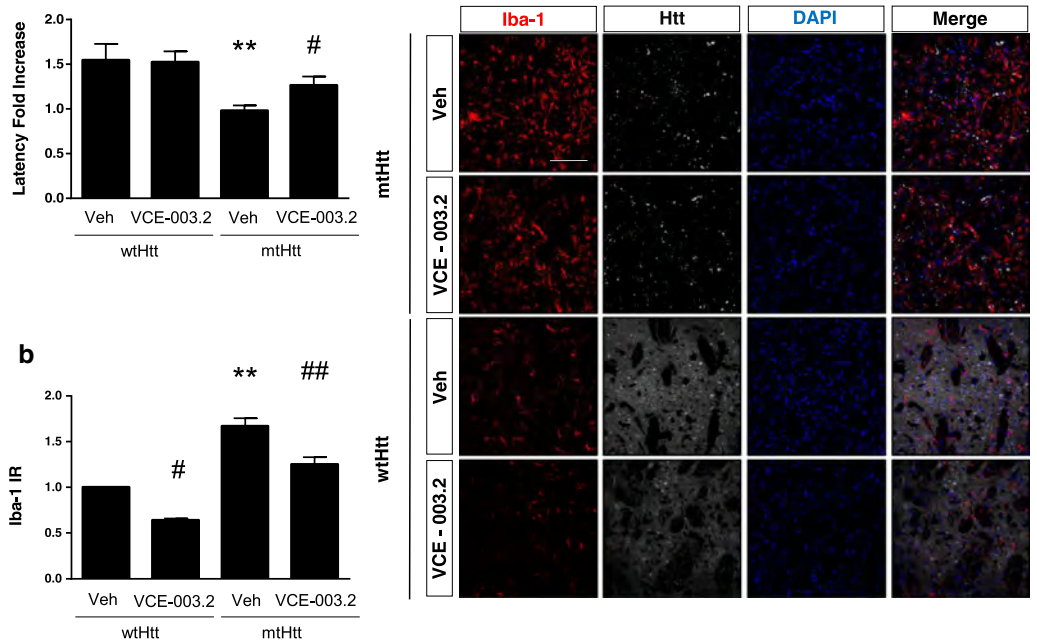


**Fig. 3** Oral administration of VCE-003.2 attenuates microglial activation and motor impairment induced by mutant-huntingtin expression. Wild type C57Bl/6 N mice were injected bilaterally with mutant huntingtin expressing AAV-htt94Q and AAV-htt16Q as control. VCE-003.2 or vehicle were administered orally daily (10 mg/kg) and mice analyzed at 2 after lesion. **a** Motor function was assessed in the RotaRod test and mean latency to fold quantified. **b** Representative confocal microscopy images of huntingtin-CFP and immunoreactivity with an antibody for microglia (Iba1). Iba1 immunoreactivity was quantified in the indicated experimental groups. AAV-htt16Q Vehicle and VCE-003.2 ($n = 3$ and 6, respectively), AAV-htt94Q Vehicle and VCE-003.2 ($n = 3$ and 5, respectively). Statistics: One-way ANOVA. **a** $F = 5.94$; $R^2 = 0.29$. $^{**}p < 0.01$; $q = 4.88$ AAV-htt16Q Veh vs. Mut-htt94q Veh and $\#p < 0.05$; $q = 3.90$ vs AAV-htt94Q Veh vs. AAV-htt94Q VCE-003.2. **b** $F = 5.87$; $R^2 = 0.91$. $\#p < 0.05$; $q = 5.32$ vs AAV-htt16Q VCE-003.2 vs. AAV-htt94Q Veh and $\#\#p < 0.01$; $q = 3.49$ vs AAV-htt94Q VCE-003.2 vs. AAV-htt94Q Veh. $^{**}p < 0.01$; $q = 9.30$ AAV-htt94Q Veh vs. AAV-htt16Q Veh. Scale bar, 100 μm

neurorepair *in vivo* by promoting SVZ-derived neurogenesis. We analyzed the SVZ neural stem cell population, identified as double-labelled GFAP/Ki-67 cells, which represents the radial glia type B cell compartment. VCE-003.2 increased the number of proliferating GFAP-positive cells in AAV-htt94Q-injected mice, indicating its positive impact on NSC mobilization (Fig. 5). Next, SVZ-derived neural progenitors were identified by immunofluorescence against Ascl1 (a transcription factor characteristic of the transit amplifying progenitor subpopulation). Mutant huntingtin expression induced an increase in $Ascl1^+$ cell number, and VCE-003.2 administration further promoted Ascl1-positive cell expansion in AAV-htt94Q-mice (Fig. 6). To determine the impact of VCE-003.2 on striatal neurogenesis we next evaluated doublecortin-positive neuroblasts after 30 days of AAV-mediated huntingtin expression and daily VCE-003.2 administration. AAV-htt94Q-induced injury resulted in a slight increase in neuroblast formation (Fig. 7a) and effective neurogenesis ($BrdU^+NeuN^+$ cells) (Fig. 7b) as compared to AAV-htt16Q. Oral administration of VCE-003.2 was effective in promoting neurogenesis in AAV-htt16Q- and AAV-htt94Q-treated mice, both determined as increased doublecortin-expressing cells and double-positive NeuN/BrdU neurons (Fig. 7a-b). Hence, oral VCE-003.2 administration is able to restore striatal neurogenesis affected by mutant huntingtin expression.

## Discussion

VCE-003.2 is an aminoquinone derivative of CBG that has been designated by the FDA as an orphan drug for HD treatment (www.accessdata.fda.gov/scripts/opdlisting/oopd/detailedIndex.cfm?cfgridkey=623717). In the present study, we demonstrate the pro-neurogenic activity of this cannabinoid derivative in a preclinical model

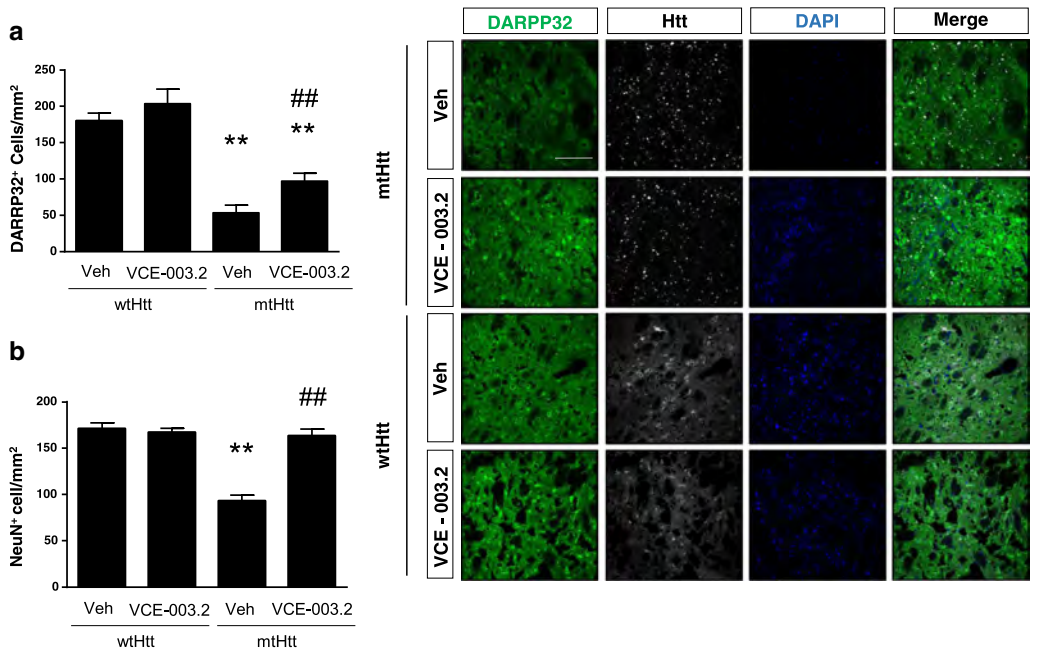


**Fig. 4** Oral administration of VCE-003.2 is neuroprotective from mutant-huntingtin-induced neurodegeneration. Wild type mice were injected bilaterally with mutant huntingtin expressing AAV-htt94Q (mtHtt) and AAV-htt16Q (wtHtt) as control. VCE-003.2 or vehicle were administered orally daily (10 mg/kg) and mice analyzed 30 days after lesion. Confocal microscopy characterization of huntingtin-CFP and using an antibody for the MSN marker DARPP32. Quantification of MSN survival after lesion for the indicated experimental groups. AAV-htt16Q (Vehicle and VCE-003.2, $n = 5$ each) and AAV-htt94Q (Vehicle and VCE-003.2, $n = 7$ each). Statistics: One-way ANOVA. **a** $F = 31.56$; $R^2 = 0.80$. ##$p < 0.01$; $q = 5.28$ AAV-htt94Q VCE-003.2 vs. AAV-htt94Q Veh. **$p < 0.01$; $q = 10.63$ vs AAV-htt94Q Veh vs. AAV-htt94Q Veh vs. AAV-htt16Q Veh and **$p < 0.01$; $q = 5.56$ vs AAV-htt94Q VCE-003.2 vs. AAV-htt16Q Veh. **b** $F = 27.15$; $R^2 = 0.78$. ##$p < 0.01$; $q = 10.74$ AAV-htt94Q VCE-003.2 vs. AAV-htt94Q Veh and **$p < 0.01$; $q = 10.85$ vs AAV-htt94Q Veh vs. AAV-htt16Q Veh. Scale bar, 100 μm

of HD that adds to its neuroprotective activity. Oral administration of VCE-003.2 exerted an anti-inflammatory and neuroprotective action in a HD experimental model. In addition, VCE-003.2 was able to augment mutant huntingtin-induced SVZ-derived neurogenesis, thus favoring neural stem cell mobilization (double-labelled $GFAP^+$/Ki-$67^+$ and $Ascl1^+$ cells), neuronal differentiation (double-$cortin^+$ cells) and effective neurogenesis (double-labelled $Brdu^+$/$NeuN^+$ cells). In agreement with previous studies, mutant huntingtin expression induced a pro-neurogenic response that was evident by the trend towards increased $Ascl1^+$, $Dcx^+$ and double-labelled $BrdU^+$/$NeuN^+$ cells. The molecular signals and mechanisms underlying injury-induced neurogenesis are diverse, and numerous therapeutic approaches aim to promote this endogenous process strategy [22]. Hence, the results obtained in this study support that striatal neurogenesis is improved by oral VCE-003.2 administration. This new mechanism of action of VCE-003.2 is relevant when considering its potential clinical applications, as it suggests that this molecule could constitute a disease-modifying drug rather than merely symptom-palliative. It is worth noting that the preclinical model of HD employed in this study is based on the expression of exon 1 of either mutant huntingtin or normal, non-pathogenic huntingtin. The validity of this approach for mechanistic and pharmacological investigations is demonstrated by the high number of studies using it [23]. However, improved animal models, for example based on the expression of full-length huntingtin, are likely to provide novel insights of additional aspects of HD.

The use of plant derived-cannabinoid ligands has been proposed to exert symptomatic relief of motor symptoms in neurodegenerative diseases, including HD-associated dystonia and chorea, levodopa-induced dyskinesia and tremor in Parkinson's disease, and multiple sclerosis-associated spasticity [6, 24]. Despite the great interest in the therapeutic potential of cannabinoids in neurodegenerative diseases, the undesired side-effects of $CB_1$ receptor agonists significantly limit

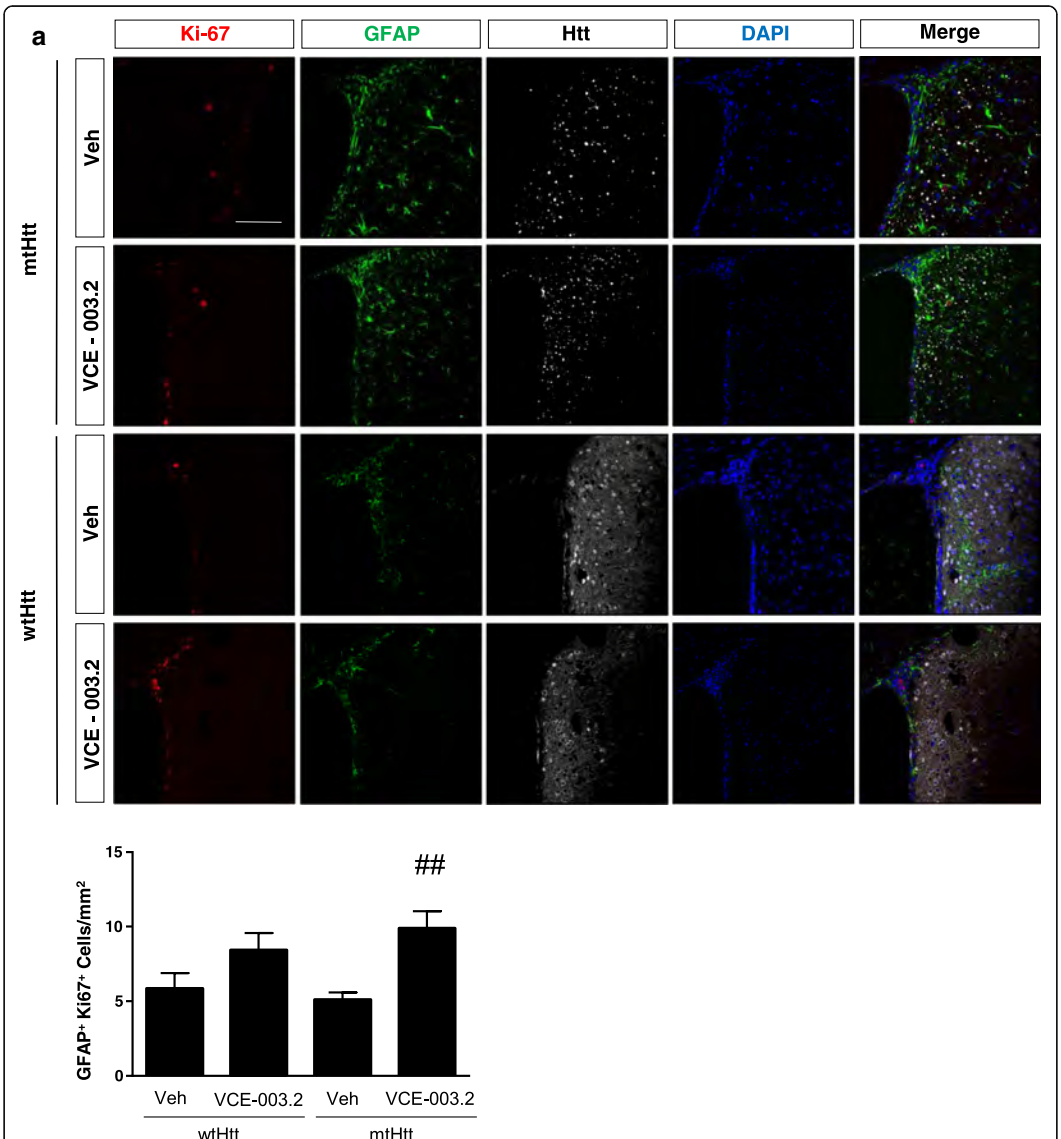


**Fig. 5** Subventricular zone neural progenitor mobilization is increased by oral administration of VCE-003.2. Mice were analyzed 4 weeks after lesion induced by AAV-htt16Q and AAV-htt94Q bilateral injection and daily treatment with vehicle or VCE-003.2 (10 mg/kg). Confocal microscopy characterization of the SVZ was performed with GFAP, htt and Ki-67-specific antibodies in the indicated experimental groups. Proliferating SVZ-neural stem cells were quantified based on GFAP and Ki-67 immunofluorescence colocalization. AAV-htt16Q (Veh and VCE-003.2, $n = 7$ and 6, respectively) and AAV-htt94Q (Veh and VCE-003.2, $n = 7$ and 8, respectively). Statistics: One-way ANOVA. $F = 5.78$; $R^2 = 0.42$. $\#\#p < 0.01$; $q = 5.29$ AAV-htt94Q VCE-003.2 vs. AAV-htt94Q Veh. Scale bar, 100 μm

their use in clinical practice. In addition, during HD progression presynaptic $CB_1$ receptor levels decline very early, even at presymptomatic stages [7, 9, 10]. Hence, despite the fact that corticostriatal projections preserve $CB_1$ receptor expression [17], the use of $CB_1$ agonists alone may have a limited therapeutic window, and the development of new cannabinoid-derived molecules acting via different signaling mechanisms and with reduced

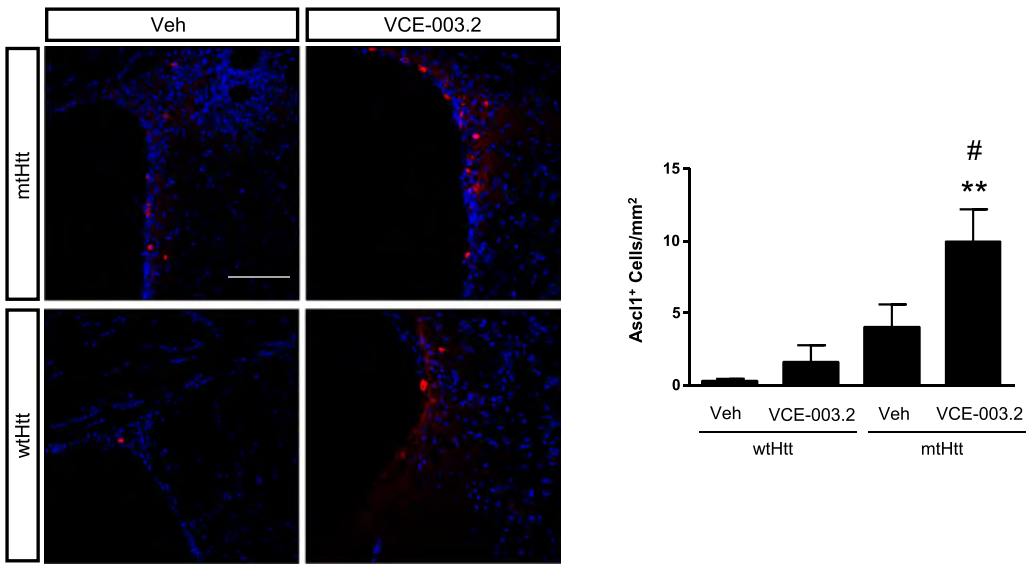


**Fig. 6** Subventricular zone neural progenitor mobilization is increased by oral administration of VCE-003.2. Mice were analyzed 4 weeks after lesion induced by AAV-htt16Q and AAV-htt94Q bilateral injection and daily treatment with vehicle or VCE-003.2 (10 mg/kg). Confocal microscopy characterization of the SVZ was performed with Ascl1-specific antibody in the indicated experimental groups. Quantification of transit amplifying progenitors labelled with Ascl1. AAV-htt-16Q (Vehicle and VCE-003.2, $n = 5$ each) and AAV-htt94Q (Vehicle and VCE-003.2, $n = 5$ each). Statistics: One-way ANOVA. $F = 10.12$; $R^2 = 0.65$. ##$p < 0.01$; $q = 4.25$ AAV-htt94Q VCE-003.2 vs. AAV-htt94Q Veh and **$p < 0.01$; $q = 7.12$ AAV-htt94Q VCE-003.2 vs. AAV-htt16Q Veh. Scale bar, 100 μm

undesired side-effects constitutes an attractive strategy to solve these limitations.

PPARγ receptors are required for appropriate neurogenesis as it controls neural progenitor cell proliferation and differentiation [25]. Noteworthy, the positive effect of PPARγ in neurogenesis, requires fine-tune regulation, as either its ablation or overactivation may hamper neuronal differentiation [26]. Under pathological conditions, for instance under an inflammatory insult, PPARγ activation can restore neurogenesis and cognitive impairment [27]. Similarly, PPARγ activation can restore neurogenesis in the OH-DA model of Parkinson's disease [28] and prevent amyloid-beta-induced cell death of human neural stem cells [29]. In HD models, the administration of PPARγ agonists protects from striatal neurodegeneration, attenuates neuroinflammation and decreases oxidative damage [30–32], supporting PPARγ as a valid target for the management of HD.

CBD is the most widely investigated phytocannabinoid devoid of psychotomimetic actions, and whereas its precise molecular mechanism of action remains the subject of research, some CBD actions, including its protective effect in counteracting amyloid-induced inflammation and neurogenesis deficits, are mediated by PPARγ receptors [33]. Hence, CBD administration can restore hippocampal neurogenesis deficits induced by different nervous system insults such as amyloid-beta pathology, chronic unpredictable stress and aging [34]. Other plant-derived cannabinoids such as CBG and tetrahydrocannabinolic acid regulate PPARγ activity [15, 35] and, hence, constitute interesting template structures for the development of new molecules with improved selectivity, reduced side-effects and better pharmacokinetic profile. Different strategies have been applied to improve CBD pharmacological properties. Fluorinated derivatives or quinone modifications have successfully generated new cannabinoid molecules with better translational perspectives (e.g., HUF-101, VCE-004). Thus, HUF-101 possesses improved anxiolytic, antidepressant and antipsychotic properties compared to the original CBD molecule [36]. Regarding CBG, its aminoquinone derivative VCE-003.2 has demonstrated efficacy as a neuroprotective molecule in HD [14], Parkinson's disease [21] and amyotrophic lateral sclerosis models [37]. Noteworthy, the VCE-003.2 compound is devoid of the side effects seen with full PPARγ-agonists and, hence, does not interfere with osteoblast differentiation and is less adipogenic [14].

Cell replacement therapy has demonstrated efficacy in HD experimental models and in preliminary studies in patients [38]. Exogenous cell grafts of either fetal tissue

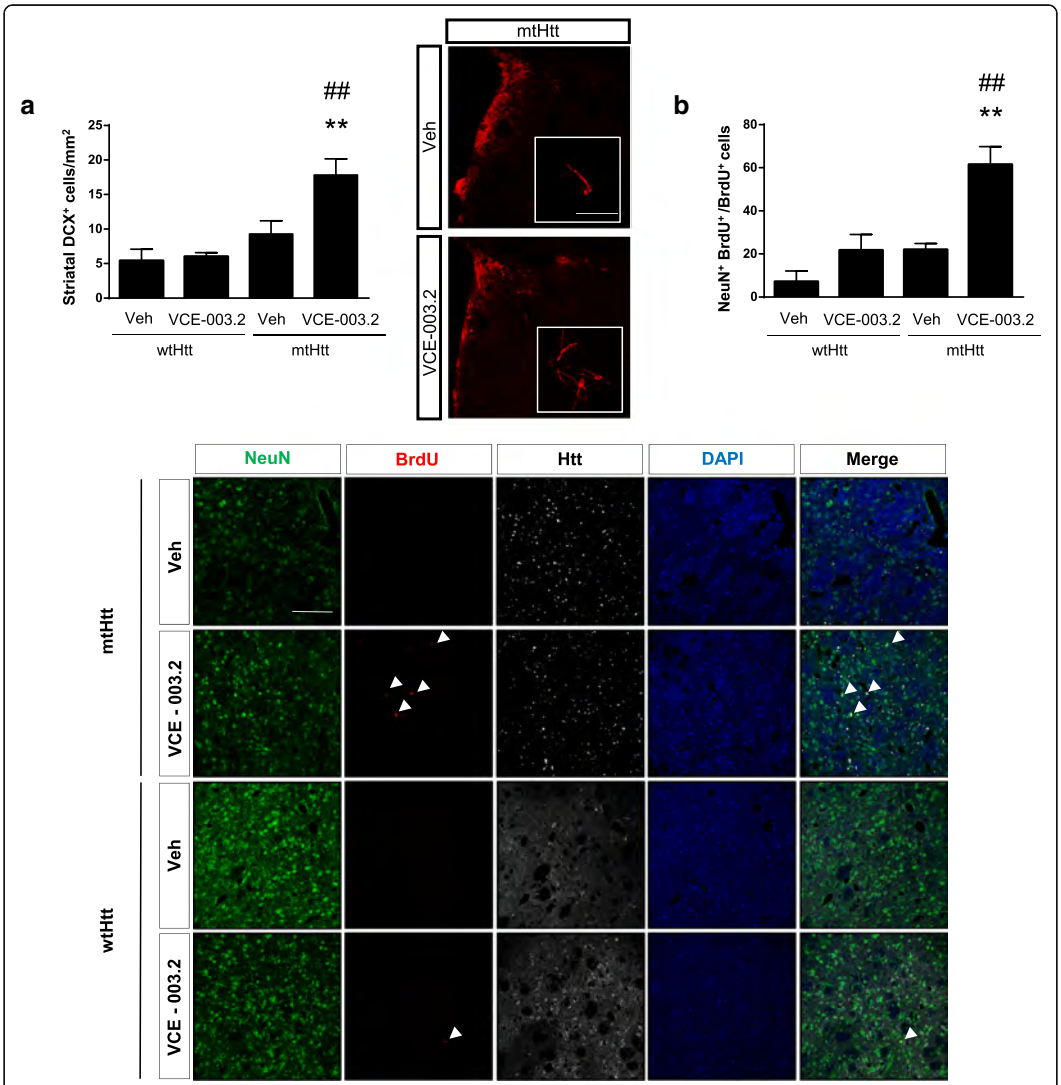


**Fig. 7** Oral administration of VCE-003.2 exerts a pro-neurogenic action. Mice were analyzed 4 weeks after lesion induced by AAV-htt16Q and AAV-htt94Q bilateral injection and administered daily with vehicle or VCE-003.2 (10 mg/kg). **a** Confocal microscopy characterization of migrating neuroblasts identified with doublecortin antibody and quantification in the striatum of the indicated mice groups. **b** Effective neurogenesis was determined by quantification of double positive cells labelled with BrdU and NeuN antibodies. AAV-htt16Q Vehicle and VCE-003.2 ($n = 7$ and 5, respectively); AAV-htt94Q Vehicle and VCE-003.2 ($n = 9$ and 11, respectively). Statistics: One-way ANOVA. **a** $F = 14.43$; $R^2 = 0.69$. ##$p < 0.01$; $q = 6.95$ AAV-htt94Q VCE-003.2 vs. AAV-htt94Q Veh and **$p < 0.01$; $q = 7.59$ AAV-htt94Q VCE-003.2 vs. AAV-htt16Q Veh. **b** $F = 13.99$; $R^2 = 0.59$. ##$p < 0.01$; $q = 6.50$ AAV-htt94Q VCE-003.2 vs. AAV-htt94Q Veh and **$p < 0.01$; $q = 7.59$ AAV-htt94Q VCE-003.2 vs. AAV-htt16Q Veh. Scale bar, 100 μm

or stem-cell derived neurons are able to survive in the striatum, as well as integrate and ameliorate motor symptoms and survival, however they face various challenges that impede their development for disease-modifying strategy. Considering that in HD postmortem tissue an increased SVZ cell proliferation and neurogenesis is evident [39], promoting endogenous SVZ-derived striatal neurogenesis constitutes an alternative approach of interest. Promoting SVZ neurogenesis by gene therapy-mediated delivery of BDNF and noggin successfully delayed progression of the

disease in the R6/2 mouse model [40, 41], and the same approach induced neurogenesis in adult squirrel monkeys [40]. These findings evidence that, even if endogenous newly-born neurons express mutant huntingtin, neurogenesis is effective and able to counteract, at least in part, neurodegeneration-evoked symptoms. In this scenario, pharmacological promotion of adult neurogenesis by cannabinoids [42, 43] may constitute a plausible alternative to gene therapy. In addition, cannabinoids could be used to promote ES-derived striatal neurogenesis *ex vivo* for mechanistic studies or cell replacement therapies.

In summary, our findings demonstrate that oral administration of VCE-003.2 exerts a neuroprotective action in a striatal neurodegeneration model that is accompanied by an improved endogenous neurogenic response. The capability of VCE-003.2 to increase effective neurogenesis suggests that this CBG derivative may possess the ability to act as a disease-modifying drug rather than only a symptomatic reliever.

## Conclusions

Oral administration of the cannabigerol derivative VCE-003.2 is neuroprotective and improves subventricular zone-derived neurogenesis in response to mutant huntingtin-induced neurodegeneration. These findings are relevant in the search for novel therapeutic strategies against Huntington's disease progression, considering the lack of undesired side actions of this novel cannabinoid-derived molecule and good bioavailability upon oral administration.

## Additional files

**Additional file 1:** Microsomal Metabolic Stability. Pooled human liver microsomes (final protein concentration 0.5 mg/mL), 0.1 M phosphate buffer pH 7.4 and the test compounds (VCE-003.2, CBG, verapamil and dextromethorphan) were pre-incubated at 37 °C prior to the addition of 1 mM NADPH to initiate the reaction. The final incubation volume was 25 μL. Each compound was incubated for 0, 5, 15, 30 and 45 min. The control (minus NADPH) was incubated for 45 min only. The reactions were stopped by the addition of 50 μL methanol containing internal standard at the appropriate time points. The incubation plates were centrifuged at 2500 rpm for 20 min at 4 °C to precipitate the protein. Following protein precipitation, the sample supernatants were analyzed using LC-MS/MS. From a plot of ln peak area ratio (compound peak area/internal standard peak area) against time, the gradient of the line was determined. Subsequently, half-life and intrinsic clearance was calculated using the equations below: Elimination rate constant (k) = (− gradient). Half-life ($t_{1/2}$) (min) = $\frac{0.693}{k}$. Intrinsic Clearance ($CL_{int}$) (μL/min/mg protein) = $\frac{V \times 0.693}{t_{1/2}}$. where V=Incubation volume mL/mg microsomal protein. (PDF 373 kb)

**Additional file 2:** Cytochrome P450 Inhibition (IC50 Determination). **CYP1A Inhibition.** VCE-003.2 (0.1, 0.25, 1, 2.5, 10, 25 μM in DMSO; final DMSO concentration = 0.3%) was incubated with human liver microsomes (0.25 mg/mL) and NADPH (1 mM) in the presence of the probe substrate ethoxyresorufin (0.5 μM) for 5 min at 37 °C. The selective CYP1A inhibitor, alpha-naphthoflavone, was screened alongside the test compounds as a positive control. **CYP2B6 Inhibition.** VCE-003.2 (0.1, 0.25, 1, 2.5, 10, 25 μM in DMSO; final DMSO concentration = 0.3%) was incubated with human liver microsomes (0.1 mg/mL) and NADPH (1 mM) in the presence of the probe substrate bupropion (110 μM) for 5 min at 37 °C. The selective CYP2B6 inhibitor, ticlopidine, was screened alongside the test compounds as a positive control. **CYP2C8 Inhibition.** VCE-003.2 (0.1, 0.25, 1, 2.5, 10, 25 μM in DMSO; final DMSO concentration = 0.3%) was incubated with human liver microsomes (0.25 mg/mL) and NADPH (1 mM) in the presence of the probe substrate paclitaxel (7.5 μM) for 30 min at 37 °C. The selective CYP2C8 inhibitor, montelukast, was screened alongside the test compounds as a positive control. **CYP2C9 Inhibition.** VCE-003.2 (0.1, 0.25, 1, 2.5, 10, 25 μM in DMSO; final DMSO concentration = 0.3%) was incubated with human liver microsomes (1 mg/mL) and NADPH (1 mM) in the presence of the probe substrate tolbutamide (120 μM) for 60 min at 37 °C. The selective CYP2C9 inhibitor, sulphaphenazole, was screened alongside the test compounds as a positive control. **CYP2C19 Inhibition.** VCE-003.2 (0.1, 0.25, 1, 2.5, 10, 25 μM in DMSO; final DMSO concentration = 0.3%) was incubated with human liver microsomes (0.5 mg/mL) and NADPH (1 mM) in the presence of the probe substrate mephenytoin (25 μM) for 60 min at 37 °C. The selective CYP2C19 inhibitor, tranylcypromine, was screened alongside the test compounds as a positive control. **CYP2D6 Inhibition.** VCE-003.2 (0.1, 0.25, 1, 2.5, 10, 25 μM in DMSO; final DMSO concentration = 0.3%) was incubated with human liver microsomes (0.5 mg/mL) and NADPH (1 mM) in the presence of the probe substrate dextromethorphan (5 μM) for 5 min at 37 °C. The selective CYP2D6 inhibitor, quinidine, was screened alongside the test compounds as a positive control. **CYP3A4 Inhibition.** VCE-003.2 (0.1, 0.25, 1, 2.5, 10, 25 μM in DMSO; final DMSO concentration = 0.3%) was incubated with human liver microsomes (0.1 mg/mL) and NADPH (1 mM) in the presence of the probe substrate midazolam (2.5 μM) for 5 min at 37 °C. The selective CYP3A4 inhibitor, ketoconazole, was screened alongside the test compounds as a positive control. **CYP3A4 Inhibition.** VCE-003.2 (0.1, 0.25, 1, 2.5, 10, 25 μM in DMSO; final DMSO concentration = 0.3%) was incubated with human liver microsomes (0.5 mg/mL) and NADPH (1 mM) in the presence of the probe substrate testosterone (50 μM) for 5 min at 37 °C. The selective CYP3A4 inhibitor, ketoconazole, was screened alongside the test compounds as a positive control. For the CYP1A incubations, the reactions were terminated by methanol, and the formation of the metabolite, resorufin, was monitored by fluorescence (excitation wavelength = 535 nm, emission wavelength = 595 nm). For the CYP2B6, CYP2C9, CYP2C19, CYP2D6, and CYP3A4 incubations, the reactions were terminated by methanol. The samples were centrifuged, and the supernatants combined for the simultaneous analysis of 4-hydroxytolbutamide, 4-hydroxymephenytoin, dextrorphan, and 1-hydroxymidazolam by LC-MS/MS. Hydroxybupropion, 6α-hydroxypaclitaxel and 6ß-hydroxytestosterone were analyzed separately by LC-MS/MS. A decrease in the formation of the metabolites compared to vehicle control was used to calculate IC50 values. (PDF 323 kb)

**Additional file 3:** hERG Channel Inhibition ($IC_{50}$ Determination). The experiments were performed on an IonWorks™ HT instrument (Molecular Devices Corporation), which automatically performs electrophysiology measurements in 48 single cells simultaneously in a specialized 384-well plate (PatchPlate™). The cells used were Chinese hamster ovary (CHO) cells stably transfected with hERG (cell-line obtained from Cytomyx, UK). A single-cell suspension was prepared in extracellular solution (Dulbecco's phosphate buffered saline with calcium and magnesium pH 7–7.2) and aliquots added to each well of a PatchPlate™. Cells were positioned over a small hole at the bottom of each well by applying a vacuum beneath the plate to form an electrical seal. The resistance of each seal was measured via a common ground-electrode in the intracellular compartment and individual electrodes placed into each of the upper wells. Electrical access to the cell was achieved by circulating a perforating agent, amphotericin, underneath the PatchPlate™ and then measuring the pre-compound hERG current. An electrode is positioned in the extracellular compartment and a holding potential of − 80 mV applied for 15 s. The hERG channels were then activated by applying a depolarizing step to + 40 mV for 5 s and then clamped at − 50 mV for 4 s to elicit the hERG tail current, before returning to − 80 mV for 0.3 s. VCE-003.2 were added to the upper wells of the PatchPlate™. Solutions were prepared by diluting 10 mM DMSO solutions of the test compound into extracellular buffer such that the final concentrations tested are 0.008, 0.04, 0.2, 1, 5 and 25 μM (final DMSO concentration 0.25%). Quinidine, an established hERG inhibitor, was included as a positive control and buffer containing 0.25% DMSO was included as a negative control. Post-

compound currents were then expressed as a percentage of pre-compound currents and plotted against concentration for each compound. Where concentration-dependent inhibition is observed, the data are fitted and $IC_{50}$ values were calculated. (PDF 322 kb)

**Additional file 4:** AMES Data Summary. AMES Experimental Procedure. Approximately ten million bacteria are exposed in triplicate to VCE-003-.2 (7.8, 15.6, 31.3, 62.5, 125 and 250 μg/ml), a negative control (vehicle) and a positive control for 90 min in medium containing a low concentration of histidine (sufficient for about 2 doublings). The cultures were then diluted into indicator medium lacking histidine and dispensed into 48 wells of a 384 well plate (micro-plate format, MPF). The plate was incubated for 48 h at 37 °C, and the number of wells showing growth were counted and compared to the vehicle control. An increase in the number of colonies of at least two-fold over baseline (mean + SD of the vehicle control) and a dose response indicates a positive response. An unpaired, one-sided Student's T-test was used to identify conditions that are significantly different from the vehicle control. Where indicated, S9 fraction from the livers of Aroclor 1254-treated rats was included in the incubation at a final concentration of 4.5%. An NADPH-regenerating system is also included to ensure a steady supply of reducing equivalents. The strains used in this study were S. typhimurium TA98 (hisD3052, rfa, uvrB/pKM10 for detection of frame-shift mutations) and S. typhimurium TA100 (hisG45, rfa, uvrB/pKM101 for detection of base-pair substitutions). VCE-003.2 was assessed for its mutagenic potential in the AMES reverse mutation assay. This test was performed in the absence and presence of S9 metabolic activation. VCE-003.2 was found to be negative for genotoxicity in this AMES study. The positive controls all behaved as expected. (PDF 568 kb)

**Additional file 5:** Effect of oral VCE-003.2 on plasmatic biomarkers. Plasma samples from the indicated groups of animals ($n = 6$) were pooled and subjected to mouse cytokine array (ARY028; R&D Systems) and mouse adipokine array (ARY013; R&D Systems) analysis. The relative expression of the indicated biomarkers is shown. (PDF 338 kb)

**Additional file 6:** 3-Nitroproprionic acid model of striatal neurodegeneration. 16-week- old C57BL/6 N male mice (Harlan Ibérica, Barcelona, Spain) were subjected to seven intraperitoneal (i.p.) injections of 50 mg/kg 3-NP (one injection each every 12 h prepared in phosphate-buffered saline (PBS)]. 3-NP-treated animals and their respective non-lesioned controls (injected with PBS) were used for pharmacological studies with VCE-003.2. Treatments consisted of oral gavage every 24 h with VCE-003.2 at a dose of 10 mg/kg using sesame oil as vehicle. 12 h after the last injection of 3-NP motor activity, hindlimb clasping and kyphosis were evaluated as previously described [12]. Animals were euthanized at the indicated time after huntingtin-AAV infection or 12 h after the last injection of 3NP and their brains removed. Statistical analysis: One-way ANOVA followed by the Tuckey's post hoc test was used to determine the statistical significance. All the *in vivo* data were expressed as mean ± SEM. Kruskal-Wallis test was used to determine the statistical in the case of non-parametric analysis. a) Hindlimb Clasping ($F = 8.069$; $p = 0.0047$) post hoc test: $p = 0.0036$ 3NP vs Veh; Locomotor activity ($F = 18.62$; $p = 0.0001$) post hoc test $p < 0.0001$ 3NP vs Veh, $p = 0.0027$ 3NP + VCE-003.2 vs 3NP; Kyphosis ($F = 28.24$ $p < 0.0001$) post hoc test: $p < 0.0001$ 3NP vs Veh, $p < 0.0001$ 3NP + VCE-003.2 vs 3NP. b) TNF-α ($F = 18.17$ $p = 0.0028$) post hoc test: $p = 0.0027$ 3NP vs Veh, $p = 0.0138$ 3NP + VCE-003.2 vs 3NP. IL-6 (Kruskal-Wallis statistic = 6.880 $p = 0.0071$) post hoc test: $p = 0.0265$ 3NP vs Veh. c) Average number of neurons per field ($F = 15.69$ $p = 0.0012$) post hoc test: $p = 0.0011$ 3NP vs Veh, $p = 0.0086$ 3NP + VCE-003.2 vs 3NP; Number of $Iba1^+$ cells ($F = 10.82$ $p = 0.0040$) post hoc test: $p = 0.0101$ 3NP vs Veh, $p = 0.0059$ 3NP + VCE-003.2 vs 3NP. (PDF 325 kb)

## Abbreviations

AAV: Adeno associated virus; CBG: Cannabigerol; HD: Huntington's disease; Htt: Huntingtin; MSN: Medium spiny neuron; PPAR: Peroxisome proliferator-activated receptor; SVZ: Subventricular zone

## Acknowledgements

We are thankful to J. Díaz-Alonso and L. Bellochio for intellectual input to the project, assistance designing and preparing AAV constructs and particles; E. Resel for grant administration and the rest of Galve-Roperh, Guzmán and Muñoz laboratories for enriching scientific environment.

## Funding

This work was supported by the MINECO grant RTC-2015-3364 to EM and IGR cofounded by the European Development Regional Fund in the Framework of the Operative Program "Reinforcement of research, technological development and innovation". IGR was also supported by grant PI15–00310 and PI18–00941 cofinanced by the European Development Regional Fund "A way to achieve Europe" and EM by the MINECO grant SAF2017–87701-R. JA and JPL were supported by FPI and FPU program fellowship (Ministerio de Educación, Cultura y Deporte) and DGR by Fundación Tatiana de Guzmán el Bueno. BP is a predoctoral fellow supported by the i-PFIS program, Instituto de Salud Carlos III (IFI15/00022; European Social Fund "Investing in your future").

## Availability of data and materials

The datasets used and/or analyzed during the current study are available from the corresponding author on reasonable request.

## Authors' contributions

JA, JPL, BP, RB, CN, AR, DGR and EGT performed *in vivo* and *in vitro* experiments; JA, JPL, BP, CN, IGR and EM collected and analyzed the data. IGR and EM managed and designed the overall study; MG, EM and IGR contributed to the literature research; JA and BP performed statistical analysis and MG, EM and IGR wrote the manuscript. All authors read and approved the final manuscript.

## Ethics approval and consent to participate

Animal studies were approved by ethics committee of Complutense University and Cordoba University (Spain). Consent to participate is not applicable.

## Consent for publication

Not applicable.

## Competing interests

EM is scientific advisors of Emerald Health Pharmaceuticals.

## Author details

[1]Instituto Ramón y Cajal de Investigación Sanitaria (IRYCIS), Ctra. Colmenar Viejo, km, 9100 Madrid, Spain. [2]Departamento de Bioquímica y Biología Molecular and Instituto Universitario de Investigación Neuroquímica, Universidad Complutense, Madrid, Spain. [3]Centro de Investigación Biomédica en Red sobre Enfermedades Neurodegenerativas (CIBERNED), Madrid, Spain. [4]Instituto Maimónides de Investigación Biomédica de Córdoba (IMIBIC), Córdoba, Spain. [5]Departamento de Biología Celular, Fisiología e Inmunología, Universidad de Córdoba, Córdoba, Spain. [6]Hospital Universitario Reina Sofía, Córdoba, Spain. [7]Emerald Health Pharmaceuticals, San Diego, USA.

Received: 22 November 2018 Accepted: 15 February 2019
Published online: 08 March 2019

## References

1. Ross CA, Aylward EH, Wild EJ, Langbehn DR, Long JD, Warner JH, Scahill RI, Leavitt BR, Stout JC, Paulsen JS, Reilmann R, Unschuld PG, Wexler A, Margolis RL, Tabrizi SJ. Huntington disease: Natural history, biomarkers and prospects for therapeutics. Nat Rev Neurol. 2014;10:204–16.
2. Conforti P, Besusso D, Bocchi VD, Faedo A, Cesana E, Rossetti G, Ranzani V, Svendsen CN, Thompson LM, Toselli M, Biella G, Pagani M, Cattaneo E. Faulty neuronal determination and cell polarization are reverted by modulating HD early phenotypes. Proc Natl Acad Sci U S A. 2018;115:E762–71.
3. Lim RG, Salazar LL, Wilton DK, King AR, Stocksdale JT, Sharifabad D, Lau AL, Stevens B, Reidling JC, Winokur ST, Casale MS, Thompson LM, Pardo M, AGG D-B, Straccia M, Sanders P, Alberch J, Canals JM, Kaye JA, Dunlap M, Jo L, May H, Mount E, Anderson-Bergman C, Haston K, Finkbeiner S, Kedaigle AJ, Gipson TA, Yildirim F, Ng CW, Milani P, Housman DE, Fraenkel E, Allen ND, Kemp PJ, Atwal RS, Biagioli M, Gusella JF, ME MD, Akimov SS, Arbez N, Stewart J, Ross CA, Mattis VB, Tom CM, Ornelas L, Sahabian A, Lenaeus L, Mandefro B, Sareen D, Svendsen CN. Developmental alterations in Huntington's disease neural cells and pharmacological rescue in cells and mice. Nat Neurosci. 2017;20:648–60.

4. Godin JD, Colombo K, Molina-Calavita M, Keryer G, Zala D, Charrin BC, Dietrich P, Volvert M-L, Guillemot F, Dragatsis I, Bellaiche Y, Saudou F, Nguyen L, Humbert S. Huntingtin Is Required for Mitotic Spindle Orientation and Mammalian Neurogenesis. Neuron. 2010;67:392–406.
5. Barnat M, Le Friec J, Benstaali C, Humbert S. Huntingtin-Mediated Multipolar-Bipolar Transition of Newborn Cortical Neurons Is Critical for Their Postnatal Neuronal Morphology. Neuron. 2017;93:99–114.
6. Di Marzo V, Stella N, Zimmer A. Endocannabinoid signalling and the deteriorating brain. Nat Rev Neurosci. 2015;16:30–42.
7. Blázquez C, Chiarlone A, Sagredo O, Aguado T, Pazos MR, Resel E, Palazuelos J, Julien B, Salazar M, Börner C, Benito C, Carrasco C, Diez-Zaera M, Paoletti P, Díaz-Hernández M, Ruiz C, Sendtner M, Lucas JJ, de Yébenes JG, Marsicano G, Monory K, Lutz B, Romero J, Alberch J, Ginés S, Kraus J, Fernández-Ruiz J, Galve-Roperh I, Guzmán M. Loss of striatal type 1 cannabinoid receptors is a key pathogenic factor in Huntington's disease. Brain. 2011;134:119–36.
8. Dowie MJ, Bradshaw HB, Howard ML, Nicholson LFB, Faull RLM, Hannan AJ, Glass M. Altered CB1 receptor and endocannabinoid levels precede motor symptom onset in a transgenic mouse model of Huntington's disease. Neuroscience. 2009;163:456–65.
9. McCaw EA, Hu H, Gomez GT, Hebb ALO, Kelly MEM, Denovan-Wright EM. Structure, expression and regulation of the cannabinoid receptor gene (CB1) in Huntington's disease transgenic mice. Eur J Biochem. 2004;271:4909–20.
10. Van Laere K, Casteels C, Dhollander I, Goffin K, Grachev I, Bormans G, Vandenberghe W. Widespread decrease of type 1 cannabinoid receptor availability in Huntington disease in vivo. J Nucl Med. 2010;51:1413–7.
11. Volkow ND, Baler RD, Compton WM, Weiss SRB. Adverse Health Effects of Marijuana Use. N Engl J Med. 2014;370:2219–27.
12. Valdeolivas S, Navarrete C, Cantarero I, Bellido ML, Muñoz E, Sagredo O. Neuroprotective Properties of Cannabigerol in Huntington's Disease: Studies in R6/2 Mice and 3-Nitropropionate-lesioned Mice. Neurotherapeutics. 2015;12:185–99.
13. Chiang MC, Cheng YC, Nicol CJ, Lin KH, Yen CH, Chen SJ, Huang RN. Rosiglitazone activation of PPAR??-dependent signaling is neuroprotective in mutant huntingtin expressing cells. Exp Cell Res. 2015b;338:183–93.
14. Díaz-Alonso J, Paraíso-Luna J, Navarrete C, Del Río C, Cantarero I, Palomares B, Aguareles J, Fernández-Ruiz J, Bellido ML, Pollastro F, Appendino G, Calzado MA, Galve-Roperh I, Muñoz E. VCE-003.2, a novel cannabigerol derivative, enhances neuronal progenitor cell survival and alleviates symptomatology in murine models of Huntington's disease. Sci Rep. 2016;6:29789.
15. Granja AG, Carrillo-Salinas F, Pagani A, Gómez-Cañas M, Negri R, Navarrete C, Mecha M, Mestre L, Fiebich BL, Cantarero I, Calzado MA, Bellido ML, Fernandez-Ruiz J, Appendino G, Guaza C, Muñoz E. A cannabigerol quinone alleviates neuroinflammation in a chronic model of multiple sclerosis. J NeuroImmune Pharmacol. 2012;7:1002–16.
16. Díaz-Alonso J, Aguado T, Wu C-S, Palazuelos J, Hofmann C, Garcez P, Guillemot F, Lu H-C, Lutz B, Guzmán M, Galve-Roperh I. The CB (1) cannabinoid receptor drives corticospinal motor neuron differentiation through the Ctip2/Satb2 transcriptional regulation axis. J Neurosci. 2012;32:16651–65.
17. Chiarlone A, Bellocchio L, Blazquez C, Resel E, Soria-Gomez E, Cannich A, Ferrero JJ, Sagredo O, Benito C, Romero J, Sanchez-Prieto J, Lutz B, Fernandez-Ruiz J, Galve-Roperh I, Guzman M. A restricted population of CB1 cannabinoid receptors with neuroprotective activity. Proc Natl Acad Sci. 2014;111:8257–62.
18. Deiana S, Watanabe A, Yamasaki Y, Amada N, Arthur M, Fleming S, Woodcock H, Dorward P, Pigliacampo B, Close S, Platt B, Riedel G. Plasma and brain pharmacokinetic profile of cannabidiol (CBD), cannabidivarine (CBDV), Δ 9-tetrahydrocannabivarin (THCV) and cannabigerol (CBG) in rats and mice following oral and intraperitoneal administration and CBD action on obsessive-compulsive behav. Psychopharmacology (Berl). 2012;219:859–73.
19. Arlotta P, Molyneaux BJ, Chen J, Inoue J, Kominami R, Macklis JD. Neuronal Subtype-Specific Genes that Control Corticospinal Motor Neuron Development In Vivo. Neuron. 2005;45:207–21.
20. Ruiz-Calvo A, Maroto IB, Bajo-Grañeras R, Chiarlone A, Gaudioso Á, Ferrero JJ, Resel E, Sánchez-Prieto J, Rodríguez-Navarro JA, Marsicano G, Galve-Roperh I, Bellocchio L, Guzmán M. Pathway-Specific Control of Striatal Neuron Vulnerability by Corticostriatal Cannabinoid CB1 Receptors. Cereb Cortex. 2018;28:307–22.
21. García C, Gómez-Cañas M, Burgaz S, Palomares B, Gómez-Gálvez Y, Palomo-Garo C, Campo S, Ferrer-Hernández J, Pavicic C, Navarrete C, Luz Bellido M, García-Arencibia M, Ruth Pazos M, Muñoz E, Fernández-Ruiz J. Benefits of VCE-003.2, a cannabigerol quinone derivative, against inflammation-driven neuronal deterioration in experimental Parkinson's disease: possible involvement of different binding sites at the PPARγ receptor. J Neuroinflammation. 2018;15:19.
22. Shohayeb B, Diab M, Ahmed M, Ng DCH. Factors that influence adult neurogenesis as potential therapy. Transl Neurodegener. 2018;7:4.
23. Brooks SP, Dunnett SB. Mouse Models of Huntington's Disease. Curr Top Behav Neurosci. 2015;22:101–33.
24. Saft C, von Hein SM, Lücke T, Thiels C, Peball M, Djamshidian A, Heim B, Seppi K. Cannabinoids for Treatment of Dystonia in Huntington's Disease. J Huntingtons Dis. 2018;7:167–73.
25. Stergiopoulos A, Politis PK. The role of nuclear receptors in controlling the fine balance between proliferation and differentiation of neural stem cells. Arch Biochem Biophys. 2013;534:27–37.
26. Taheri M, Salamian A, Ghaedi K, Peymani M, Izadi T, Nejati AS, Atefi A, Nematollahi M, Ahmadi Ghahrizjani F, Esmaeili M, Kiani Esfahani A, Irani S, Baharvand H, Nasr-Esfahani MH. A ground state of PPARγ activity and expression is required for appropriate neural differentiation of hESCs. Pharmacol Rep. 2015;67:1103–14.
27. Ormerod BK, Hanft SJ, Asokan A, Haditsch U, Lee SW, Palmer TD. PPARγ activation prevents impairments in spatial memory and neurogenesis following transient illness. Brain Behav Immun. 2013;29:28–38.
28. Bonato JM, Bassani TB, Milani H, Vital MABF, de Oliveira RMW. Pioglitazone reduces mortality, prevents depressive-like behavior, and impacts hippocampal neurogenesis in the 6-OHDA model of Parkinson's disease in rats. Exp Neurol. 2018;300:188–200.
29. Chiang M-C, Nicol CJ, Cheng Y-C, Lin K-H, Yen C-H, Lin C-H. Rosiglitazone activation of PPARγ-dependent pathways is neuroprotective in human neural stem cells against amyloid-beta–induced mitochondrial dysfunction and oxidative stress. Neurobiol Aging. 2016;40:181–90.
30. Chiang M-C, Cheng Y-C, Nicol CJ, Lin K-H, Yen C-H, Chen S-J, Huang R-N. Rosiglitazone activation of PPARγ-dependent signaling is neuroprotective in mutant huntingtin expressing cells. Exp Cell Res. 2015a;338:183–93.
31. Chiang M-C, Chern Y, Huang R-N. PPARgamma rescue of the mitochondrial dysfunction in Huntington's disease. Neurobiol Dis. 2012;45:322–8.
32. Jin J, Albertz J, Guo Z, Peng Q, Rudow G, Troncoso JC, Ross CA, Duan W. Neuroprotective effects of PPAR-γ agonist rosiglitazone in N171-82Q mouse model of Huntington's disease. J Neurochem. 2013;125:410–9.
33. Esposito G, Scuderi C, Valenza M, Togna GI, Latina V, de Filippis D, Cipriano M, Carratù MR, Iuvone T, Steardo L. Cannabidiol reduces Aβ-induced neuroinflammation and promotes hippocampal neurogenesis through PPARγ involvement. PLoS One. 2011;6:e28668.
34. Campos AC, Fogaça MV, Scarante FF, Joca SRL, Sales AJ, Gomes FV, Sonego AB, Rodrigues NS, Galve-Roperh I, Guimarães FS. Plastic and neuroprotective mechanisms involved in the therapeutic effects of cannabidiol in psychiatric disorders. Front Pharmacol. 2017;8:269.
35. Nadal X, del Río C, Casano S, Palomares B, Ferreiro-Vera C, Navarrete C, Sánchez-Carnerero C, Cantarero I, Bellido ML, Meyer S, Morello G, Appendino G, Muñoz E. Tetrahydrocannabinolic acid is a potent PPARγ agonist with neuroprotective activity. Br J Pharmacol. 2017;174:4263–76.
36. Breuer A, Haj CG, Fogaça MV, Gomes FV, Silva NR, Pedrazzi JF, Del Bel EA, Hallak JC, Crippa JA, Zuardi AW, Mechoulam R, Guimarães FS. Fluorinated Cannabidiol Derivatives: Enhancement of Activity in Mice Models Predictive of Anxiolytic. Antidepressant and Antipsychotic Effects. PLoS One. 2016;11:e0158779.
37. Rodríguez-Cueto C, Santos-García I, García-Toscano L, Espejo-Porras F, Bellido M, Fernández-Ruiz J, Muñoz E, de Lago E. Neuroprotective effects of the cannabigerol quinone derivative VCE-003.2 in SOD1G93Atransgenic mice, an experimental model of amyotrophic lateral sclerosis. Biochem Pharmacol. 2018;157:217–26.
38. Rosser A, Svendsen CN. Stem cells for cell replacement therapy: A therapeutic strategy for HD? Mov Disord. 2014;29:1446–54.
39. Curtis MA, Penney EB, Pearson AG, van Roon-Mom WMC, Butterworth NJ, Dragunow M, Connor B, Faull RLM. Increased cell proliferation and neurogenesis in the adult human Huntington's disease brain. Proc Natl Acad Sci U S A. 2003;100:9023–7.
40. Benraiss A, Toner MJ, Xu Q, Bruel-Jungerman E, Rogers EH, Wang F, Economides AN, Davidson BL, Kageyama R, Nedergaard M, Goldman SA. Sustained mobilization of endogenous neural progenitors delays disease progression in a transgenic model of huntington's disease. Cell Stem Cell. 2013;12:787–99.
41. Cho SR, Benraiss A, Chmielnicki E, Samdani A, Economides A, Goldman SA. Induction of neostriatal neurogenesis slows disease progression in a

transgenic murine model of Huntington disease. J Clin Invest. 2007;117:2889–902.
42. Galve-Roperh I, Chiurchiù V, Díaz-Alonso J, Bari M, Guzmán M, Maccarrone M. Cannabinoid receptor signaling in progenitor/stem cell proliferation and differentiation. Prog Lipid Res. 2013;52:633–50.
43. Prenderville JA, Kelly ÁM, Downer EJ. The role of cannabinoids in adult neurogenesis. Br J Pharmacol. 2015;172:3950–63.

*See you, Space Cowboy...*